Experimental Studies and Modelling of Chitosan Based Proton Exchange Membrane Fuel Cell (PEMFC)

Thesis Submitted by:

RABIRANJAN MURMU

Doctor of Philosophy (Engineering)

Department of Chemical Engineering

Faculty Council of Engineering & Technology

Jadavpur University

Kolkata, India

2024

JADAVPUR UNIVERSITY

KOLKATA 700032, INDIA

INDEX NO. 189/19/E

1. **Title of the thesis:** "Experimental Studies and Modelling of Chitosan Based Proton Exchange Membrane Fuel Cell (PEMFC)".

2. **Name, Designation & Institution of the Supervisor/s:**

(1) **Dr. Debashis Roy,** Professor, Department of Chemical Engineering, Jadavpur University, Kolkata 700032, WB, India.

(2) **Dr. Harekrushna Sutar,** Assistant Professor, Department of Chemical Engineering, Indira Gandhi Institute of Technology, Sarang, Dhenkanal-759146, Odisha, India.

3. List of Publications

I. **R. Murmu**, D. Roy, S.C. Patra, H. Sutar, P. Senapati, "Preparation and characterization of the SPEEK/PVA/Silica hybrid membrane for direct methanol fuel cell (DMFC)", **POLYMER BULLETIN**, 79, 2061-2087, 2021.

II. **R. Murmu**, D. Roy, H. Sutar, P. Senapati, Effect of Sulfuric Acid on the physiochemical properties of Chitosan-PVA blend for direct methanol fuel cell, **JOURNAL OF POLYMER MATERIALS**, 39(1-2), 89-109, 2022.

III. **R. Murmu**, D. Roy, S. Jena, H. Sutar, Development of chitosan based hybrid membrane modified with Ionic Liquid and Carbon Nanotubes for direct methanol fuel cell operating at moderate temperature, **POLYMER BULLETIN**, 80, 3949-3980, 2022.

IV. **R. Murmu**,D. Roy**,** H. Sutar, P. Senapati, S.C. Patra, Development of the highly performed chitosan based thin film towards the sustainability of direct methanol fuel cell, **POLYMER-PLASTICS TECHNOLOGY AND MATERIALS**, 62(6), 732-755, 2022.

V. **R. Murmu**, D. Roy, S.C. Patra, H. Sutar, B. Choudhary, Preparation and characterization of Red Mud modified chitosan-PVA composite membrane for direct methanol fuel cell, **JOURNAL OF ELECTROCHEMICAL ENERGY CONVERSION AND STORAGE**, 20(3), 031008, 2023.

VI. **R. Murmu**, D. Roy, H. Sutar, Mathematical modelling and simulations of active DMFC, **JOURNAL OF POLYMER MATERIALS**, 40 (3-4), 125-139, 2023.

4. List of Patents: NIL

5. List of Presentations in National/ International/ Conferences/ Workshops:

I. **R. Murmu**, D. Roy, H. Sutar, "Effect of Ionic Liquid on the properties of Chitosan Based membrane for Direct methanol Fuel Cell Application" in International Conference on Recent Advances in Mechanical Engineering Research and Development (ICRAMERD-2023) July 20-22, 2023. **(Oral)**

6. PROFORMA 1

JADAVPUR UNIVERSITY

KOLKATA 700032, INDIA

Statement of Originality

I, Shri Rabiranjan Murmu, registered on 27th June 2019 do hereby declare that this thesis entitled "Experimental Studies and Modelling of Chitosan Based Proton Exchange Membrane Fuel Cell (PEMFC)" contains literature survey and original research work done by the undersigned candidate as a part of Doctoral studies.

All information in this thesis have been obtained and presented in accordance with existing academic rules and ethical conduct. I declare that, as required by these rules and conduct, I have fully cited and referred all materials and results that are not original to this work.

I also declare that I have checked this thesis as per the "Policy on Anti Plagiarism, Jadavpur University, 2019", and the level of similarity as checked by iThenticate software is **10 %**.

Rabiranjan Murmu
Signature of the candidate:

Date: 08.11.2023

Certified by Supervisors

(DR. DEBASHIS ROY)

1._____ Signature of the supervisor and date with official seal

Professor
CHEMICAL ENGINEERING DEPARTMENT
JADAVPUR UNIVERSITY
Kolkata-700 032

Date: 08.11.2023

2._____ Signature of the Co-Supervisor and date with official seal

Harekrushna Sutar
Assistant Professor
Chemical Engineering Dept.
I.G.I.T, Sarang

Date: 08.11.2023

6. PROFORMA 2

JADAVPUR UNIVERSITY

KOLKATA 700032, INDIA

Certificate from the Supervisors

This is to certify that the thesis entitled "**Experimental Studies and Modelling of Chitosan Based Proton Exchange Membrane Fuel Cell (PEMFC)**" submitted by Shri Rabiranjan Murmu, who got his name registered on 27th June 2019 for the award of Ph.D. (Engineering) degree of Jadavpur University is absolutely based upon his own work under the supervision of Dr. Debashis Roy (Professor, Department of Chemical Engineering, Jadavpur University) and Dr. Harekrushna Sutar (Assistant Professor, Department of Chemical Engineering, Indira Gandhi Institute of Technology, Sarang, Odisha) and that neither this thesis nor any part of the thesis has been submitted for any degree / diploma or any other academic award anywhere before.

(DR. DEBASHIS ROY)

Professor
CHEMICAL ENGINEERING DEPARTMENT
JADAVPUR UNIVERSITY
Kolkata-700 032

1. _____

Signature of the supervisor
and date with official seal
Date: 8.11.2023

Harekrushna Sutar
Assistant Professor
Chemical Engineering Dept.
I.G.I.T, Sarang

2. _____

Signature of the Co-Supervisor
and date with the official seal
Date: 8.11.2023

7. Acknowledgement

First and foremost, I would like to express my sincere gratitude to my supervisor Dr. Debashis Roy, Professor, Department of Chemical Engineering, Jadavpur University, Kolkata, India, for his guidance, supervision, precious suggestions and insightful advice during the research work. I am grateful to him for his outreach suggestions during the research work. I am also thankful to him for his invaluable academic support. I am extremely grateful for the opportunity to work on my Ph.D. under his supervision.

I would like to express my gratitude to my co-supervisor Dr. Harekrushna Sutar, Assistant Professor, Department of Chemical Engineering, Indira Gandhi Institute of Technology, Sarang, Dhenkanal, Odisha, India, for his guidance, supervision, precious suggestions and insightful advice during the research work.

I am thankful to all the staff and faculty members of Chemical Engineering Department, Jadavpur University, Kolkata, India for their consistent encouragement and support.

I am also thankful to the staff members of the office, store and library of the Chemical Engineering Department, Jadavpur University for their help and support during my Ph.D. tenure.

I would like to express my gratitude to everyone who helped me, directly or indirectly to finish my research work.

I would like to express my gratitude to my respected parents for their unfailing love, care, and blessings. They are always encouraging me to give it my all. It would have been impossible to accomplish the research without their affection and blessings. I would want to express my gratitude to my wife, Mrs. Parbati Tudu, for her continuous support throughout the ups and downs of my Ph.D. work.

Rabiranjan Murmu
Department of Chemical Engineering
Jadavpur University

Dedicated

to

My Parents

TABLE OF CONTENTS

List of Figures

List of Tables

Nomenclature

DMFC: Direct Methanol Fuel Cell

AFC: Anode Flow Channel

ACL: Anode Catalyst layer

D_b: Diffusion coefficient of methanol at ADL, cm^2/s

D_m: Diffusion coefficient of methanol through membrane, cm^2/s

$I_{0,ref}^{MeOH}$: Electron transfer density of methanol, A/cm^2

$I_{0,ref}^{O_2}$: Electron transfer density of oxygen, A/cm^2

g: Specific surface area of anode, cm^2

U^{O_2}: Potential for oxygen oxidation, V

U^{MeOH}: Potential for methanol oxidation, V

t_a: Anode catalyst layer thickness, cm

t_b: Anode baking layer thickness, cm

t_m: Membrane thickness, cm

σ: Proton conductivity, S/cm

J: Volumetric current density at anode, (A/cm^3)

m_d: Electro-osmotic drag coefficient of methanol

r: Tafel slope

c_{o_2}: Oxygen concentration at CCL/Membrane interface

$c_{o_2,ref}$: Oxygen concentration at cathode inlet

c_{ref}^{a}: Methanol concentration at ACL/Membrane interface

β_a: Charge transfer at anode interface

β_c: Charge transfer at cathode interface

ABSTRACT

Proton exchange membrane fuel cell (PEMFC) is commonly used to generate electricity in three primary applications: transportation, stationary, and portable electronics. The development of an electrolyte membrane by Chitosan material is appealing for PEMFC due to its lower methanol cross-over, biodegradable, widely available and lower cost. However, it has lower proton conductivity as well as poor mechanical, thermal and dimension stability. For potential applications, Chitosan membrane is modified with polyvinyl alcohol (PVA), fillers, cross-linking agents and ionic liquid to improve its properties. The crosslinking of Chitosan-PVA blend by H_2SO_4 improves ion transport capacity, proton conductivity as well as mechanical and thermal properties. The addition of filler likes red mud, zirconia and multiwall carbon nanotubes to the Chitosan-PVA blend improves bound water content. Moreover, the addition of fillers deplete crystalline domain of the membrane and reduces glass transition temperature. The addition of ionic liquid and hygroscopic zirconia to the CP blend significantly increases proton conductivity and reduces methanol permeability. The highest proton conductivity was observed in a zirconia and ionic liquid modified CP blend. Moreover, it provides the lowest methanol permeability of 9.4×10^{-8} cm^2/s which is significantly lower than the commercial N117 membrane (2.74×10^{-6} cm^2/s). At 70°C, zirconia and ionic liquid modified CP blend provides the highest power density of 97 mW/cm^2 at a current density of 440 mA/cm^2. A one dimensional analytical model of direct methanol fuel cell (DMFC) is proposed by modelling the kinetics of methanol transport at anode flow channel (AFC), membrane and cathode catalyst layer. The proposed model is validated with the experimental results and can be used to predict DMFC performance.

Key words: PEMFC, IEC, Bound Water (%), Proton Conductivity, Methanol Permeability, Power density, Polarization Curve, Anode Flow Channel, Analytical Model.

(265 words) (1736 Characters)

CHAPTER 1

INTRODUCTION

1. INTRODUCTION

1.1 Fuel Cell

The use of petroleum based fuel like petrol and diesel in a portable devices produces toxic gas. The emission of toxic gas, polluted green environment and it is harmful for human beings. At present, the demand of petroleum fuel is gradually increasing. However, the resources of petroleum fuel is depleting due to their over consumption. The main drawbacks of using petroleum fuel in a portable devices are higher cost and potential harmful toxic gas emissions [**1, 2**]. In a current scenario, use of green energy in a portable and stationary device is quite appealing for maintaining healthy environment. The researcher has worked hard over the last few years to develop a potential device for replacing petroleum fuel. Fuel cell received more attention for the potential replacement of petroleum fuel. Proton exchange membrane fuel cell (PEMFC) generates electricity by electrochemical reaction. During electrochemical reaction, fuel (hydrogen or methanol) is oxidized at anode and generate electric current. The researchers have invented many types of highly prospective fuel cells to replace internal combustion (IC) engines [**2**]. The IC engine generates highly toxic pollutants and uses depleted fuel like petrol and diesel. The types of fuel cell and their operating condition's is given in **Table 1.1**.

Fuel cell has wide range of operating temperature as mentioned in **Table 1.1**. However, fuel cells which operate at low temperatures are thought to be the more promising for portable applications. Fuel cells that operate at low temperatures requires little energy to heat the system and can be handled properly. There are two kinds of low temperature fuel cells that function at less than 100°C; (i) alkaline fuel cell and (ii) proton exchange membrane fuel cell (PEMFC). Alkaline fuel cell have high fuel conversion efficiency. Moreover, the oxidation kinetics of fuel at cathode was faster which make it a superior candidate to replace IC engine. However, the

higher cost of fuel, corrosive electrolytes and low tolerance of carbon dioxide limit its potential application. PEMFC is a cheap, low temperature device and efficiently converted fuel to energy [**3**]. Due to these appealing characteristics, PEMFC is considered to be a convincing candidate to replace IC engine for portable and stationary applications. PEMFC was further categorized in to two types based on the types of fuel supply (i) Hydrogen fuel cell (ii) Direct methanol fuel cell (DMFC). Hydrogen and direct methanol fuel cell are the subcategory of PEMFC and are considered to be a most convincing device for portable and stationary applications. The hydrogen fuel cell is considered to be a most attracting candidate to replace petroleum based feedstock due to its following salient features like high fuel conversion efficiency and power density, low toxic emissions. However, the high cost of fuel as well as storage and transportation problems forced us to search for a potential alternative. In a current scenario, DMFC is considered to be a more promising candidate for portable and stationary applications. Hydrogen fuel cell operates with hydrogen fuel whereas clean methanol was supplied to the DMFC. The methanol fuel is chosen over hydrogen due to the following properties like high energy density, easy to store and transfer, low cost. The supply of clean methanol to the DMFC produces negligible toxic emission. Hence, it is considered to be a green energy with no harmful emissions [**4, 5**]. Moreover, the use of methanol in a fuel cell increases its demands which encourage the plantation of sugarcane for the production of methanol. The plantation of sugarcane not only improves the economy of farmers but also creates a healthy environment. As a result, it appears to be a promising to build a high-performance DMFC for societal socioeconomic benefits.

Table 1.1: **Different kinds of fuel cells and their operating conditions.**

Fuel Cell	**Operating requirements**
Alkaline Fuel Cell (AFC)	Operating temperature: up to 80ºC Fuel: Hydrogen, Fuel efficiency: 70% Electrolyte: Porous matrix saturated by alkaline solution
Proton Exchange Membrane Fuel Cell (PEMFC)	Operating Temperature: 50-100°C Fuel: Hydrogen or methanol Electrolyte: Polymer membrane, Nafion is the best suited membrane. Developer: General Electric
Phosphoric Acid Fuel Cell (PAFC)	Operating temperature: 150-210ºC, Fuel: Hydrogen, Liquid phosphoric acid as an electrolyte
Molten Carbonate Fuel Cell (MCFC)	Operating temperature: 650ºC Fuel: Hydrogen (internal reformer to produce hydrogen) Fuel efficiency: 60% Electrolyte: Salt mixture consists of molten carbonate
Solid Oxide Fuel Cell (SOFC)	Operating temperature: 700-1000ºC, Ceramic material as an electrolyte. Fuel: Hydrogen, Fuel efficiency: 60%
Direct Methanol Fuel Cell (DMFC)	Operating temperature: 60-90ºC, Fuel used: Methanol Best suited for portable applications.

In a DMFC, proton produced at anode is transported through the electrolyte membrane for generating electric current. Polymer membrane with high proton conductivity is preferred as an electrolyte medium. The thermally dispersed platinum (Pt) and platinum-ruthenium (Pt-Ru) powder on carbon cloth are most two common catalyst used in a DMFC. The working scheme of a typical DMFC is represented in **Fig. 1.1**. During cell operation, dilute oxygen and methanol is supplied to the cathode and anode side. Methanol is oxidized at the interface of

anode catalyst whereas the reduction of dilute oxygen was observed at cathode interface. The electrochemical reaction of fuel observed in a DMFC is given below

At anode interface: $CH_3OH + H_2O \longrightarrow CO_2 + 6H^+ + 6e^-$

At cathode interface: $3/2O_2 + 6H^+ + 6e^- \longrightarrow 3H_2O$

$CH_3OH + H_2O \longrightarrow CO_2 + 6H^+ + 6e^-$

Overall cell reaction: $CH_3OH + 3/2O_2 \longrightarrow CO_2 + 2H_2O$

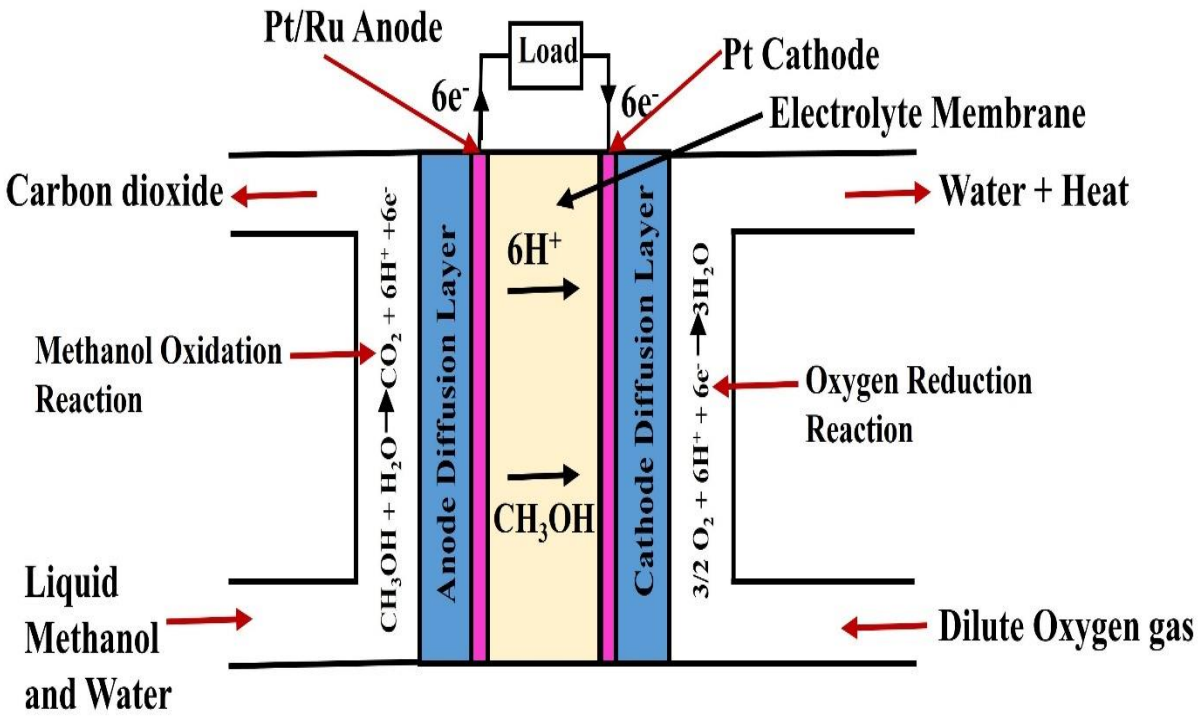

Figure 1.1: Working principle of a typical Direct Methanol Fuel Cell.

The main drawbacks of DMFC are its sluggish electrochemical reaction kinetics, fuel loss due to methanol cross-over, and improper water management [**6**]. Significant work was carried out in a recent years to address the aforementioned concerns, with a focus to improve fuel cell performance. On the very first, the polymer membrane used in the cell was modified to improve cell performance. The polymer membrane is considered to be an important part of fuel cell which control cell performance. It was used as an electrolyte to transport proton during electrochemical reaction. The desirable properties of membranes for fuel cell applications are its low cost, greater proton conductivity, low methanol cross-over and improved mechanical, thermal and hydrolytic stability. In the current scenario, Nafion membrane is most popular for the fuel cell applications. It has excellent ionic conductivity and better mechanical, thermal and chemical stability at harsh conditions. The key drawbacks of Nafion membrane are its increased methanol permeability and high cost. The higher methanol permeability through the membrane increases fuel loss and generating leakage current. The permeated methanol oxidized at cathode interface and produces leakage current which incurred voltage loss. The generation of leakage current at cathode reduces cell performance. Moreover, the higher cost of membrane makes fuel cell more expensive [**7, 8**]. Hence, it is desirable to make a low cost membrane with favourable properties to replace commercial Nafion membrane. The researcher has put in additional effort to build a low-cost membrane with desirable qualities such as strong proton conductivity, low methanol cross-over, and improved mechanical, thermal, and hydrolytic stability.

1.2 Research Gap in a DMFC

The DMFC is a greener energy technology that generates power from methanol. In a near future, it has the greater potential to replace petroleum based fuel in stationary and portable devices. In a DMFC, Nafion membrane is used as an electrolyte. The Nafion membrane provides higher proton conductivity as well as better mechanical, thermal and hydrolytic

stability. The main drawbacks of Nafion membrane are its significant fuel cross-over and higher cost. For potential application of DMFC in a stationary and portable applications, the performance of Nafion membrane should be enhanced or to develop a potential alternative membrane. The use of Nafion membrane is not attractive due to its higher cost. Moreover, the use of Nafion membrane in a DMFC increases fuel cross-over. The increase of fuel cross-over through the membrane increases leakage current. Due to the increase of fuel cross-over, higher fuel loss was occurred. Therefore, it is more convincing to develop a potential alternative of Nafion membrane with low cost and better properties. The literature study reveals that the use of Chitosan as an electrolyte membrane reduces methanol permeability. Therefore, it is an attractive candidate for the development of an electrolyte membrane. The major advantages of Chitosan is its biodegradability and low cost which make it a potential alternative of Nafion membrane. However, there are some issues in Chitosan membrane which needed be addresses for its potential application in stationary and portable devices. The use of Chitosan as an electrolyte membrane in a DMFC causes following drawbacks

i. Poor conductivity
ii. Higher swelling area which causes dimension instability
iii. Poor thermal and mechanical stability
iv. Poor performance at reduced humidity conditions
v. Operate only for lower conc. of methanol

Apart from the above issues, DMFC faces following challenges like poor water management and sluggish electrochemical oxidation of methanol. Poor water management can be remedied by constructing an appropriate membrane with a lower water uptake capacity or operating the fuel cell at a medium temperature. To improve DMFC performance, Chitosan membrane should be modified by adopting different strategy like blending, crosslinking, inorganic filler or ionic liquid incorporation.

1.3 Poly (ether-ether ketone) Membrane

In a recent years, poly (ether-ether ketone) membrane has garnered interest as a potential replacement for Nafion membrane due to its cost effectiveness. The PEEK membrane was functionally modified to improve its stability (mechanical, thermal and hydrolytic) and ionic conductivity [**9**]. The main limitations of PEEK membrane are its poor proton conductivity and higher fuel cross-over. A lot of effort has been made in modifying the PEEK-based membrane to improve proton conductivity and reduce fuel cross-over. To improve PEEK membrane performance, different strategy was employed by the researcher. The sulphonation of PEEK membrane with sulphuric acid increases its ion transport capacity, ionic conductivity and stability (mechanical and thermal). The blending of PEEK with another organic polymer material is proved to be good for enhancing performance of the PEEK membrane [**10, 11**]. Moreover, it was observed that introducing a hygroscopic filler to the PEEK backbone increases proton conductivity at low humidity conditions [**12, 13**]. The PEEK polymer is blended to a polyvinyl alcohol and hygroscopic silica to achieve better performance. The properties of the developed membrane are compared with the commercial Nafion membrane.

1.4 Chitosan Based Hybrid Membrane

The synthesis of electrolyte membrane with biodegradable material is attractive for DMFC applications. In a recent years, a substantial effort has been made by the researcher to produce a cost-effective electrolyte membrane by biodegradable materials. Because of its biodegradability, low cost, simple manufacturing procedure, and high methanol blocking ability, Chitosan is now regarded a possible choice for DMFC applications [**14, 15**]. Chitin is a nitrogenous polymer found mostly in the exoskeleton and internal organs of invertebrates [**16**]. The sources and potential application of Chitosan is shown in **Fig. 1.2**. Chitin obtained from the food sector was the primary source of Chitosan production. The Chitin was disposed to the outside environment which leads to potential air pollution. Therefore, a potential use of

chitin should be found to avoid air pollution. The use of Chitosan as an electrolyte in a DMFC not only generate cleaner energy but also reduces the potential air pollution incurred by chitin. Chitosan was obtained from the chemical treatments of chitin. The most frequent method for producing Chitosan from chitin is the deacetylation of chitin with sodium hydroxide solution. During chemical treatment, acetyl group of the chitin was removed. The chitin is highly hydrophilic due to the presence of water attracting acetyl group. Therefore, the chitin membrane has high swelling degree and poor mechanical strength. To enhance its mechanical, thermal and dimension stability, acetyl group of the chitin is removed.

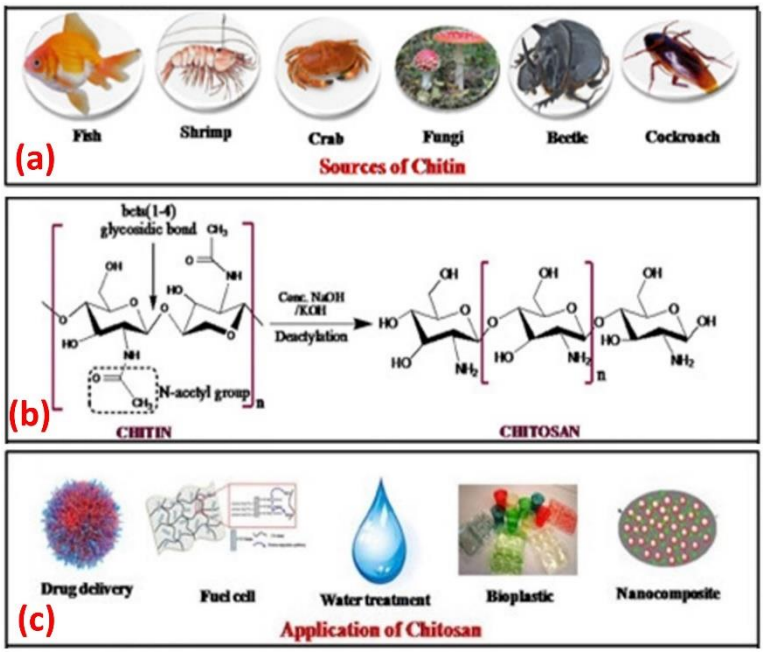

Figure 1.2: (a) Different sources of Chitin through which Chitosan is extracted. (b) Chemical treatment of Chitin to extract Chitosan. (c) Different applications of Chitosan. [16]

1.5 Modified with Polyvinyl Alcohol (PVA)

Polyvinyl alcohol is considered to be a good candidate for preparing membrane for fuel cell application. It is synthetically produced from poly (vinyl acetate) by hydrolysis reaction. The degree of hydrolysis affects physical and chemical properties of the polyvinyl alcohol [**17**]. It was also confirmed that the higher degree of hydrolysis produces harder PVA which is difficult to dissolve in a water. Therefore, partially hydrolysed PVA is preferred for the

synthesis of membrane. The partially hydrolysed PVA was easily dissolved in a water and make it more attractive for the synthesis of membrane. The PVA was dissolved in a water at the temperature range of 60-70°C [**18**]. It has good stability (mechanical, thermal and hydrolytic) which attracted for its possible consideration as a membrane material. It offers good methanol blocking ability. However, it contains more hydroxyl group which make it crystalline in nature. Due to its higher crystalline phase, it is harder but breaks at lower strain. Hence, for its practical application, crystalline phase of the PVA should be reduced. Moreover, it has lower proton conductivity and selectivity which make it unsuitable for fuel cell applications. The architecture of the PVA was modified to improve its selectivity. The PVA was modified by crosslinking reaction, blending with other polymer, incorporating nanoparticles as a fillers. It is highly biocompatible with the other polymers which make it attractive for the manufacture of composite membrane. The composite membrane provides excellent properties as compared to the virgin polyvinyl alcohol. It was ideal to develop a composite membrane by blending Chitosan with polyvinyl alcohol [**19-21**]. The blending of Chitosan and PVA reduces methanol permeability. Moreover, it increases hydrolytic stability of the membrane by reducing swelling degree of Chitosan [**21**]. It is believed that the blending of PVA and Chitosan along with the addition of filler improves selectivity of the composite membrane.

1.6 Modified with Filler and Ionic Liquid

The use of filler (inorganic and hygroscopic) and ionic liquid for preparing electrolyte membrane is more appealing. It was reported that the incorporation of filler to the base materials (SPEEK, Nafion, Chitosan) improves their physiochemical properties as well as proton conductivity [**22-26**]. Therefore, it is more convincing to develop a potential membrane by incorporating inorganic filler to the Chitosan membrane. Moreover, the use of inorganic filler to the Chitosan membrane improves bound water [**19, 22**]. The higher bound water content membrane provides more proton conductivity at moderate temperature and low

humidity conditions. The proton transport was controlled by bound water regulated Grotthuss mechanism [**22**]. The higher proton conductivity at reduced humidity conditions improves cell performance. Therefore, it was more appealing to modify Chitosan membrane by adding inorganic filler. The ionic liquid has a favourable properties like low vapour pressure and high ion exchange capacity [**27**]. The addition of ionic liquid to the membrane increase ion migration sites. The increase of ion migration sites in a membrane improves proton conductivity. It was reported that the addition of ionic liquid to the Chitosan membrane improve its proton conductivity [**28**]. It is not evaporated at low to moderate temperature due to its low vapour pressure. Moreover, the presence of ionic salt increases bound water of the membrane. The ionic liquid is strongly interacted with the water. The strongly interacted bound water is not evaporated at its boiling point and it will participated for proton transport by Grotthuss mechanism. Therefore, the ionic liquid modified membrane provides good performance at reduced humidity condition. Moreover, it improves thermal property of the membrane. The presence of pendant group of the ionic liquid prevents degradation of polymer chain at lower temperature. Due to the above properties, ionic liquid can be a considered as potential candidate for membrane preparation. However, the higher swelling nature of ionic liquid reduces hydrolytic stability of the membrane. Due to its higher swelling nature, swelling degree of the membrane was increases which reduces mechanical property of the membrane. Therefore, it is desirable to add a filler to the ionic liquid modified membrane for its mechanical property improvement. It is believed that the modifications of Chitosan membrane with the ionic liquid and filler will improves cell performance at reduced humidity conditions. Moreover, the amount of water produced by electrochemical reactions can be maintained properly by operating the fuel cell at moderate temperature.

CHAPTER 2

LITERATURE REVIEW

2. LITERATURE REVIEW

The rise in social and economic growth has resulted in an increase in demand for various fuel cells in our society. The rising scarcity of energy has compelled researchers to concentrate on renewable biological resources in order to produce suitable membranes that can meet this need. The usage of a bio-membrane in a fuel cell not only decreases fuel cross-over but also creates a clean environment. The use of Chitosan as an electrolyte membrane will significantly reduce fuel cross-over in a fuel cell. However, it is highly hydrophilic in nature and provide low proton conductivity. Hence, different technique was used by the researcher to develop a lost cost, high performance membrane from the Chitosan Therefore, it was blended with a compatible material to make it a suitable membrane. Moreover, to improve its proton conductivity, different filler, crosslinking agents or ionic liquid was incorporated in the blend.

Due to their advantageous features, Chitosan and polyvinyl alcohol (PVA) have received more interest for the fabrication of fuel cell membranes in recent years [**14, 17-19**]. Chitosan derived from prawn shells is biocompatible, low in production costs, abundant in nature, and environmentally benign [**21**]. Chitosan-based membranes can reduce methanol permeability across the membrane, improving fuel cell performance [**22-25, 28**]. PVA membranes are becoming increasingly popular for DMFC applications due to their hydrophilic property, increased electrochemical selectivity, and improved mechanical and thermal adaptability [**29-31**]. Because of their higher degree of crystalline phase, which raises elastic modulus, PVA and Chitosan membranes have poor mechanical and thermal stability. Chitosan and PVA were blended to improve physiochemical characteristics and proton conductivity [**32-34**]. The Chitosan-PVA combination offers improved electrochemical selectivity as well as better mechanical and thermal stability. At lower temperatures, the blend improves proton conductivity [**34**]. However, at lower temperatures, fuel cell performance was substantially

reduced due to inadequate water management, which is the most serious issue in a fuel cells. To address the aforementioned difficulty, fuel cells are operated at higher temperatures, close to the boiling point of water. The condition of water in the membrane, i.e. bound water and free water, is important for proton transport and is controlled by the Grotthuss mechanism [**35**]. The blend has low proton conductivity at higher temperatures because to a dramatic fall in free water in the membrane, which restricts proton transfer via the Grotthuss mechanism. In this condition, bound water of the membrane plays important role for proton transport. The membrane with higher bound water content provides better proton conductivity at a medium temperature. The proton transfer was aided by the Grotthuss mechanism, which was regulated by bound water [**36**]. Several attempts have been undertaken, such as cross-linking [**36**], inorganic fillers [**38, 39**], nanoparticles addition [**40-42**], to improve the physiochemical characteristics and bound water content of the Chitosan-PVA blend. According to the literature, modifying the membrane with an inorganic filler increases the bound water content, which increases proton conductivity. It was also confirmed that introducing hygroscopic filler not just increases bound water content but also improves mechanical, thermal, and hydrolytic stability of the membrane [**40, 43**].

Carbon nanotubes (CNTs) and hygroscopic zirconia are regarded potential fillers for the construction of composite membranes due to their exceptional mechanical and thermal properties [**42**]. It was discovered that dispersing CNT fluid and hygroscopic zirconia in the Chitosan matrix increases mechanical and thermal strength while also lowering methanol permeability through the composite [**42, 43**]. Ionic liquids (IL) have garnered a lot of interest in recent years for the fabrication of fuel cell membranes due to their non-volatility and high ionic conductivity. The key benefits of ILs are their low vapour pressure, strong mechanical and thermal stability, and high ion conductivity [**44-46**]. As a result, ILs are widely regarded as a promising candidate for the fabrication of suitable membrane materials for medium

temperature fuel cell applications [**47, 48**]. The IL will serve as a mobile charge carrier for proton transport, which will be governed by a vehicular mechanism. The ions are migrated by the mobile carrier of IL thereby increasing ionic conductivity. The impregnation of IL, introduces the extra charge carrier sites in the polymer matrix which eventually elevates ion transport capacity. It was also confirmed that adding bulky ionic liquid to a polymer matrix limits the migration sites for methanol transport and lowers methanol permeability [**49**].

The major goal of this work is to create a Chitosan-based composite membrane with higher proton conductivity, reduced methanol permeability, and superior mechanical, thermal, and hydrolytic stability. A membrane with higher proton conductivity and great methanol blocking capabilities is considered as a viable contender for DMFC applications. Our research focuses on the successful inclusion of IL, hygroscopic zirconia, red mud nanoparticles, and CNT in Chitosan composites and characterising their properties using various experimental techniques. Following the development of composite membranes, fuel cell performance in a single cell of direct methanol fuel cell will be investigated. Our work focuses on increasing the power density of the DMFC by improving selectivity of the composite membranes. The physiochemical properties of the composite membranes will be studied by different experimental technique like FESEM, FTIR, DSC, TGA, DMA and tensile test. As a green energy carrier that has gained practical importance for fuel cells and for potential applications, hybrid membranes need to have higher mechanical, thermal, and hydrolytic stability. The strategy of this work is to fabricate a hybrid thin film with the goal of improving selectivity as well as membrane stability (mechanical, thermal, and hydrolytic). Furthermore, the fuel cell assembled with the developed hybrid thin film should provide higher power density under reduced humidity conditions. The power density and cell voltage of the single cell of DMFC will be obtained from the polarization curve.

CHAPTER 3

AIMS & OBJECTIVES

3. AIMS & OBJECTIVES

Fuel cell is recognised as one of the most promising clean energy devices because of its low toxic gas and other hazardous chemical emissions. It is currently a prominent research topic in all major vehicle and energy industries, and it is also thought to be approaching commercialisation. Among the various kinds of fuel cells, polymer electrolyte membrane fuel cells (PEMFC) are easily miniaturised and suitable as energy sources for autos, home purposes, and portable electronics. The polymer membrane is a crucial part of PEMFC that determines fuel cell performance. The PEMFC is categorized in to two type (i) hydrogen fuel cell (ii) direct methanol fuel cell. My research topic focuses on the fabrication of Chitosan-based membranes for direct methanol fuel cells and the estimation of fuel cell power density. After estimating fuel cell performance, the properties of Chitosan based membranes are compared with a possible SPEEK-based membrane and traditional Nafion membrane.

Aims & Objectives of the research work are as follows;

To develop highly selective chitosan based low cost membranes (modified with red mud, ionic liquid with different fillers) able to deliver high power density.

I. Fabrication of cost effective bio-membrane based on Chitosan.

In the current scenario, Nafion membrane is used as electrolyte membrane in a PEMFC. However, the cost of Nafion membrane is very high. The higher cost of membrane increases the cost of fuel cell. Therefore, the preparation of electrolyte membrane by a cheap material is more appealing. The use of low cost chitosan as membrane material is more attractive due to its excellent methanol blocking ability. The main objective of this work is to develop a cost effective chitosan based membrane focusing on higher proton conductivity as well as selectivity.

II. Improve thermal, mechanical and hydrolytic stability of the composite membrane.

The electrolyte membrane with better mechanical and thermal stability is desirable for fuel cell applications. The membrane with better mechanical stability provides excellent performance at stressed conditions. Moreover, it should have better hydrolytic stability. The membrane with poor hydrolytic stability reduces fuel cell performance. Due to poor hydrolytic stability, membrane swells more which drastically affects fuel cell performance. The chitosan membrane has poor hydrolytic stability due to its excessive swelling property. Moreover, it has also poor mechanical and thermal stability. Therefore, it should be blended with other polymers as well as fillers to improve its mechanical, thermal and hydrolytic stability.

III. Reduce fuel cross-over across the membrane.

The electrolyte membrane with higher methanol cross-over is not desirable for fuel cell application. Due to higher methanol cross-over, fuel loss was occurred in a fuel cell. Moreover, the permeated methanol takes part for oxidation reaction at cathode interface and produces leakage current. The generation of more leakage current drastically reduces fuel cell performance. Therefore, it is more appealing to develop a cost effective membrane with lower methanol cross-over. The chitosan is a potential candidate for the development of electrolyte membrane due to its good methanol blocking ability.

IV. Improve membrane selectivity and proton conductivity.

The electrolyte membrane with better proton conductivity is desirable for fuel cell application. The membrane with higher proton conductivity as well as excellent methanol blocking ability provides excellent performance. The chitosan membrane has lower proton conductivity. Due to its poor proton conductivity, it has lower selectivity. Hence, pure chitosan membrane provides poor performance. Therefore, it is desirable to improve its proton conductivity by adding fillers.

V. Improve power density of a fuel cell at low to moderate temperature.

The highly selective membrane is preferred for fuel cell application. The highly selective membrane provides better cell performance. The more power density will be achieved by the highly selective membrane. The main objective of this work is to develop highly selective chitosan based membrane to achieve high power density.

VI. Mathematical modelling of fuel cell.

An analytical model will be developed to predict fuel cell performance at different operating conditions. The model equation will be developed by steady state assumption in a flow channel of fuel cell attack. The model equation will be solved to predict leakage current and polarization curve of a fuel cell. Finally, the polarization curve predicted by the analytical model will be compared with the experimental polarization curve.

VII. To compare the performance of Chitosan based membrane with a potential SPEEK based membrane and commercial Nafion Membrane.

The SPEEK membrane is considered to be a potential candidate for fuel cell application. The main drawbacks of the SPEEK based membrane is its higher cost. The properties of chitosan based membranes will be compared with the commercial Nafion membrane and prospective SPEEK based membrane. The properties of the chitosan based membranes will be compared to confirm its feasibility towards fuel cell applications.

CHAPTER 4

MATERIALS AND METHODS

4. MATERIALS AND METHODS

4.1 Materials & Chemicals

Chitosan (De-acetylated degree ≥ 75%, $\bar{M}_{av}$ ≈310,000-375,000), Poly (ether-ether ketone) powder (d_p=80μm), Sulphuric acid (>98%), Polyvinyl alcohol (99 % hydrolysed, $\bar{M}_{av}$≈85000-124000), Ionic Liquid, 1-Allyl-3-methylimidzolium bis (trifluormethylsulfonyl)imide (CAS No.: 655249-87-9, 5g) and glacial acetic acid (Anhydrous, 100%) were purchased from Sigma-Aldrich. Dimethylacetamide solvent, PTFE beaker and silica gel were procured from Noble enterprise, Berhampur. Zirconium oxide (99.0%, APS: 20nm, SSA: 30-60m^2/g), Multi-wall Carbon Nanotubes (OD: 10-20NM and length: 10-30UM), Hydrochloric acid, Sodium Chloride crystal, Sodium hydroxide pellet, methanol (Anhydrous, 99.8%) and Phenolphthalein indicator were procured from Otto Chemie Pvt. Ltd, Mumbai, Maharashtra. Water purifying system supplied by Ion Exchange ltd. was used to produce deionised and distilled water. Red mud powder was collected from the sites of NALCO power plant Angul, Odisha, India. The catalyst powder (Platinum: 40%, Platinum: 20%-Ruthenium: 10%) along with carbon cloth required for making anode and cathode catalysts were procured from Duralyst Energy Pvt. Ltd. Chennai, Tamil Nadu, India.

4.2 Size Reduction of Red Mud and Silica Particle

The size of red mud and silica particle was reduced by wet milling process. The wet milling process was a conventional method to obtain fine particle size without aggregation. The wet milling process was carried out in a dual drive planetary ball mill. Using an acetone solvent, the material was well distributed in the grinding ball of a planetary ball mill. Milling duration and disc rotating speed were optimised during the milling process to achieve fine particle size. The milling duration and disc rotational speed have a considerable impact on the final particle

size of the sample. The milling process carried out for longer duration of time produces finer particle size. The wet milling process of the sample was carried out at 150 rpm and 25-30h milling time. Before milling process, sample was dried in a hot air oven at 70-100°C to reduce moisture content. The weight ratio between the ball and sample was maintained at 8:1. After milling process, finer particle was separated by sieve shaker and dehydrated in a hot air oven at 60°C for 4h. The size of the particles is analysed by laser scattering particle size distribution analyser (Model No. LA-960).

4.2.1 Analysis of Particle Size

The size of fine particles produced by the planetary ball mill was determined using a particle size analyser. The grain size distribution of red mud particles is depicted in **Fig. 4.1(a)**. Particle sizes are narrowly distributed in the 18-28nm range. The planetary ball mill produces very fine particle size in the nanometre range. From the size distribution curve, the mean grain size of particles were 19±10nm. The maximum size of red mud particles was observed in the grain size of 22nm. It was observed that with the increase of sieving tray diameter, the population of undersize particles increases. The maximum population of particles was observed in the grain size range of 20-25nm. According to the curve, more than 90% of the sample population was larger than 18nm in diameter, 5% is smaller than 18nm in diameter, and 10% is larger than 24nm in diameter.

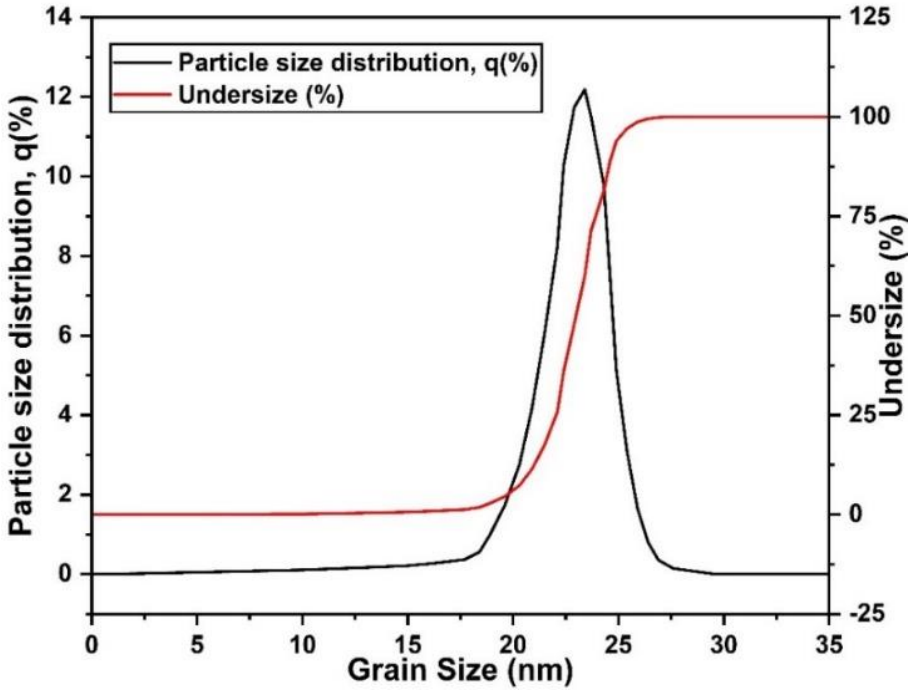

Figure 4.1 (a): Grain size plot of finely produced red mud particles.

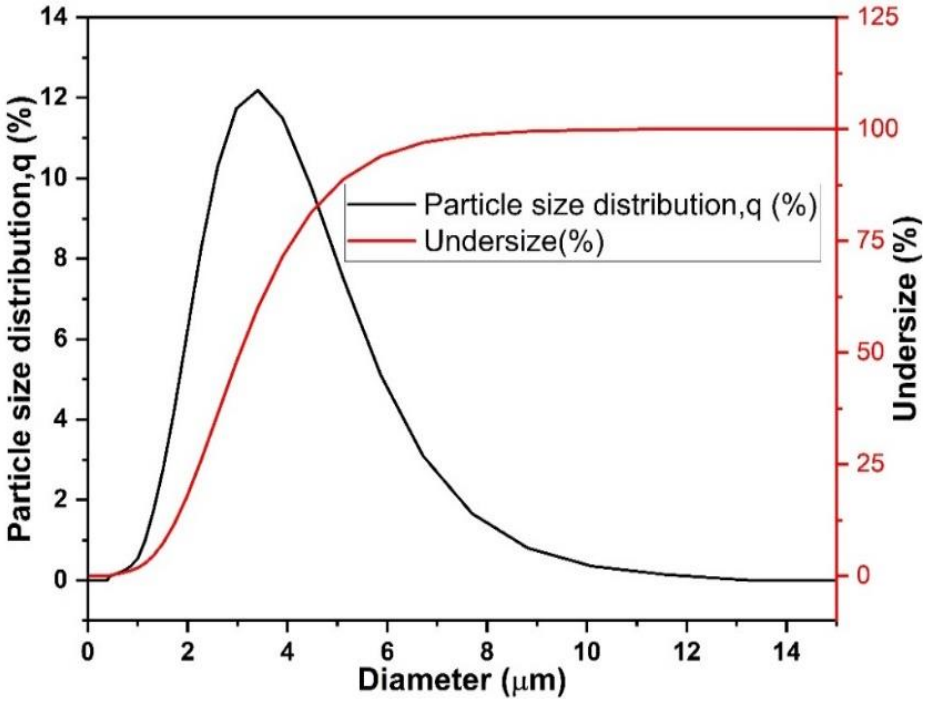

Figure 4.1 (b): Grain size plot of finely produced silica particles.

The particles size distribution of silica acquired by the wet milling process is depicted in **Fig. 4.1(b)**. Silica particles were widely distributed in the grain size diameter range of 1.5-8μm. The maximum population of the silica particles were observed in the grain size diameter of 4μm. From the curve, it was observed that the percentage of undersize particle reached 100% when the size of tray was above 6μm in diameter. It indicates that, very trace amount of silica particles with more than 6μm diameter was present in the sample. The average size of the particles obtained from the wet milling process was in the range of 2-6μm.

4.3 Membrane Preparation

4.3.1. Preparation of Chitosan-Polyvinyl Alcohol Blend

The Chitosan-polyvinyl alcohol blend was made using solution casting process. The different weight ratio of blends were prepared. For preparing the weight ratio between Chitosan and polyvinyl alcohol of 10:90, 4.5g of polyvinyl alcohol solution was blended with 0.5g of Chitosan solution. Both the solutions of Chitosan and polyvinyl alcohol was prepared separately and mixed together. The polyvinyl alcohol powder (4.5g) was mixed in a 50ml distilled water under vigorous stirring for 1hr at 65°C. The Chitosan (0.5g) was mixed in a 50ml glacial acetic acid (1vol. %) for 1hr at 60°C followed by sonication. For preparing 1vol. % of glacial acetic acid, 1ml of concentrated glacial acetic acid was mixed with a 99ml of deionized water. Then both the solutions of Chitosan and polyvinyl alcohol were blended thoroughly by vigorous stirring in a magnetic stirrer at 65°C for 1hr followed by sonication. At the end, a homogeneous solution was obtained which was poured in to a flat glass petri dish. After that, solution was kept in a hot air oven for 24hr at 45°C. During this stage, volatile matter and moisture was escaped and a thin film was developed. Here, the chain of Chitosan and PVA were interacted with each other. The possible chain interaction between the Chitosan and polyvinyl alcohol is represented in **Fig. 4.2**. Chitosan and polyvinyl alcohol interact strongly with one another due to the creation of an intermolecular hydrogen bond [**6**]. The hydroxyl

groups of Chitosan and polyvinyl alcohol combine to generate a strong hydrogen bond, as seen in **Fig. 4.2(a)**. However, there was no chemical modification of the polymer chain was observed during mixing. It was also observed an intra-molecular interaction between the ether and hydroxyl group of chitosan as shown in **Fig. 4.2(a)** [**82**]. The volatile matter and moisture was escaped from the solution. A thin film of membrane was developed on the surface of Petri dish and was peeled off from the surface. After that, it was stored in a desiccator for further analysis. The prepared thin film was labelled as CP membrane. The Chitosan-polyvinyl alcohol blend with the weight ratio of 20:80 and 30:70 were prepared by similar procedure and labelled as CP-1 and CP-2 respectively.

4.3.2 Cross-linking by Sulfuric Acid

All the chitosan-polyvinyl alcohol blends were cross-linked by diluted sulfuric acid. The Chitosan-PVA blends were cross-linked to improve its performance. During cross-linking reaction, all the blends were dipped in a sulfuric acid (2M) for 24hr. The blends were sulfonated by the insertion of sulfonic acid ($-SO_3$) group to the polymer chain. It is believed that the insertion of sulfonic acid group to the Chitosan-PVA blend improves ion transport sites and water uptake capacity. During crosslinking reaction, SO_4^{2-} ion diffuses in to the membrane and created an extra ionic sites in the membrane. The creation of an extra ionic sites in a cross-linked membrane is responsible for the enhancement of IEC. The ionic sites in a blend membrane act as a proton transport channel. The increase of ion transport sites in a blend increases ion exchange capacity [**26, 29**]. After cross-linking reaction, all the blends were removed from the sulfuric acid solution and kept it in a controlled chamber (used as a desiccator) for 2 days. The cross-linked membranes were labelled as CPH, CPH-1 and CPH-2 respectively. The possible reaction scheme of the blends during cross-linking reaction is shown in **Fig. 4.2(b)**. The sulfuric acid produces two ions in the solution i.e. H^+ and SO_4^{2-}. The sulfuric acid converts the amine group of Chitosan to NH_3^+ in the blend. The $-NH_2$ group of Chitosan

was protonated by H^+ ion to form NH_3^+ ion. A new ionic bond was created due to the interaction between the NH_3^+ and SO_4^{2-} ion [**26**]. The creation of a strong ionic bond in a cross-linked membrane as a result of acid-base coupling is depicted is depicted in **Fig. 4.2(b)**.

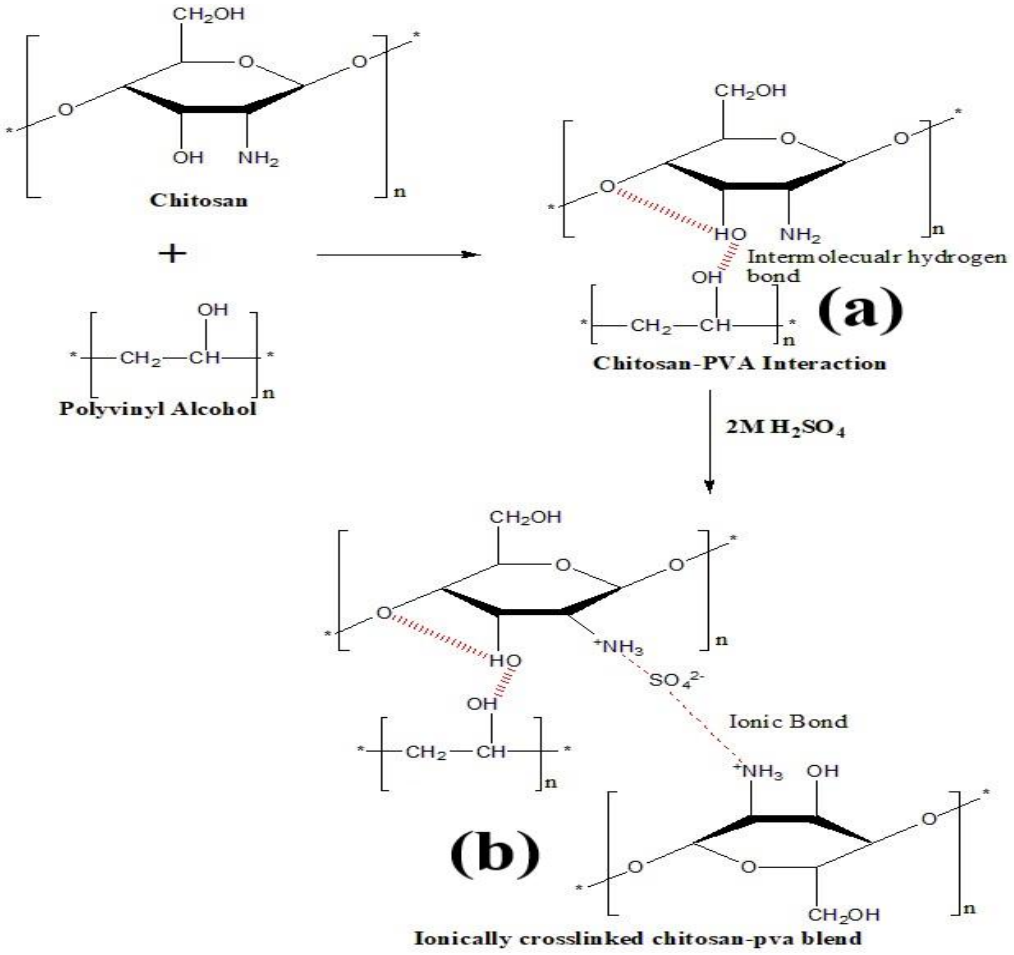

Figure 4.2: Possible reaction scheme of Chitosan-PVA blends cross-linked with sulfuric acid.

4.3.3 Modifying with Red Mud Filler

The Chitosan-polyvinyl alcohol blend with a weight ratio of 10:90 provides better mechanical, thermal and dimension stability than the other blends like CP-1 and CP-2 blend. Hence, it was consider as electrolyte membrane for DMFC application. However, the blend provides poor proton conductivity and high methanol cross-over which decreases its selectivity. Hence, to

improve its selectivity, the blend was modified by adding different hygroscopic filler like red mud, zirconia, and multi-wall carbon nanotubes. The Chitosan-polyvinyl alcohol blend was modified by impregnating red mud filler. The preparation step of CP blend was discussed in the earlier section. The mixture of Chitosan-polyvinyl alcohol blend was prepared and red mud filler was added to fabricate hybrid membrane. The red mud particles were well dispersed in a Chitosan-polyvinyl mixture by using probe sonicator. The different weight (%) of red mud particles *(*1, 2, 3 & 4 wt. (%)) were added in the Chitosan-polyvinyl alcohol blend to develop hybrid membrane and designated as Chitosan-PVA-x hybrid membrane, here x stands for weight (%) of red mud particles added to the Chitosan-PVA blend. Final solution mixture was poured in to a flat glass plate and dried in a hot air oven for 24hr at 45°C. During heating process, moisture and volatile solvents were escaped from the mixtures and a thin sheet of membrane was developed. After drying, thin film was separated from the surface of glass plate and stored in a dehumidified container for further investigations.

4.3.4 Modifying with Carbon Nanotubes and Ionic Liquid

Chitosan-polyvinyl alcohol blend was further modified by adding multi-wall carbon nanotubes and ionic liquid. The varied weight percentages (i.e., 0.5%, 1%, 1.5%, and 2% of Chitosan) of carbon nanotubes was added to the Chitosan-polyvinyl blend, and the resulting hybrid membrane is termed as CPCN-x, where x stands for the weight percentage of carbon nanotubes. To make an ionic liquid modified membrane, 0.05ml of ionic solution was added to the final combination. The ionic liquid modified hybrid membrane is designated as CPCN@IL-x. The resulting solution was placed into a flat glass plate and dried for 24 hours at 35°C in a hot air oven. The thin layer formed on the surface of the glass plate was scraped off and kept in a dehumidifying chamber for future examination. The fabrication steps of the hybrid membrane is depicted in **Fig. 4.3**. The potential reaction schemes occurred during the synthesis of hybrid

membrane is represented in **Fig. 4.4**. The amine group of Chitosan was interacted with the base of ionic liquid to form a strong covalent bond [**17**]. Due to the addition of ionic liquid to the composite, sulfonate (SO_3) group was impregnated which has the potential to improve its ion exchange capacity [**44**]. The hydroxyl group of Chitosan interacts with the positive ion of an ionic liquid, resulting in the creation of an electron donor electron receiver (EDA) complex [**50**]. In this case, the ionic liquid's cation (N^+) functions as a receptor for electrons, while the Chitosan's hydroxyl group (OH^-) acts as a donor of electrons [**51**]. The chemical reaction between hydroxyl group and cation of ionic liquid creates a strong ionic bond which is represented in **Fig. 4.4**. The amine group of IL@CP complex was strongly interacted with the carbon of multi-wall carbon nanotubes as shown in **Fig. 4.4**.

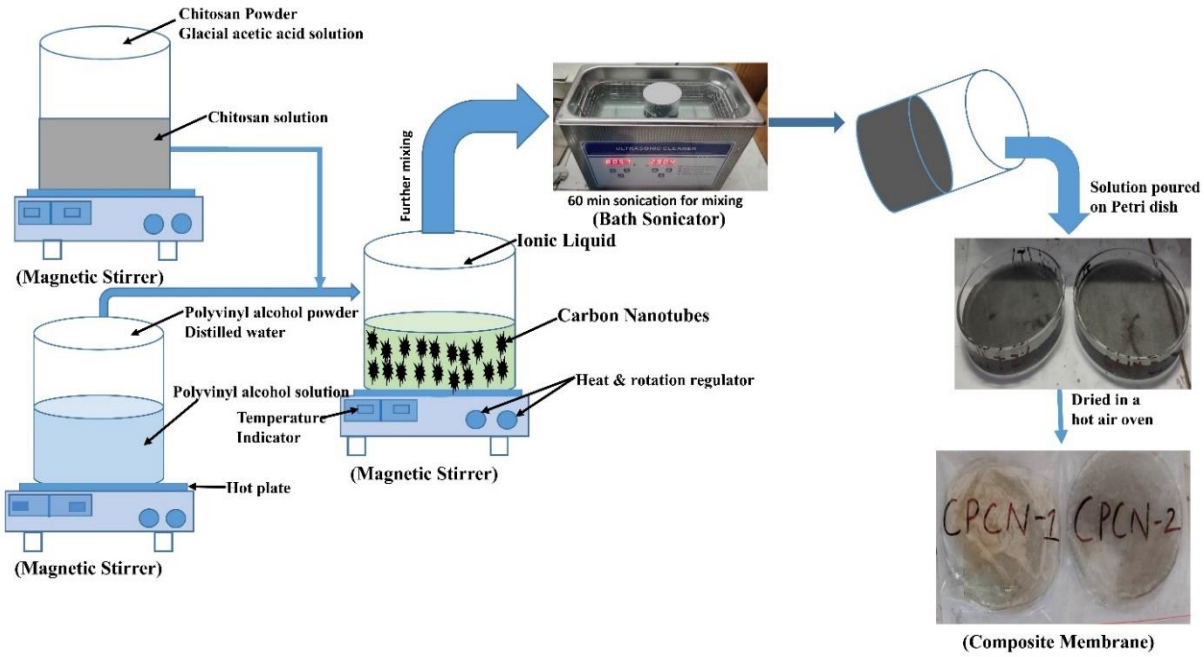

Figure 4.3: Different step involve for the preparation of multiwall carbon nanotubes and ionic solution modified Chitosan membrane.

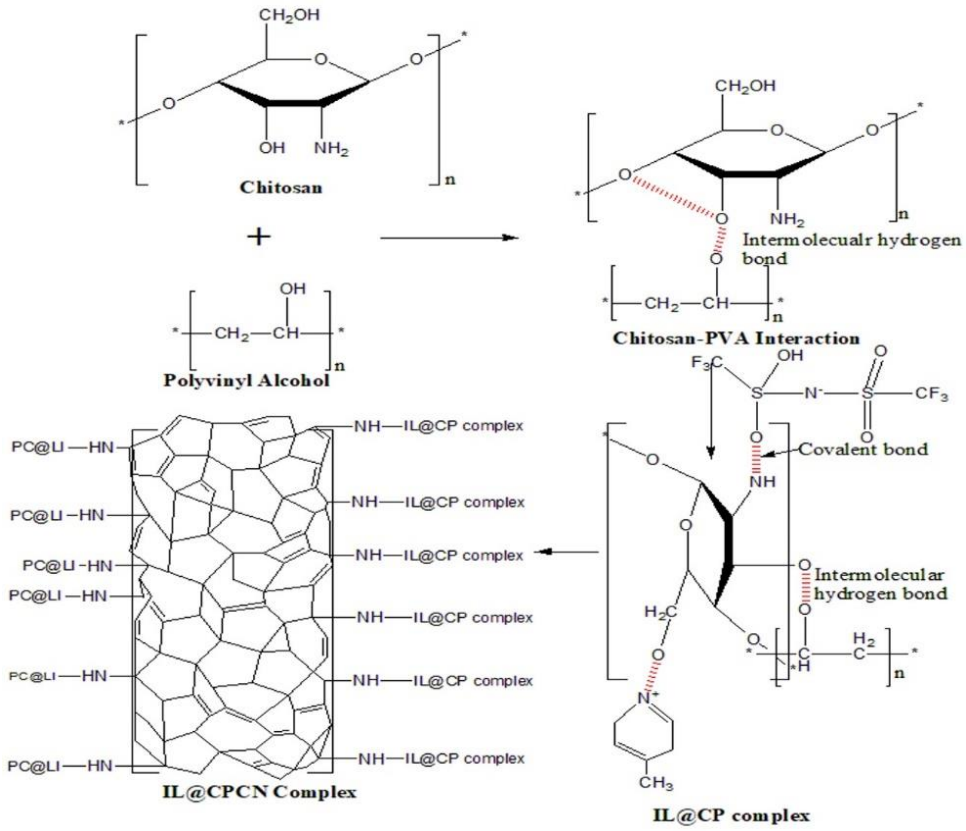

Figure 4.4: Possible reaction scheme of the multiwall carbon nanotubes and ionic solution modified Chitosan membrane.

4.3.5 Modifying with Hygroscopic Zirconia and Ionic Liquid

Next, Chitosan-polyvinyl alcohol blend was modified by impregnation hygroscopic zirconia and ionic liquid. The detailed preparation step for hybrid membrane is represented in **Fig. 4.5**. The different weight % (0.5, 1, 1.5 & 2%) of zirconia was added to the Chitosan-polyvinyl alcohol bend and designated as CPZr-x, where x stands for weight (%) of zirconia. For developing ionic liquid modified membrane, the resultant mixture was treated with 0.05ml of ionic solution. After that; the solution mixture was placed into a flat glass plate and dried for 24 hours at 35°C in a hot air oven. During heating process, volatile matter and moisture were escaped and a thin film of membrane was developed. The thin layer that forms on the surface of the Petri dish was scraped off and preserved in a dehumidifier chamber for future examination. The possible chain interaction and functional group reaction during the synthesis of hybrid membrane is represented in **Fig. 4.6**. The hydroxyl group of Chitosan interacts with

the zirconium atom. The zirconium atom and the hydroxyl group engage via a strong connection, as illustrated in Fig. 4.6 [**82**]. When ionic liquid was added, the reactivity of zirconium atom was suppressed by the cation of ionic liquid. In this situation, the cation interacts with the hydroxyl group of Chitosan and forms a strong ionic bond, as illustrated in Fig. 4.6. The development of the electron donor electron receiver (EDA) complex results in the creation of a strong ionic interaction [**50, 52**]. The development of EDA complexes as a result of ionic liquid addition has already been studied. Moreover, the base of ionic solution was interacted with the amine group of Chitosan to establish a strong covalent bond. The base of ionic liquid comprises a sulfonate (S=O) group, which was imbedded in the hybrid membrane. The incorporation of sulfonate group in a hybrid membrane is attractive for the preparation of highly performed hybrid membrane. The presence of sulfonate group in an electrolyte membrane improves ion transport capacity and proton conductivity. The higher proton conducting membrane improves fuel cell performance.

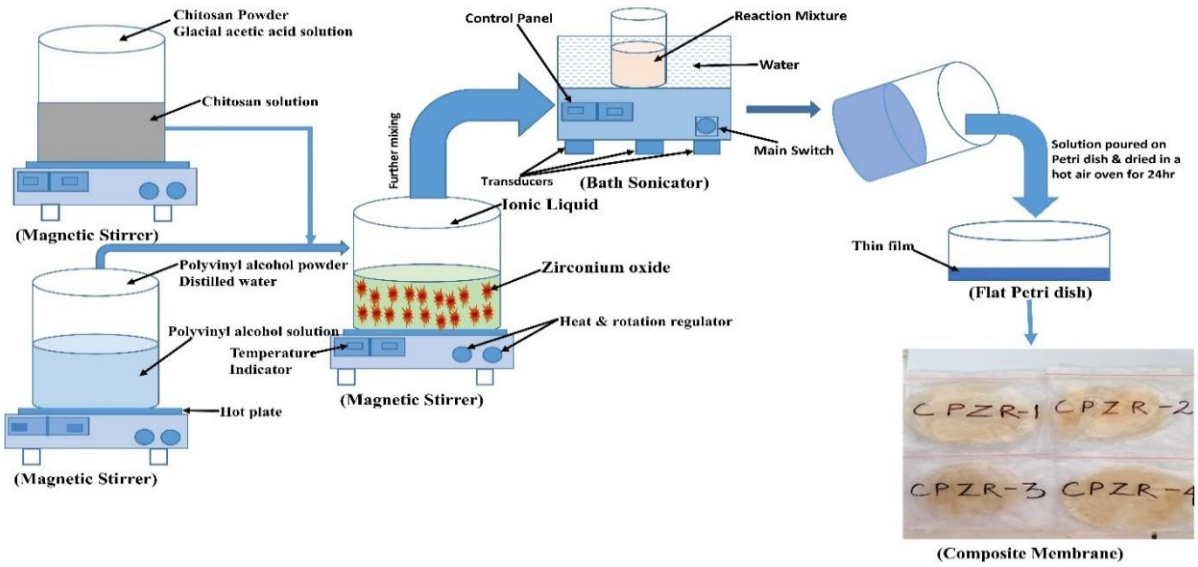

Figure 4.5: Scheme adopted for the development of zirconia and ionic liquid modified Chitosan membrane.

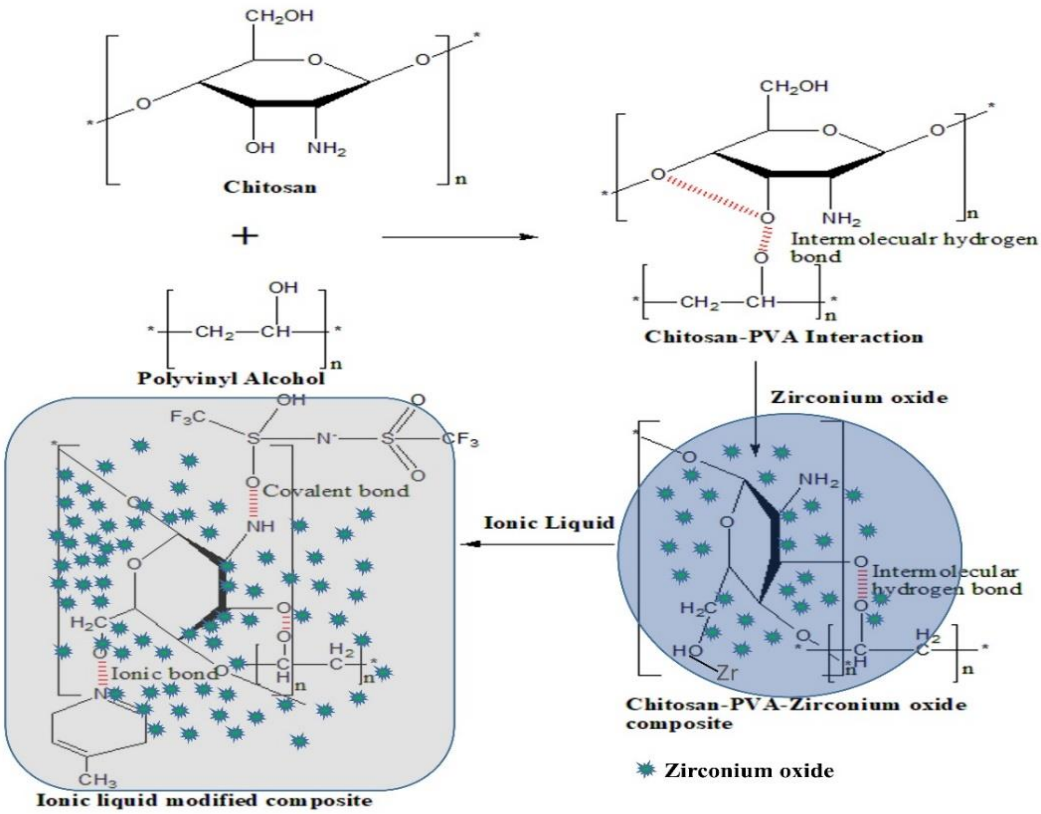

Figure 4.6: Possible reaction mechanism during the development of zirconia and ionic liquid modified Chitosan membrane.

4.3.6 Synthesis of Poly (ether-ether ketone) (PEEK) Hybrid Membrane

The poly (ether-ether ketone) hybrid membrane was developed by solvent casting process. PEEK polymer was sulfonated by sulphuric acid to achieve high degree of sulfonation (DS). During sulfonation reaction, reaction time was controlled to achieve specific DS. The higher reaction time increases DS of the PEEK polymer. A membrane with a greater DS is preferred for fuel cell applications. As we increases the DS of membrane, more sulfonate group (S=O) of the sulphuric acid were impregnated to the polymer sample. The presence of more sulfonate group (S=O) group in a membrane increases transport capacity. The increased ion transport capacity of the membrane boosts proton conductivity and power density of the fuel cell. Hence, higher DS of PEEK was synthesized and used as a reference material for the development of hybrid membrane. The DS of the synthesized PEEK polymer was 73.72%. For preparing hybrid membrane, SPEEK polymer was blended with polyvinyl alcohol in a different weight

ratio and optimized to get a favourable properties. The SPEEK-PVA blend with the weight ratio of (70:30) provides better mechanical, thermal and hydraulic property. However, the blend provides poor proton conductivity and higher methanol cross-over. Moreover, the bound water of the blend was lower which reduces fuel cell performance at reduced humidity conditions. Therefore, SPEEK-PVA was further modified by impregnating silica filler. For preparing the blend of SPEEK and PVA, both the component were dissolved in a suitable solvents. The needed amount of SPEEK granules were added to a dimethylacetamide (DMA) solvent. The polyvinyl alcohol powder was dissolved in a distilled for 1hr at 65°C. The two solutions were then blended in a magnetic stirrer and sonicator. The different weight (%) (1, 2, 3, 4 & 8%) of silica powder was added to the solution and the hybrid membrane were classified as SPS-1, SPS-2, SPS-3, SPS-4 & SPS-5 respectively. The resulting solution was put into a flat glass plate and dried for 48 hours at 40°C in a hot air oven. The volatile matter and moisture were escaped from the solution and a thin film was developed. The thin film was scraped off from the glass plate and placed in a dehumidifier chamber for further examination. The scheme of reactions during the synthesis of hybrid membrane is represented in **Fig. 4.7**. During the sulfonation of PEEK, sulfonate group (S=O) was inserted to the PEEK backbone leaving out water as a condensation product [**50, 53**]. The possible interaction between SPEEK and polyvinyl alcohol is represented in **Fig. 4.7(b)**. The hydroxyl group of polyvinyl alcohol was strongly interacted with the sulfonate group of SPEEK to from hydrogen bond [**54**]. However, the addition of silica disturbs the interaction between SPEEK and polyvinyl alcohol. The silica has higher reactivity towards the sulfonate group of SPEEK. The silica atom will be reacted with the sulfonate group of SPEEK and the possible reaction scheme is represented in Fig. 4.7(b) [**55, 56**]. The polyvinyl alcohol was strongly reacted with the silanol group of silica, forming a strong intermolecular bond [**54**].

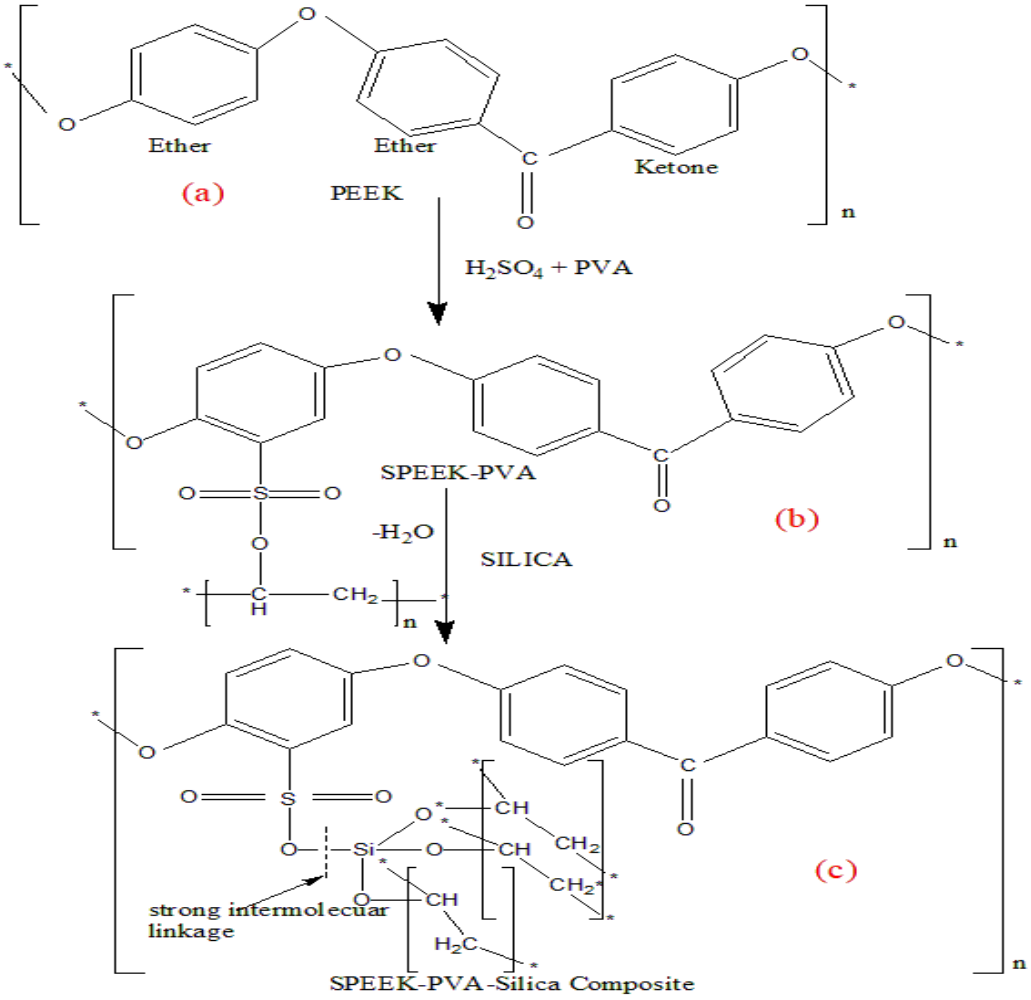

Figure 4.7: Possible reaction scheme of SPEEK based polymer membrane modified with silica and polyvinyl alcohol.

4.4 Physical and Chemical Properties Measurement

4.4.1 Ion Exchange Capacity (IEC)

The membrane with higher ion transport capacity is considered to be a potential candidate for fuel applications. Proton conductivity is improved by using a membrane with a higher IEC. It is also defined as the number of ions involved in proton transport through the electrolyte membrane. The ion exchange ability of the membrane was measured by titration analysis. Before analysis, test membrane was heated in a hot air oven for 2 hours at 60°C and its dry weight, W_d, was determined. The sample was then dipped in a 0.1M hydrochloric acid solution for 24 hours. During this period, H^+ or proton produced by the dissociation of hydrochloric acid was transported to the test membrane. After 24 hours, test membrane was taken out from the hydrochloric acid solution and placed in a 0.1M sodium chloride solution. The amount of proton present in the membrane was now swapped for the Na^+ ion of sodium chloride solution. The H^+ ions present in the membrane were all transferred to the sodium chloride solution. The quantity of H^+ ion present in the sodium chloride solution was determined by titrating it with 0.01M sodium hydroxide solution. The following expression is used to calculate the ion transport capacity of the test membrane

$$IEC\ (meq/g) = \frac{V_{NaOH} \times C_{NaOH}}{W_d} \qquad (4.1)$$

In this expression, V_{NaOH} denotes the volume of sodium hydroxide utilised during the titration process, (ml), C_{NaOH} denotes the amount of sodium hydroxide used for titration analysis, 0.01M and W_d denotes the dry weight of the membrane, gram.

4.4.2 Water Uptake and Swelling Degree

The water absorption capacity of all the membranes were determined experimentally. For measuring water absorption capacity, dry membrane was equilibrated in a deionized water for 30 hours. During experiment, weight of dry and equilibrated membrane was measured. First, the membrane was dried in a hot air oven at 60°C for 2 hours and its weight, W_d, was

determined. The dry membrane was then equilibrated in deionized water for 30 hours. At regular intervals, the membrane was kept out from the deionized water and surface was thoroughly cleaned. After cleaning surface water, weight of membrane was measured. A similar approach was followed until the membrane reached equilibrium weight in a deionized water. The expression used to calculate water uptake capacity (%) of the membrane is given below

$$WU\ (\%) = \frac{W_w - W_d}{W_d} \times 100 = \frac{Change\ in\ weight}{Initial\ dry\ weight} \times 100 \qquad (4.2)$$

Here, W_d and W_w are the weight of dry and equilibrated membrane respectively.

The swelling area of the membrane was measured to ensure its dimension stability. The membrane with higher swelling area provides poor dimension stability. As a result, the membrane with the lowest swelling area is deemed a promising contender for fuel cell usage. During a water uptake test, the swelling area of the membrane was assessed. The area of dry and wet membrane was determined. The following expression was used to calculate swelling area of the membrane

$$\text{Swelling degree, SA (\%), Area} = \frac{A_w - A_d}{A_d} \times 100 \qquad (4.3)$$

Here, A_w and A_d are the area of equilibrated and dry membrane respectively.

Hydration number is an important parameter of a fuel cell membrane. The water molecules were absorbed by the sulfonate group of membrane. The membrane with higher hydration number absorbs more water. It signifies the amount of water molecules absorbed by sulfonate group of the membrane. The hydration number plays a crucial role for fuel cell performance. The following expression was proposed by the different investigators to calculate hydration number of the membrane

$$\lambda = \frac{10 \times WU(\%)}{IEC \times M_{H_2O}} = \frac{10 \times WU\ (\%)}{IEC \times 18} \qquad (4.4)$$

In this expression, λ is the hydration number, WU (%) and IEC are water upatke and ion exchange capacity of the membrane, and M_{H_2O} is the molar mass of water, 18 gram/mol.

The water transported through the membrane was controlled by fickian diffusion. Water diffusion has a substantial impact on fuel cell performance. Water flooding in the membrane was caused by inadequate water diffusion, which lowers cell performance. The kinetics of water diffusion was modelled to predict water diffusivity. To analyse water diffusivity via the membrane, many scientists suggested various diffusion models. **Lue et al.** suggested a fickian model to forecast the diffusivity of water [**57**]. The proposed diffusion model is considered to be more successful at measuring water diffusivity. The fickian model is given below

$$ln\ (1-\frac{M_t}{M_\infty}) = \ln(\frac{8}{\pi^2}) - \frac{\pi^2 Dt}{L^2} \qquad (4.5)$$

In this equation, M_t represents the amount of water absorbed by the membrane at time t, M_∞ is the amount of water absorbed by the equilibrated membrane, L is the thickness of membrane and D is the water diffusivity in cm^2/s. A linear curve is drawn between $\ln(1 - \frac{M_t}{M_\infty})$ vs time and the slope of the curve is used to obtain water diffusivity value.

Void fraction of the membrane influence its mechanical and thermal properties. The void fraction of the membrane increases water absorption capacity. As more water was absorbed, the membrane's bound water content increased. The increase of bound water is crucial for fuel cell operation at reduced humidity conditions. The presence of bound water improves proton conductivity of the membrane. Under low humidity levels, bound water enhances proton transport via the Grotthuss mechanism. The increase of proton conductivity of the membrane improves cell performance. Moreover, when void fraction increases, glass transition temperature of the membrane was significantly reduces. The polymer chain will move freely, accelerating the phase shift from glassy to rubbery. The temperature at which glassy phase of polymer converted to rubbery phase is called glass transition temperature. The

membrane with lower glass transition temperature is less rigid and highly flexible. However, the membrane with higher void fraction provides poor mechanical properties and excessive fuel loss due to fuel cross-over. Due to its higher void fraction, glass transition temperature of the membrane was increases which makes the membrane more rigid and less flexible. The methanol molecules will migrate easily through the membrane. Hence, the void fraction of the membrane should be optimized to reduce methanol cross-over and improves mechanical stability. The following expression is used to compute the void fraction available in the membrane.

$$\epsilon = \frac{\lambda\left(\frac{1}{EW_m}+\frac{w}{MW_p}\right)}{\lambda\left(\frac{1}{EW_m}+\frac{w}{MW_p}\right)+\frac{r_{m/w}}{EW_m}+\frac{w.r_{p/w}}{MW_p}} \qquad (4.6)$$

In this expression, ϵ is the void volume available in the membrane, λ is the hydration number of membrane, $r_{m/w}$ and $r_{p/w}$ are the ratio of partial molar volume of membrane to water and filler to water respectively. Here, w denotes the amount of filler presence in the sample, MW_p is the molecular weight of filler. EW_m is the membranes equivalent weight. To determine the partial molar volume of the membrane, its volume is measured. A known amount of solvent was used to dissolve the membrane. After dissolution, sample volume was measured. The quantity of water absorbed at equilibrium conditions is called partial molar volume of water. The equivalent weight of the membrane is related to the IEC of the membrane by the following relationship.

$$EW_m = \frac{1}{IEC} \times 1000 \qquad (4.7)$$

Here, EW_m is the membranes equivalent weight in gm.meq^{-1}.

4.4.3 Methanol Permeability

The fuel cross-over through the membrane is a major drawbacks in a DMFC. The membrane with higher methanol cross-over produces more leakage current which reduces power density

of the DMFC. Moreover, higher methanol cross-over incurred fuel loss in a DMFC. Hence, methanol cross-over is the important parameter of fuel cell which should be minimized. A custom built diffusion cell was used to evaluate how much methanol passes through the membrane. The schematic representation of a glass diffusion cell is shown in **Fig. 4.8**. The diffusion cell has two compartments, donor (A) and receiver (B). Methanol (2M) and distiller water were placed in donor and receiver compartments, respectively. Between the two chambers, the test membrane was sandwiched. During experiment, both the chambers were properly agitated using agitator. Methanol diffuses from compartment A to compartment B due to concentration gradient. The amount of methanol diffuses over time was measured by refractometer. Methanol diffusion through the membrane was tested for 30 hours. After 30 hours, approximately 0.20 ml of sample solution was taken from the compartment B for examination. The refractive index of the permeated methanol was measured. A reference curve was drawn between methanol concentrations and their refractive index. The amount of methanol that went through the membrane was graphically obtained by fitting its refractive index data to a reference plot. The following expression was used to calculate the methanol cross-over through the membrane.

$$P=\frac{C_B(t)V_BL}{AC_A(t_0)} \qquad (4.8)$$

In this expression, P is amount of methanol passes through the membrane over time or methanol permeability (cm^2s^{-1}), C_A (t_0) is the initial methanol concentration in donor chamber (A), C_B (t) is the concentration of permeated methanol at time, t in a receiver chamber, V_B is the volume of sample collected from the receiver compartment B (0.2ml), L and A are the sample thickness and area respectively. The average thickness and diameter of the membrane was measured by digital varnier caliper.

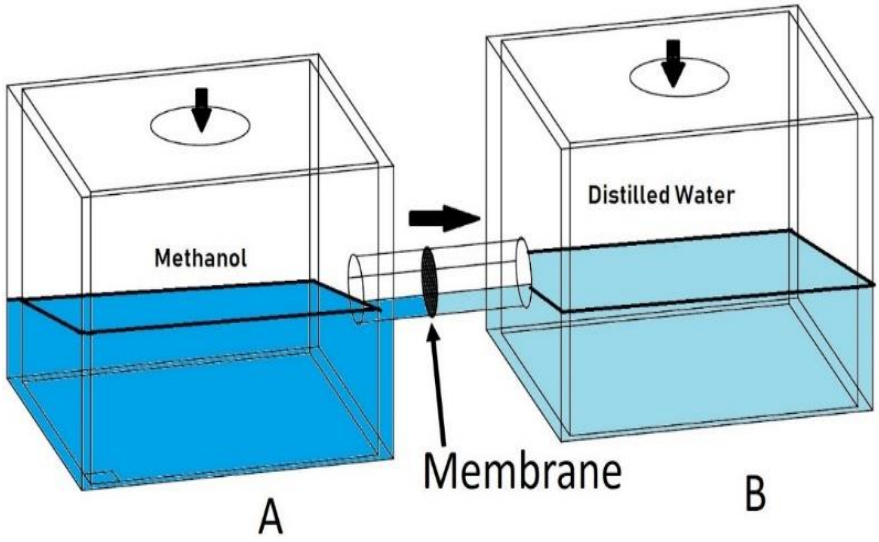

Figure 4.8: Schematic diagram of a glass diffusion cell for measuring methanol permeability of the membranes.

4.4.4 Proton Conductivity

The membrane with the highest proton conductivity is selected for fuel cell applications. A four probe impedance analyzer was used to measure the amount of proton transferred through the electrolyte membrane. The test membrane was hold between the two electrodes of impedance equipment and temperature of cell was controlled by temperature sensor. The test was conducted at a variable frequency range of 0.1-10^6Hz and 0.05V. The impedance test was performed at different temperature to obtain impedance data. The electrolyte or membrane resistance (R_b) was obtained from the impedance data. There are various methods to obtain membrane resistance from impedance data like Nyquist plot, Zimm plot and equivalent circuit model. In a Nyquist plot method, intercept of the impedance plot gives membrane bulk resistance. The membrane bulk resistance is given by the intercept of the real impedance axis in the high frequency semicircle region. In an equivalent circuit model analysis, impedance response of the sample was fitted to an appropriate circuit model available in Z-view software. The membrane bulk resistance was determined from the model parameters. After determining membrane resistance, the following expression is used to compute proton conductivity.

$$\sigma = \frac{L}{R_b A} \qquad (4.9)$$

In this expression, σ is the ionic conductivity of the test membrane (Scm^{-1}), L and A are the membranes thickness and area respectively.

4.5 Membrane Characterization

4.5.1 Fourier Transform Infrared Spectroscopy Analysis (FTIR)

Functional group of the membranes were confirmed by infrared spectroscopy analysis. During analysis, sample was scanned by passing infrared light in a FIIR machine (IR-Prestige 21, FTIR machine, Japan). The sample was scanned at 400-4000cm^{-1} wavelength range, and light deflection at the specific wavelength value indicates the presence of functional group.

4.5.2 X-ray Diffraction Analysis (XRD)

Crystal size and phase of the membranes were studied using an X-ray diffraction machine (Philips, PW1720, USA). X-ray light generated by the radiation of Cu-kα element is passed to the sample at 40kV and 30mA. During the study, X-ray radiation was transmitted through the material at diffraction angles ranging from 5-85°. X-ray light was deflected by the presence of crystal in the sample. From the crystalline peak, area of crystalline phase was calculated. Area of amorphous phase was obtained by subtracting the area of crystalline phase from the total area of XRD peak. The following equation is used to calculate the sample's degree of crystallinity.

$$\chi_C\ (\%) = \frac{A_C}{A_C + A_A} \times 100 \qquad (4.10)$$

In this expression, χ_c is the degree of crystalline phase (%), A_C and A_A are the area of amorphous and crystalline phase of the sample respectively.

The average size of crystal (D, nm) presence in the sample was calculated by using Scherrer equation. The Scherrer equation used for calculating the size of crystal is given below

$$D=\frac{K\lambda}{\beta Cos\theta} \quad (4.11)$$

In this expression, D is the average size of crystal presence in the sample (nm), K is the Scherrer constant, λ is the wavelength of X-ray light which is passed to the sample (1.79Å), θ is the diffraction angle and β is the FWHM (radians). The Gaussian curve is fitted to a crystalline peak of the sample to obtain β value. The crystal particles are considered to be sphere in shape. The Scherrer constant of the sphere particle is K=0.9.

4.5.3 Field Emission Scanning Electron Microscopy Analysis (FESEM)

The surface image and elemental analysis of the membranes were characterized by FESEM (Quanta FEG 250, USA). The gold coated specimen was put in to the sample holder and capture images at different magnification and resolution. The mapping of different elements present in the membrane was conducted during analysis.

4.5.4 Differential Scanning Calorimetry Analysis (DSC)

The flow behaviour and bound water of the sample was analysed by DSC (Perkin-Elmer DSC7, MA, USA). The test membrane was heated in a nitrogen gas environment from -70-300°C at the rate of 10°C/ min. During testing, sample was examined by performing experiment at two heating and one cooling cycle. The appearance of exothermic and endothermic peaks during the heating and cooling cycle was used to investigate the phase transition behaviour of membranes. The crystallisation peak observed during the cooling cycle was used to calculate the sample's bound water.

The bound water (%) of the sample was obtained from the following expression

$$\text{Bound water (\%)} = \frac{W_b}{W_d}\times 100 \quad (4.12)$$

Here, W_b is the amount of bound water presence in the sample (gram); W_d is the samples dry weight (gram). The quantity of free water presence in the sample was used to compute bound water (%). The quantity of free water presence in the sample was obtained from the area of first crystallization peak observed during cooling cycle. The quantity of strongly bonded waster (bound water) was then estimated by subtracting the quantity of free water from the amount of

water absorbed by the membrane. The relationship between the amount of free and strongly bonded water presence in the sample is given below

$W_b = W_t - W_f$ (4.13)

Here, W_b is the weight of bound water (gram), W_t is the amount of water absorbed by the membrane (gram) and W_f is the weight of free water (gram). The weight of free water was obtained from the first crystallization peak.

4.5.5 Thermo-gravimetric Analysis (TGA)

The thermal stability and degradation behaviour of the samples were examined by TGA (Perkin-Elmer TGA, MA, USA). The test sample was heated in a nitrogen gas environment from 28-800°C at a rate of 10°C/minute. The degradation characteristics of polymer samples at various temperatures were investigated.

4.5.6 Dynamic Mechanical Analysis (DMA)

The temperature dependent mechanical behaviour of the membranes were studied by DMA (Q800 model, M/S TA instruments, USA). The samples were made in the dimension of 41×8.5×3mm size. The test was conducted as per ASTM D5026 to evaluate its viscoelastic properties. In a nitrogen atmosphere; temperature ranging from 28 to 300°C, the test membranes were evaluated in a variable frequency mode with an oscillation amplitude of 0.2mm. The effect of temperature on chain mobility and modulus of membrane were evaluated. The influence of temperature on tan δ of the sample was studied. The tan δ peak was used to obtain glass transition temperature of the membrane.

4.5.7 Tensile Test

The mechanical property of the membrane was evaluated by performing tensile test in a universal testing machine (UTM3382, Norwood, MA, USA). The sample was prepared as per ASTM D638 (Type I, gauge length 50mm) and tested in tension mode. During testing, crosshead speed was maintained at 10mm/min. The membrane's elastic modulus, ultimate

strength, and strain at break were all measured. The membrane's ductility and brittleness were investigated.

4.6 Fabrication of Membrane Electrode Assembly (MEA)

The performance of a fuel cell was evaluated in a custom-built membrane electrode assembly (MEA). The MEA was fabricated by first preparing an anode and a cathode catalyst. The pictorial representation of single cell of membrane electrode assembly is shown in Fig. 4.9. The anode catalyst was prepared by thermally pressing of Pt-Ru catalyst powder on carbon cloth @4mg/cm^2. The similar procedure was followed to prepare cathode catalyst. The platinum powder was thermally pressed on carbon cloth @2mg/cm^2. Then membrane and electrodes were assembled to make MEA. Here, test membrane was sandwiched between the two electrodes. Two graphite plates with feed flow channels sandwiched the MEA. The MEA was connected with external load. The temperature sensor was connected to control cell temperature. During test, dilute methanol and oxygen gas are introduced on both sides of the cell with the flow rate of 1ml/min and 100ml/min respectively. The anode and cathode feed flow rates are controlled by a rota metre. The cell performance was studied at 70°C and various molar concentrations of methanol. The cell's power density and polarisation curve were recorded using an externally connected EIS work station (EIS, CH Instrument, USA).

Figure 4.9: Single cell membrane electrode assembly setup with EIS work station.

4.7 Mathematical Modelling of Active Fuel Cell

4.7.1 Model Assumptions

A simple isothermal model of DMFC was developed by considering the diffusion and transport of methanol. The methanol was transported to a feed flow channel and oxidized at anode layer. The oxidation kinetics of methanol at catalyst layer was modelled to predict the cell potential and leakage current. The electrochemical reaction of methanol at anode and cathode interface was considered during the analysis. The simulation environment of an active DMFC was developed by considering the following assumptions

1. The electrochemical reaction in a DMFC is considered to be liquid phase reaction. We assumed that the carbon dioxide formed during the reaction was remains in a liquid phase due to its higher solubility towards water.
2. Electrochemical oxidation of methanol follows Tafel kinetics.
3. Electrochemical reaction is considered to be isothermal reaction, temperature remains constant.
4. Uniform ionic conductivity and methanol cross-over throughout the electrolyte membrane.
5. The catalyst film was considered to be homogeneous porous electrode and thus the electrochemical reaction occurred at electrode interface was assumed to be homogeneous reaction.
6. One dimensional flow of feed (methanol and oxygen) was considered during analysis. The flow was considered to be perfectly plug flow with negligible back mixing.

Tafel kinetics:

Tafel kinetics relates the rate of an electrochemical reaction to the over potential. It describes the dependency of electric current through an electrode on voltage difference between the electrode and electrolyte.

Tafel equation can be used for predicting anode and cathode side over potential. The general expression of tafel equation for a single electrode is given below

$$\eta = \pm A.\ \log_{10}\left(\frac{I}{I_0}\right) \qquad (4.14)$$

Here, plus sign refers to an anode side reaction and minus sign refers to cathode side reaction. η is the over potential of the cell (Volt), A is tafel slope (Volt), I is current density (A/cm^2) and I_0 is the exchange current density (A/cm^2). It assumes that the concentrations at electrode interface are practically equal to the concentrations in the bulk electrolyte. It also assumes that the electrode mass transfer rate is much greater than the reaction rate.

The electrochemical reaction between fuel (methanol) and O_2 gas, produces heat and electrical energy in a DMFC. The electrical energy produced in a single cell of DMFC is called open circuit voltage, V_{oc}. The electrochemical reaction of a DMFC is represented in **Fig. 1.1**. In a DMFC, loss of voltage was occurred due to polarization loss. Polarization curve characterises the voltage with the function of current. It also predicts the efficiency of fuel cell at any operating current. During current flow, voltage loss was occurred due to the resistance of current flow at anode and cathode interface. It was affected due to the limitations of reaction rate, mass transport and resistance at catalyst surface. Due to the loss of current, sharp drop of open circuit voltage was occurred. Due to the voltage drop, fuel cell efficiency decreases. The polarization loss was categorized in to three types i.e. active, ohmic and concentration polarization loss. The voltage loss occurred due to the limitations of reaction rate is called active polarization loss. The limitations of mass transport incurred concentration polarization

loss. The ohmic loss was occurred due to the resistance of current at catalyst interface. In most cases, ohmic loss was dominated over the other and it has significant effect on cell voltage. The cell voltage (V_{Cell}) is defined as the net amount of electrical energy produced in a DMFC. The electrochemical reactions of methanol as well as its diffusion kinetics are modelled to predict the polarization loss of cell. The theoretical cell voltage (V_{Cell}) of the cell was predicted by using following the expression [**58**]

$$V_{Cell} = U_{O_2} - U^{MeOH} - \eta_A - \eta_C - \frac{\delta_M I_{Cell}}{K} \qquad (4.15)$$

In this expression, V_{Cell} is the cell voltage (volt), $U_{O_2}$and U^{MeOH} are the potential of oxygen reduction and methanol oxidation respectively, η_A and η_C are the anode and cathode over potentials respectively. The last term in the expression represents ohmic loss across the membrane. Ohmic loss was calculated at different current density (I_{cell}) by using the known parameters of δ_m and k.

A simplified one dimensional approach of anode flow channel (AFC) in a DMFC is represented in **Figure 4.9**. The anode flow channel was modelled to predict the methanol cross-over rate through the membrane and anode over-potential. The concentration distribution and flow direction of methanol in an AFC is shown in the figure. The model considered the AFC in to three partition layer i.e. anode diffusion layer (ADL), anode catalyst layer (ACL) and membrane. The methanol concentration and thickness of each partition layer is represented. The liquid methanol is transported in X- direction and the boundary conditions for each partition layer is given below

ADL: Thickness (t_b); At X=0: c=c_b; At X=X_1: c=c_I^b

ACL: Thickness (t_a); At X=X_I: c=c_I^a; At X=X_{II}: c=c_{II}^a

Membrane: Thickness (t_m); At X=X_{II}: c=c_{II}^m; At X=X_{III}: c=c_{III}^m

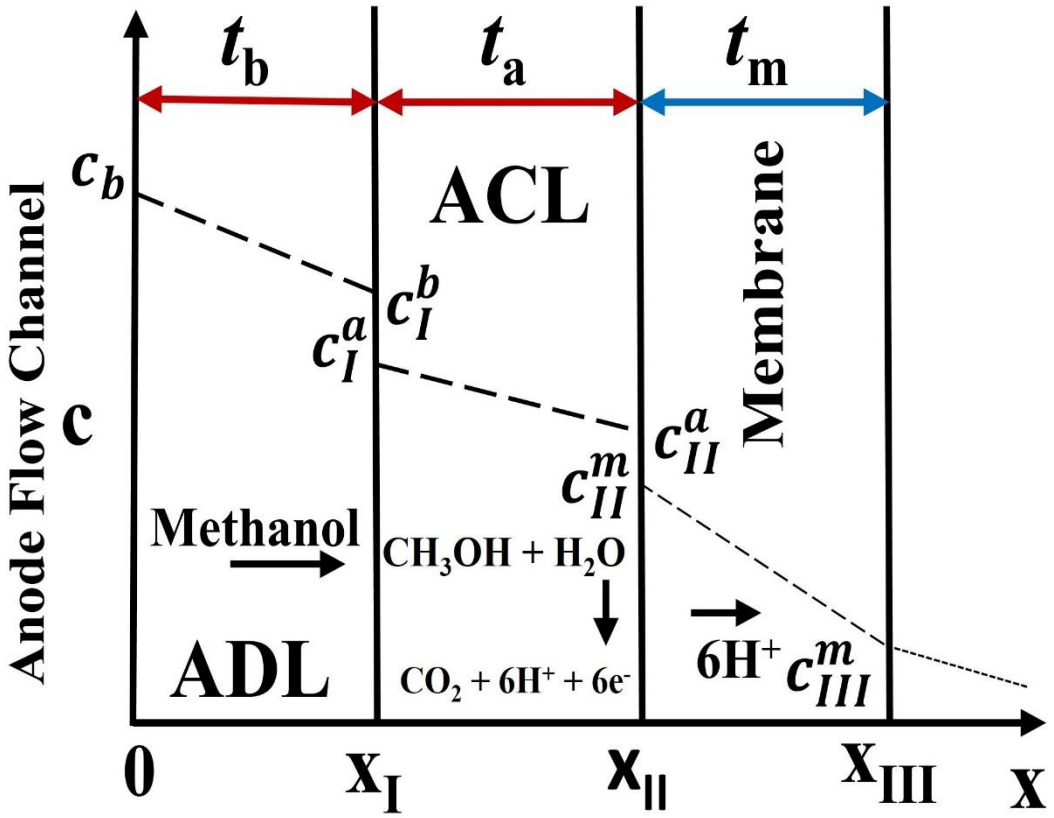

Figure 4.10: A simplistic one dimensional approach of anode flow channel in a DMFC.

4.7.2 Modelling of Anode Flow Channel (AFC)

The kinetics of methanol transport in an AFC was modelled to propose methanol cross-over rate and anode side over-potential. The methanol transported in an ADL was assumed to be controlled by first order fickian diffusion. The methanol molar flux through the ADL was expressed by fickian diffusion law. The diffusion of methanol in ADL is expressed by first order fickian law as given below

$$N_{MeOH,X} = -D_b \frac{dc_{MeOH}}{dX} \qquad (4.16)$$

Here, $N_{MeOH,X}$ is the molar flux of methanol diffuses in the ADL, c_{MeOH} is the concentration of methanol diffuses in ADL, x is the distance of diffusion and D_b is the diffusivity of methanol in an ADL ($cm^2/s.$).

Methanol diffusion through the membrane was thought to be a combination of diffusion and electro-osmotic drag. The methanol molecules were dragged by the convective effect of proton and crosses through the membrane. Hence, the expression of methanol flux expressed by fickian laws was modified. The modified expression of methanol molar flux is given below

$$N_{m,cross} = -D_m \frac{dc^m_{MeOH}}{dx} + m_d \frac{I_{Cell}}{F} \frac{c^a_{MeOH}}{c^a_w} \qquad (4.17)$$

Here, $N_{m,cross}$ is the molar flux of methanol transported through the test membrane. D_m is the diffusivity of methanol through the membrane, F is the Faradays constant, c^a_{MeOH} is the concentration of methanol at anode interface. The analytical solution of methanol molar flux was proposed by solving equation-4.17. The molar flux equation (equation-4.17) was solved by using boundary conditions at membrane interface. The boundary conditions at membrane interface was mentioned earlier. The above equation was analytically solved by considering the boundary conditions at interfaces. The equation was solved to get the general expression of methanol molar flux through the membrane. The general expression of methanol molar flux through the membrane was proposed by A.A. Kulikovsky [**59**]. The expression of methanol molar flux proposed by A.A. Kulikovsky was modified as per the boundary conditions presented in our model which is schematically shown in **Fig. 4.10**. The general expression for predicting the methanol molar flux though the membrane is given below

$$N_{m,cross} = \frac{I^a_{lim}}{6F}\left(\frac{\gamma + m_d \frac{I_{cell}}{I_w}}{1+\gamma+m_d \frac{I_{cell}}{I_w}}\right)\left(1-\frac{I_{cell}}{I^a_{im}}\right) \qquad (4.18)$$

Here, $\gamma=\frac{D_m t_b}{D_b t_m}$, $I_w=\left(\frac{F}{M_{H_2O}}\right)\left[\frac{D_b}{t_b}\right]$ and $I^a_{lim}=6F\frac{D_b C_b}{t_b}$

Here, I^a_{lim} denotes the amount of limiting current generated at anode interface, β is the constant and I_w is the equivalent current related to the geometry of anode flow channel. The methanol transported through the membrane was controlled by diffusion and electro-osmotic drag of

proton. The methanol molecules were dragged through the membrane by the proton. The drag coefficient (m_d) is defined as the number of methanol molecules dragged by one proton. Oxidation of permeated methanol at cathode interface produces leakage current. As the methanol permeation increases through the membrane, more amount of methanol will take part for oxidation reaction. As a result, more leakage current was produced in the cell which decreases its performance. The production of leakage current should be declined to improve cell performance. Hence, the methanol permeated through the membrane should be minimized to decline leakage current.

The anode side over-potential was predicted by solving the diffusion kinetics of methanol. A.A. Kulikovsky [**59**] proposed a theoretical model to predict anode side over potential. In his study, diffusion, oxidation reaction of methanol was considered for developing the model. The kinetic of methanol oxidation and oxygen reduction at AFC and cathode catalyst layer was considered in this model. The model equation proposed for predicting the anode over-potential (η_A) is given below

$$\eta_a = 2r\ln\left(\frac{I_{cell}}{I^a}\right) - \ln k_h - \ln\left(1-\frac{I_{cell}}{I^a_{lim}}\right) + \ln(1+\gamma) \qquad (4.19)$$

Here, $I^a = \frac{2\sigma r}{t_a}$ and $k_h = \frac{t_a J}{I^a}\left(\frac{c_b}{c^a_{ref}}\right)$

In this expression, r is the constant for tafel slope, C_b and c^a_{ref} are the concentration of methanol at anode and ACL/membrane interface, J is the volumetric current density (A/cm^3).

The equation (6) is used to predict the anode side over-potential.

4.7.3 Modelling of Cathode Catalyst Layer

The diluted oxygen was reduced at the cathode interface. The reduction of oxygen at cathode interface is represented in **Fig. 1.1**. Water was produced in the cathode diffusion layer as a result of reduction reaction. The permeated methanol was also oxidized at the catalyst layer leaving out electric current (leakage current) and heat. Garcia et al. proposed a theoretical

model to relate leakage current with cathode over-potential. In their model, kinetics of oxygen reduction was considered. The kinetic equation of oxygen reduction at the catalyst interface was modelled. The proposed theoretical model is given below

$$I_{Cell} + I_{leak} = I_{0,ref}^{O_2} \frac{c_{o_2}}{c_{o_2,ref}} e^{\frac{F\beta_c\eta_C}{RT}} \qquad (4.20)$$

Here, I_{leak} is the leakage current generated by the oxidation of methanol at cathode (A/cm^2), β_c is the transfer coefficients at cathode interface and η_C is the over potential produced at cathode interface (Volt). $I_{0,ref}^{O_2}$ is the electron transfer density of oxygen, A/cm^2. I_{cell} is the current density of cell (mA/cm^2). Electron transfer density of oxygen is defined as the generation of electric current due to the reduction of oxygen at cathode. The model parameters and their values is given in **Table 4.1**.

The leakage current is also related with the methanol permeation flux through the electrolyte membrane. The expression used for predicting the loss of electricity in a fuel is given below

$$I_{leak} = 6FN_{M,cross} \qquad (4.21)$$

The **equation-4.19** is further simplified to get the expression of cathode over potential (η_c). The general expression for calculating cathode over potential is

$$\eta_c = \frac{RTy}{F\beta_c} \ln\left(\frac{I+j}{qx}\right) \qquad (4.22)$$

Here, j=I_{Cell}, I=I_{leak}, q=$I_{0,ref}^{O_2}$, x=c_{o_2} and y=$c_{o_2,ref}$

The expression of anode and cathode side over-potential are substituted in **equation-4.15** to predict cell voltage. The simplified I-D model of active DMFC was developed to predict the cell voltage at different current density. The proposed model of an active DMFC was simultaneously solved at different current density to predict polarization curve. The model equations were solved by developing MATLAB code for different methanol feed

concentration. The model parameter used for predicting the polarization curve is given in **Table 4.1**. The leakage current of the DMFC was predicted by using the **equation-4.21**. For predicting leakage current, methanol molar flux was calculated from **equation-4.18**. The leakage current was calculated at different methanol feed concentrations. The model equations was simultaneously solved in a MATLAB environment at different current density and predicts the leakage current.

Table 4.1: Different model parameters and their values.

Parameters	**Symbol**	**Values**	**Reference**
Specific surface area of anode, cm^2	g	1000	Garcia et al. [**58**]
Diffusion coefficient of methanol at ADL, cm^2/s	D_b	1.8×10^{-5}	Patrabansh et al.[**61**]
Diffusion coefficient of methanol through the membrane, cm^2/s	D_m	1.08×10^{-7}	Measured
Electron transfer density of methanol, A/cm^2	$I_{0,ref}^{MeOH}$	$9.425\times10^{-3}\exp[\frac{35570}{R}\left(\frac{1}{353}-\frac{1}{T}\right)]$	Wang et al. [**60**]
Electron transfer density of oxygen, A/cm^2	$I_{0,ref}^{O_2}$	$4.222\times10^{-3}\exp[\frac{73200}{R}\left(\frac{1}{353}-\frac{1}{T}\right)]$	Wang et al.
Rate constant	k	7.5×10^{-4}	Garcia et al.
Potential for methanol oxidation, V	U^{MeOH}	0.03	Wang et al.
Potential for oxygen oxidation, V	U^{O_2}	1.24	Wang et al.
Charge transfer at anode interface	β_a	0.52	Garcia et al.
Charge transfer at cathode interface	β_c	1.55	Garcia et al.
Anode catalyst layer thickness, cm	t_a	0.0023	Garcia et al
Anode baking layer thickness, cm	t_b	0.015	Garcia et al
Membrane thickness, cm	t_m	0.012	Measured
Proton conductivity, S/cm	σ	0.1265×10^{-2}	Measured
Volumetric current density at anode, (A/cm^3)	J	0.01	A.A. Kulikovsky [**59**]
Faradays constant	F	96487 C/mol.	Assumed
electro-osmotic drag coefficient of methanol	M_d	2	A.A. Kulikovsky
Tafel slope	r	0.075	Assumed
Oxygen concentration at CCL/Membrane interface	c_{o_2}	0.14 kg/m^3 or 4.37 $mol./m^3$	Assumed
Oxygen concentration at cathode inlet	$c_{o_2,ref}$	0.17 kg/m^3 or 5.32 $mol./m^3$	Measured
Methanol concentration at ACL/Membrane interface	c_{ref}^{a}	0.001	A.A. Kulikovsky

CHAPTER 5

MORPHOLOGY ANALYSIS

5. MORPHOLOGY ANALYSIS

5.1 Pure and Cross-linked Chitosan-PVA blend

5.1.1 FTIR analysis

The functional of group of Chitosan-PVA (CP) blend and cross-linked with sulfuric acid is analyzed by FTIR. The transmittance peak of the blends are represented in **Fig. 5.1**. The presence of a prominent peak at 600cm^{-1} confirms C-C interaction between chitosan and polyvinyl alcohol. There was no C-C bond interaction in a CP blend. The absence of C-C bond interaction signifies its non-compatibility structure [**62**]. However there was formation of intermolecular hydrogen bonds between the –OH and –NH groups in chitosan and the –OH group of polyvinyl alcohol [**63**]. The C-O group interaction of the blends are confirmed by the appearance of strong peak at 1100cm^{-1}. The appearance of C-O bond confirms the miscibility of the blend [**63**]. Due to crosslinking reaction with sulfuric acid, the peak intensity of C-O group in a blend was decreases. During crosslinking reaction, hydroxyl group was interacted with the sulfonate group of cross-linking agent and reduces the amount of hydroxyl group. Therefore, the peak intensity of C-O group decreases in a cross-linked membrane. The acid (H^+ ion) of sulfuric acid protonated amine group of Chitosan. The existence of a prominent peak at 3400^{-1} confirms the protonation of amine group and is ascribed as N^+H bond interaction. The existence of a prominent peak at 1200cm^{-1} confirms the interaction between SO_4^{2-} and NH_3^+. The peak intensity of ionic bond interaction in a CP blend was higher than the CP-1 and CP-2 blends. Hence, the ionic bond interaction between SO_4^{2-} and NH_3^+ was higher in a CP blend as compared to CP-1 and CP-2 blend. It signifies that the CPH blend was more compatible as compared to CPH-1 and CPH-2 blend. Moreover, due to ionic bond interaction, cross-linked bond was more compatible than neat CP blend. The presence of prominent peaks at 1400 and

2900cm^{-1} confirms the C-H interaction in a blends. The presence of a prominent peak at 1650cm^{-1} confirms the N-H bending of the amino group.

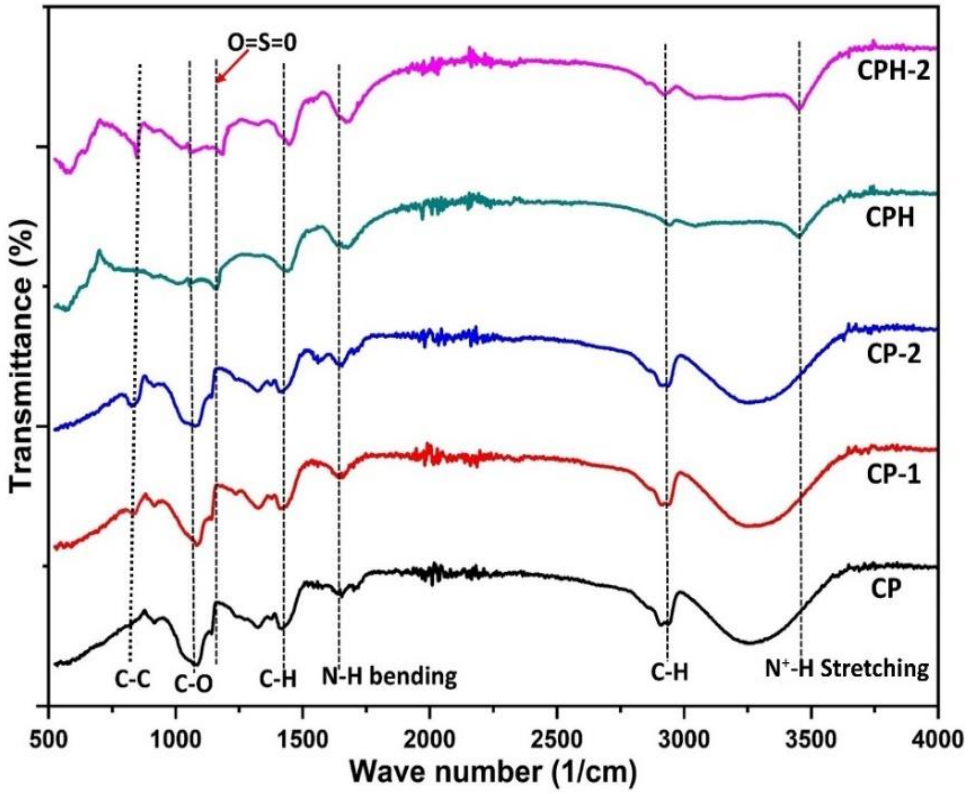

Figure 5.1: IR transmittance peak of pure and cross-linked CP blends.

5.1.2 X-ray diffraction analysis

The XRD profile of the blends are shown in **Fig. 5.2**. The sharp high intensity peak represents crystalline phase whereas amorphous phase is identified from the region of low intensity broad peak. PVA has crystalline peaks at 10° (002), 19.8° (101) and 28° (200) planes, whereas Chitosan has strong peaks at 10.3° (002), 15.2° (002) and 21.9° (102) [**34, 64**]. The crystalline phase of the blend was allocated to the steep peak seen at 9 & 33° (002), 18° (101) and 28° (200). In a CP blends, hydroxyl and amino group are responsible for the formation of crystalline phase. It was observed that the peak intensity at region of 9° (002) gradually decreases with the increase of Chitosan (wt. %) in a blend. The reactivity of hydroxyl groups between Chitosan and PVA were affected by the addition of more Chitosan. The increase of chitosan amount to

a CP blend reduces the inter-molecular linkage between hydroxyl groups. Due to the decline of hydroxyl group interactions, higher unreacted hydroxyl group was present in a CP-1 and CP-2 blends. The unreacted hydroxyl group of the blend contributes to the crystalline phase, causes an increase in peak intensity. Hence, crystalline peak with higher intensity was observed in a CP-1 and CP-2 blend as compared to CP blend. However, the cross-linking agent reduces crystalline phase of the blend. The amino group of Chitosan was consumed by the reaction with SO_4^{2-} and reduces the crystalline phase.

The crystalline degree (%) of the blends were calculated from the XRD peak and reported in **Table 6.1**. The highly compatible blend shows lower crystallinity as compared to the non-compatible blend. The presence of free hydroxyl groups in a blend contributes crystal phase. The amount free hydroxyl group in a non-compatible blend has higher than that of compatible blend. In non-compatible blend, there was a weak interaction between the hydroxyl groups. The CP-2 blend contributes maximum crystalline degree followed by CP-1 and CP blend. The cross-linking agent significantly reduces the crystalline degree of the blend. It was observed that the crosslinking of CP blend reduces the crystalline degree from 15.36 to 8.32%.

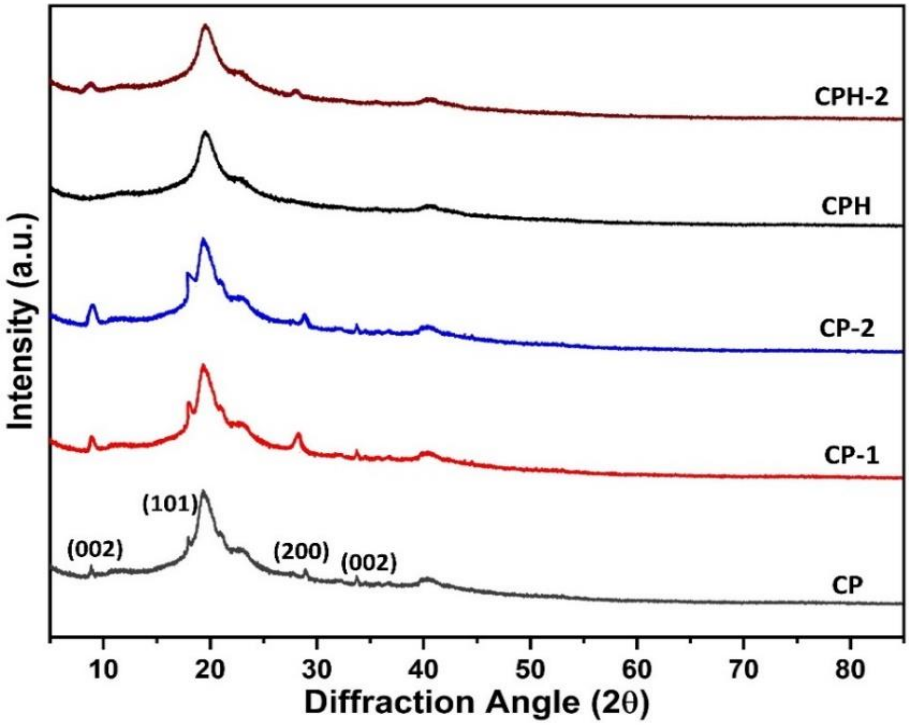

Figure 5.2: X-ray diffraction peak of the pure and cross-linked CP blends.

5.2 Chitosan-PVA blend modified with Red Mud

5.2.1 FESEM analysis

The surface image of pure and red mud modified Chitosan-PVA blend is shown **Fig. 5.3**. When red mud was added to the CP blend, the surface becomes rough. The surface roughness was clearly observed in a red mud modified membrane. Moreover, the red mud particles were aggregated on the surface of membrane. The addition of red mud filler creates void space. The polymer chain interaction in a blends was disturbed by the addition of filler. Moreover, at drying conditions, high temperature was achieved which initiates aggregation of red mud particles. There are two types of aggregation observed in a membrane, soft and hard aggregation. The soft aggregation of red mud was observed in a CPR-1 and CPR-2 membrane. The soft aggregated particles were well dispersed in the polymer domain. However, when we add more red mud particles during synthesis, hard aggregation was observed. The hard aggregation of red mud particle was observed in a CPR-3 membrane which is shown in **Fig. 5.3(d)**. During hard aggregation, the red mud particles were aggregated strongly and form a

cluster of particles. The formation of cluster in a blend is shown in **Fig. 5.3(d)** for CPR-4 membrane. The formation of cluster creates more void space in a membrane. Energy dispersive X-ray spectroscopy (EDX) technique was used to analyse the elemental content of membranes. The EDX system was attached to an FESEM machine. The EDX scan of the synthesized membrane is shown in **Fig. 5.4**. The elements of O, C, Al, Fe, and Silica are present in the synthesized membrane. The Al, Fe and silica are the oxides of red mud which was incorporated in the membrane. The atomic percentage of different elements present in a membrane is tabulated in **Table 5.1**. The main elemental constituents of CP blend were carbon and oxygen. When red mud powder was added to the blends, elements like AL, Fe and Si appeared in the membrane. These elements are the constituents of red mud originally presence in oxide form. The addition of red mud particles to a CP blend reduces the amount of oxygen content. The silica and aluminium atoms were reacted with the hydroxyl group of blend to form Si-O and Al-O bond. Hence, hydroxyl group of the blend was depleted which resulted lower atomic percentage of oxygen in a red mud modified membrane. However, the interaction between Fe atom and hydroxyl groups was not reported in literature. Moreover, the atomic percentage of Fe atom was increases in a blend. It confirms that the Fe atom was not reacted with the functional group of blend. It remains in a discrete iron oxide form of Fe_2O_3 and Fe_3O_4.

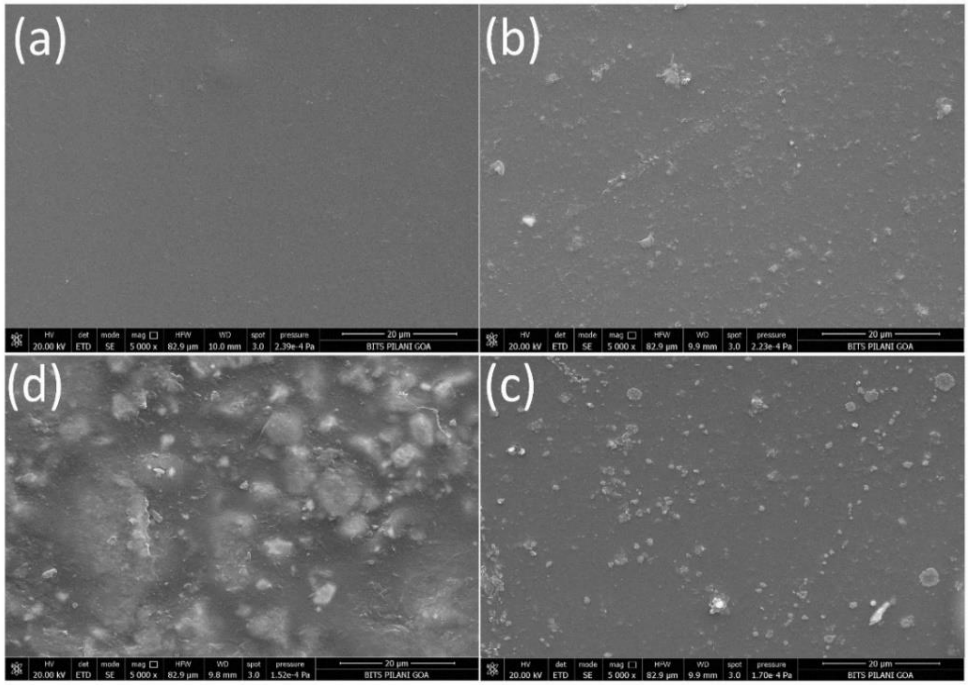

Figure 5.3: The surface images of membrane (a) CP (b) CPR-1 (c) CPR-2 (d) CPR-4.

(a)

Element	Weight %	Atomic %
C K	52.6	59.6
O K	47.4	40.4
Al K	---	---
Si K	---	---
Fe K	---	---

(b)

Element	Weight %	Atomic %
C K	53.0	60.5
O K	45.2	38.8
Al K	0.6	0.3
Si K	0.2	0.1
Fe K	0.9	0.2

(c)

Element	Weight %	Atomic %
C K	51.3	62.2
O K	36.7	34.1
Al K	1.3	0.2
Si K	7.2	2.7
Fe K	3.5	0.8

(d)

Element	Weight %	Atomic %
C K	52.8	58.1
O K	33.1	34.9
Al K	0.8	0.4
Si K	10.7	5.4
Fe K	2.6	1.2

Figure 5.4: EDX profile of CP and CPR membrane obtained from FESEM analysis.

Table 5.1: Atomic weight percentage of the red mud modified Chitosan membranes obtained from EDX analysis.

Sample Code	C (%)	O (%)	Al (%)	Si (%)	Fe (%)
Chitosan-PVA	59.6	40.4	---	---	---
CPR-1	60.5	38.8	0.3	0.1	0.2
CPR-2	62.2	34.1	0.2	2.7	0.8
CPR-3	58.1	34.9	0.4	5.4	1.2

5.2.2 FTIR analysis

The transmittance peak appeared in a red mud modified membrane is marked in **Fig. 5.5**. The presence of C-H group in all the samples was confirmed from the appearance strong peak at 2800cm^{-1}. The prominent peak appeared at 1470cm^{-1} represents the N-H bending of Chitosan. The prominent peak appeared at 1100cm^{-1} confirms the C-O-C group interaction in the blend. A weak peak was observed at the wavelength range of 400-700cm^{-1} in a red mud modified membrane. This peak was appeared due to the presence of metal oxides of red mud. The prominent peak appeared at the wavelength range of 1600-1700cm^{-1} confirms the stretching vibration of C=O group present in the amide II (O=C-NHR) of Chitosan. A strong peak appeared at 750cm^{-1} represents C-O stretching of PVA. A new peak at 3450cm^{-1} for CPR-3 membrane was assigned to Si-OH group which confirms the interaction between silica and hydroxyl group.

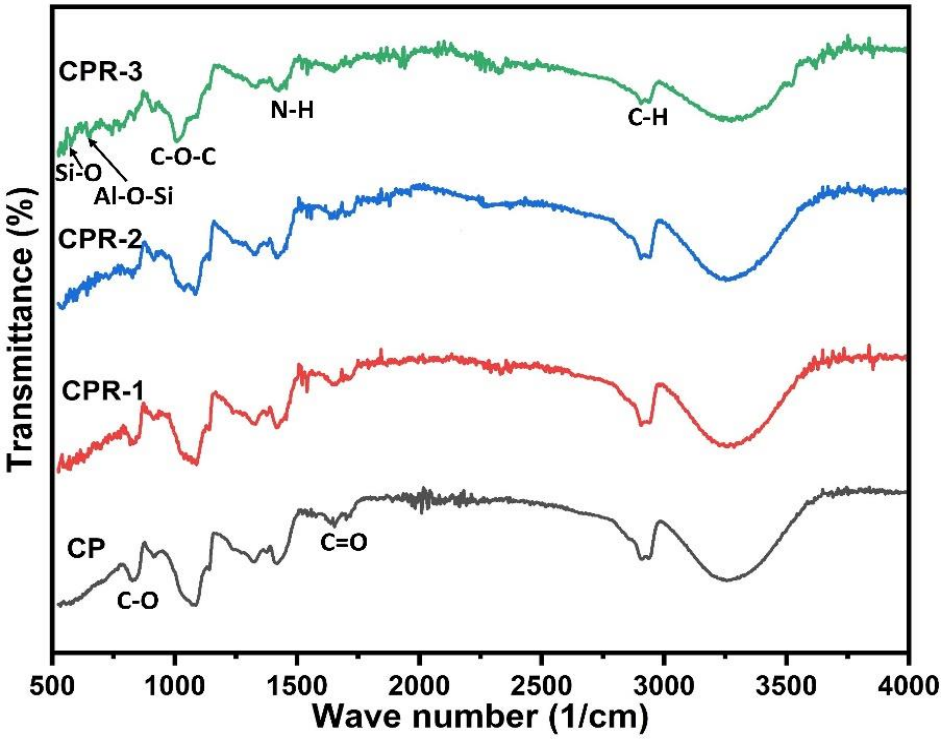

Figure 5.5: IR transmittance peak of the red mud modified Chitosan membranes.

5.2.3 X-ray diffraction analysis

The XRD plot of the red mud modified membranes are represented in **Fig. 5.6**. The strong peak appeared at 12° (002) and 20° (002) plane are assigned to be the crystal of Chitosan. A new broad peak appeared for red mud modified membrane at 13° (020) plane was assigned to the crystal of silica. Amorphous silica is the main constituents of red mud which was added as filler. The addition of PVA in a blend decreases the peak intensity of PVA crystal. The PVA crystal was depleted due to the interaction with red mud. The crystal of red mud contributes crystalline phase of the membrane. The strong crystalline peak appeared in a pure blend at 12° (002) and 25° (200) were varnished and a new peak was appeared at 13° (020) for red mud modified membrane. The appearance of crystal peak in a pure blend was due to the presence of hydroxyl and amide group. The hydroxyl group of the blend was thought to have reacted with the metal of red mud. As a result, the peak intensity owing to the hydroxyl group decreased as the red mud filler in the membrane increased. The depletion of crystal phase with the

addition of red mud filler was confirmed by calculating degree of crystallinity. The degree of crystallinity of the membranes are obtained from the crystalline peak and reported in **Table 6.2.** The incorporation of 4wt% red mud filler in a blend reduces the degree of crystallinity from 12.46% to 2.16%.

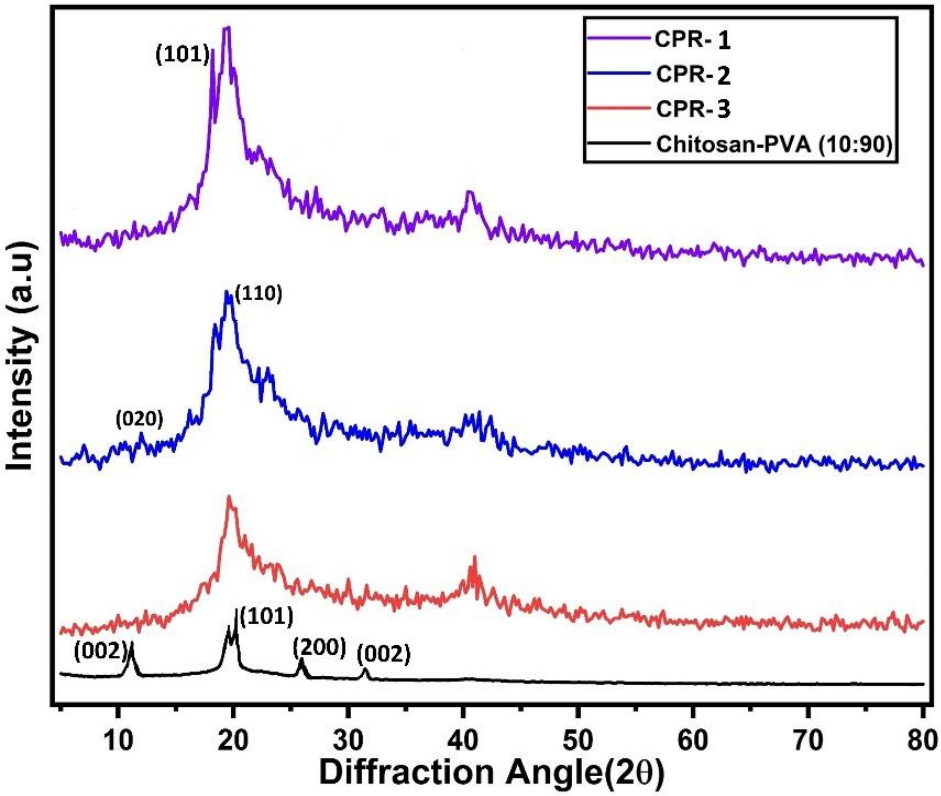

Figure 5.6: X-ray diffraction peak of the red mud modified Chitosan membranes.

5.3 Ionic liquid modified Chitosan-PVA-CNT hybrid membrane

5.3.1 FESEM analysis

The FESEM surface images of the hybrid membranes were captured at different magnification and resolution. Dispersing filler to the blend influences its mechanical and thermal properties. From the surface view, dispersion of filler and interface boding between polymer matrix and filler was analyzed. The surface image and interfacial interaction in a blends are represented in **Fig. 5.7(a)**. From the FESEM images, surface roughness and void space was observed. In CPCN-1 membrane, small void space and crack was observed. The fillers did not accumulate

on the membrane's surface. When the amount of filler increases in the hybrid membranes, fillers start to form aggregation. The formation of filler cluster on the surface of CPCN-4 membrane is shown in Fig. 5.7(b). The fillers were aggregated in a rod like morphology which is highlighted in the figure. However, when the hybrid membranes were modified by ionic liquid, there was significant decline in aggregation of filler was observed. The surface of the membrane becomes more compact and defect free. The defect free and smooth surface of membrane is shown in **Fig. 5.7 (c &d)**. The ionic liquid was interacted with the filler and a layer like structure was developed on the surface. The homogeneous distribution of filler in the matrix phase of membrane is shown in **Fig. 5.8(a)**. As illustrated in **Fig. 5.8(b)**, the aggregated filler in the CPCN@IL-4 membrane is denoted by a rectangular box.

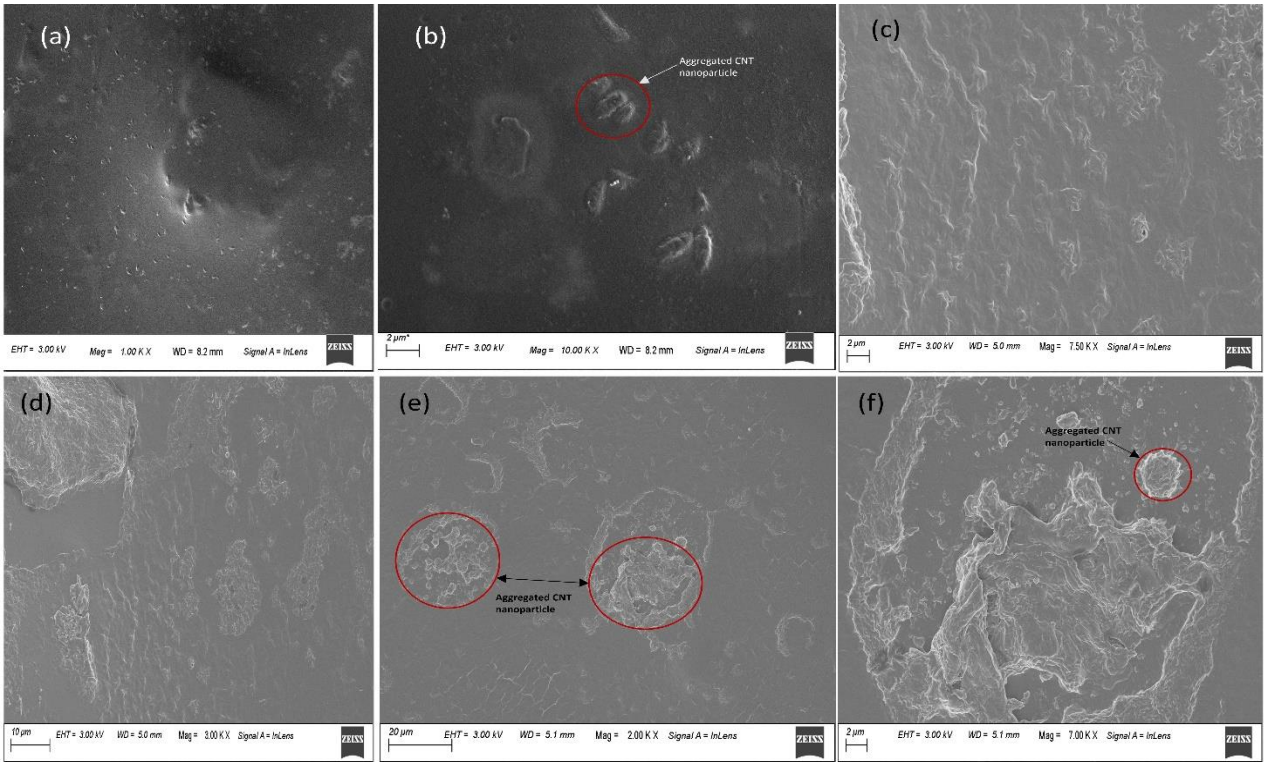

Figure 5.7. FESEM images of the membrane (a) CPCN-1 (b) CPCN-4 (c) CPCN@IL-1, Mag=7.50KX (d) CPCN@IL-1, Mag=3.00KX (e) CPCN@IL-4, Mag=2.00KX (f) CPCN@IL-4, Mag=7.00KX.

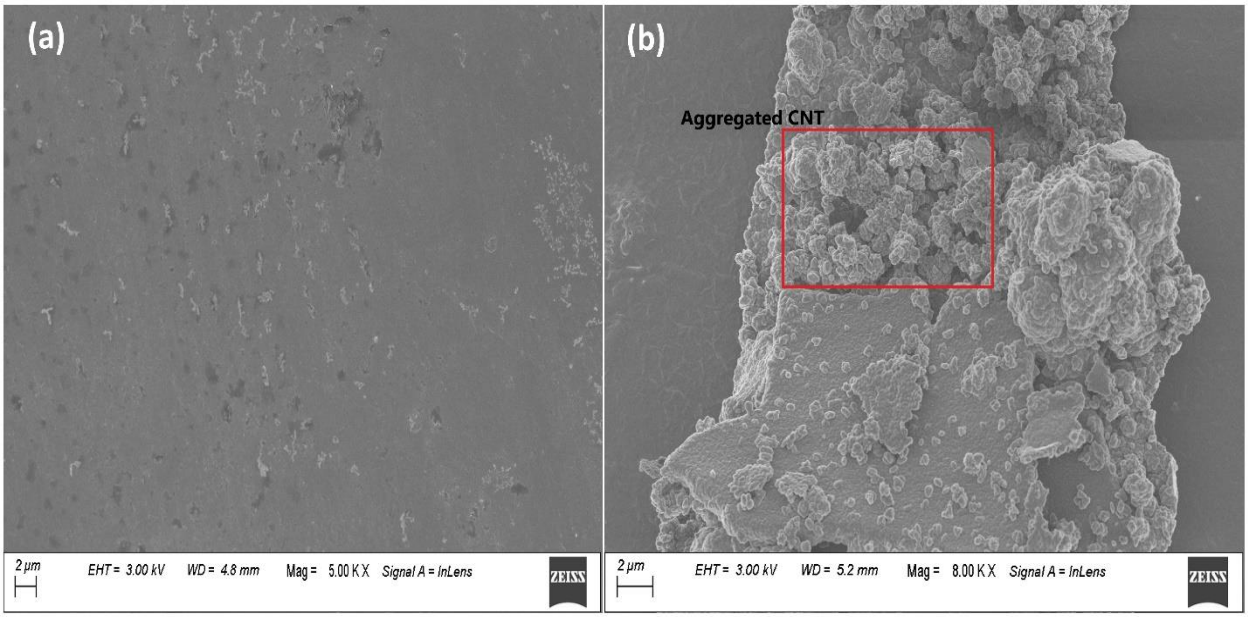

Figure 5.8. FESEM images of (a) CPCN@IL-1 (b) CPCN@IL-4.

5.3.2 FTIR analysis

The FTIR transmittance peak of the Chitosan-PVA blend modified with hygroscopic CNT is shown in **Fig. 5.9(a)**. The appearance of strong peak at 1000cm^{-1} for CPCN hybrid membrane reveals the presence of hydroxyl group. The peak intensity of the hydroxyl group region decreases with the increase of CNT filler loading. The hydroxyl group was interacted with the filler and depleted its concentration. As a result, the peak intensity of the hydroxyl group decreased as filler loading increased. The appearance of strong characteristic peak at 1250 and 2150cm^{-1} are due to C-H bending and stretching respectively. The presence of a prominent peak at 1700cm^{-1} confirms the C-C interaction in a hybrid membrane. A strong peak at 1700cm^{-1} confirms N-H bending of amide group. The peak intensity of the amide group gradually decreases with the increase of filler loading. The amide group was interacted with the filler and depleted its concentration. The FTIR peak of the ionic liquid modified hybrid membrane is shown in **Fig. 5.9(b)**. The hydroxyl group of the blend was reacted with the cation of ionic liquid. The hydroxyl group was consumed due to ionic liquid interaction. Hence, there is no sharp peak observed for the wavelength of hydroxyl group region. Due to addition of ionic liquid, new peak was appeared at 1350 and 1650cm^{-1} which were due to S=O and imidazole ring stretching. A strong peak appeared at 1980cm^{-1} is assigned to the stretching of imidazolium cation.

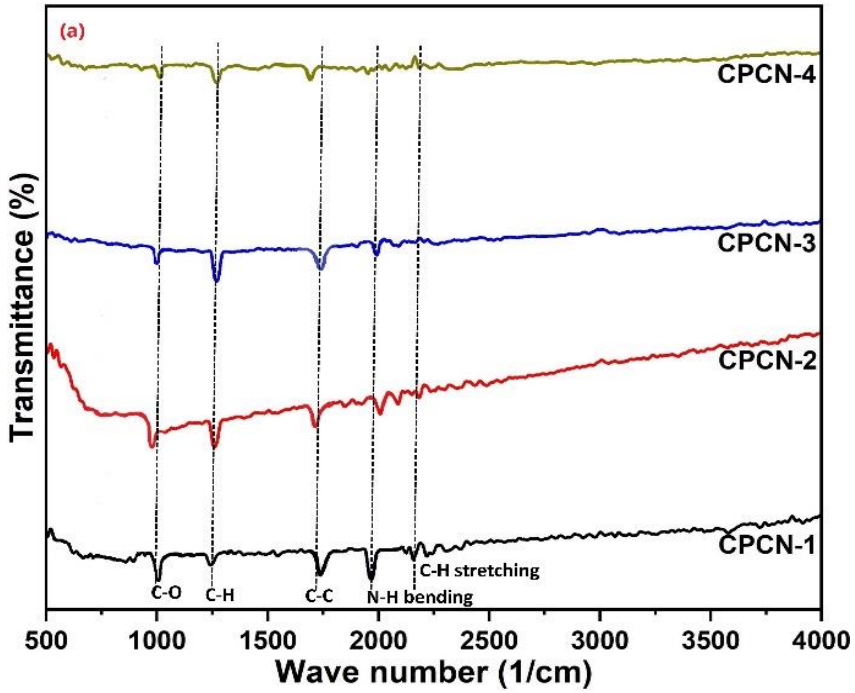

Figure 5.9 (a): IR transmittance peak of the CPCN membranes.

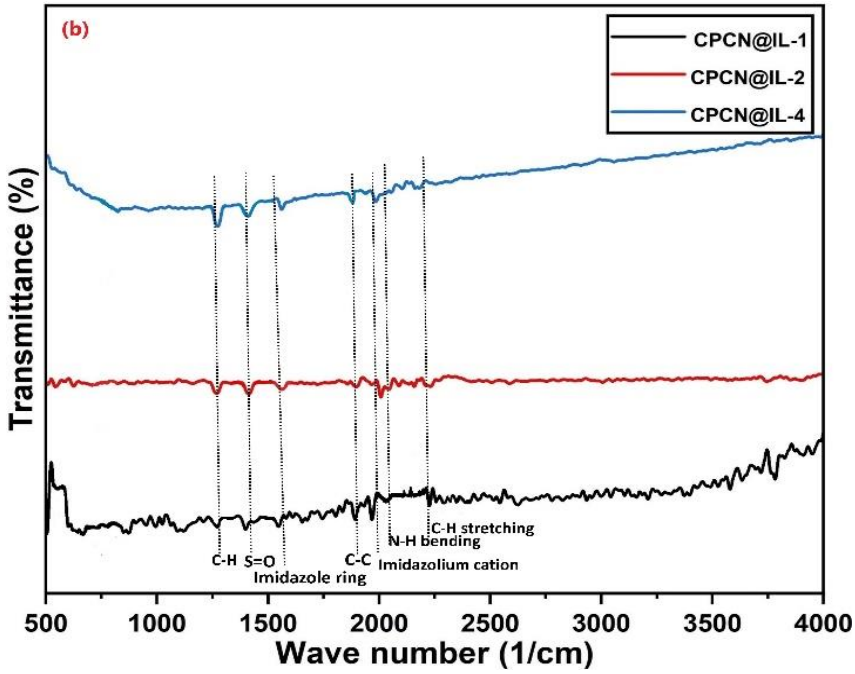

Figure 5.9 (b): IR transmittance peak of the CPCN@IL membranes.

5.3.3 X-ray diffraction analysis

The XRD profile of the CNT filled hybrid membrane is shown in **Fig. 5.10**. A sharp peak appeared at 21° (110) plane is assigned to the crystal of Chitosan. The peak intensity and area gradually decreases with the increase of filler content. However, when the membrane was treated with ionic liquid, peak area was broadening. It signifies that the crystal phase was converted to amorphous phase at the presence of ionic liquid. The maximum phase shifting was observed in a CPCN@IL-3 membrane. The peak intensity was shifted to a lower 2θ angle and area becomes broader. A new peak appeared at 2θ=19° is assigned to the amorphous phase of the membrane. A sharp peak appeared at 23° (110) plane is assigned to the crystal phase of CNT crystal.

The effect of filler (carbon nanotubes) and ionic liquid on the crystalline degree of Chitosan-PVA blend are studied. The crystalline degree of the hybrid membranes are calculated from the XRD Peak and reported in **Table 6.3**. The addition of CNT filler to a CP blend increases crystalline phase of the blend. The crystal of zirconia contributes crystalline phase of the blend. However, the increases of CNT filler in a membrane reduces crystalline phase. The CNT filler was interacted with the hydroxyl and amide group of blend and depleted crystalline phase. In a CP blend, hydroxyl and amide groups are responsible for the formation crystalline phase. The interaction of CNT with the hydroxyl and amide group of CP blend was confirmed from functional group analysis. With ionic liquid treatment, crystalline phase of the membrane was further reduced. The ionic liquid reacted with the crystal phase of the membrane and depleted crystalline phase. The ionic liquid will have a plasticizing effect which weakening the well-ordered structure of the membrane. The phase transition of the hybrid membrane was observed due to the plasticizing effect of ionic liquid. Moreover, ionic liquid improves chain flexibility of the hybrid membrane. The ionic liquid modified hybrid shows lower crystalline degree as compared to the non-treated hybrid membrane.

The average size of CNT crystal present in the hybrid membrane was calculated by Scherer's equation (equation-4.11). The effect of filler (CNT) amount on the average size of CNT crystal in a hybrid membrane is shown in **Fig. 5.11**. The increase of filler amount in a hybrid membrane increases average size of CNT crystal. The filling effect of CNT in the membrane creates lattice distortion of crystal. Moreover, the lattice distortion and growth of crystal was assisted by the formation of void space in the membrane. The ionic liquid modified hybrid membrane has lower crystal size than pure hybrid membrane. The growth of CNT crystal was affected by the reduction of void space in the hybrid membrane. The ionic liquid reduced void space in a hybrid membrane, as confirmed by FESEM analysis. Moreover, the growth of CNT crystal was controlled by the interfacial adhesion among filler and polymer matrix. Better interfacial adhesion between the filler and the polymer matrix promotes the growth of crystal size. The distribution of filler to a polymer matrix influences interfacial adhesion. The well dispersed filler in a polymer matrix provides better interfacial adhesion. Hence, the hybrid membrane modified with 1.5wt. (%) filler has bigger crystal size than the other membrane.

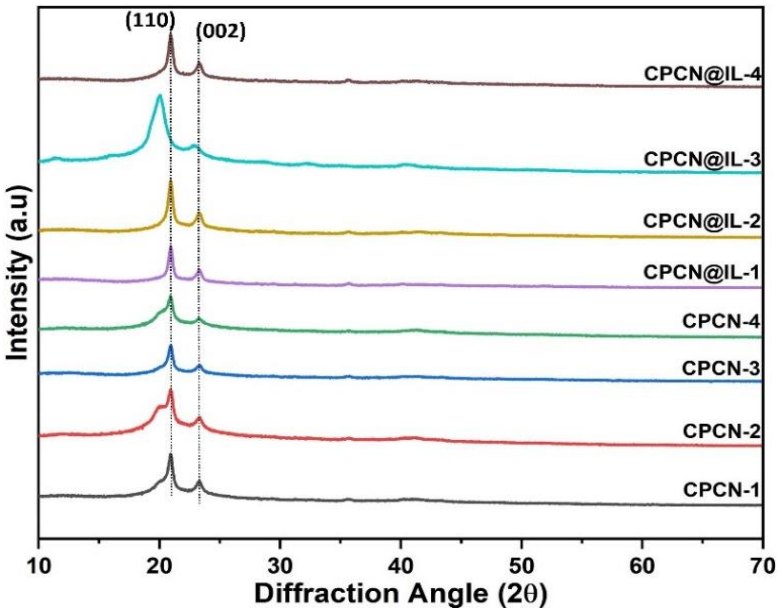

Figure 5.10: X-ray diffraction peak of the CPCN and CPCN@IL membranes.

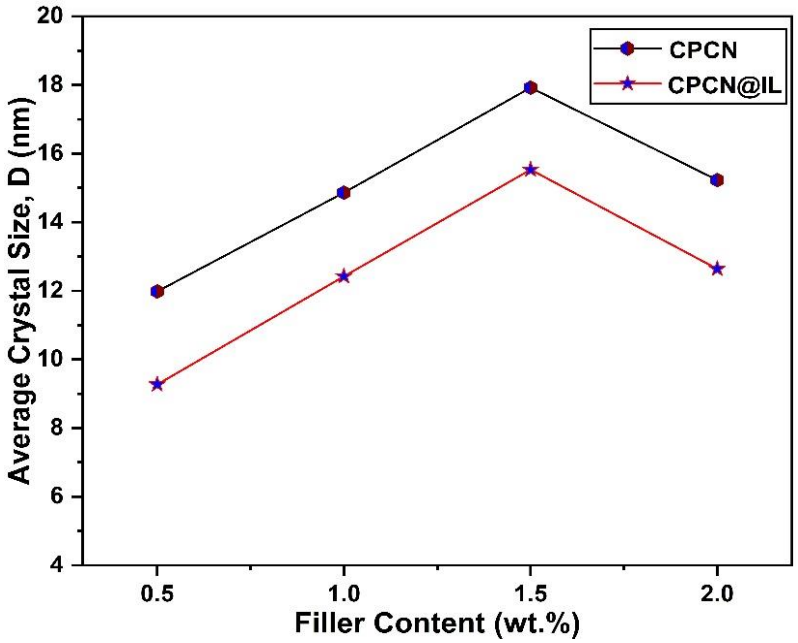

Figure 5.11: Effect of MWCNT amount on the growth of crystals in a CPCN and CPCN@IL membranes.

5.4 Ionic liquid modified Chitosan-PVA-Zirconia hybrid membrane

5.4.1 FESEM analysis

The topographic morphology of the membranes was examined using FESEM images. The FESEM images of the membranes taken at different magnifications are displayed in **Fig. 5.12(a. & b)**. For ease of analysis, surface images were captured at different magnification and resolutions. The FESEM images of the hybrid membrane captured at 300X magnification is shown in **Fig. 5.12**. The well dispersed zirconia particles was observed in all the membranes except CPZr-4. In a CPZr-4 membrane, zirconia particles were aggregated which is highlighted by rectangular box in Fig. 5.13(c). A void space was also created on the surface of membrane. The void space of the membranes were analyzed from high magnification images. The void space created on the surface of CPZr-1 membrane is highlighted in **Fig. 5.13(a)**. However, the depletion of void space was noticed with the increase of filler loading. When the membrane was modified with an ionic liquid, membrane becomes defect free with no void space. The ionic liquid was interacted with the polymer matrix and a root like morphology was observed. The ionic liquid avoids particle clustering on the membrane surface. However, when the amount of particles in a membrane exceed more than 2wt. (%), aggregation started. The interaction between zirconia and ionic liquid becomes least significant. The aggregated zirconia in CPZr@IL-4 membrane is highlighted in **Fig. 5.13(d)**. The mapping of zirconia metal in a pure and ionic liquid modified CPZr-3 membrane is shown in **Fig. 5.14**. The zirconia particles were aggregated on the surface of CPZr-3 membrane. However, when the membrane was treated with ionic liquid, particles were well dispersed on the surface. The ionic liquid enhances the dispersion of zirconia metal on membrane surface. The well dispersion of zirconia in CPZR@IL-3 membrane is shown in **Fig. 5.14(b)**.

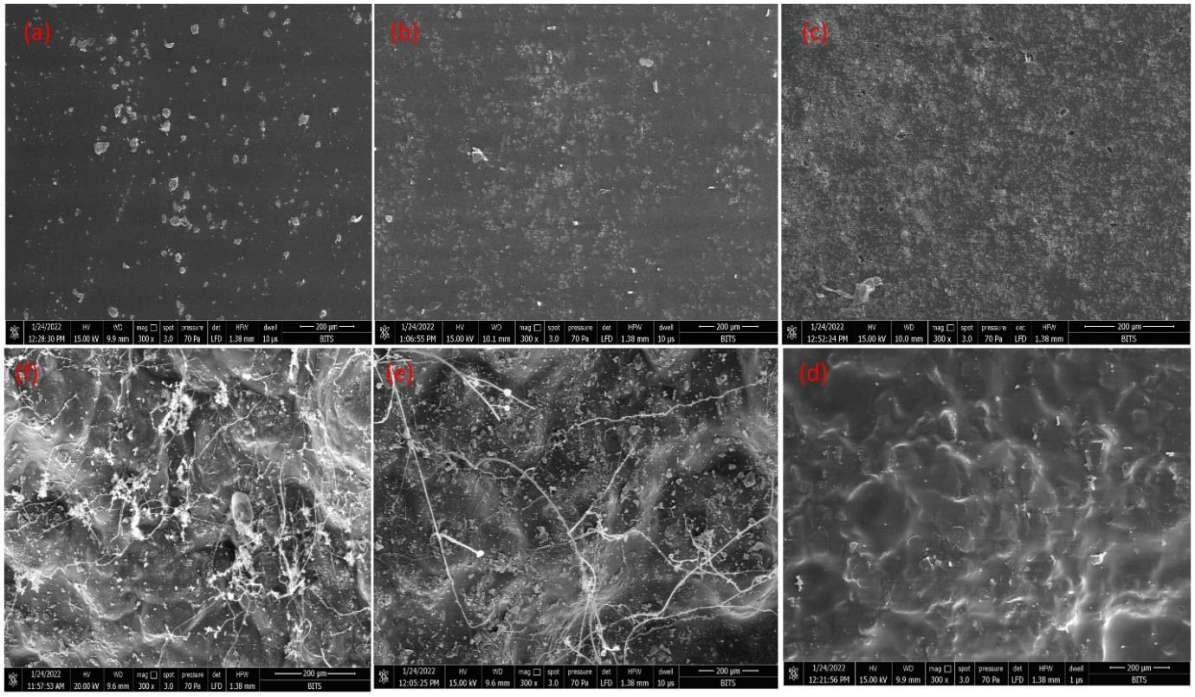

Figure 5.12: Surface image of hybrid membranes captured at 300X magnification and 200µm resolution. (a) CPZr-1 (b) CPZr-2 (c) CPZr-3 (d) CPZr@IL-1 (e) CPZr@IL-2 (f) CPZr@IL-3.

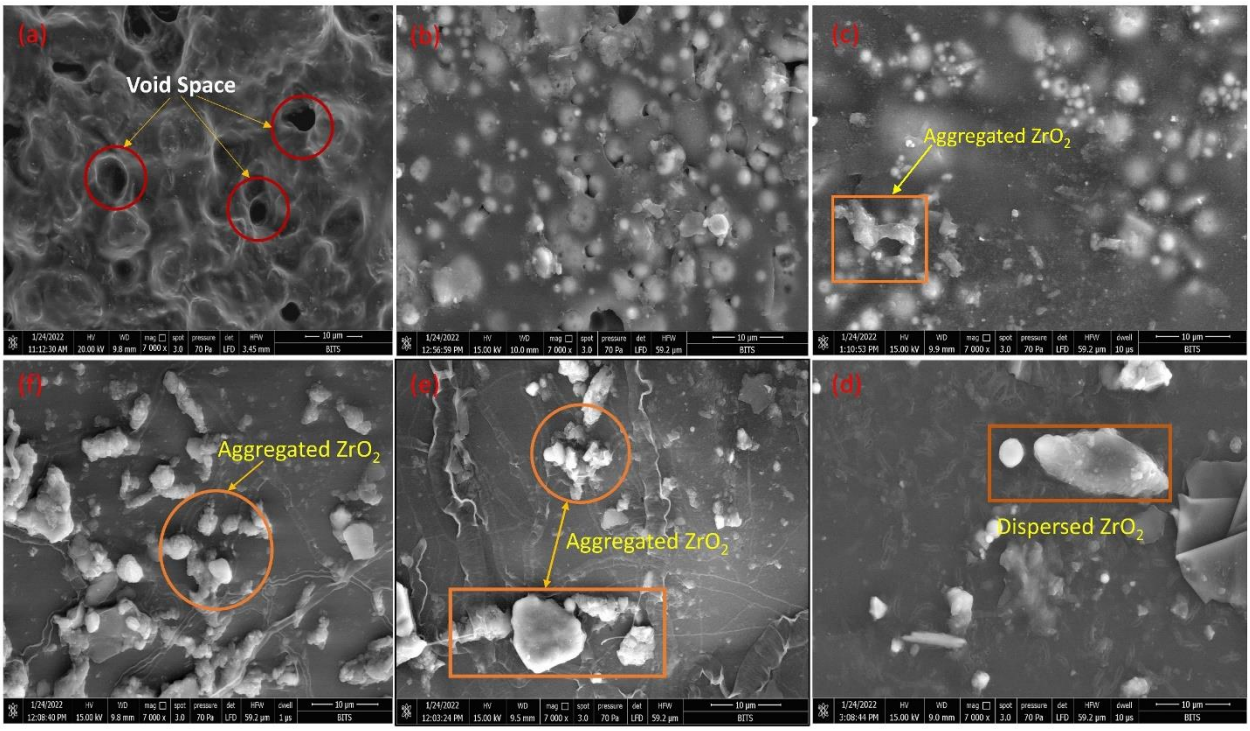

Figure 5.13: Surface images of hybrid membrane captured at 7000X magnification and 10µm resolution. (a) CPZr-1 (b) CPZr-2 (c) CPZr-4 (d) CPZr@IL-1 (e) CPZr@IL-4 (f) CPZr@IL-4.

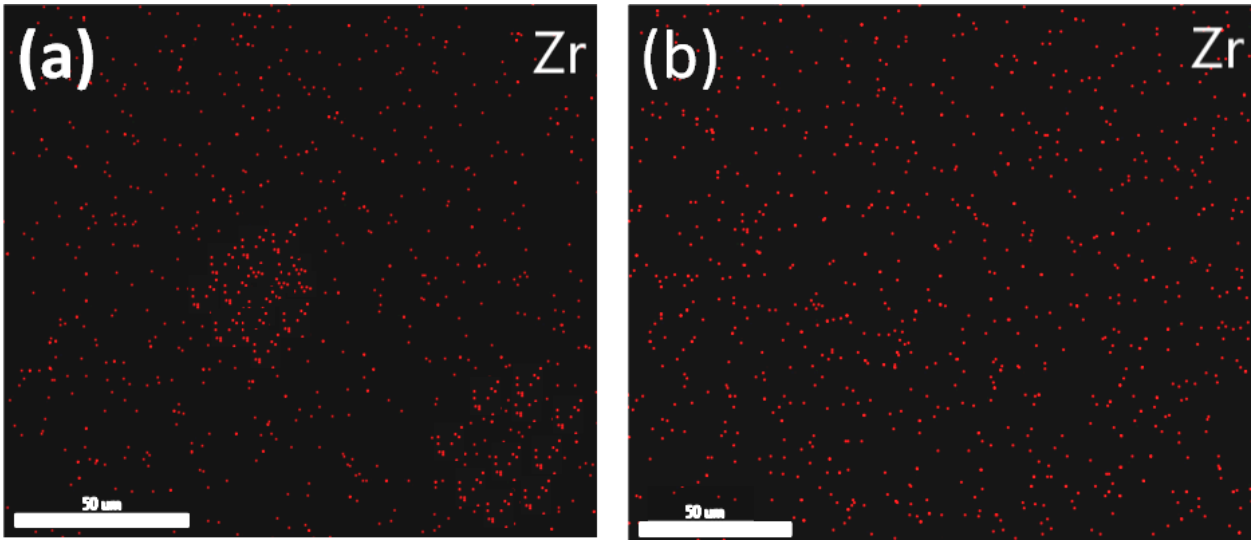

Figure 5.14: EDS mapping of zirconium metal in a composite membrane (a) CPZr-3 (b) CPZr@IL-3

5.4.2 FTIR analysis

The FTIR transmittance peak of the zirconia filled hybrid is shown in **Fig. 5.15(a)**. A strong peak appeared at 550cm^{-1} confirms the Zr-O interaction in a hybrid membrane. Here, the acidic nature of zirconia atom interacts with the oxygen atom of hydroxyl group. The electronic interaction between zirconia and oxygen atom was heavily reliant on zirconia, and thus the dependence of zirconia grows with the increase of zirconia amount. Hence, the peak intensity of Zr-O interaction gradually increases with the increase of zirconia content. A strong peak appeared at 650cm^{-1} is assigned to the stretching vibration of hydroxyl group. The peak strength of the hydroxyl group steadily diminishes with the increase of zirconia amount to a membrane. The hydroxyl group was depleted due to the formation of bond between hydroxyl group and zirconia element. The strong peak appeared at 1180, 1600 and 2200cm^{-1} are assigned to CH_2 bending and stretching of C-C and CH_2 respectively. The appearance of strong peak at 1850cm^{-1} confirms the bending of amide (NH_2) group. The functional group of the ionic liquid modified hybrid membrane is analyzed from **Fig. 5.15(b)**. During membrane synthesis, cation of ionic liquid was interacted with the hydroxyl group of Chitosan-PVA blend. A strong peak appeared

at 730cm^{-1} is assigned to C-O interaction in a hybrid membrane. The peak intensity at the region of C-O interaction was gradually decreasing with the increase of filler loading. It suggest that the hydroxyl group presence in the blend was consumed due to interaction with ionic liquid. Two sharp peak appeared at 1180 and 1620cm^{-1} represents the stretching vibration of S=O and imidazole ring. Moreover, a new peak was noticed at 1830cm^{-1} which signifies the stretching vibration of imidazolium cation.

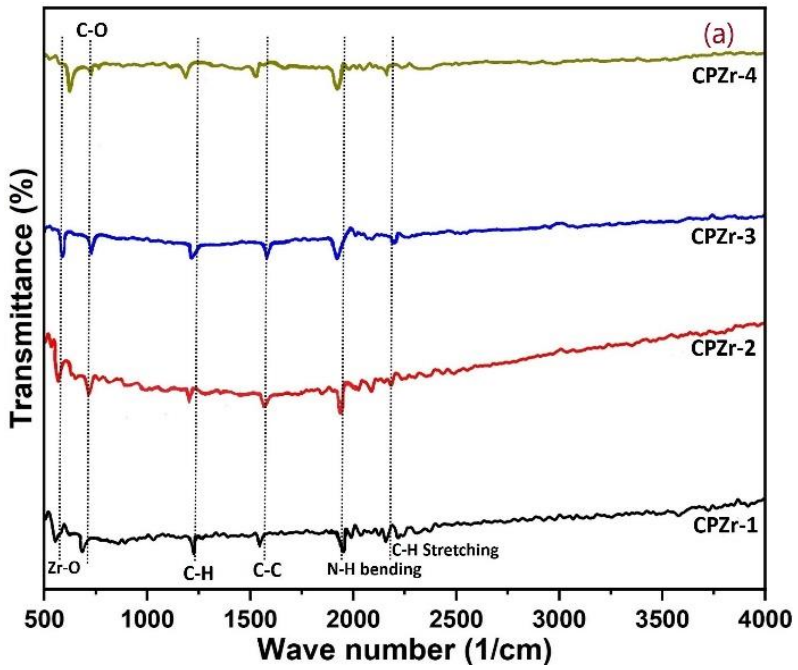

(a)

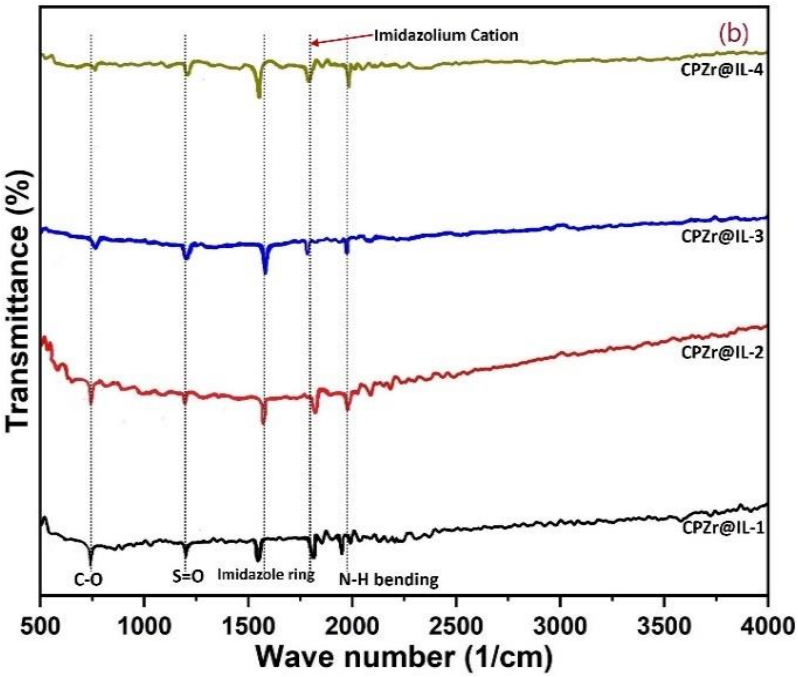

(b)

Figure 5.15(a): FTIR transmittance peak of Chitosan membranes modified with hygroscopic zirconia. (b) FTIR transmittance peak of Chitosan membranes modified with hygroscopic zirconia and ionic liquid.

5.4.3 X-ray diffraction analysis

The XRD profile of the zirconia modified hybrid membrane is shown in **Fig. 5.16**. There are two sharp peak was observed at 21° (110) and 23° (002) plane. The sharp peak appeared at 21° (110) and 23° (002) plane are assigned to the crystal of Chitosan and zirconia. The peak intensity of the Chitosan crystals was reduces with the increase of zirconia in the membrane. The groups which are responsible for the appearance of crystal peak in a CP blend were consumed due to the reaction with zirconia. The zirconia reacted with the hydroxyl group, which was confirmed. The depletion of hydroxyl group in the blend reduces peak intensity of Chitosan crystal. It was observed that the peak area was shifted to a lower diffraction angle with the increase of zirconia loading. The shifting of crystalline peak in a CPZr-2 and CPZr-3 membrane is as shown in XRD plot. Moreover, the peak area was broadening which signifies the phase transition from crystalline to amorphous phase. The addition of zirconia in a Chitosan-PVA blend depleted crystalline phase. The highest crystal phase transition was observed in a CPZr-2 hybrid membrane. The similar phase transition was occurred in an ionic liquid modified hybrid membrane. The ionic liquid will act as plasticizer which reduces the polymer chain interaction and depleted crystalline phase. The shifting of crystalline peak was clearly observed in a CPZr@IL-3 and CPZr@IL-4 membrane. A broad high intensity peak was appeared at $2\theta=19°$ and assigned to the amorphous phase of the membrane.

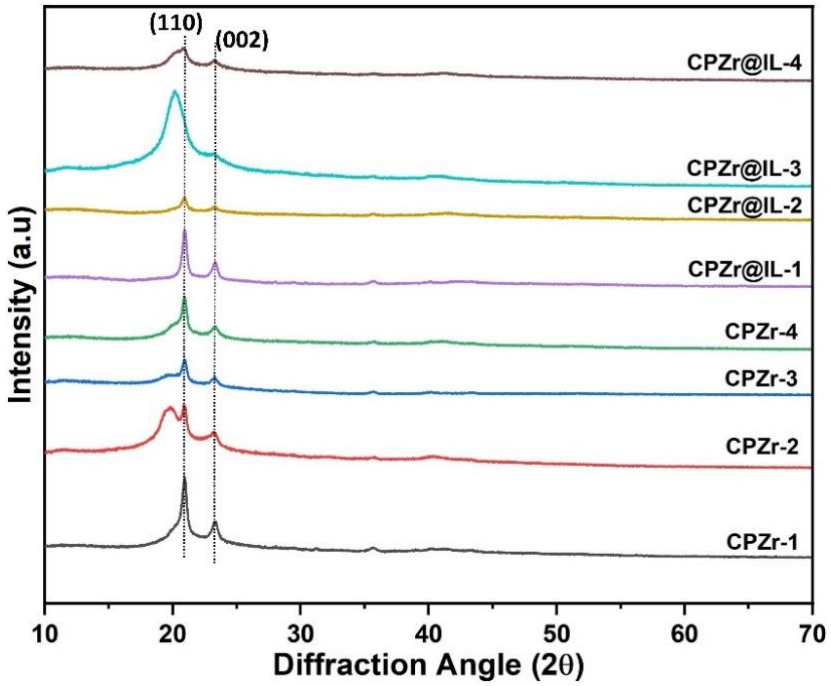

Figure 5.16: XRD profile of the Chitosan membranes modified with hygroscopic zirconia and ionic liquid.

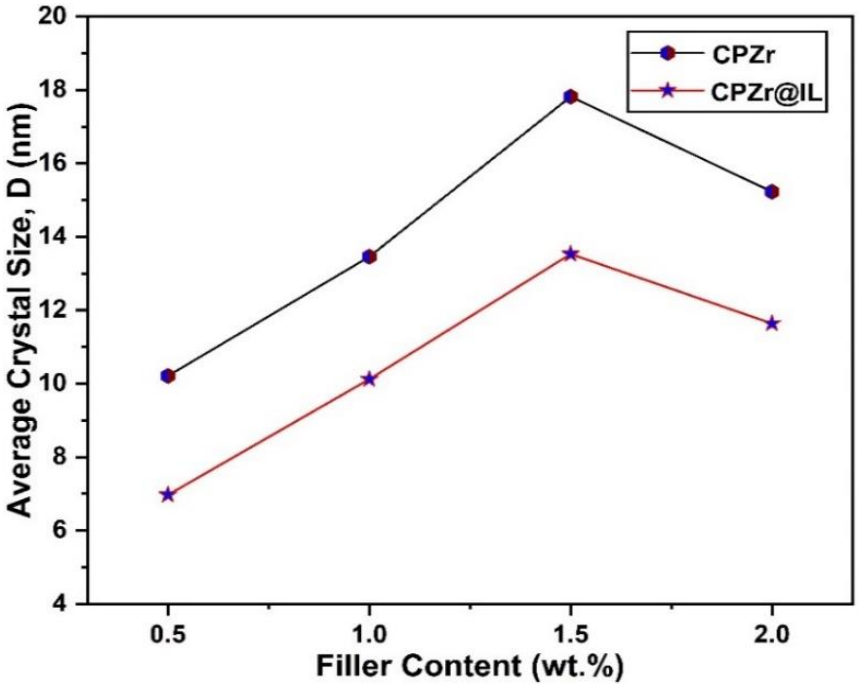

Figure 5.17: Average size (D) of the crystallites in a zirconia and ionic liquid modified CP blends.

The crystalline degree of the zirconia and ionic liquid modified hybrid membrane was calculated and reported in **Table 6.3**. The average crystal size of zirconia filler in a modified membrane is represented in **Fig. 5.17**. Filler crystal size grows as filler quantity increases in a hybrid membrane. The plasticizing effect of filler causes lattice distortion. Moreover, the lattice distortion was supplemented by the formation of void space. Due to lattice distortion, more number of zirconia particles were participated for crystallization process. The influence of filler amount on the growth of crystals in a hybrid membrane was calculated and represented in **Fig 5.17**. However, the creation of particles cluster in a CPZr-4 membrane prevents crystal growth. Hence, the crystal size of zirconia in a CPZr-4 hybrid membrane was lower than the other membranes. Ionic liquid was used to exhaust the empty space in an ionic liquid modified membrane. The ionic liquid affects the growth of zirconia crystal. The hybrid membrane modified with ionic liquid reduces average crystal size of zirconia filler.

5.5 SPEEK-PVA-silica hybrid membrane

5.5.1 Porosity and density analysis

The void volume and density of the membrane was determined and shown in **Fig. 5.18**. The incorporation of silica particles to a membrane increases its void space and density. Moreover, the silica particles enhances compactness and tortuosity of the membrane. The void space was created due to the filling effect of silica. The void space will act as proton transport channel which is a favourable properties of fuel cell membrane. However, the void space should be optimized to prevent the migration of methanol through the membrane.

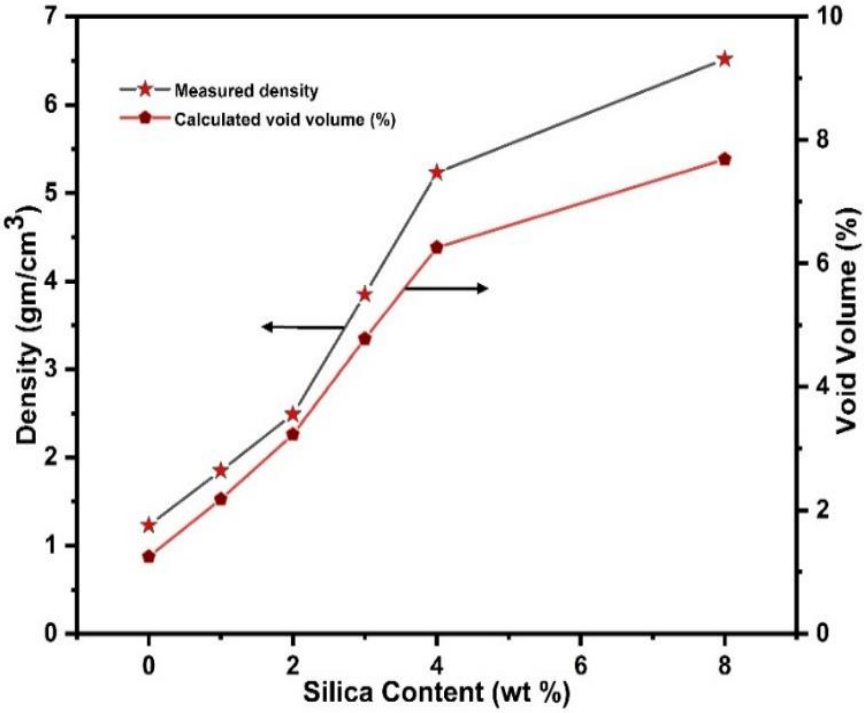

Figure 5.18: Effect of silica amount on the density and void volume fraction of the SPEEK-PVA-silica hybrid membranes.

5.5.2 FTIR analysis

The functional group of the developed membrane was analysed from the FTIR transmittance peak. The transmittance peak appeared for all the membrane is marked in **Fig. 5.19**. A sharp peak appeared at of 620 and 750cm^{-1} confirms the interaction between silica and hydroxyl group of PVA. Here, strong peak was attributed to the stretching of Si-O group. The Si-O-Si stretching was responsible for a prominent peak at 900cm^{-1}. The strong peak noticed at 1023, 1074 and 1469cm^{-1} were attributed to the stretching vibration of O=S=O and S=O groups. A prominent peak denotes the carbonyl (C=O) group of the polymer backbone in the region of 1596-1645cm^{-1}. The presence of strong peak in the range of 3300-3550cm^{-1} confirms the stretching of O-H group.

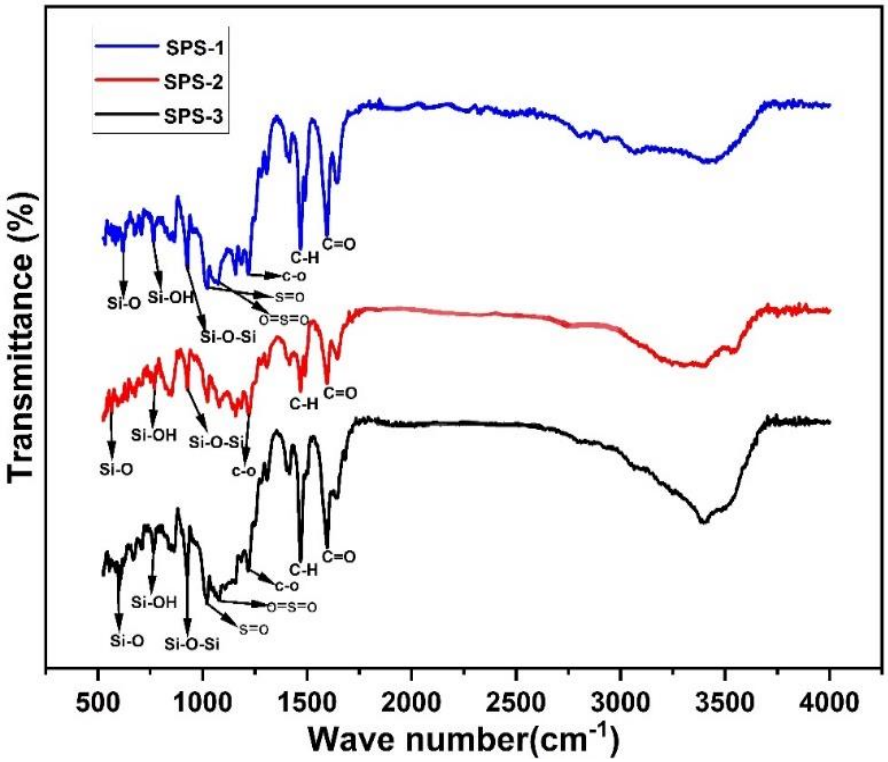

Figure 5.19: FTIR transmittance peak of the silica filled SPEEK-PVA hybrid membranes.

5.5.3 X-ray diffraction analysis

The XRD profile of SPEEK-PVA-silica hybrid membrane is shown in **Fig. 5.20**. The membrane shows three sharp peak at 21° (101), 26° (200) and 34° (002), which are assigned to the crystal of PVA. When filler was added to the SPEEK-PVA domain, sharp peak appeared at 21° (101) was varnished due to the interaction with silica. Moreover, the peak area at 26° (200) was gradually broadening with the increase of silica filler. The hydroxyl group of PVA was reacted with the silica. The crystal phase of the membrane was converted to amorphous phase. A broad peak appeared at 2θ=22° is assigned to the amorphous domain of the membrane. The degree of crystallinity of the SPEEK-PVA-silica hybrid membranes was calculated from the peak of XRD plot. The incorporation of silica particles to membrane decline its crystalline phase. The addition of 4wt. (%) silica to a SPEEK-PVA domain reduces the crystalline phase from 24.21 to 5.82%. It was believed that using smaller molecules as a filler influenced the crystal phase of the membranes. The polymer chain interaction was highly influenced by the

surface area of filler. The filler with a high surface area significantly reduces the interaction of polymer chain in a membrane. The filler weakens the firmly interacted polymer matrix and converts it to a loosely oriented amorphous phase. The small molecules were strongly interacted with the polymer matrix.

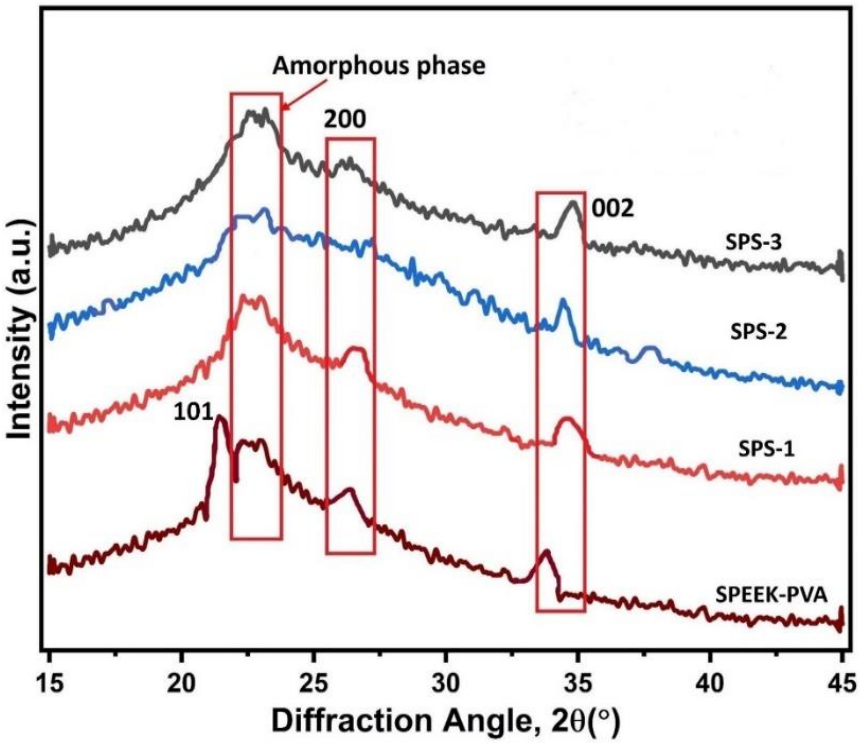

Figure 5.20: XRD plot of the silica filled SPEEK-PVA hybrid membranes.

CHAPTER 6

RESULTS AND DISCUSSIONS

6. RESULTS AND DISCUSSIONS

6.1 Ion Exchange Capacity and Water Uptake Studies

The fuel cell performance was controlled by the chemical properties of electrolyte membrane. The ion exchange capacity (IEC) and water absorption ability of the membrane has an impact on fuel cell performance. The fuel cell performance was highly dependent on proton conductivity of the electrolyte membrane. The proton conductivity was highly influenced by the availability of water in a membrane. There are typically two states of water exiting a membrane, which are known as free and bound water. Free water is similar to the properties of bulk water. The hydrogen bond holds the bound water tightly to the polymer chain. The proton transported though the membrane by two key mechanism (i) Grotthuss and (ii) Vehicular [**65**]. Proton transport by Grotthuss and vehicular mechanism is shown in **Fig. 6.1**. The mechanism of proton transport by Grotthuss mechanism is shown in **Fig. 6.1**. In Grotthuss mechanism, proton passes through the membrane by the formation of hydrogen bond with the water [**66**]. The bonding between water and proton is called hydronium ion (H_3O^+). The resulting hydronium ion will transfer proton along the conduction pathway by subsequent rearrangement between nearly water molecules [**66**]. The vehicular mechanism involves the transport of proton through self-diffusion proton carriers. Moreover, the proton transport was highly influenced by the state of water. In a membrane, higher proton conductivity was achieved by proton transport via the Gotthus mechanism. The proton transport via Grotthuss mechanism was regulated by the presence of free water. At lower temperature, fuel cell performance was influenced by the availability of free water as well as IEC of the membrane. The membrane achieved increased proton conductivity by free water, and proton transport was controlled by the Grotthuss mechanism. However, fuel cell provides lower power density due to poor water management.

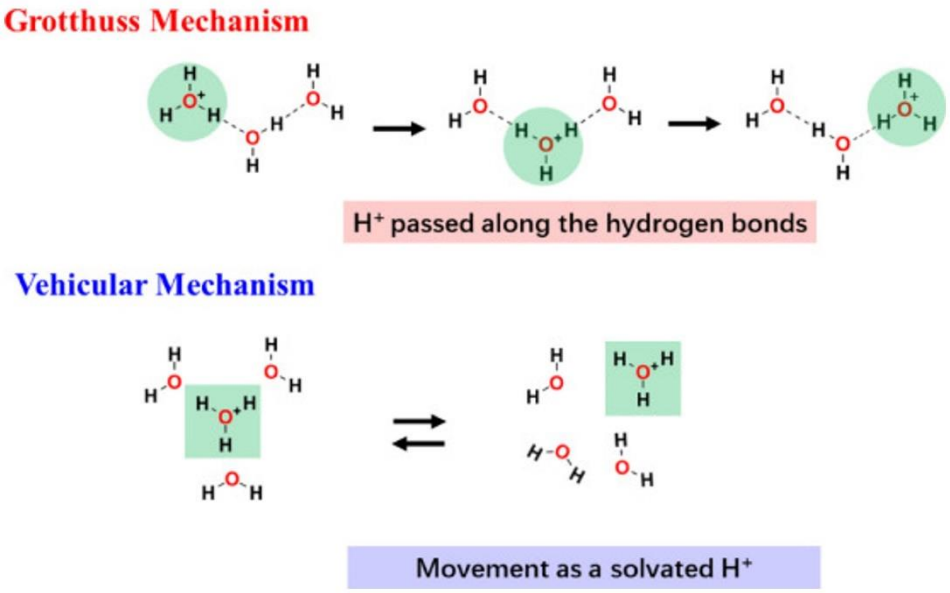

Fig. 6.1: Proton conduction by Grotthusss and vehicular mechanism. [66]

The water was formed due to electrochemical reaction which drastically reduces fuel cell performance. The proton conductivity of the membrane was greatly dependent on its hydration level. The properly hydrated membrane provides better proton conductivity. Hence, hydration states of the membrane should be maintained properly to achieve higher proton conductivity as well as power density. It was more challenging to keep the membrane hydrated at lower temperatures. The formation of water causes membrane flooding which negatively impact proton conductivity. Hence, it is appealing to operate fuel cell at more than room temperature to avoid membrane flooding. However, at moderate temperature (low humidity conditions), amount of free water presence in the membrane was escaped due to evaporation loss. In this condition, bound water plays a crucial role for fuel cell performance. The proton transport was controlled by bound water regulated Grotthuss mechanism [**65**]. Moreover, free water will act as a vehicle to transport proton by vehicular mechanism. The amount of proton transport by vehicular mechanism was significantly lower than that of Grotthuss mechanism. The membrane with higher bound water content is considered to be a potential candidate of fuel cell application at moderate temperature.

The water uptake capacity and IEC of the different CP blends are reported in **Table 6.1**. The increase of Chitosan weight (%) in a blend improves water absorption capacity. The hydrophilic property of Chitosan was thought to boost the blend's water absorption capabilities. The CP-2 blend absorbs maximum water as compared to other blend. The membrane with higher water uptake capacity provides poor dimension stability. Due to excessive swelling, dimension stability of the CP-2 blend will decreases. Hence, CP blend is considered to be a better candidate for fuel cell application. Moreover, the cross-linking of CP blend with sulphuric acid increases water uptake capacity. The water molecules were strongly attached with the sulfonate groups (S=O) of crosslinking agent by hydrogen bond interaction. It was confirmed that the crosslinking reaction transform the membrane to more compact and dense due. The void space available in the membrane was depleted. Due to the lack of free space, the intake of free water will reduces. However, it was observed that the cross-linking reaction improves water uptake capacity. The water absorbed in the membrane were strongly attached with the polymer chain and are termed as bound water. Due to cross-linking, higher bound water was present in the membrane. The bound water has significant impact on water absorption capacity of the membranes. The enhancement of water absorption capacity was noticed with the increase of bound water. The CPH blend has lower water absorption capacity than the CPH-1 and CPH-2 blends. Moreover, the increase of bound water in a CP blend improves its dimension stability. The CP blend have more ion exchange sites as compared to CP-1 and CP-2 blend. Due to more ion transport sites, CP blend has higher IEC than other blend. Moreover, the cross-linking reaction improves ion transport sites in the blend. During cross-linking, sulphuric acid gives H^+ and SO_4^{2-} ion in a polymer solution. The diffusion of SO_4^{2-} ions to the backbone of blend creates extra in transport sites. Hence, cross-linked blend provides more IEC than the pure blend. It was observed that the CPH blend provides maximum IEC among the blends. Moreover, Chitosan and PVA were highly compatible with each other

in the CPH blend. The IEC and water uptake study suggest that the CPH blend will be good candidate of DMFC application. However, for practical application, IEC of the blend should be enhanced to achieve better proton conductivity. The dimension stability of the blend should be improved to provide better stability at stressed conditions. The architecture of the CP blend was modified to achieve better proton conductivity at reduced humidity conditions. The different filler like red mud, multiwall carbon nanotubes, hygroscopic zirconia and ionic liquid were incorporated in a CP blend to improve its bound wand, IEC as well as dimension stability at reduced humidity conditions.

Table 6.1: Physical, mechanical and chemical properties of the CP blends.

Samples	**Water Uptake (%)**	**IEC (meq/g)**	**χ_c (%)**	**Tensile Strength (MPa)**	**Elastic Modulus (MPa)**	**Methanol Permeability, P×10^{-7} (cm^2/Sec.)**
CP	133	0.575	15.46	42.08	1379.41	2.42
CP-1	136	0.413	18.24	38.73	1250.23	3.18
CP-2	145	0.328	22.34	20.41	402.46	4.67
CPH	138	0.832	8.32	46.12	448.44	0.34
CPH-1	147	0.71	12.46	41.28	387.19	1.46
CPH-2	154	0.64	17.38	23.82	405.44	1.74

The water uptake and IEC of the red mud modified CP blends are represented in **Table 6.2**. The addition of red mud nanoparticles as a filler increases water uptake capacity. The presence of hygroscopic group like SiO_2, Al_2O_3 and Fe_2O_3 are responsible for the enhancement of water absorption capacity in a membranes. The water absorbing ability of the membrane gradually increases with the increase of red mud weight percent. The maximum water uptake capacity was observed in CPR-4 membrane. The hydrogen bond tightly linked the water molecules to the hygroscopic filler. The interaction between water and SiO_2 by strong hydrogen bond was

confirmed in a literature studies [**67**]. Moreover, addition of filler creates a void space inside the membrane. The polymer chain interaction was disturbed by the filler and creates a void space inside the membrane. The formation of void space in a membrane due to the addition filler was confirmed in a literature [**68**]. The water uptake was enhanced by the combined effect of hygroscopic filler and void volume in a composite membrane. Due to strong interaction of water with the filler, bound water content in a membrane was increases. The interaction between filler and water via hydrogen bond was highly reliant with the increase of red mud weight in a composite membrane. The more amounts of silica or alumina atom were bonded with water and improves bound water content. The bound water content of the membranes were measured from the endothermic peak of DSC heating scan. During the heating scan, an endothermic peak at 0°C was noted for all samples, which was attributed to ice melting or enthalpy of fusion of water. After measuring enthalpy of fusion, bound water of the membrane was obtained. The detailed procedure for obtaining bound water from enthalpy of fusion was reported by Awang et al. [**69**]. The bound water acquired by the membranes are reported in **Table 6.2**. The bound water of the membrane was increased as the amount of filler increased. The higher bound water was observed in a CPR-4 membrane. At moderate temperature, membrane with higher bound water provides favourable performance. The proton transport was governed by bound water and improves fuel cell performance. The addition of 4wt. (%) red mud filler to a CP blend raises the bound water from 4.68 to 13.73%. Moreover, dimension stability of the membrane was enhanced with a decline in free water. The membrane becomes less hydrophilic with better dimension stability. The diffusion of water in a membrane was assumed to be controlled by fickian diffusion. Water uptake data reported at different time intervals was fitted to a fickian diffusion model to determine water diffusivity. The proposed fickian diffusion model is represented in **equation-4.5**. The goodness of fit of a model (R^2) to the experimental data for different membrane is reported in **Table 6.2**. The experimental water

uptake data of all the membranes were perfectly fitted to a model. The obtained diffusivity of the membranes were in the order of 10^{-6}. In a literature, similar result was reported for Chitosan based membrane [**38**]. The impregnation of hygroscopic filler to a membrane increases water diffusivity. The water diffusion was catalysed by the presence of hygroscopic filler.

The addition of red mud to a CP blend increases IEC. The ion transport sites of the membrane was enhanced due to the availability of free space in a polymer blend. The creation of free space in a polymer domain increases ion transport sites. The CPR-3 membrane provides maximum IEC among the modified membranes. We have observed that the red mud particles were soft aggregated in a polymer domain of CPR-3 membrane. Due to well dispersed and softly aggregated red mud particles, it has least significant impact on IEC of the membrane. Moreover, the presence of silica dioxide increases ion transport sites of the membrane. It was reported in a literature that the inclusion of silica oxide to a membrane increased its IEC [**68**]. The IEC of the CPR-4 membrane was lower than CPR-3 and CPR-2 membrane. The red mud particles were hardly aggregated in the polymer domain which restricted ion migration. Moreover, the ion migration sites was depleted in a CPR-4 membrane. The hard aggregation of red mud particles in a CPR-4 membrane was confirmed in a FESEM images.

Table 6.2: Water uptake capacity, IEC, degree of crystallinity and bound water content of the red mud modified CP blends.

Samples	**Diffusivity (cm^2/sec) × 10^{-6}**	**Fickian Fit (R^2)**	**Water Uptake (%)**	**IEC (meq/g)**	**Bound Water (%)**	**χ_c (%)**	**Young's Modulus (MPa)**
CS/PVA	3.78	92.7	133±5	0.57±0.04	4.68	12.46	1379.41
CPR-1	5.26	94.3	136±8	0.61±0.03	7.42	9.21	175.47
CPR-2	6.78	98.2	144±6	0.66±0.05	9.89	7.46	109.7
CPR-3	9.02	99.5	149±3	0.71±0.06	12.26	3.72	102.79
CPR-4	9.87	99	153.5±4	0.62±0.04	13.73	2.16	----

The water uptake and IEC of the CNT and ionic liquid modified hybrid membranes are reported in **Table 6.3**. The addition of CNT as a filler reduces water uptake capacity of the CP blend. The CPCN-1 blend provides lower water uptake capacity. The hydrophobic nature of CNT reduces water absorption capacity of the membrane. However, increasing the amount of filler resulted in a considerable improvement in water uptake. **Figure 6.2(a)** depicts the influence of CNT quantity on membrane water uptake. The filler will creates a void space in the polymer domain which improves water uptake capacity. The formation of void space in a polymer domain was confirmed in a FESEM analysis. The CPCN-3 membrane provides maximum water absorption capacity. The water uptake capacity in a CPCN-4 was lower than the CPCN-3 membrane. The water absorption capacity was reduced due to the aggregation of CNT filler in the polymer domain. Due to aggregation, void space available in the membrane was drastically reduces which eventually decreases water uptake capacity. The ionic liquid incorporated hybrid membrane provides higher water uptake capacity. The ionic liquid contained a sulfonate (S=O) group that reacted with water to form a hydrogen bond. The hydrophilic nature of an ionic liquid was enhanced by the presence of sulfonate group. Hence, ionic liquid modified hybrid membrane provides better water absorption capacity. The bound and free water of the hybrid membrane was experimentally determined and reported in **Table 6.3**. The bound water of the hybrid membrane was gradually increased with the increase of CNT filler. The highest bound water was observed in an ionic liquid modified hybrid membranes. The water molecules were strongly attached with the base of ionic liquid, increasing the amount of water bonded to it. **Figure 6.2(b)** depicts the influence of CNT quantity on the swelling degree of the hybrid membrane. The swelling degree of CPCN hybrid membrane was lower than the ionic liquid modified membrane. Due to hydrophilic nature of ionic liquid, membrane modified by ionic liquid provides higher swelling degree. It was believed that the CPCN hybrid provides better dimension stability that the ionic liquid modified

membrane. The addition of CNT as a filler in a CP blend reduces IEC. It was believed that the hooping sites for ion migration was blocked due to the filling effect of CNT. Moreover, the free water of the membrane was reduced, limiting ion movement. The increase of filler content in a hybrid membrane increases IEC. The significant improvement of IEC was observed in an ionic liquid modified membrane. The presence of ionic liquid aided migration sites of ion transport. The IEC of the CPCN@IL-4 hybrid membrane was highest among the fabricated membrane.

Table 6.3: Physical, chemical and mechanical properties of the MWCNT and ionic liquid modified CP blends.

Samples	**IEC (meq/g)**	**Water Uptake (%)**	**Swelling Ratio, SR (%)**	**Free Water (%)**	**χ_c (%)**	**Tensile Strength (MPa)**	**Elastic Modulus (MPa)**	**Tensile Strain at Break (%)**
CPCN-1	0.08	89.36	27.28	23.62	25.25	18	126	94.26
CPCN-2	0.12	118.4	41.62	22.98	23.73	16	89.25	113.94
CPCN-3	0.16	140	51.85	20.63	22.90	13	78	127.46
CPCN-4	0.22	128.43	46.71	19.21	16.75	10	56	138.52
CPCN@IL-1	0.18	132.14	52.78	19.10	23.38	15.36	82.46	178.57
CPCN@IL-2	0.35	170.58	62.50	17.62	21.15	12.63	59.47	162.58
CPCN@IL-3	0.74	184.38	74.16	15.23	18.73	9.41	30.18	134.51
CPCN@IL-4	0.86	144.23	68.08	12.87	14.76	6.2	23.97	112.58

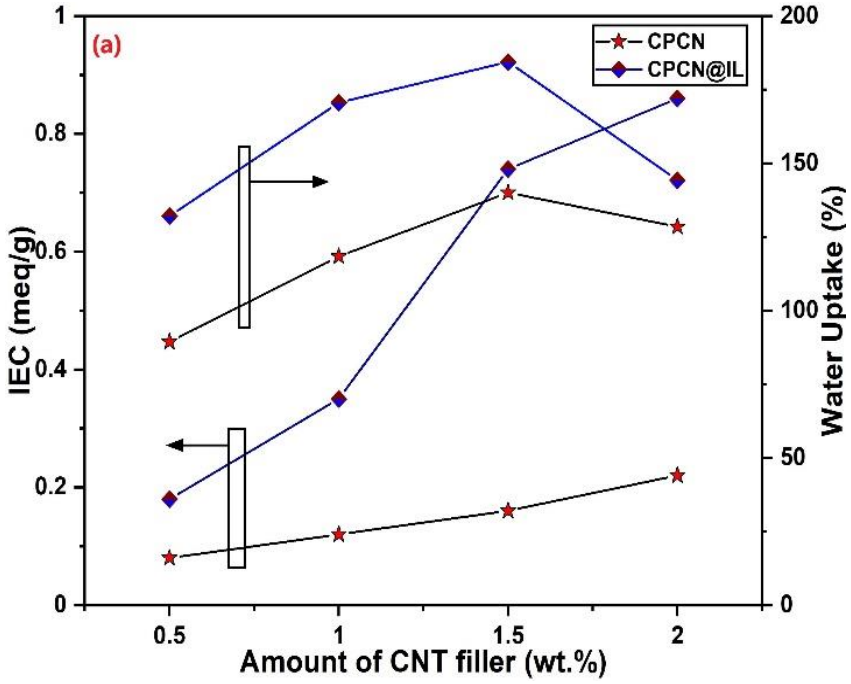

Figure 6.2 (a): Effect of MWCNT content on IEC and water uptake of the membranes.

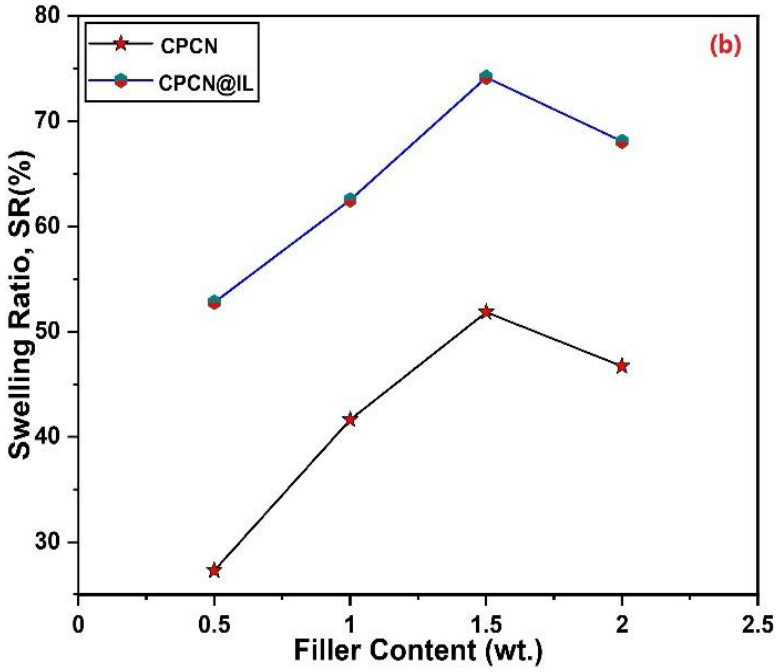

Figure 6.2 (b): Effect of MWCNT content on swelling area of the membranes.

The CP blend was further modified with hygroscopic zirconia and ionic liquid to improve its IEC and bound water content. The incorporation of hygroscopic zirconia to a CP blend increase water uptake capacity and bound water content. The water uptake and bound water content of the CPZr hybrid membrane is reported in **Table 6.4**. It was confirmed that the addition of zirconia to a blend depleted void volume. The depletion of void space in a membrane was confirmed by FESEM analysis. The depletion of void space in a membrane reduces free water intake. Hence, the overall water uptake was reduced in a hybrid membrane. However, bound water content of the membrane was increases. The zirconia atom was strongly interacted with the water molecules and improves bound water content. The enhancement of membrane's bound water by zirconia was reported in a literature [**70**]. Due to this fact, free water of the membrane was gradually reduces as the amount of zirconia increases. The presence of sulfonate group (S=O) in an ionic liquid modified membrane contributes additional bound water content. The base of ionic liquid i.e. sulfonate group was strongly interacted with water molecules via hydrogen bond. The increase of bound water in an ionic liquid modified membrane was due to the combine effect of zirconia and ionic liquid. The increase of bound water in an ionic liquid modified membrane is reported and CPZr@IL-4 hybrid membrane provides highest bound water content. The increase of bound water in a membrane is beneficial for fuel cell application at moderate temperature. The presences of bound water in a membrane reduces loss of water due to evaporation and improves proton conductivity. Hence, the modified membrane is considered to be a potential candidate for fuel cell application. However, the hydrophilic nature of ionic liquid enhances swelling area of the membrane. It was observed that the swelling degree of the membrane was controlled by zirconia amount. The influence of zirconia amount on swelling degree of the hybrid membranes are represented in **Fig. 6.3(b)**. The swelling degree of the membrane was reduces with the increase of zirconia amount. The swelling degree of CPZr hybrid membrane was lower than the ionic liquid modified hybrid

membrane. It is believed that the CPZr hybrid membrane provides better dimension stability than the ionic liquid modified hybrid membrane. The impact of filler on IEC of the membrane is represented in Fig. 6.3(a). The addition of filler to a polymer domain depleted ion migration sites thereby reducing IEC. The similar result was reported in a literature [30, 43 & 50]. However, the modification of CPZr hybrid membrane with ionic liquid increases IEC. The presence of ionic liquid in a membrane creates extra ion migration sites for ion transport. Therefore, ionic liquid membrane provides better IEC than the CPZr hybrid membrane. Adding an aprotic liquid to the hybrid membrane introduces additional imidazolium cations and increases IEC [**71**]. However, the aggregation of filler in an ionic liquid modified hybrid membrane influence IEC of the membrane. The ion migration sites were blocked by the presence of aggregated zirconia. Hence, CPZr@IL-4 hybrid membrane provides lower IEC than the CPZr@IL-3 hybrid membrane.

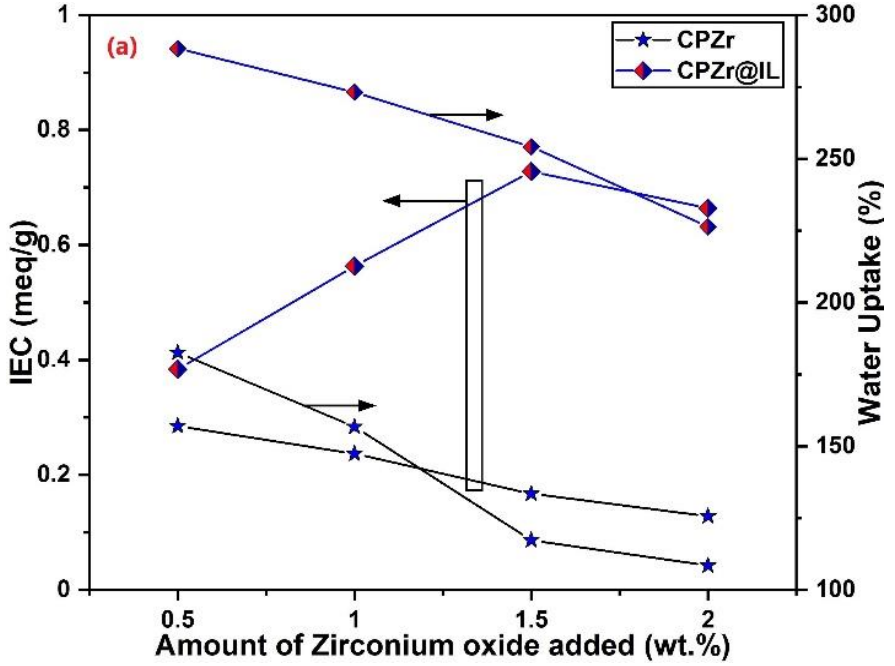

Figure 6.3 (a): Effect of zirconia content on IEC and water uptake of the membranes.

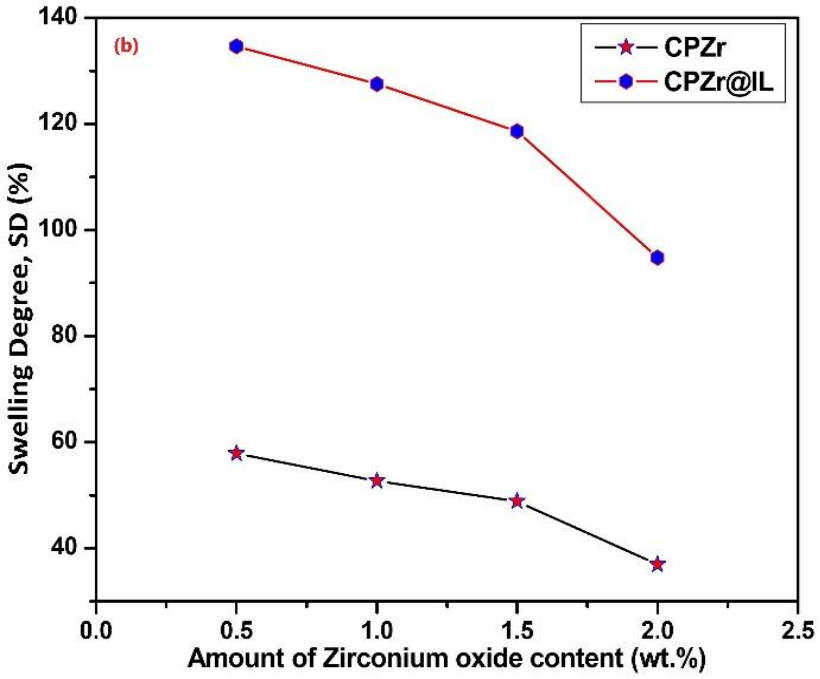

Figure 6.3 (b): Effect of zirconia content on swelling degree of the membranes.

Table 6.4: Physical, chemical and mechanical properties of CP blends modified with hygroscopic zirconia and ionic liquid.

Sample Code	IEC (meq/g)	WU (%)	Swelling Degree, SR (%)	Free Water (%)	χ_c (%)	Tensile Strength (MPa)	Young's Modulus (MPa)	Elongation at Break (%)
CPZr-1	0.285	182.50	57.89	62.13	25.05	15.89	129.18	113.94
CPZr-2	0.237	156.74	52.72	43.36	14.86	17.39	92.17	167.16
CPZr-3	0.167	117.31	48.83	40.79	11.22	13.56	59.47	142.58
CPZr-4	0.128	108.41	36.95	36.73	9.59	11.29	30.18	29.43
CPZr@IL-1	0.384	288.33	134.63	35.26	22.32	16.53	44.36	128.61
CPZr@IL-2	0.563	273.21	127.5	31.68	11.94	18.19	23.97	145.38
CPZr@IL-3	0.728	254.21	118.64	24.47	8.47	10.59	17.52	156.74
CPZr@IL-4	0.664	226.36	94.83	14.38	7.51	6.72	14.41	171.28

The IEC, water uptake and bound water of the Chitosan based membranes are compared with SPEEK based hybrid membrane. The IEC, water uptake and bound water content of the SPEEK based hybrid membranes are reported in **Table 6.5**. The modification of SPEEK membrane with PVA and silicon dioxide reduces its IEC. The filling effect of SiO_2 depleted migration sites for ion transport. However, it was also observed that the water absorption capacity of the membrane was enhanced. The hygroscopic nature of silicon dioxide improves water uptake capacity of the membrane. The silicon dioxide was strongly interacted with water molecules via hydrogen bond. Due to strong interaction with water molecules, bound water content of the membrane was enhanced. The hydration number of all the membranes are calculated and reported in **Table 6.5**. The number of water molecules linked per sulfonate group increased as the filler amount increased. Hence, bound water content of the membrane was increases in a modified membrane. The SPS-3 membrane provides highest bound water content. The filler was aggregated in the polymer domain of SPS-4 membrane which reduces IEC, water uptake and bound water content. The aggregated silica blocks ion migration sites in a polymer domain. The water diffusivity of the membrane was increases with the increase of filler amount. The

IEC of Chitosan based membrane was lower than the SPEEK based membrane. However, Chitosan based membrane provides higher water uptake and bound water content which is beneficial for low temperature application. Moreover, the chitosan membrane has higher bound water content which it preferable candidate for moderate temperature applications. The higher bound water content in a Chitosan based membrane improves proton conductivity at moderate temperature.

Table 6.5: Physiochemical properties of the SPEEK-PVA-silica hybrid membranes.

Sample	IEC (meq/g)	DS (%)	λ	WU (%)	Bound Water (%)	Methanol Uptake (%)	Water Diffusivity ($cm^2/sec.)\times10^{-6}$
Recast SPEEK	2.12	73.72	7.34	28	1.23	38	5.21
SPEEK-PVA	1.84	62.28	7.54	25	1.16	35	4.29
SPS-1	1.79	60.29	9.31	30	3.14	33	7.39
SPS-2	1.75	58.72	10.79	34	5.46	27	9.16
SPS-3	1.64	54.46	12.19	36	7.83	22	10.42
SPS-4	1.46	47.68	12.17	32	4.26	18	8.56
N117	0.93	----	----	25	2.15	27	3.91

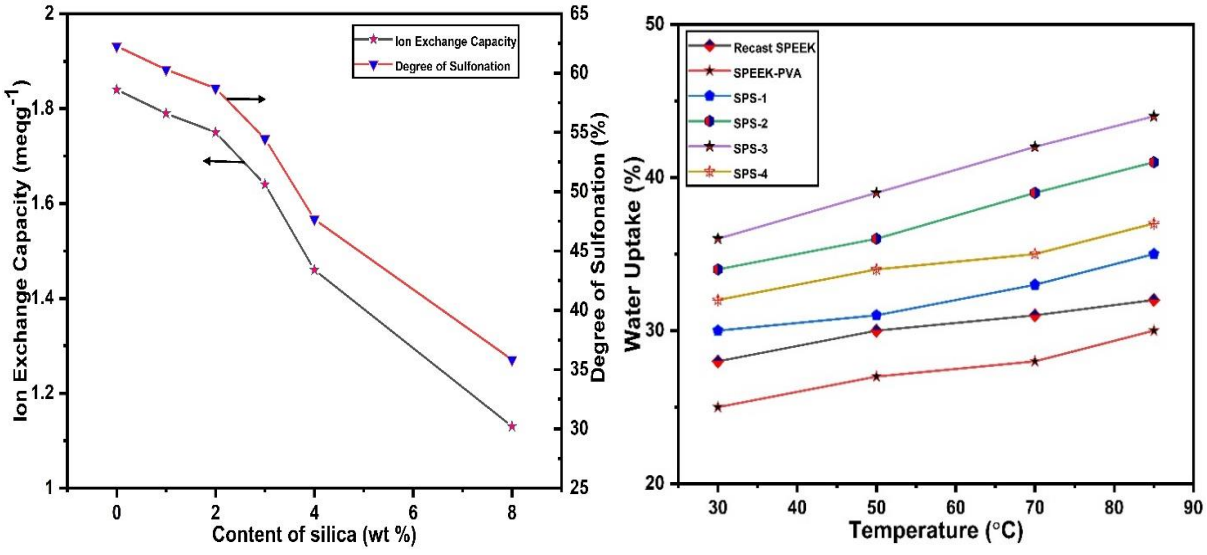

(a) **(b)**

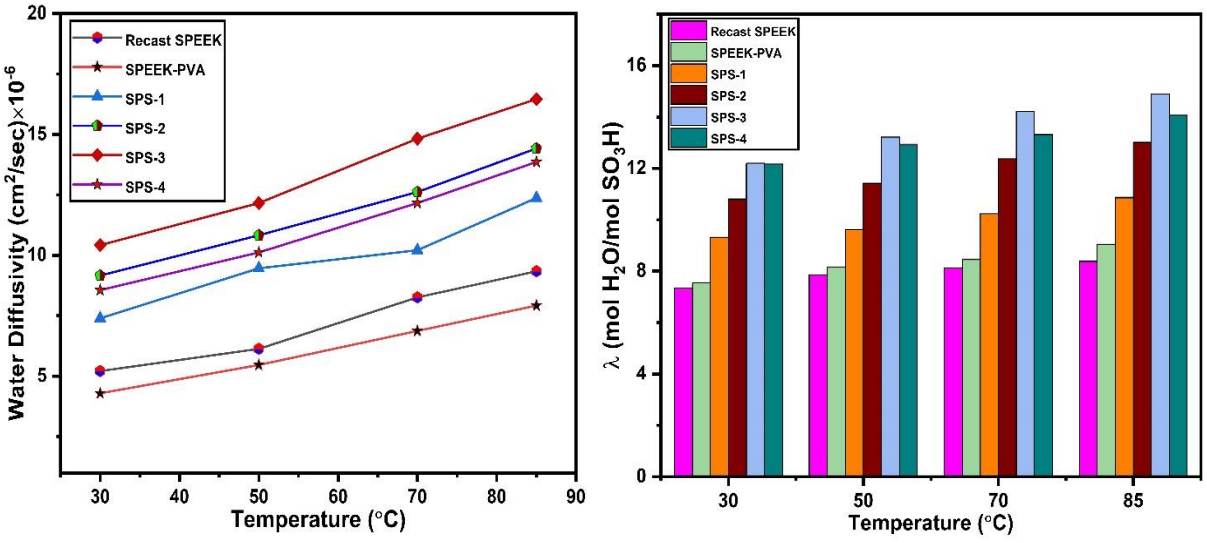

(c) **(d)**

Figure 6.4: Physical and chemical properties of the SPEEK-PVA-silica hybrid membranes (a) Effect of silica content on IEC and DS of the membranes; Effect of temperature on (b) water uptake capacity (c) Water diffusivity and (d) Hydration number.

6.2 Thermal Property Analysis

6.2.1 Differential Scanning Calorimetry Analysis

The temperature dependent phase transition behaviour of the membranes are studied. The glass transition temperature (T_g) of the membranes was evaluated from the phase transition behaviour. The T_g is an important parameter of an electrolyte membrane which affects fuel cell performance. The stability (mechanical and thermal) of the membranes were greatly influenced by their glass transition temperature. The membrane with high T_g breaks at lower strain which reduces its mechanical stability. The fuel cell is designed using the knowledge of glass transition and melting temperature of an electrolyte membrane. The glass transition temperature of the membrane plays a crucial role during MEA preparation. The membrane was hot pressed in an electrode by thermal treatment process. The MEA was thermally treated in the range of 120-140°C to increase the interfacial adhesion between membrane and electrodes. Therefore, T_g of the developed membrane should be in the range of 120-140°C to provide better interfacial stability of the MEA. In general, amorphous and crystalline phase of membrane contributes glass transition and melting temperature respectively. The DSC heating scan of the membrane was conducted to evaluate its glass transition and melting temperature. During heating scan, two sharp endothermic peak was appeared for semi crystalline membrane. The first peak relates to the phase change from glassy to rubber phase, or glass transition temperature, and the second peak corresponds to crystal melting, or melting temperature. However, in case of non-compatible blend, two stage phase transition was observed at amorphous region. First and second stage phase transition correspond to the phase relaxation of PVA and Chitosan. The glass transition and melting temperature of the CP blends were evaluated from the heating curve of DSC and reported in **Table 6.6**. The DSC heating scan of the CP blends are shown in **Fig. 6.5.** In the table, T_{g1} and T_{g2} corresponds to the glass transition temperatures of PVA and Chitosan in a non-compatible blend. Moreover, the glass transition

temperature of the compatible blends are represented by T_g. The appearance of a strong endothermic peak at higher temperatures corresponds to crystal melting. The CP blend provides lower glass transition temperature. Non-compatible blends, on the other hand, have higher glass transition temperatures than CP blend. The increased crystalline phase in a non-compatible blend limited the mobility of the polymer chain. The increased of crystalline phase in a non-compatible blend was confirmed by XRD analysis. Moreover, the presence of more crystalline phase delayed melting temperature. The cross-linking of CP blend with sulphuric acid fastened phase transition from glassy to rubbery phase. The mobility of the polymer chain was fastened due to the depletion of crystalline phase. The sulfonate group of sulphuric acid was interacted with the hydroxyl group of CP blend and depleted the crystalline phase. T_g value of the CPH blend was 110°C which was slightly lower than the CPH-1 and CPH-2 blend. Moreover, the crosslinking reaction reduces melting temperature of the blend.

The CP blend was further modified with red mud nanoparticles and their phase transition behaviour was studied. The addition of red mud to a CP blend depleted crystalline phase. The depletion crystalline phase in a CPR membrane was confirmed by XRD analysis. Due to depletion of crystalline phase, mobility of the polymer chain was enhances. Moreover, the addition of filler creates a free space in the polymer domain which catalysed polymer chain mobility. The fastening of polymer chain mobility enhances phase transition from glassy to rubbery phase. As a result, the glass transition temperature of the CPR membrane was lower than that of the CP blends. The addition of 4wt. (%) red mud nanoparticle to a CP blend reduces the T_g value from 134°C to 117°C. The glass transition temperature of the CPR membrane was lower than the CPH blend. The lower glass transition temperature of the membrane reduces its mechanical strength and increases its swelling degree. Due to its lower glass transition temperature, MEA was treated at lower temperature. However, hot pressing of membrane in an electrodes at lower temperature resulted poor interfacial adhesion. Moreover, the interfacial

adhesion was weakened due to the dimension change of membrane. The dimension change was occurred due to its higher swelling degree. The fuel cell performance was reduce due to its poor interfacial stability. The glass transition temperature of the membrane should be optimized to improve fuel cell performance. The melting temperature of the membrane was reduces with the increase of red mud amount. The crystalline phase of the membrane contribute melting temperature. It was confirmed that the increase of filler amount to a CP blend reduces crystalline phase. Due to the depletion of crystalline phase, melting temperature of the crystalline phase was reduces.

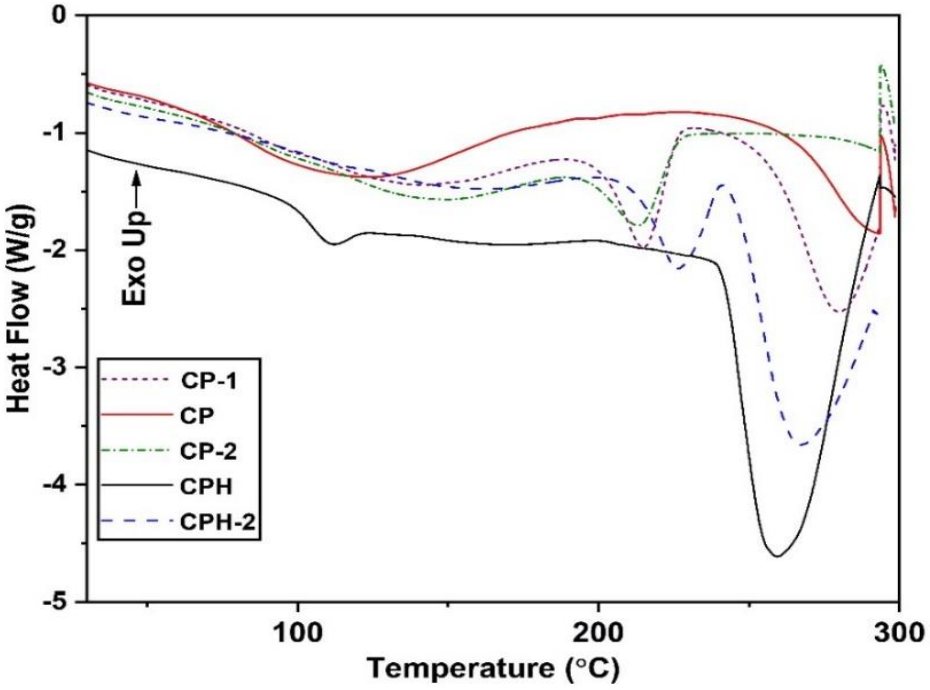

Figure 6.5: DSC heating plot of the CP and cross-linked membranes.

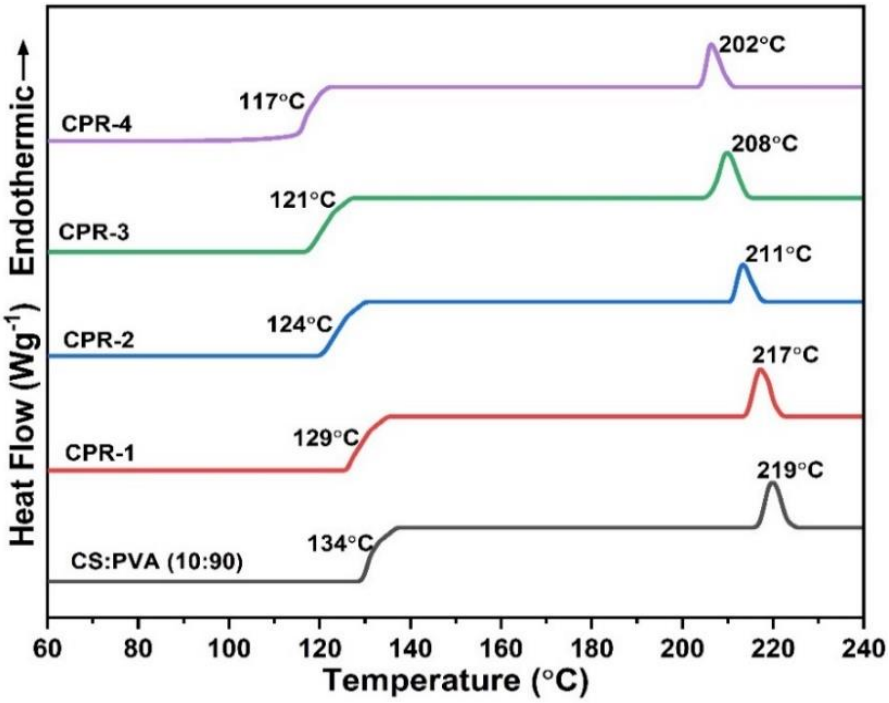

Figure 6.6: DSC heating plot of the red mud modified CP blends.

The CP blend was modified with ionic liquid and carbon nanotubes (CNT) to improve its thermal stability. The effect of ionic liquid and CNT filler on phase transition behaviour of CP blends were studied. The DSC heating profile of the modified membranes are shown in **Fig. 6.7.** The addition of CNT to the CP blend improves polymer chain mobility. The CNT filler will act as a plasticizing effect which reduces glass transition temperature. The CNT filler depleted the crystalline domain of the membrane and improves polymer chain mobility. The glass transition temperature of the membrane was reduced as a result of increased chain mobility. The CNT modified CP blends provide higher glass transition temperature than the red mud modified membranes. The T_g values of the CPCN membranes was between 115 and 135°C. The CPCN membranes were considered to be an ideal candidate for fuel cell application. However, CPCN membrane provides lower water uptake capacity. To improve its water uptake capacity, it was modified with ionic liquid. However, ionic liquid reduces glass transition temperature of membrane. The ionic liquid interacted with the groups which are responsible for crystalline phase in the membrane. The membrane's crystalline phase was depleted as a result of ionic bond interaction. The ionic liquid has an ability to reduce T_g of the membrane by depleting crystalline phase [**71, 72**]. The phase transition from glassy to rubbery phase was fastened due to the depletion of crystalline phase. The ionic liquid improves chain flexibility of the membrane. But membrane provides poor interfacial stability due to its lower glass transition temperature. The ionic liquid has significant effect on interfacial stability of the CPCN membrane. There was no significant changes in melting temperature of the membrane.

To improve fuel cell performance at moderate temperature, CP blend was further modified with hygroscopic zirconia and ionic liquid. The hygroscopic zirconia was added to increase its water uptake capacity. Moreover, ionic liquid was added to increase ion migration sites in the membrane. The glass transition temperature of the membrane was evaluated to measure its

thermal stability. The glass transition and melting temperature of the modified membrane were obtained from DSC heating profile. The heating curve of the modified membranes obtained from DSC experiment is shown in **Fig. 6.8**. The glass transition temperature of CPZr-1 membrane was 146.78°C which was slightly higher than CP blend. The hygroscopic zirconia contributes crystalline phase of the membrane. However, with the increase of zirconia amount, crystalline degree of the membrane was reduces. The zirconia atom interacted with the hydroxyl group of blend and reduces crystalline phase. Hence, the mobility of the polymer chain was enhanced. Moreover, the creation of void volume in a polymer channel catalyzer phase transition behavior. The CPZr membranes provide the T_g values between 126 and 147°C. The interfacial stability of CPZr membranes were higher than the CPCN membranes. However, the modification of CPZr membrane with ionic liquid reduces its interfacial stability. The modified membrane will provide lower glass transition temperature. The ionic liquid enhances polymer chain mobility which fastened phase transition behavior. The glass transition temperature of the CPZr@IL membranes are in the range of 120-135°C. The T_g values of the CPZr@IL membrane was slightly higher than the CPCN@IL membrane. The use of an ionic liquid had least impact on thermal stability of the CPZr membrane. The CPZr@IL membrane will provide better thermal stability and an ideal candidate for fuel cell application.

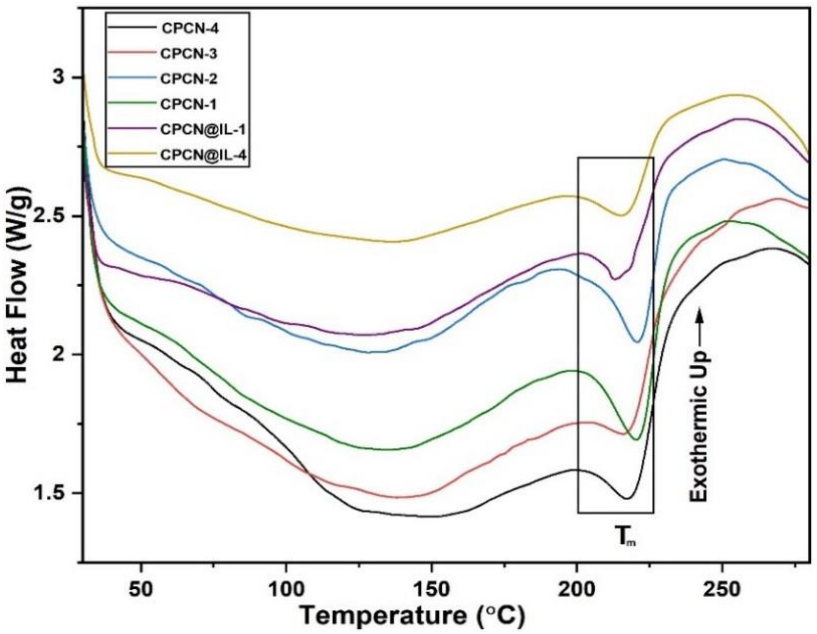

Figure 6.7: DSC heating plot of the MWCNT & ionic liquid modified CP blends.

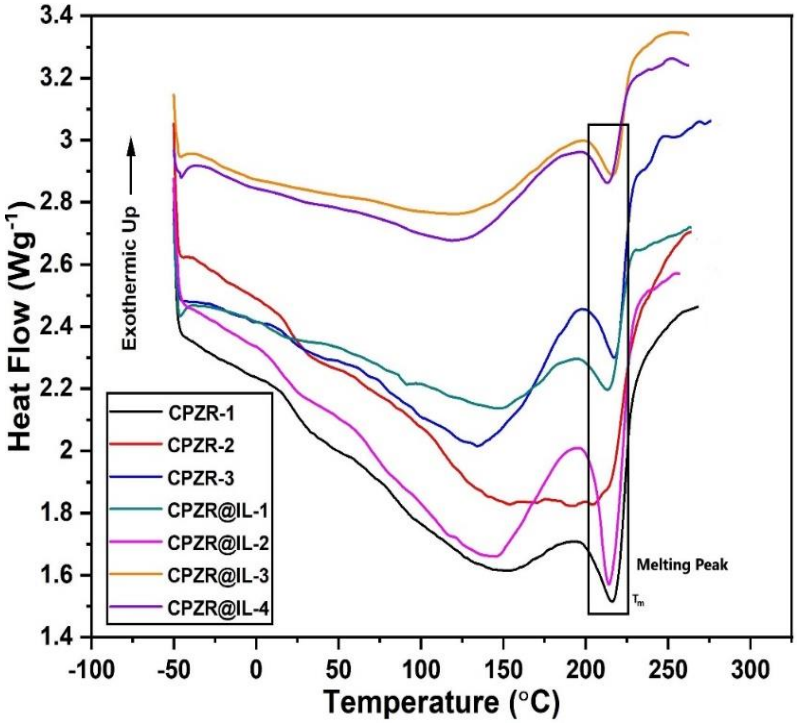

Figure 6.8: DSC heating plot of the zirconia & ionic liquid modified CP blends.

The T_g values of the Chitosan based membranes were compared to the SPEEK-based membranes and commercial Nafion membranes. The heating curve obtained from the DSC scan of SPEEK hybrid membrane is shown in **Fig. 6.9**. The SPEEK membrane modified with polyvinyl alcohol reduces glass transition temperature. It was owing to a possible decrease in the crystalline phase of the membrane, which increases mobility of the polymer chain. The glassy phase was converted to rubbery phase at lower temperature. The SPEEK-PVA blend provides lower glass transition temperature than the pristine SPEEK membrane. Further reduction of glass transition temperature was observed in a silicon dioxide modified SPEEK-PVA blend. The incorporation of silicon dioxide to a SPEEK-PVA blend reduces crystalline phase. Moreover, a void space was created in a polymer which helps the polymer chain movement. The T_g values of the SPEEK hybrid membranes were found in the range of 128-146°C. The obtained T_g values of the membranes were slightly higher than the Chitosan based modified membranes and commercial N117 membrane. The T_g value of the commercial N117 membrane was reported in the range of 107-130°C [**72**]. The electrolyte membrane with low glass transition temperate provides poor interfacial stability. Moreover, the increase of glass transition temperature also break at low strain. Hence, glass transition temperature of the membrane should be optimized to improve its thermal stability. The thermally stabile electrolyte membrane provides better fuel cell performance. The T_g value of the CPH and CPR membrane was lower than the SPEEK hybrid membrane and N117 membrane. Due to their lower glass transition temperature, CPH and CPR membranes will provide poor interfacial stability during MEA preparation. However, the glass transition temperature of the CPCN and CPZr membrane was similar to the SPEEK hybrid membrane and N117 membrane. The DSC result suggests that the Chitosan based membrane modified with CNT and zirconia provides good thermal property than the N117 membrane. Moreover, it provides better interfacial stability during MEA fabrication.

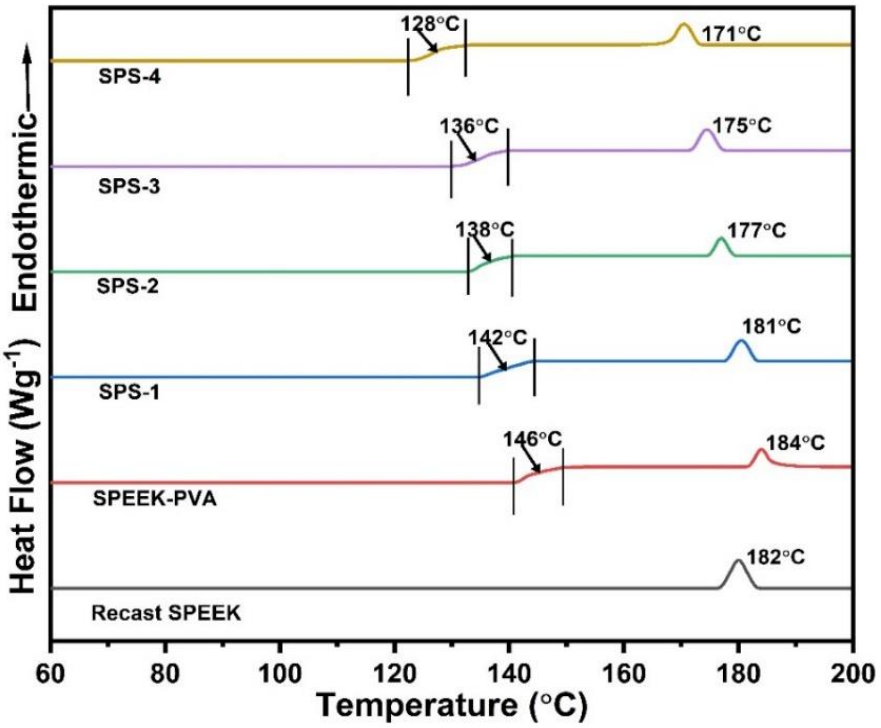

Figure 6.9: DSC heating plot of the SPEEK-PVA-silica hybrid membranes.

6.2.2 Thermo-gravimetric Analysis

The thermal degradation stability of the membrane has a significant impact on fuel cell performance. The membrane with higher thermal degradation stability improves its longevity. Moreover, fuel cell provides better performance for long duration of time without membrane replacement. The membrane with higher thermal degradation stability was appealing for sustainability of fuel cell. The degradation stability of the membrane was studied from the weight loss curve obtained at different temperature. The electrolyte membrane with lower weight loss at 80-200°C was considered for ideal candidate for fuel cell application. In this temperature range, weight loss was mainly occurred in a membrane by evaporation of free water and volatile solvents. The electrolyte membrane with higher bound water content decreases weight loss. The presence of free water was mostly responsible for the weight loss. The presence of bound water kept the proton conductivity at a greater level. Hence, fuel cell will provide better performance at less humidity conditions. The weight loss curve of the membrane was obtained by performing thermal treatment of the membrane in a thermo-gravimetric analyser. The obtained weight loss curve of the pure CP blend and cross-linked with sulphuric acid is shown in **Fig. 6.10**. The weight loss of the blends were categorized in to three stages. During first stage of weight loss, amount of water presents in the membrane was evaporated. Moreover, volatile solvents i.e. acetic acid was also evaporated during this stage. The degradation of oxygen functional group and side chain was observed in second stage of weight loss [**73**]. Moreover, in case of cross-linked blend sulfonate group was degraded. During the third stage of weight reduction, polymer backbone degraded. The weight loss of the blends at different stage is reported in **Table 6.6**. During first stage, weight loss observed in a CP-1 and CP-2 blend was lower than the CP blend. The amount of free water present in the CP blend was greater than the CP-1 and CP-2 blends. Due to its higher free water content, higher weight loss was observed in a CP blend. However, the cross-linking of CP blend reduces weight loss.

The bound water content of the blends was enhances due to strong interaction between sulfonate group and water. The increase of bound water in a blend delays evaporation loss. The lowest weight loss was observed in CPH blend. Due to its lower weight loss, it was considered to be an ideal candidate for fuel cell application. Moreover, it will provides higher thermal stability due to its lower weight loss. During second stage, bound water was escaped from the polymer domain. The second weight loss stage of the blends was noticed at a temperature ranging from 200 to 400°C. The higher weight loss was observed in a CP blend. In this stage, CP blend was less thermally stable than the other blend. The CPH blend provides excellent thermal degradation stability at the range of 200-370°C. However, when the temperature exceed 370°C, CPH blend provides significant weight loss. The degradation kinetics of the blend was catalysed by presence of sulfonate group and it reduces its thermal stability. During third stage, the polymer backbone of non-compatible blend degraded faster as compared to compatible blend. The final residue in a CPH blend was higher among other blend.

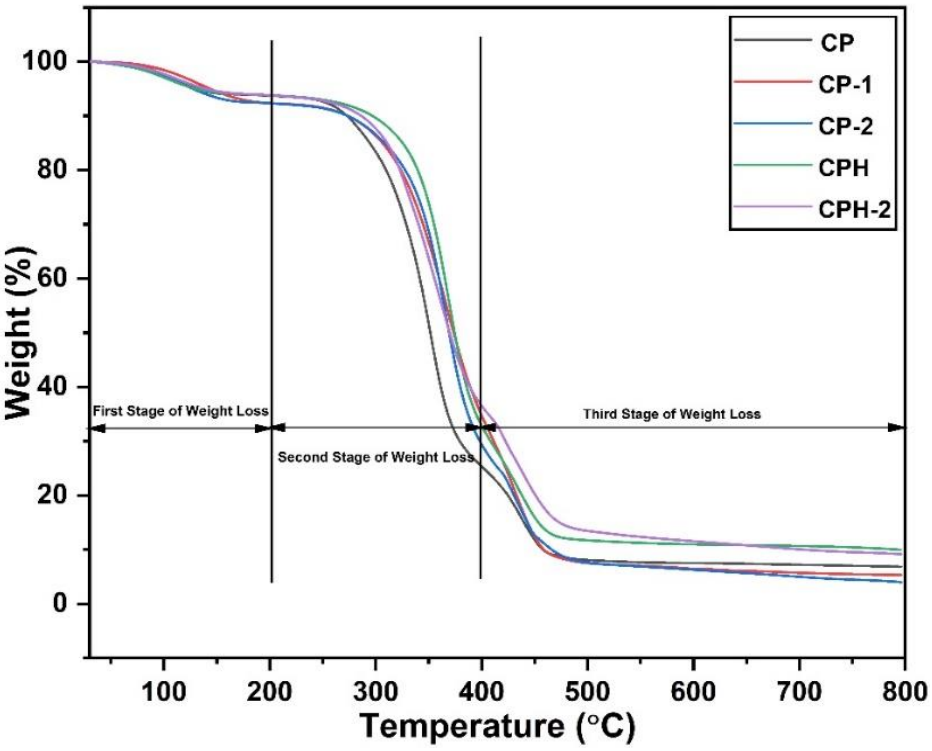

Figure 6.10: Weight loss curve of the CP blends.

Table 6.6: Summary of the obtained DSC and TGA results of CP blends.

Sample Code	$T_{g,1}$ (°C)	T_g (°C)	T_m (°C)	TGA profile data			
				1st stage of weight loss at 200°C (%)	2nd stage of weight loss between 200-400°C (%)	2nd stage of weight loss at 450°C (%)	Final Residue at 790°C (%)
CP	---	133.57	280.17	13.92	42.36	88.18	6.87
CP-1	136.05	---	286.76	7.66	57.64	87.59	5.33
CP-2	143.18	---	293.57	7.82	62.8	87.32	4.08
CPH	---	110.82	259.97	6.14	61.03	84.02	10.03
CPH-1	132.72	---	263.42	6.18	59.61	81.72	9.84
CPH-2	137.40	---	265.27	6.21	57.28	79.75	9.22

The CP blend was further modified with red mud nanoparticles to improve its bound water content and degradation stability. The weight loss curve of the modified membrane is shown in **Fig. 6.11**. During first stage, free water contributes maximum weight loss. Moreover, volatile solvent was evaporated during this stage. The weight loss in a CPR membrane was lower than the CP blend. The addition of red mud nanoparticles in a CP blend reduces free water. The increase of bound water in a CPR blend was already reported. The free water contributes weight loss of the membrane. Therefore, CPR membranes provide lower weight loss as compared to the CP blend. During this stage, CPR membrane provides higher thermal stability than the CP blend. The second stage of weight reduction was noticed at the temperature between 200 and 400°C. During this stage, side chain and oxygen functional group of the membrane was degraded. Moreover, bound water of the membrane also escapes from the polymer domain. At temperature ranging from 200 to 370°C, CPR membrane provides minor weight reduction as compared to CP blend. The presence of filler in a blend prevents side chain deformation of the polymer backbone. The filler like silicon and aluminium oxides are strongly interacted with the polymer backbone. The side chain of the membranes are degraded by the formation of free radicals which initiates degradation reaction. The free radicals were captured by the oxide of fillers and prevents degradation reaction. However, higher weight loss was observed in a CPR membrane when the temperature exceed 370°C. The polymer backbone was degraded faster in a CPR membrane. It was believed that the degradation kinetics was catalysed by the presence of filler in a blend.

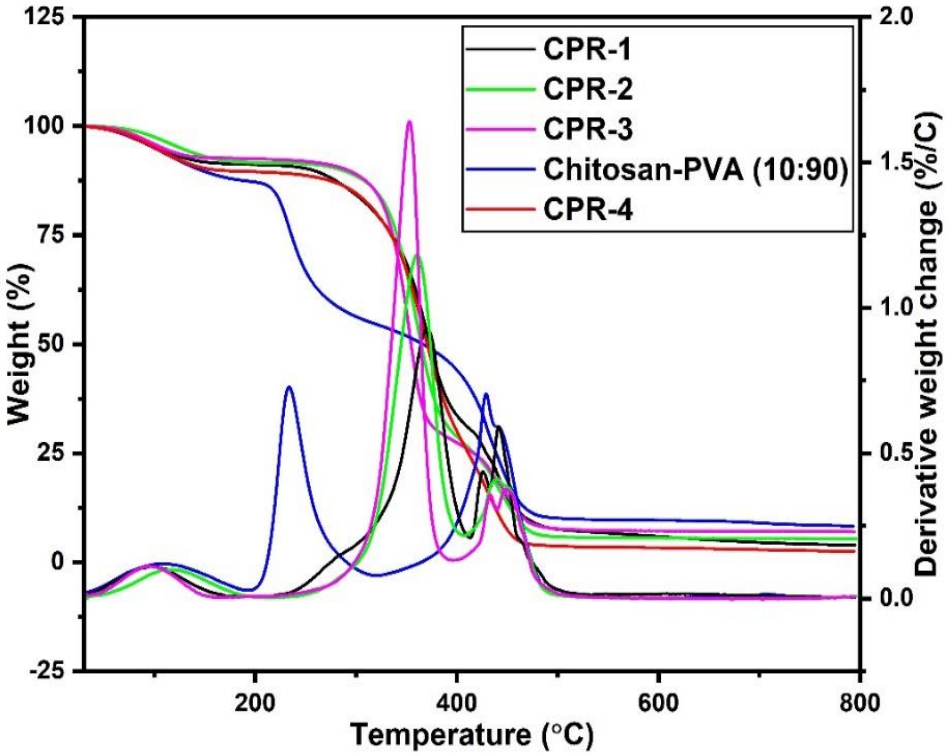

Figure 6.11: Weight loss curve of the red mud modified CP blends.

The effect of ionic liquid and carbon nanotubes on thermal degradation stability of the CP blend was studied. The thermal degradation stability of the modified membranes were analyzed from the TGA curve as shown in **Fig. 6.12**. The first stage of weight reduction was noticed at the range 30-240°C. The summary of weight loss in a CPCN membrane at different temperature region is summarized in **Table 6.7**. The weight loss in a CPCN membrane at 200°C was lower than the CP blend. At 200°C, the amount of water (free water) and volatile solvent evaporated in a CPCN membrane was lower than CP blend. It was also confirmed that the addition of filler (CNT) in a CP blend reduces free water. Therefore, weight loss in a CPCN membrane was lower. When the temperature exceed 200°C, bound water and residual solvent was escaped from the polymer domain. The deformation of side chain along with oxygen and carboxyl group of the membrane was responsible in a second stage of weight loss. In this stage, the strongly attached bound water was escaped from the ionic liquid modified membrane. The CNT modified membrane provides higher weight loss. The degradation of carboxyl group in a membrane contributes maximum weight loss. The carboxyl group present in a membrane was degraded faster. The addition of CNT to a CP blend increases carboxyl group. However, the modification of CPCN membrane with ionic liquid improves thermal stability by reducing weight loss. The ionic liquid was strongly interacted with the functional group (carboxyl group) of the CNT and delays its degradation. The primary weight reduction was noticed due to the breaking of pendant group and bound water evaporation. In literature, it was reported that the pendant group of ionic liquid was degraded between 220 to 350°C [**44**]. However, it was observed that the CPCN@IL-4 membrane provides higher weight loss between 300 to 400°C. The ionic liquid was weakly reacted with the functional group of CNT. The carboxyl group of the CNT was degraded, which contributed to more weight reduction. The main constituents of the membrane was degraded between 450 to 800°C. The weight reduction in an ionic liquid modified membrane was lower than the CPCN membrane.

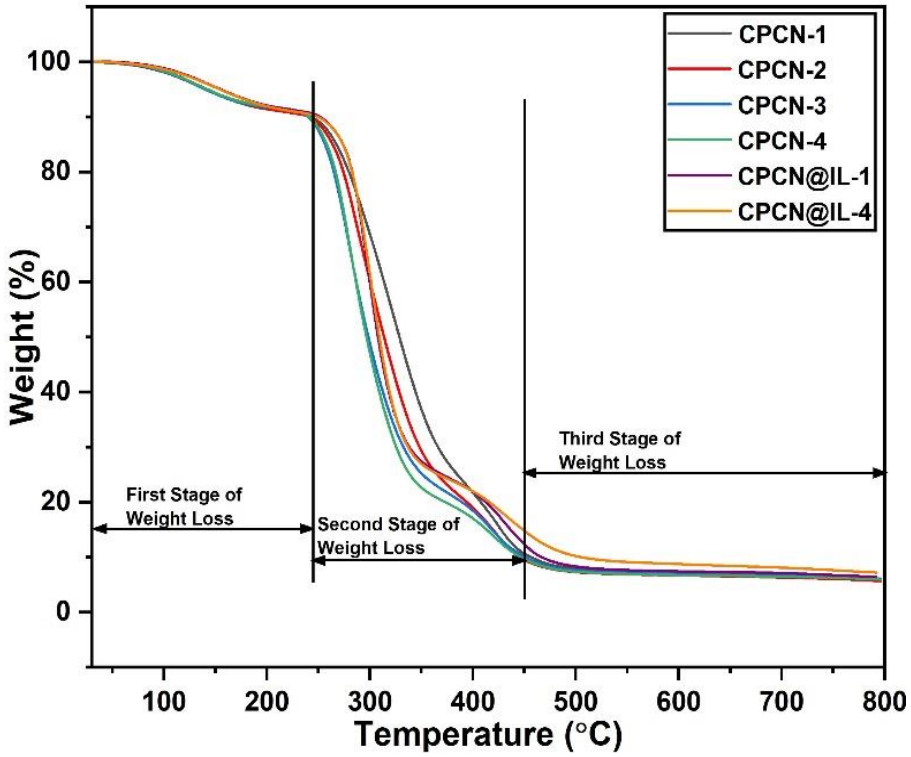

Figure 6.12: Weight loss curve of the MWCNT & ionic liquid modified CP blends.

Table 6.7: Summary of DSC and TGA results of the CP blends modified with MWCNT and ionic liquid.

Sample Code	T_g (°C)	T_m (°C)	TGA profile data			
			1st stage of weight loss at 240°C (%)	2nd stage of weight loss between 240-375°C (%)	2nd stage of weight loss at 450°C (%)	Final Residue at 790°C (%)
CPCN-1	138.07	221.99	9.50	67.19	94.39	5.82
CPCN-2	128.27	219.69	8.846	69.41	93.92	5.64
CPCN-3	126.58	217.58	8.150	69.90	91.46	6.08
CPCN-4	125.32	218.73	8.011	71.36	89.13	5.92
CPCN@IL-1	134.72	217.61	8.857	66.50	87.65	6.43
CPCN@IL-2	131.22	215.81	7.698	64.73	86.21	7.08
CPCN@IL-3	124.38	213.42	6.368	62.92	85.16	7.82
CPCN@IL-4	122.48	214.51	8.611	66.56	83.41	7.21

The CP blend was further modified with ionic liquid and hygroscopic zirconia to improve its bound water content and thermal property. The thermal degradation stability of the membranes were studied from TGA curve which is depicted in **Fig. 6.13**. The different stages of weight reduction noticed in the membrane is highlighted in **Fig. 6.13(a)**. The derivative weight reduction curve of the membrane is depicted in **Fig. 6.13(b)**. The first stage of weight reduction was noticed at the temperature ranging from 30 to 240°C. The water (free and bound water) and solvent were evaporated from the polymer domain. The free water evaporated between 100 and 150°C, whereas the bound water escaped at temperatures above 200°C. The addition of zirconia to the CP blend delays evaporation loss of water. The zirconia particles were strongly interacted with the water and improves bound water. The bound water was escaped from the polymer domain at a higher temperature. Hence, the stability of the membrane was improved at a lower temperature. The weight loss in a CPZr membrane was slightly higher than the CPCN membrane. However, the modification of CPZr membrane with ionic liquid significantly increases its weight loss. The free water contributes maximum weight loss in the membrane. The second stage of weight reduction was witnessed between 240 to 375°C. The side chain along with the oxygen and carboxyl group of membranes were degraded during this stage. The CPZr-1 membrane provides higher weight loss as compared to the other membrane. The increase of zirconia amount in a membrane improve its thermal stability. The zirconia atoms were strongly interacted with the hydroxyl groups of blend which prevents the degradation of oxygen function group. The oxygen function groups were degraded at higher temperature. Due to this fact, carbon atoms were degraded at higher temperature. The amount carbon atoms degraded during this stage was gradually decreases with increase of zirconia amount. The decrease in carbon atom loss in a CPZr membrane is depicted in **Fig. 6.13(b)**. Hence, CPZr membrane with higher zirconia amount provides better thermal stability. At low zirconia concentrations, CPZr membranes modified with ionic liquid reduces weight loss. The zirconia

atoms were reacted with the oxygen functional groups of the membrane and delays its degradation. However, the interaction between zirconia atoms and oxygen suppressed at high concentrations. The ionic liquid was interacted with the oxygen functional group. The weight loss was occurred in an ionic liquid modified CPZr membrane due to the cleavage of pendant group. Moreover, the degradation kinetics of organic compounds was catalyzed by the presence of imidazolium cation [**73**]. Due to thermal splitting of pendant and organic compounds, maximum weight loss of occurred in CPZr@IL-3 and CPZr@IL-4 membrane.

Table 6.8: Glass transition temperature, melting temperature and weight loss values of the CP blends modified with zirconia and ionic liquid.

Hybrid Membrane	T_g (°C)	T_m (°C)	TGA Profile		
			Initial stage of weight loss, 240°C (%)	Total weight loss between 240-375°C (%)	Weight loss of the film at 450°C (%)
CPZr-1	146.79	217.36	10.38	57.91	84.07
CPZr-2	143.49	214.42	10.12	57.07	83.18
CPZr-3	134.77	218.52	9.46	56.88	81.34
CPZr@IL-1	141.87	215.08	16.36	46.42	81.89
CPZr@IL-2	136.74	214.51	14.48	53.88	84.56
CPZr@IL-3	126.17	217.89	13.56	59.53	85.62
CPZr@IL-4	129.43	214.87	19.91	58.56	81.59

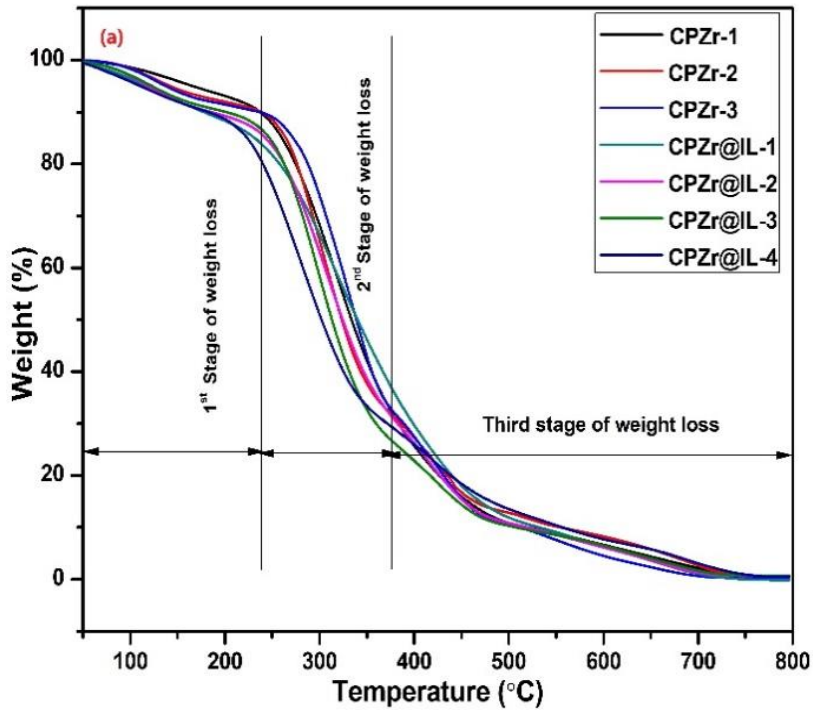

Figure 6.13 (a): Weight loss curve of the zirconia & ionic liquid modified CP blends.

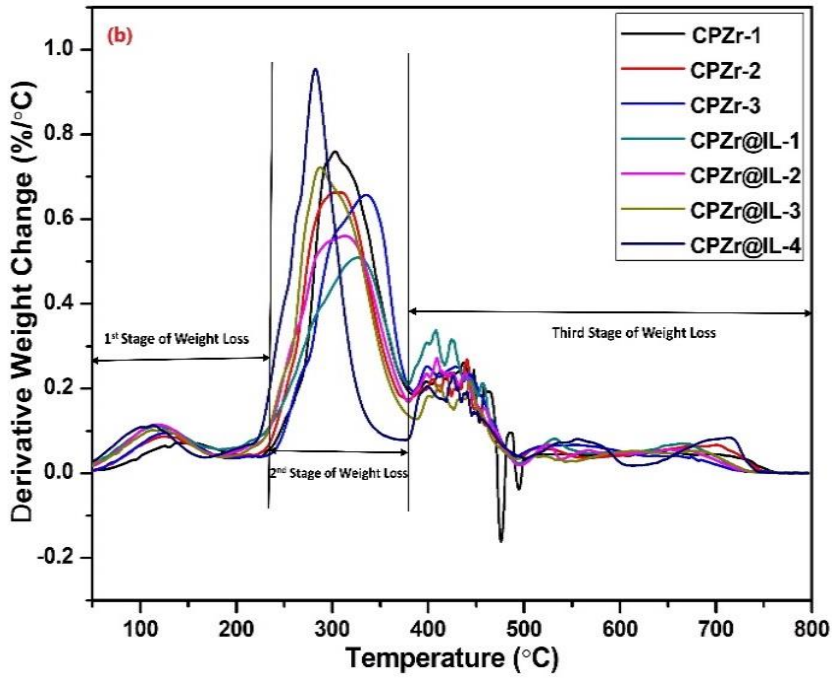

Figure 6.13 (b): Effect of temperature on the derivative weight change of membranes.

The thermal degradation stability of the SPEEK hybrid membranes were studied from the weight reduction profile. The obtained weight reduction profile of the membranes are depicted in **Fig. 6.14**. The three important weight reduction stages was observed in the membrane. The weight reduction stages are highlighted in the TGA profile. In first stage of weight loss, moisture (free and bound water) and volatile solvent were evaporated. The weight reduction was occurred at the temperature between 100 and 200°C. In this stage, dimethyl-acetamide (boiling point: 165°C) was escaped from the polymer domain. During second stage of weight loss, PVA backbone and sulfonate groups were degraded. The increase of silica amount to the SPEEK-PVA domain improves thermal stability. The addition of silica prevents the deformation of oxygen functional group of membrane. The silica particles were strongly interacted with the hydroxyl group of PVA. Due to strong interaction, degradation of PVA backbone was delayed. Therefore, SPS membrane provides lower weight loss than the pristine SPEEK. However, SPS-4 membrane provides more weight loss as compared to other SPS membrane. The silica particles were aggregated to the domain of membrane and not interacted with the PVA. The hydroxyl group of PVA was degraded which increase weight loss of the membrane. Moreover, the strongly attached bound water also escaped from the polymer domain. Finally, the polymer backbone of membrane was degraded between 650 to 800°C. The primal SPEEK membrane degraded faster as compared to the other membrane. The inclusion of filler improves thermal degradation stability of the SPEEK hybrid membranes. Moreover, degradation of membrane's substituents by thermal oxidation was shifted to a higher temperature.

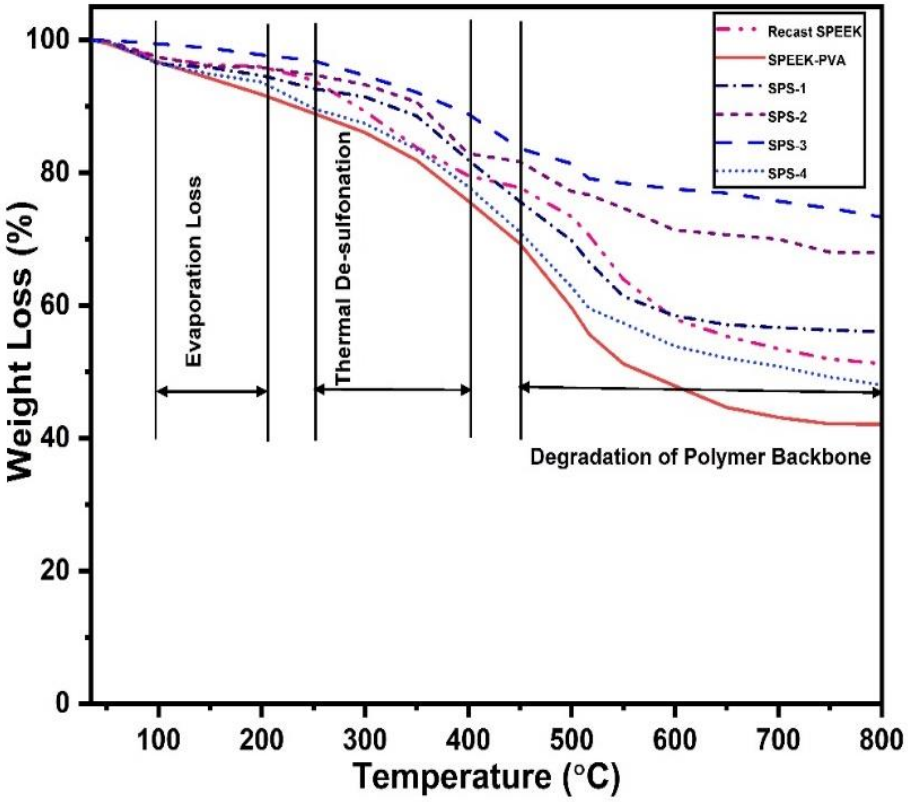

Figure 6.14: Weight loss curve of the SPEEK-PVA-silica hybrid membranes.

6.3 Mechanical Property Analysis

6.3.1 Dynamic Mechanical Analysis

The influence of temperature on phase transition behaviour of the membranes was studied by DMA. The mechanical property of the membranes was highly reliant on its phase transition behaviour. Moreover, the viscoelastic properties of the membranes were studied. The glass transition temperature of the membranes was predicted from the appearance of tan δ peak in a DMA curve. The phase transition behaviour of the CP blends are represented in **Fig. 6.15(a. &b)**. The response of storage modulus of the blend with temperature is shown in **Fig. 6.15(a)**. During phase transition, storage modulus of the blends was changes with temperature. The different stages of phase transition occurred in a blend was highlighted in a storage modulus curve. The phase shifting of the blends was influenced by the presence of crystalline phase and compatibility structure. The phase transition from glassy to rubbery was observed at the temperature range of 100-150°C. The compatibility of the blend enhances phase transition from glassy to rubbery phase. The phase transition of the non-compatible was delayed due to the presence of higher crystalline phase. The glassy zone of the CP blend was observer at the temperature below 100°C. The CP blend provides lower storage modulus as compared to CP-1 and CP-2 blend. Due to its lower storage modulus, CP blend was flexible and breaks at higher strain. The cross-linking reaction improves mobility of the CP blend. The phase transition behaviour of the cross-linked blend was fastened. The higher mobility of the polymer chain reduces storage modulus. The cross-linked blend has a lower storage modulus than the pure blend. The temperature reliant viscoelastic behaviour of blends were examined from the tan δ curve. The two stages of phase relaxation was occurred in a non-compatible blend. The two immiscible and non-compatible phase of Chitosan and PVA were relaxed during heat treatment. The damping behaviour of the blends are studied. During first stage of phase relaxation, tan δ value gradually decreases with temperature. It suggest that the elastic

behaviour of the blends was dominated over viscous property. The polymer chain flexibility was enhanced. However, at the temperature between 100 and 180°C, viscous property was dominated. The non-compatibility of the blends improves dissipation of energy. In a compatible blend, glass transition temperature was occurred during the first stage of phase relaxation. In a non-compatible blends, tan δ peak appeared at second stage of phase relaxation was attributed to its glass transition temperature. The height and area of tan δ peak provides the information about the amount of energy absorbed and chain mobility of the blends. In a non-compatible blend, polymer chain mobility was restricted by a cross-linking agent. The height of tan δ peak was reduces in a cross-linked blend as noticed between 230-250°C. It suggest that the viscous property was dominated over elastic property.

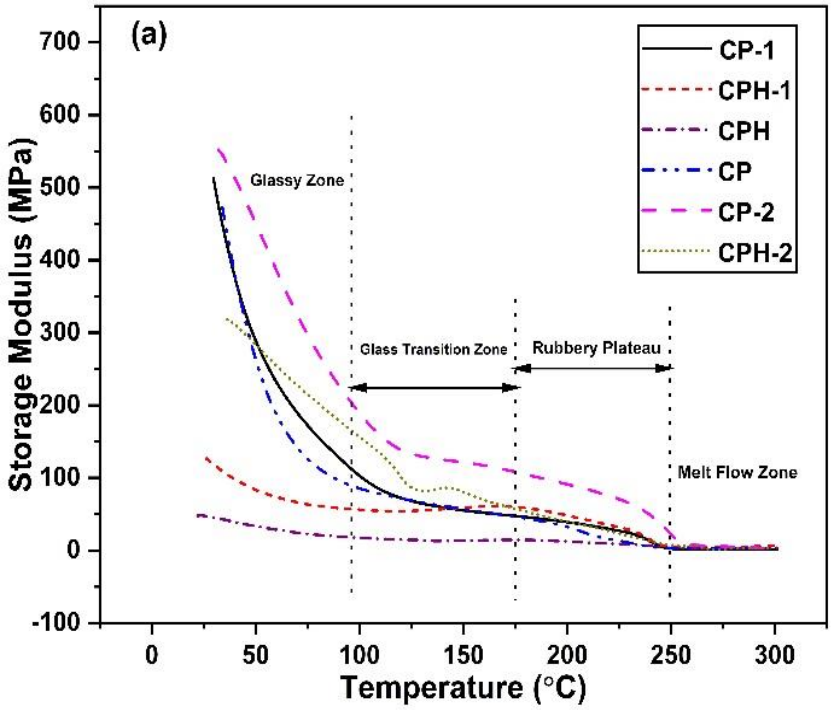

Figure 6.15 (a): Effect of temperature on storage modulus of the membrane.

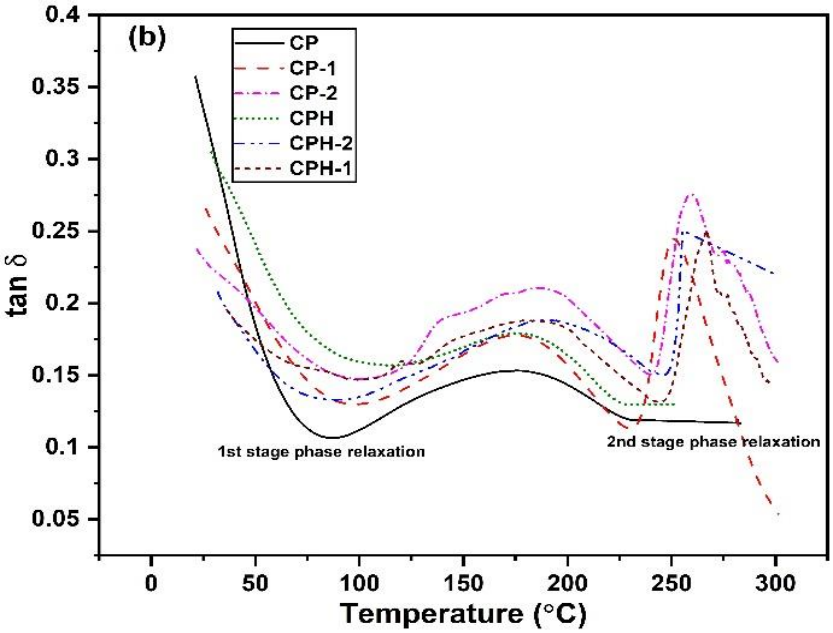

Figure 6.15 (b): Effect of temperature on tan δ curve of the membrane.

The phase transition behavior and damping properties of the red mud modified membranes were evaluated to predict their mechanical stability. The phase relaxation behavior of the red mud modified CP blends were represented in **Fig. 6.16(a)**. The response of storage modulus at different phase transition zone was represented in the curve. The glassy state of the blends were observed at the temperature below 75°C. The CP blend provides lower storage modulus than the other modified membranes. The incorporation of red mud particles to a membrane reduces its crystalline phase which fastening mobility of the polymer chain. Hence, red mud reduces storage modulus of the membrane and improves its chain flexibility. At temperatures ranging from 75 to 230°C, the phase shift from glassy to rubbery occurred. The damping properties of the blends were predicted from the tan δ curve as depicted in **Fig. 6.16(b)**. The relaxation of polymer membrane at different phase transition state was represented. In a glassy state, tan δ value of CP blend was higher than the modified membrane. The addition of red mud to a CP blend improve its elastic property. However, viscous property of the red mud modified membrane was dominated at the glass transition state. The inclusion of red mud in a CP blend enhances dissipation of energy. The T_g of the blends were evaluated from the peak of tan δ curve. The addition of red mud in a CP blend shifted tan δ peak to a lower temperature. Due to depletion of crystalline phase, amount of energy required to convert glassy phase of the CPR membranes were lower than CP blend.

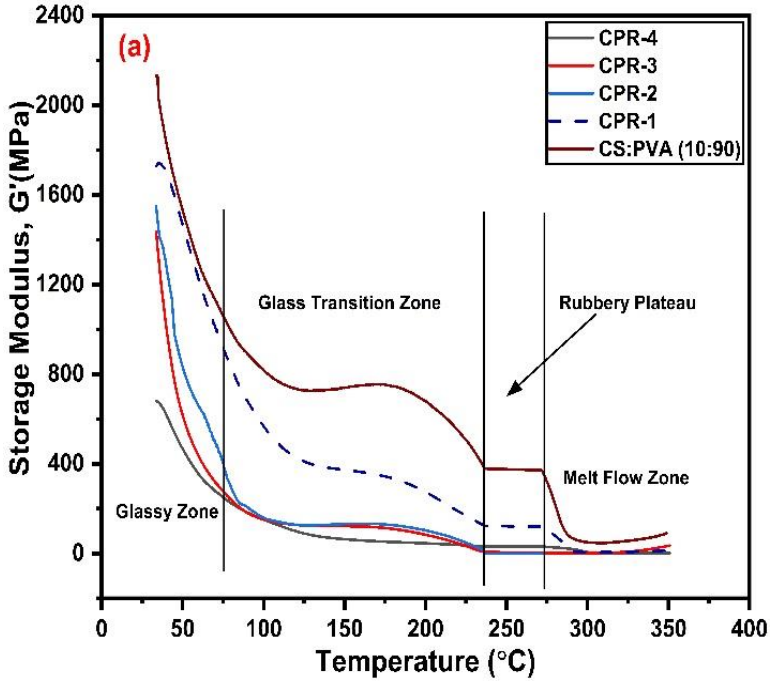

Figure 6.16 (a): Effect of temperature on storage modulus of the membrane.

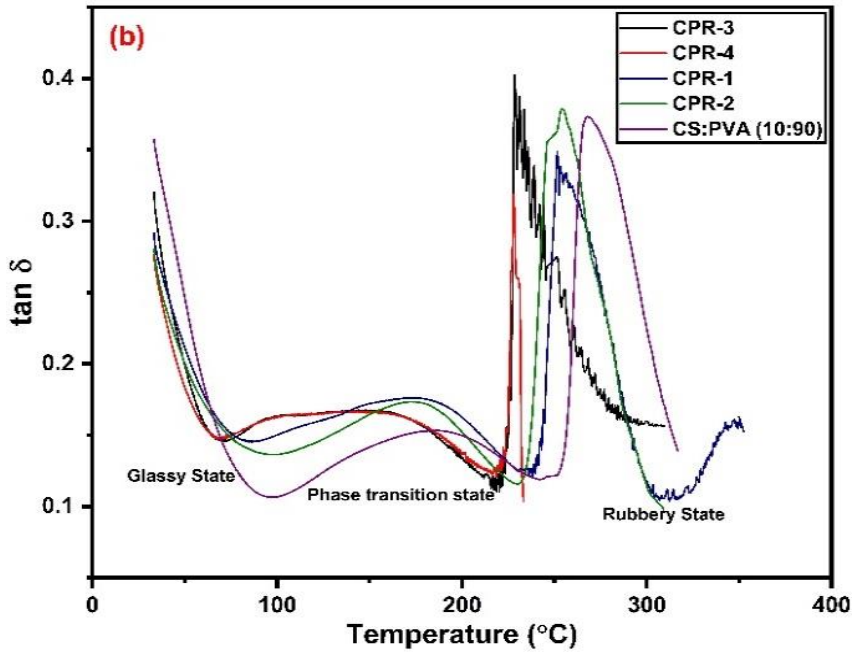

Figure 6.16 (b): Effect of temperature on ten δ curve of the membrane.

The effect of CNT filler on the phase transition behaviour of CP blend was studied. The temperature dependent mechanical property of the membranes were investigated. The mechanical property of the membranes were predicted by evaluating their storage modulus. The response of storage modulus at different phase transition stage is depicted in **Fig. 6.17**. The CNT filler was act as a filler which reduces the intermolecular cohesive force of polymer chain. The membrane becomes more flexible due to the enhancement of polymer chain movement. Hence, the increase of CNT amount to a membrane reduces its storage modulus. Moreover, the ionic liquid further reduces the storage modulus of CPCN membrane. The ionic liquid fastening the phase transition from glassy to rubbery phase. The storage modulus of the membranes decreased steadily as temperature increased. The polymer chain movement was increased at higher temperatures, which reduced the storage modulus.

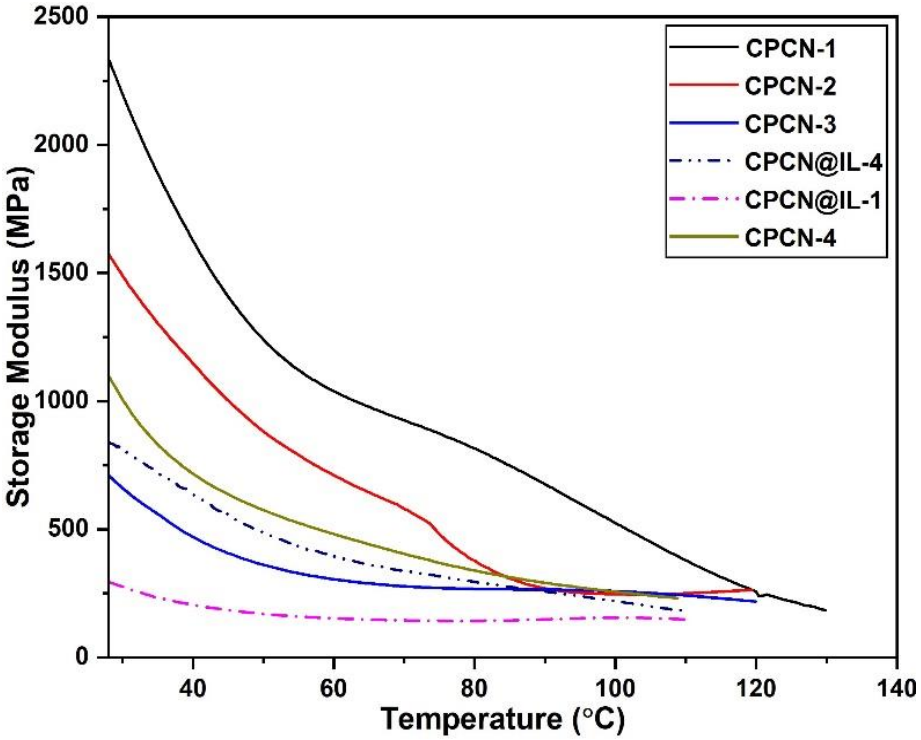

Figure 6.17: Effect of temperature on storage modulus of the MWCNT and ionic liquid modified CP blends.

The phase transition behavior of the zirconia and ionic liquid modified hybrid membranes is represented in **Fig. 6.18(a)**. Hygroscopic zirconia and ionic liquid were impregnated into the CP blend to modify it. The plasticizing effect of zirconia and ionic liquid improves mobility of the CP blend. The enhancement in mobility of the chain reduces storage modulus. The increase of zirconia amount in a membrane gradually improves chain mobility. Therefore, the membrane with more amount of zirconia provides lower storage modulus. Moreover, it was found that increasing the temperature reduces storage modulus. At higher temperature, kinetic energy of the polymer chain was enhanced which improves its chain mobility. The membrane becomes soft, flexible and break at higher strain. However, the strength of the membrane was reduces due to the reduction of storage modulus. The ionic liquid improves chain mobility of the CPZr membrane. The presence of ionic liquid significantly affects the interaction between zirconia and polymer domain. Moreover, ionic liquid was interacted with the polymer domain of CPZr membrane. The interaction between ionic liquid and polymer domain improves chain flexibility. Therefore, the storage modulus of ionic liquid modified membranes was lower than the CPZr membrane. The damping properties of the membranes are evaluated from the tan δ curve as depicted in **Fig. 6.18(b)**. The glassy phase of the membrane was observed at the temperature below 100°C. In this stage, tan δ values were gradually decreasing for all membranes. The polymer membranes has more ability to absorb energy and elastic response was dominated. The tan δ values of CPZr membrane gradually decreases with the increase of zirconia amount. The zirconia filler improves elastic property of the membrane. The addition of ionic liquid further improves its elastic property. However, viscous property was dominated in a CPZR@IL-3 membrane. The presence of ionic liquid improves dissipation of energy. At temperatures ranging from 130 to 170°C, the phase shift from glassy to rubbery was observed. During phase transition stage, tan δ peak was increases. It suggest the improvement of viscous property. The polymer chains will dissipate more energy. The amount of energy absorbed and

polymer chain mobility was evaluated from the area of tan δ peak. The tan peak steadily decreased as the amount of zirconia increases. The viscous property was dominated with the increase of zirconia amount. The increase of zirconia amount in a membrane shifted the tan δ peak to a lower temperature. Moreover, tan δ peak was appeared at a lower temperature in an ionic liquid modified membrane. The addition of ionic liquid improves polymer chain mobility and phase transition was occurred at lower temperature. The glass transition temperature of membranes obtained in this investigation was slightly higher than that found in the DSC analysis.

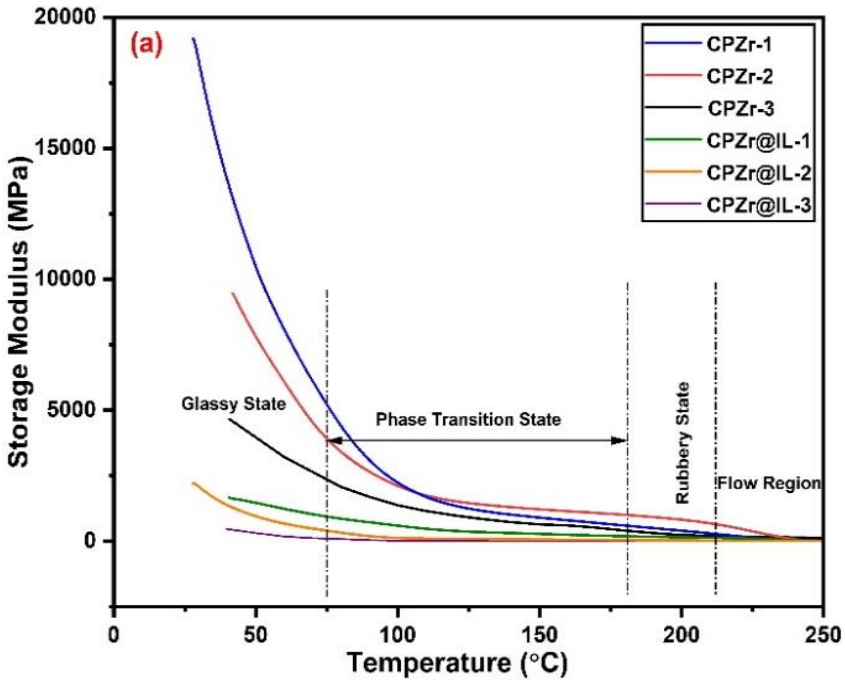

Figure 6.18 (a): Influence of temperature on storage modulus of the membrane.

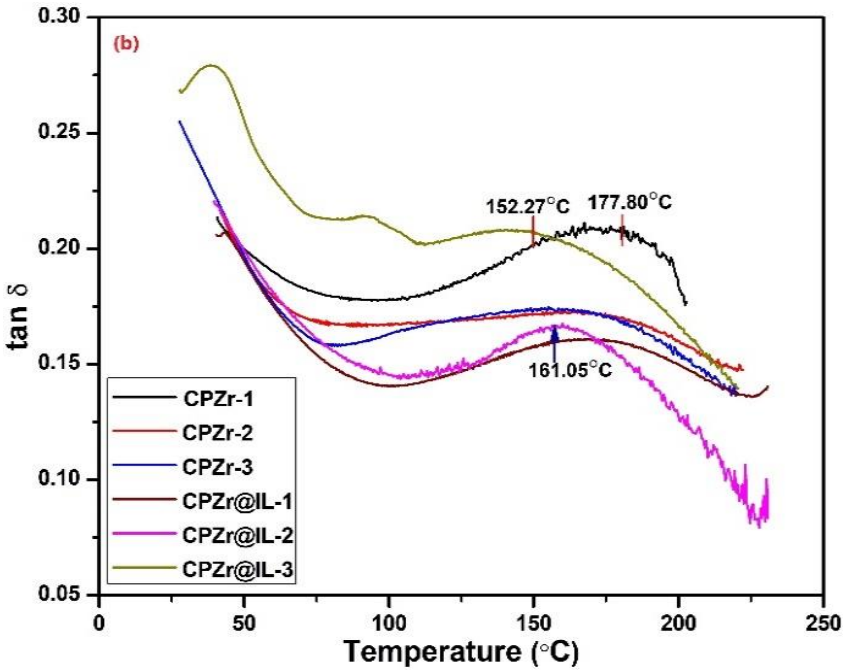

Figure 6.18 (b): Influence of temperature on tan δ curve of the membrane.

The effect temperature on the phase transition behaviour of SPEEK-PVA-silica hybrid membrane was studied. The response of storage modulus and tan δ during phase transition of the hybrid membranes are shown in **Fig. 6.19**. The SPEEK membrane was modified with PVA and silica. The temperature dependency of the storage modulus of membranes was investigated. The addition of silica and PVA to a SPEEK membrane significantly changes its chain mobility. The response of the storage modulus was found to be substantially temperature dependent. At lower temperature i.e. up to 120°C, all the membranes were behaved like glassy polymer. The storage modulus of membrane was increased as the amount of silica increases. The viscous property of the membranes were dominated over elastic property. The viscous property dominated due to the dissipation of energy. The increase of silica amount improves polymer chain mobility which enhances dissipation of energy. However, the aggregation of silica particles limits dissipation of energy. Therefore, the storage modulus of SPS-4 membrane was lower. At higher temperature, elastic property was dominated over viscous response. The tan δ peak was used to obtain the phase shift temperature of the membranes. The temperature

dependent tan δ curve of all the fabricated membrane are depicted in **Fig. 6.19(b)**. The addition of PVA and silica to a SPEEK membrane transit the tan δ peak to a lower temperature. The addition of filler increases polymer chain mobility, which accelerates the phase change from glassy to rubbery. The polymer chain mobility was enhanced due to the depletion of well-ordered crystalline phase in a membrane. In a pristine SPEEK membrane, tan δ peak was occurred at higher temperature as compared to other membrane. The area of the tan peak was used to calculate the amount of energy absorbed by the membrane. The region under the tan peak rapidly decreased as the amount of silica increased. The pristine SPEEK membrane absorb more energy and behaves like an elastic material. However, the inclusion of silica to a SPEEK membrane decline its elastic property. The viscous property was dominated over elastic response.

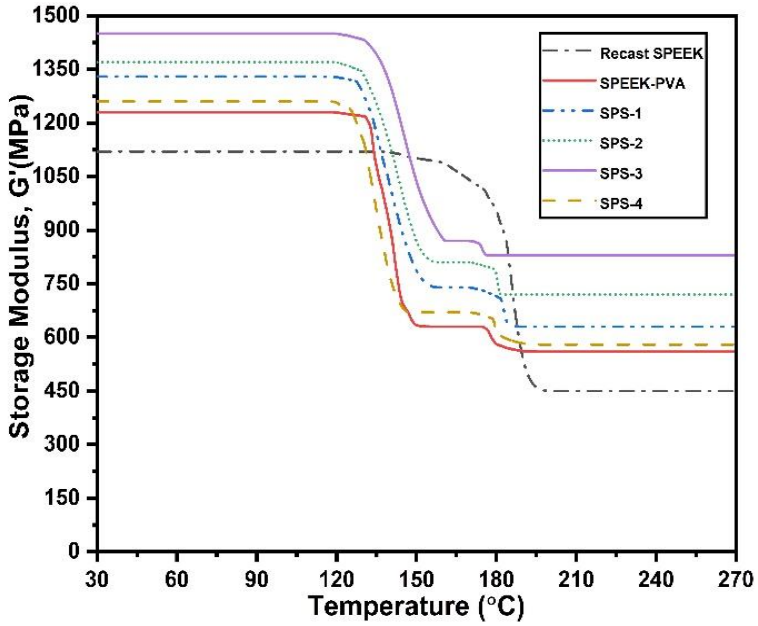

Figure 6.19 (a): Influence of temperature on storage modulus of the membrane.

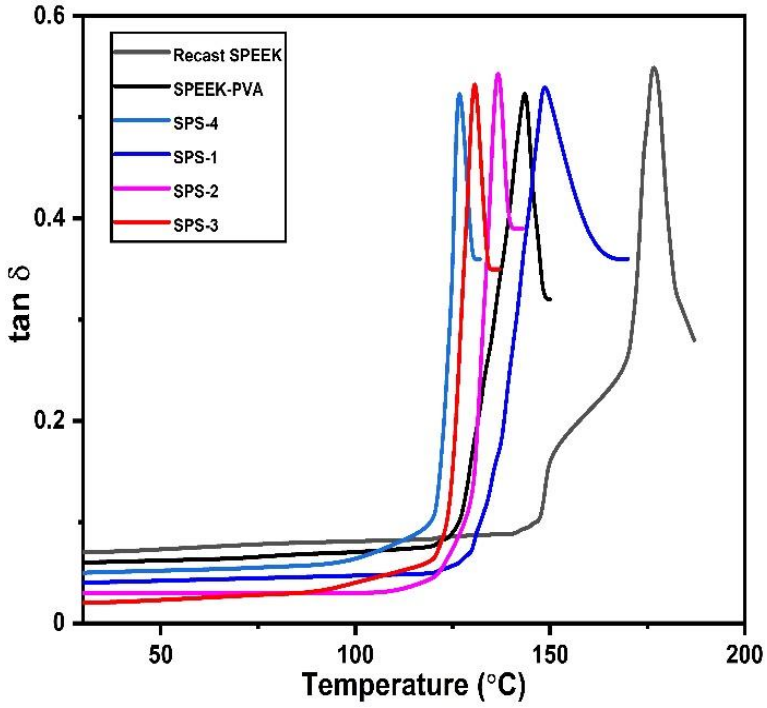

Figure 6.19 (b): Influence of temperature on tan δ curve of the membrane.

6.3.2 Tensile Property

The mechanical strength of the membrane plays a crucial role for fuel cell performance. The membrane with higher tensile strength as well as a better dimension stability improve its durability. The tensile stress, elastic modulus and elongation at break of the membranes were obtained from the stress-strain curve and reported in **Table 6.1**. The compatibility of the blend affects its mechanical property. The highly compatible CP blend provides higher tensile strength as compared to non-compatible CP-1 and CP-2 blend. Moreover, the elastic modulus of CP blend was higher. It was also confirmed that the CP blend has more elongation at break. CP blend offers a better tensile strength because to its high compatibility. The CP blend was more flexible due to the presence of dominant amorphous phase. Hence, it has higher elongation at break point. It was also noticed the CP-1 and CP-2 blends has higher crystalline phase but provides lower modulus. The reason for the reduction of storage modulus in a non-

compatible was not known. It may be the effect of non-compatibility of the blend. Moreover, due to presence of more crystalline phase, non-compatible blends were break at lower strain. The CP blend has a tensile strength of 55.06MPa, which was much higher than the N117 membrane, 28.57MPa [**74, 75**]. The tensile strength of CP blend was similar to the reported work [**38**]. The cross-linked blend provides higher tensile strength as compared to pure blend. The cross-linking agent (SO_4^{2-} ion of sulphuric acid) strongly binds the polymer chain and improves tensile strength. Due to cross-linking reaction, tensile strength of CP blend was increased from 42.08 to 46.12MPa. Moreover, the cross-lined CP blend provides highest tensile strength as compared to other membrane. However, the cross-linking reaction depleted crystalline domain of the blend. Due to depleted crystalline domain, modulus of the blend was reduced and the membrane breaks at higher strain. The cross-linked membrane has more tensile strength and elastic modulus. The cross-linked membrane can be considered as a suitable candidate for fuel cell application. It can provide higher mechanical stability at higher stress.

The effect of red mud particles as filler on the mechanical property of CP blend was studied. The stress-strain curve was used to investigate the tensile strength, elastic modulus, and elongation at break of the membranes. The tensile stress-strain curve of the membranes are obtained and depicted in **Fig. 6.20**. It was found that the addition of red mud to a CP blend improves chain flexibility. The reduction in crystalline phase due to the addition of RM to CP blend was confirmed from XRD analysis. Due to the depleted crystalline phase, elastic modulus reduces. Moreover, the modified membrane provides higher elongation at break. The increase of red mud amount in a CP blend gradually decreases tensile strength and CPR-1 membrane provides higher tensile strength. The filling effect of red mud has a substantial effect on the tensile strength of the blend. It was reported that the red mud particles were well dispersed in a CPR-1 membrane and prevents the distortion of well-ordered structure at lower stress. Moreover, the presence of more crystalline phase in a CPR-1 membrane improves its tensile

strength. The CPR-2 membrane provides lowest storage modulus and breaks at lower strain as compared to other modified membranes. The CPR-1 membrane has higher tensile strength and elastic modulus. It can provide better mechanical stability at higher stress. The obtained tensile strength of CPR-1 membrane was 29.02MPa. The similar result was reported for N117 membrane. However, as the amount of red mud increased, the tensile strength of the membrane was decreases. The tensile strength of CPR-2 and CPR-3 membrane was 18 and 11MPa respectively. Due to decline their tensile strength, mechanical stability of the membrane were reduces.

The influence of MWCNT filler and ionic liquid on the mechanical features of CP blend was studied. The tensile curve of membranes obtained at room temperature is shown in **Fig. 6.21**. Form the tensile curve, tensile strength and elastic modulus of the membranes were obtained. Moreover, tensile strength and elastic modulus of all the fabricated membranes was reported in **Table 6.3**. It was found that adding more filler to a CP blend reduces tensile strength and elastic modulus. It was confirmed that the addition of filler and ionic liquid depleted crystalline phase. Hence, tensile strength of the membranes were dropping. Due to the depletion of crystalline phase, membrane becomes soft and flexible. Hence, the increase of filler amount and ionic liquid incorporation to a CP blend increases elongation at break. The CPCN membrane provides higher tensile strength than the ionic liquid modified membrane. However, the tensile strain of CPCN membrane was lower as compared to ionic liquid modified membrane. The ionic liquid increases the chain flexibility of the polymer domain while decreasing tensile strength [**76**]. The developed membrane has lower tensile stress than the N117 membrane. The ionic liquid modified membrane provides moderate tensile strength with higher strain at break.

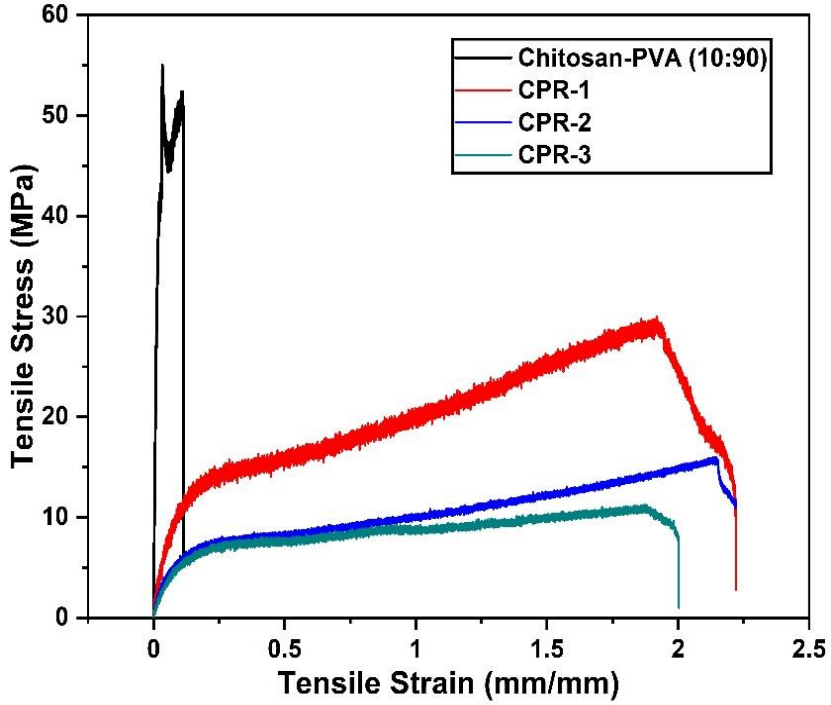

Figure 6.20: Stress-strain curve of the red mud modified CP blends.

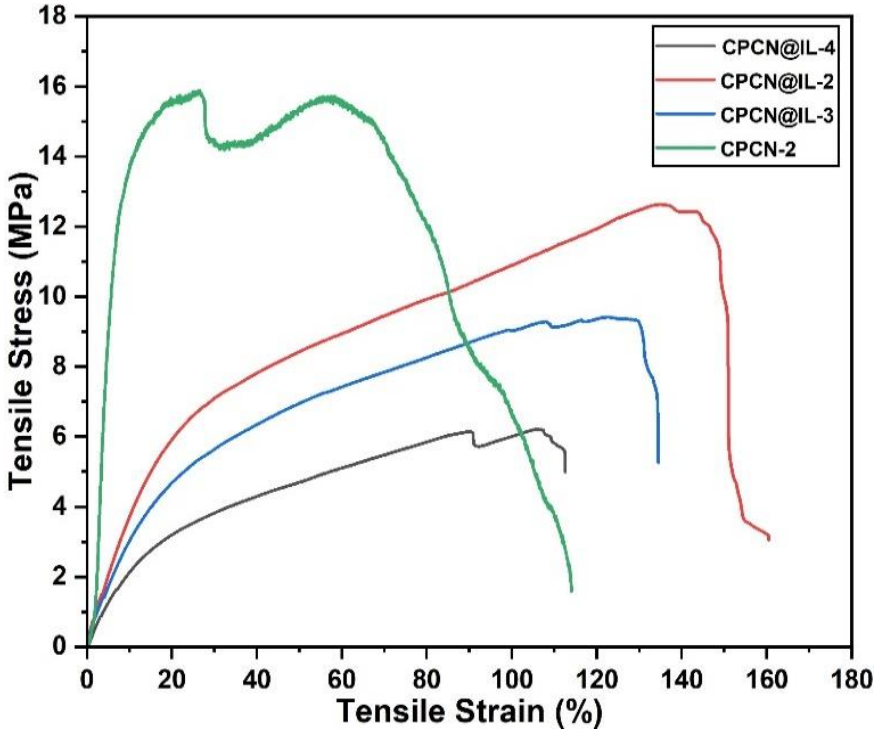

Figure 6.21: Stress-strain curve of the MWCNT and ionic liquid modified CP blends.

The tensile stress, elastic modulus and elongation at break of the zirconia and ionic liquid modified CP blend were evaluated form the stress-strain curve. The obtained stress-strain curve of the developed membranes are depicted in **Fig. 6.22**. The tensile strength, elastic modulus and strain at break of the membranes are obtained and reported in **Table 6.4**. The tensile strength of the membranes were obtained in the range of 6.72-18.19MPa. The addition of zirconia to a CP blend reduces its tensile strength. The tensile strength was reduces due to the reduction of well-ordered phase. Among the pure membrane, CPZr-2 provides higher tensile strength of 17.39MPa. The well dispersion of filler in a CPZr-2 membrane improves its tensile strength. However, a noticeable drop of tensile strength was observed in CPZr-3 and CPZr-4 membrane. The zirconia particles were start to aggregate on the polymer domain which reduces the intermolecular force of interactions. Moreover, the crystalline phase was depleted in CPZr-2 and CPZr-4 membrane. Therefore, CPZr-3 and CPZr-4 membrane provides lower tensile strength. The modifications of CPZr membrane with ionic liquid improves tensile strength. The ionic liquid modified CPZr-2 membrane provides the highest tensile strength of 18.19MPa. The elastic modulus of the membranes were gradually decreases with the increase of zirconia amount. The membrane becomes soft and break at higher strain. The addition of ionic liquid further reduces elastic modulus and improves polymer chain flexibility. It was observed that the ionic liquid modified membrane provides higher tensile stress and elastic modulus. The CPZr@IL-2 membrane (18.19MPa) has lower tensile stress than the N117 & N112 membrane [**38, 77**]. The membrane with higher strength and modulus was considered to be potential application of fuel cell. Therefore, ionic liquid membrane can be considered as an ideal candidate for fuel cell.

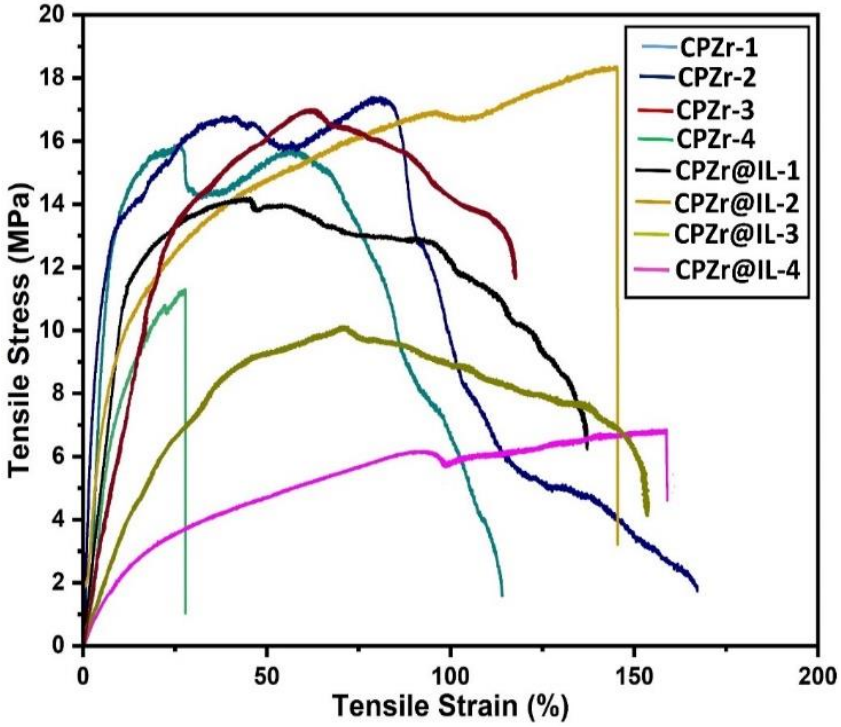

Figure 6.22: Stress-strain profile of the zirconia and ionic liquid modified CP blends obtained at 27°C and 54% humidity.

6.4 Methanol Permeability

The methanol permeability is a crucial properties of an electrolyte membrane which affects fuel cell performance. The membrane with higher methanol permeability provides poor cell performance. The methanol permeability across the membrane was conducted for 2M methanol feed. It was reported that the commercial N117 membrane provides the methanol permeability of $5.2\times10^{-7}cm^2/s$ [**20, 77**]. Moreover, higher methanol permeability produces leakage current. For improving fuel cell performance and preventing fuel loss, methanol permeability across the membrane should be lower. The goal of the work is to create a low-cost membrane with lower methanol cross-over than the current NII7 membrane. The methanol cross-over values of the produced membranes were compared to the N117 membrane.

6.4.1 Chitosan-Polyvinyl Alcohol Blend

The methanol cross-over through the CP blend was measured in a glass diffusion cell and reported in **Table 6.10**. The result reveals that the non-compatibility of CP blend causes higher methanol cross-over. The highly compatible blend provides lower methanol cross-over. The lowest methanol permeability was found in a highly compatible CP blend, 2.42×10^{-7} cm^2/sec. The similar results was reported for the CP blend in a literature [**25, 38**]. It was believed that the presence of hydroxyl group in a CP blend was responsible for methanol cross-over. The hydroxyl group was interacted with the methanol by strong hydrogen bond [**25**]. Therefore, the CP blend with more hydroxyl groups will suffer higher methanol cross-over. It was confirmed that the non-compatible blend like CP-1 and CP-2 blend has more hydroxyl group as compared to compatible CP blend. The CP blend cross-linked with sulphuric acid drastically reduces its methanol cross-over. The free hydroxyl group presence in the CP blend was further reacted with the sulfonate group of sulphuric acid. The cross-linking reaction consumes hydroxyl group's presence in the blend and blocks the methanol transport channel. Moreover, the crosslinking agent was strongly interacted with the polymer chain of CP blend by ionic bond.

The blend becomes harder, compact and tortuous. The free space available for the methanol transport was depleted which eventually reduces methanol cross-over through the blend. The lowest methanol permeability was found in a CPH-1 blend, 0.34×10^{-7} cm^2/sec. The methanol permeability occurred in a CPH-1 blend was significantly lower than the N117 membrane.

6.4.2 Modified with Red Mud Filler

The methanol permeability values of the red mud modified CP blends were reported in **Table 6.12**. It was observed that the addition of red mud as a filler reduces the methanol permeability of CP blend. The red mud particles has the ability to depleted hydroxyl group of CP blend. The red mud particles like silica and alumina were interacted with the hydroxyl group of blends. The hydroxyl groups in a blend were consumed by the filler and improves the methanol blocking ability. The depletion of hydroxyl groups in a blend reduces the interaction between hydroxyl group and methanol. Therefore, the methanol permeability value decreases in a red mud modified CP blends. The membrane becomes dense and depleted the migration sites for methanol transport. The free space available for the migration of methanol was depleted by the inclusion of red mud. Moreover, methanol migration was prevented by the existence of distinct iron oxide in a blend .It was reported in a literature that the existence of iron oxide in a membrane reduces methanol permeability [**78, 79**]. It was observed that the increase of filler amount to a CP blend gradually decreases methanol cross-over. The lowest methanol permeability was found in a CPR-3 membrane, $0.72\times10^{-7}cm^2/s$. The methanol cross-over occurred across the CPR membrane was much lower than the reported N117 membrane [**80**]. The methanol cross-over across the CPR-3 membrane was slightly higher than the cross-linked CP blends. However, CPR-3 membrane provides higher proton conductivity than the cross-linked CP blends. The CPR-3 membrane was considered to be an ideal candidate for fuel cell application. It was observed that the CPR-4 membrane suffers higher methanol cross-over. The increase of filler to a CP blend creates void space and increases porosity. The red mud particles

were aggregated and creates huge void space in a membrane. Due to the formation of void space, methanol will migrated though the polymer channel which eventually increases methanol permeability. Therefore, CPR-4 membrane was not suitable for fuel cell application.

6.4.3 Modified with Carbon Nanotubes and Ionic Liquid

The impact of MWCNT and ionic liquid on methanol permeability of the CP blend was studied. The methanol cross-over across the modified membrane was obtained and reported in **Table 6.14**. The addition of MWCNT as a filler gradually decreases methanol cross-over of the CP blend. The lowest methanol permeability was observed in a CPCN-3 membrane, $2.16\times10^{-7}cm^2/s$. The obtained values of the CPCN membranes was marginally lesser than the reported value of CP blends. There was no significant improvement of methanol permeability was observed in a CPCN membrane. The methanol cross-over across the CPCN membranes was superior to the N117 membrane. It was also observed that CPCN-4 membrane suffers higher methanol cross-over. In a CPCN-4 membrane, MWCNT particles were aggregated to a bulky phase and increase void space. The migration sites for methanol transport was enhanced which increase methanol permeability. Therefore, further modifications in architecture was required to decrease methanol cross-over. The modification of CPCN membrane with ionic liquid significantly decreases methanol permeability. The ionic liquid was strongly interacted with the polymer chain and depleted the methanol migration sites. Moreover, the presence of bulky pendant group of ionic liquid blocks the methanol transport channel in a CP blend [**75**]. Therefore, methanol permeability in an ionic liquid modified CPCN membrane was lower as compared to CPCN membrane. The lowest methanol permeability was observed in an ionic liquid modified CPCN-3 membrane ($0.726\times10^{-7}cm^2/s.$) which was similar to the CPR membrane. The methanol permeability in an ionic liquid modified CPCN membrane was significantly lower than the N117 membrane.

6.4.4 Modified with Hygroscopic Zirconia and Ionic Liquid

The methanol permeability through the zirconia and ionic liquid modified membrane was studied by performing permeation test. The methanol permeability of the modified membranes are reported in **Table 6.16**. The addition of zirconia to a CP blend reduces methanol permeability. The hydroxyl group of the CP blend was interacted with the zirconia and ionic liquid. Due to the interaction, hydroxyl group was depleted in a membrane. The depletion of hydroxyl group reduces the interaction between methanol and hydroxyl group. The affinity of the methanol towards the polymer domain was gradually reduces. Moreover, the addition of zirconia to a CP blend increases bulk density, compactness and tortuosity thereby impeding the migration sites for methanol transport. Hence, the hybrid membrane modified with zirconia and ionic liquid provides lower methanol cross-over as compared to the CP blends. Among the pure CPZr membrane, CPZr-4 membrane provides the lowest methanol cross-over of 6.18×10^{-7} cm^2s^{-1}. The addition of ionic liquid to the CPZr membrane further reduces the methanol permeability. The ionic liquid was interacted with the zirconia particles and prevents to aggregate on the polymer matrix. Moreover, a layer like structure was developed on the membrane surface which mitigate the migration path of methanol. The methanol migration sites was depleted on the membrane domain which lower the methanol permeability. Moreover, the addition of bulky pendant groups of ionic liquid to the blend blocks migration sites for methanol transport which resulted lower methanol cross-over [**80, 81**]. The lowest methanol permeability was observed in a CPZr@IL-4 membrane, 0.94×10^{-7} cm^2s^{-1}. The highly selective CPZr@IL-3 membrane provides the methanol permeability of 1.08×10^{-7} cm^2s^{-1}. The methanol permeability in a CPZr@IL membrane was slightly more than the CPCN@IL membrane. However, it provides lower methanol permeability than the Nafion (N117) and Nafion based hybrid membrane [**30**].

6.4.5 SPEEK-PVA-Silica Hybrid Membrane

The methanol cross-over across the SPEEK-PVA-silica hybrid membrane was measured in a glass diffusion cell and reported in **Table 6.18**. The addition of silica to the SPEEK-PVA blend increases its compactness. Due to polymer chain compactness, migration sites for methanol transport was depleted. The permeability of methanol steadily declines with increasing silica content to a certain point and then increases. In SPS-4 membrane, silica particles were aggregated and enhances void space or porosity. Therefore, it provides higher methanol permeability. The methanol permeability in a SPEEK-PVA-silica hybrid membrane was slightly lower than the N117 membrane. However, it provides higher methanol permeability the CPCN and CPZr hybrid membrane. Among the fabricated membranes, the ionic liquid modified CPZr hybrid had the lowest methanol cross-over. The membrane with the lower methanol permeability is considered to be a potential candidate for fuel cell application.

6.5 Proton Conductivity

The proton conductivity of the membranes was obtained by measuring the bulk or electrolyte resistance. The bulk or electrolyte resistance of the membrane was determined using an impedance test. The EIS data obtained from the impedance experiment was fitted to the most appropriate equivalent model. The different circuit model was available in the z-view software. It was observed that the EIS data was properly fitted to the Randles circuit model. After fitting, bulk resistance (R_b) was obtained from the model parameters. The Randles circuit model is represented in **Fig. 6.23**. The different model parameters and their significance is mentioned below.

Randles circuit model parameter:

R_b represent bulk or electrolyte resistance in Ω. R_c is the electrode resistance in Ω and C_b is the constant phase element of the model which represents capacitor in the experiment.

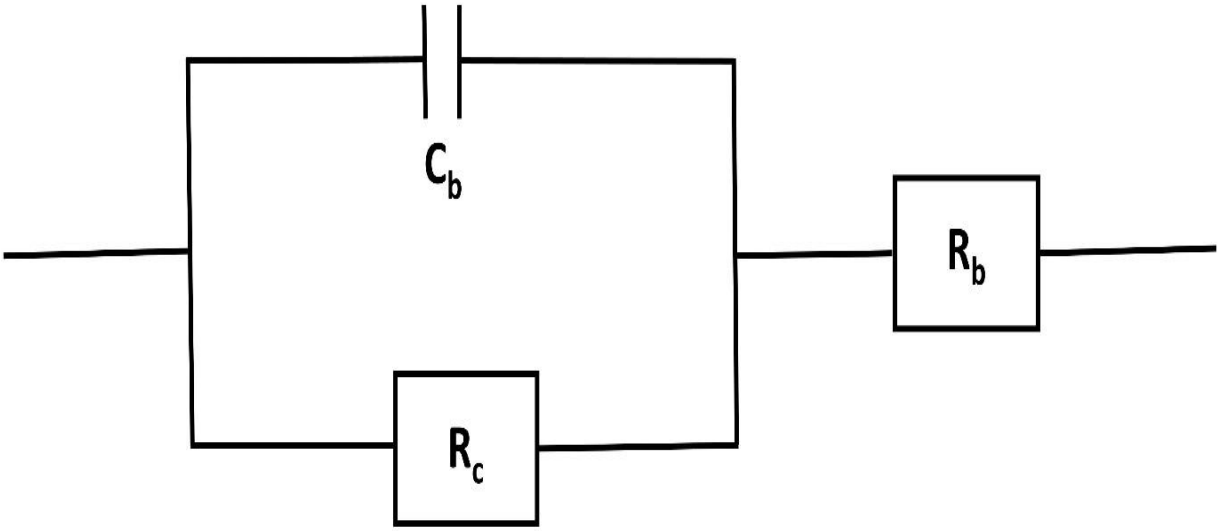

Figure 6.23: Schematic diagram of the Randles circuit model for obtaining electrolyte resistance of the membranes.

After obtaining the electrolyte resistance, the proton conductivity of the membrane was estimated using **equation-4.9**. The fuel cell performance was highly reliant on electrolyte resistance of the membrane. The membrane with higher electrolyte resistance provides lower cell voltage and power density. The membrane with lower electrolyte resistance is considered to be a suitable candidate for fuel cell application.

The proton transport through the electrolyte membrane is controlled by two key mechanism (i) Grotthuss (ii) Vehicular mechanism. The proton transport by Grotthuss mechanism was higher than the vehicular mechanism. The Grotthuss mechanism was controlled by free water. The free water was combined with the proton to form hydronium ion and transported through the ion transport channel of electrolyte membrane. However, the lack of free water at medium temperature restrict proton transport by Grotthuss mechanism. At this conditions, proton transport was governed by vehicular mechanism. The trace amount of free water will act as a vehicle to transport proton through the polymer channel. At medium temperature and low humidity conditions, bound water of the electrolyte membrane plays a crucial role for the proton transport. The proton transport was controlled by the bound water facilitated Grotthuss mechanism.

The bulk or electrolyte resistance and proton conductivity of the membranes are reported in **Table 6.9**. It was observed that the crosslinking of CP blend with the sulphuric acid decreases its bulk resistance. The crosslinking reaction incorporated extra proton migration sites to the CP blend. Therefore, In comparison to the pure CP blend, the crosslinking blend has higher proton conductivity. Moreover, the proton conductivity of the blend was increased with increasing temperature. The increase of temperature improves the mobility of the proton thereby increases proton conductivity. The effect of temperature on the proton conductivity of different CP blend is represented in **Fig. 6.24(a)**. At medium temperature, a significant increase of proton conductivity was noticed in a cross-linked CP blend. The proton transport was

controlled by bound water regulated Grotthuss mechanism. In a cross-linked blend, higher bound water was present which contribute maximum proton conductivity. The sulfonate group of the crosslinking agent was strongly interacted with the water and increases bound water of the membrane. The strongly interacted bound water not escape from the polymer domain at a medium temperature. The bound water facilitate higher proton conductivity by Grotthuss mechanism. Moreover, the presence of trace amount of free water also contribute some proton conductivity by vehicular mechanism. However, in a pure blend, the free water was weakly interacted with the polymer domain. Hence, at medium temperature, free water was escaped from the polymer matrix. Due to the lack of free water, proton transport was controlled by vehicular mechanism. The proton transport by vehicular mechanism provides lower proton conductivity. Therefore, proton conductivity in a cross-linked blend was significantly higher than the pure CP blends. The proton conductivity of the cross-linked CP blend was compared to that of the commercial NN17 membrane. It was observed that the proton conductivity of the CP blend was significantly lower than the N117 membrane [**25**]. The proton conductivity value was lower than the magnitude of two order than the N117 membrane. For possible application in a fuel cell, its proton conductivity should be improved to a higher level.

Table 6.9: Electrolyte resistance (R_b) and Proton conductivity (σ) of the CP blends obtained at 28ºC and 70ºC.

Sample Code	Membrane Resistance, R_b (Ω)		Proton Conductivity, σ (Scm^{-1}) ×10^{-3}	
	28ºC	70ºC	28ºC	70ºC
CP	278.51	226.29	0.13	0.16
CP-1	402.29	329.15	0.09	0.11
CP-2	905.17	517.24	0.04	0.07
CPH	32.32	26.23	1.12	1.38
CPH-1	53.24	38.93	0.68	0.93
CPH-2	77.03	51.72	0.47	0.70

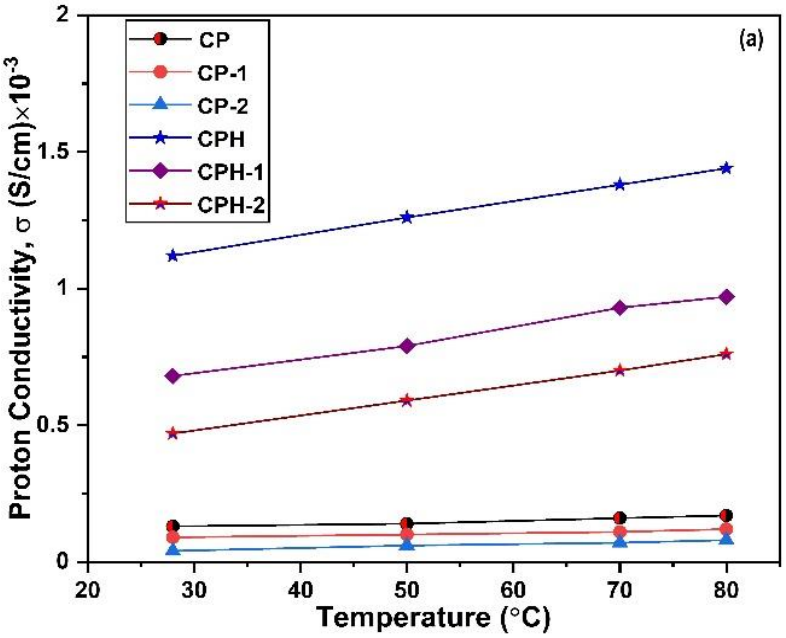

Figure 6.24 (a): Effect of temperature on the proton conductivity of the CP blends. (b) Arrhenius plot for obtaining activation energy.

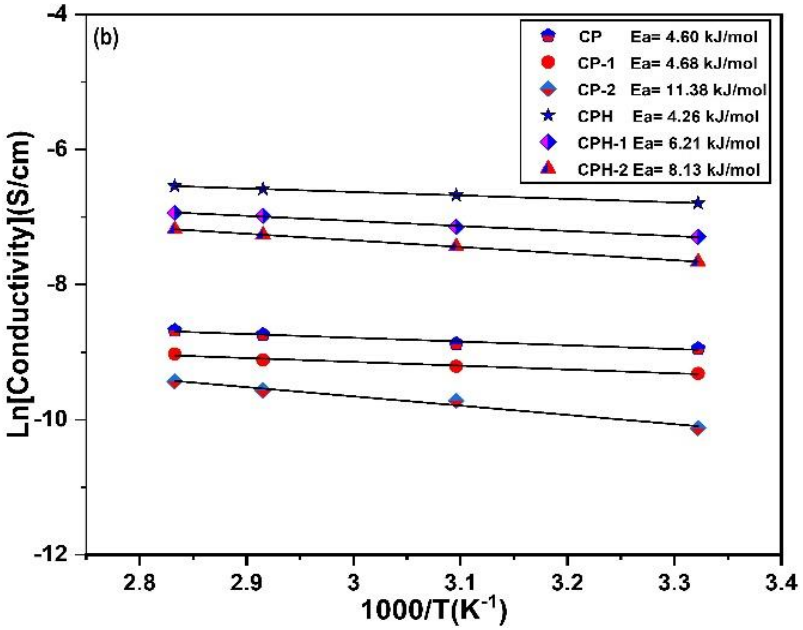

Figure 6.24 (b): Arrhenius plot for obtaining activation energy.

The effect of temperature on the proton conductivity of blend was evaluated by determining the activation energy. The Arrhenius equation is used to calculate the lowest energy required for proton transport via the electrolyte membrane. The Arrhenius equation describes the relation between proton conductivity and temperature. Proton conductivity of the blend was measured at various temperatures to evaluate activation energy. The general form of the Arrhenius equation for proton conductivity is represented in the following expression

$$\ln [\sigma] = \ln [\sigma_0] - \frac{Ea}{RT} \qquad (22)$$

Here, σ and σ_0 are the proton conductivity and pre-exponential factor of membrane respectively, in S cm^{-1}, Ea is the activation energy required for proton transport in kJ/mol., R is the universal gas constant (8.314 J/mol. K) and T is the absolute temperature in Kelvin. The Arrhenius plot of all the CP blends are represented in **Fig. 6.24(b)**. The activation energy of the blends were calculated from the slope of Arrhenius plot. The activation energy of each blend is illustrated in the Arrhenius plot in **Fig 6.24(b)**. The obtained activation energy of the blends ranged from 4.26 to 11.38 kJ/mol. The activation energy of the Nafion membranes such as N112 and N117 is 10.39 and 7.46 kJ/mol, respectively [**38, 69 & 82**]. The non-compatibility of the CP blend increases activation energy. The activation energy of the CP blend was found to be lower than that of the CP-1 and CP-2 blends. The proton transport was highly influenced in a non-compatible blends like CP-1 and CP-2 blend. It signifies that the proton transport was controlled by Grotthuss mechanism in a compatible CP blend. Due to Grotthuss dominate proton transport, CP blend provides higher proton conductivity. The CP and CP-2 blend cross-linked with the sulfuric acid decreases activation energy. The proton transport was least influenced by temperature. Moreover, the proton transport mechanism was highly dominated by Grotthuss mechanism. However, there was a contrasting trend in a CP-1 blend. It was

observed that the crosslinking of CP-1 blend increases its activation energy. The proton transport was highly influenced by temperature. The electrolyte membrane with high selectivity is preferred for fuel cell application. The highly selective membrane improves performance of fuel cell. Therefore, it is desirable to develop electrolyte membrane with higher selectivity. The membrane's selectivity was calculated using the following expression:

$$S\ (S.sec./cm^3) = \frac{Proton\ Conductivity,\sigma}{Methanol\ Permeability,P} \qquad (6.1)$$

The membrane with higher proton conductivity and excellent methanol blocking ability improves its selectivity. The selectivity of all the blends were calculated and reported in **Table 6.10**. The selectivity of the CP blend was higher than the less compatible CP-1 and CP-2 blend. The highly compatible CP blend has improved proton conductivity and methanol blocking capabilities. Therefore, the selectivity of CP blend was higher as compared to CP-1 and CP-2 blend. The crosslinking of CP blend with sulphuric acid significantly improves its selectivity. Among the cross-linked blend, CPH blend provides higher selectivity than the CPH-1 and CPH-2 blend. The selectivity was enhanced due to the improvement of proton conductivity. The crosslinking of CP blend with the sulphuric acid increases selectivity from 0.54×10^3 to 32×10^3 S.sec./cm^3. However, the selectivity of the CPH blend was lower than the N117 and N212-GO membrane. The proton conductivity of the CPH membrane was lower than the commercial N117 membrane. Due to its inferior proton conductivity, it provides lower selectivity than the commercial N117 membrane. Methanol is effectively blocked by the CPH blend which is beneficial for fuel cell application. The proton conductivity of the CPH blend should be improved to achieve higher selectivity. The lower methanol blocking ability of the chitosan blend encourages for further investigation. The CP blend was further modified by incorporating filler like red mud, multiwall carbon nanotubes, zirconia and ionic liquid to increase selectivity of the membrane.

Table 6.10: Proton conductivity (σ), methanol permeability (P) and selectivity (S) values of CP blends obtained at 28°C.

Sample Code	Proton Conductivity, σ (S/cm)×10^{-3}	Methanol Permeability, P (cm^2/sec.)×10^{-7}	Membrane Selectivity, S (S.sec./cm^3)×10^3
CP	0.13	2.42	0.54
CP-1	0.09	3.18	0.28
CP-2	0.011	4.67	0.024
CPH	1.12	0.34	32.94
CPH-1	0.68	1.46	4.65
CPH-2	0.47	1.74	2.71
N117 [26]	71	5.2	139.2
N212-GO [78]	40	0.792	50.51

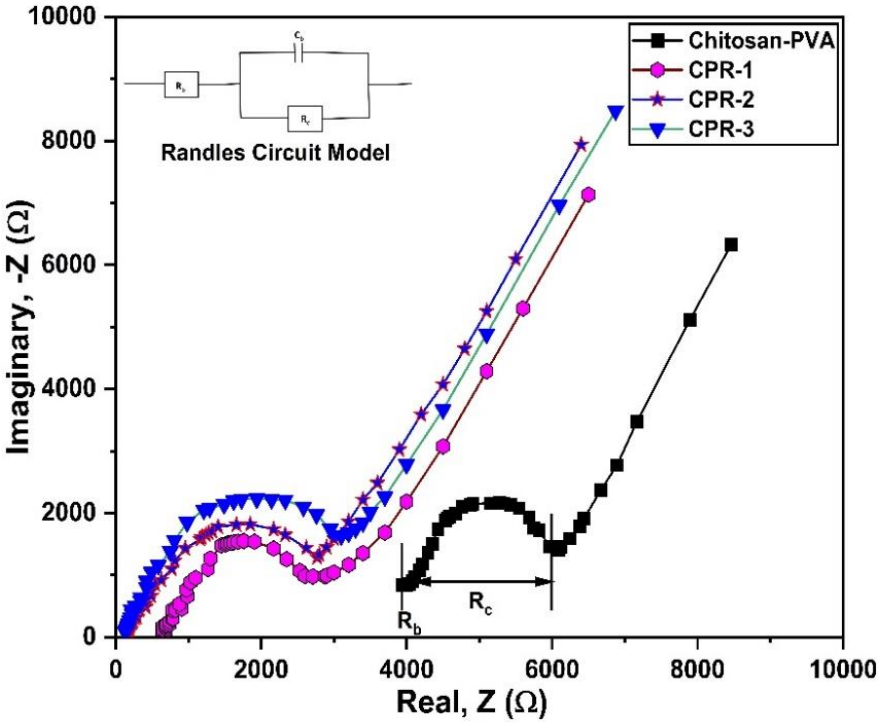

Figure 6.25: Fitting of an impedance data of the red mud modified CP blends in an equivalent circuit model.

The CP blend was modified by incorporating red mud nanoparticles to improve its selectivity. The effect of red mud nanoparticles on the proton conductivity and selectivity of the membrane was studied. The proton conductivity of the membranes are obtained at different temperature. The electrolyte resistance of the membranes are evaluated to obtain proton conductivity. The electrolyte resistance of the membrane was calculated by fitting the impedance values to an equivalent circuit model. The fitted impedance values to a circuit model is depicted in **Fig. 6.25**. After fitting the EIS data, the lower intercept of the semicircle region was used to calculate electrolyte resistance. The electrolyte resistance of the membrane measured at 30 and 70°C is reported in **Table 6.11**. After evaluating electrolyte resistance, proton conductivity of the membrane was obtained. The electrolyte resistance of the membrane steadily decreased as the red mud content increased. The membrane with lower electrolyte resistance provides higher proton conductivity. The CPR-3 membrane provides highest proton conductivity among the fabricated membranes. It provides more proton conductivity due to its higher IEC value. However, the electrolyte resistance of the CPR-4 membrane increased dramatically. Due to its higher electrolyte resistance, it provides lower proton conductivity. It was also confirmed that the red mud particles were aggregated in a CPR-4 membrane. Due to the aggregation of red mud particles, proton migration sites was blocked which reduces its proton conductivity. The effect of temperature on the proton conductivity the membrane is shown in **Fig. 6.26(a)**. The proton conductivity of the membrane increased as temperature increased. The mobility of the proton was enhanced at higher temperature which increases proton conductivity of the membrane. At 70°C, bound water content of the membrane plays role for proton transport. The free water available in the membrane was start to escape from the polymer domain. Hence, the proton transport by Grotthuss mechanism was declined. However, the presence of bound water will contributes higher proton conductivity. The proton transport was controlled by bound water regulated Grotthuss mechanism. Therefore, the membrane with higher bound water

provides better proton conductivity. It was noticed that the CPR-3 membrane provides highest proton conductivity among the fabricated membrane. The proton conductivity of the CPR-4 membrane was dropped dramatically. The CPR-3 membrane had a greater proton conductivity than the CP blends. However, it has lesser proton conductivity than the N117 membrane.

Table 6.11: Electrolyte resistance (R_b) and proton conductivity (σ) of the red mud modified CP blends obtained at 30ºC and 70ºC.

Sample Code	Membrane Resistance, R_b (Ω)		Proton Conductivity, σ (Scm^{-1}) ×10^{-4}	
	30ºC	70ºC	30ºC	70ºC
CP (10:90)	3689	2693	0.11	0.16
CPR-1	426.7	342.09	1.01	1.26
CPR-2	218.74	174.46	1.34	1.68
CPR-3	122.8	109.4	3.51	3.94
CPR-4	603	370.3	0.61	0.97

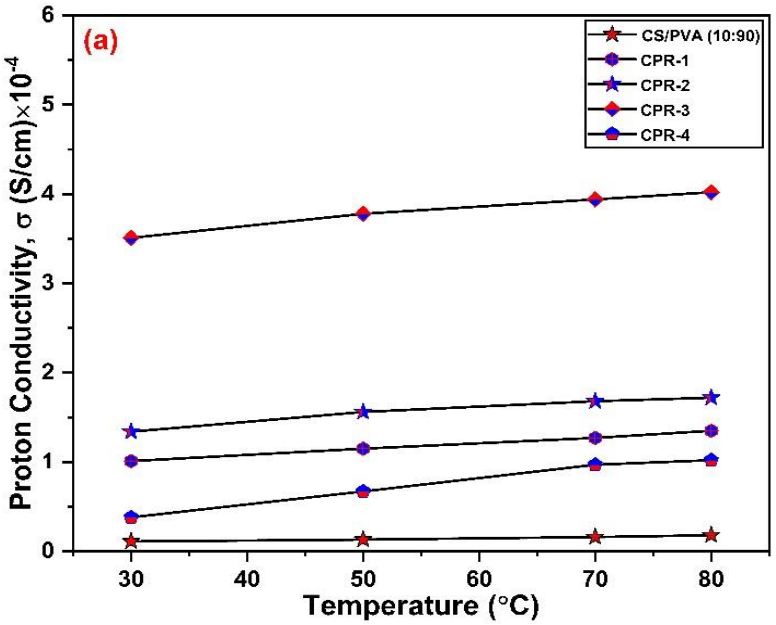

Figure 6.26 (a): Effect of temperature on the proton conductivity of red mud modified CP blends.

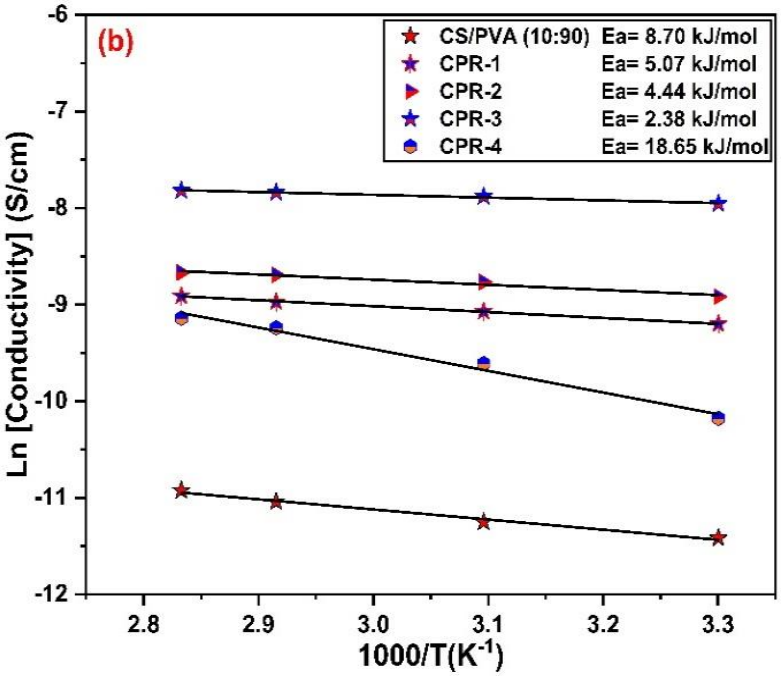

Figure 6.26 (b): Arrhenius plot for obtaining activation energy.

The Arrhenius plot of the red mud modified membrane is shown in **Fig. 6.26(b)**. The activation energy of the membranes are obtained from the slope of Arrhenius plot and reported in **Fig. 6.26(b)**. The activation energy of the red mud modified CP blend was found in the range 2.38-18.65 kJ/mol. The addition of red mud particles to the CP blend decreases its activation energy. It was also reported in a literature that the presence of iron oxide in a membrane reduces activation energy [**83**]. It was observed that the increase of red mud amount to the CP blend gradually decreases its activation energy except CPR-4 membrane. The lowest activation energy was observed in a CRR-3 membrane. The decline of activation energy signifies the least dependency of temperature on proton transport. The proton transport was highly controlled by Grotthuss mechanism. Due to Grotthuss control proton transport, CPR-3 membrane provides higher proton conductivity. The proton transport was controlled by vehicular mechanism in a CPR-4 membrane. Moreover, the proton transport was highly influenced by temperature. Therefore, CPR-4 membrane has lesser proton conductivity than the CPR-3 membrane.

The selectivity of the red mud modified CP blend was calculated and reported in **Table 6.12**. It was observed that the selectivity of the membrane was increases with the increase of red mud amount except CPR-4 membrane. The maximum selectivity was achieved in a CPR-3 membrane. The CPR-3 membrane has improved selectivity due to its superior methanol blocking ability and low proton conductivity. The CPR-4 membrane provides poor proton conductivity which reduces its selectivity. The selectivity of the CPR-3 membrane was lesser than the CPH blend. Therefore, further modification is required to achieve higher selectivity. The selectivity of the CPR-3 membrane was lower the commercial N117 membrane. The CPR-3 membrane was shown to be extremely effective in methanol blocking. The CPR-3 membrane has lesser methanol cross-over than the N117 membrane. Hence, proton conductivity of the CPR membrane plays crucial role for its selectivity. The proton conductivity of the CPR membrane was lower than the N117 membrane. The proton conductivity of the CPR membrane

should be enhanced to achieve higher selectivity. The proton conductivity of the CPR membrane can be improved by modifying its architecture or proton transport channel. Therefore, more research is needed to improve its proton conductivity.

Table 6.12: Proton conductivity (σ), methanol permeability (P) and selectivity (S) values of the red mud modified CP blends obtained at 30°C.

Sample	Proton Conductivity, σ (S/cm) $\times 10^{-3}$	Methanol Permeability, P ($cm^2/sec.$)$\times 10^{-7}$	Membrane Selectivity, S ($S.sec./cm^3$) $\times 10^{3}$
CP (10:90)	0.011	2.38	0.046
CPR-1	0.101	1.24	0.814
CPR-2	0.134	0.97	1.381
CPR-3	0.351	0.72	4.87
CPR-4	0.061	1.46	0.26

The CP blend was further modified with multiwall carbon nanotubes and ionic liquid to increase its proton conductivity. The impedance values were fitted to a circuit model and obtained electrolyte resistance. From the model parameters, electrolyte resistance was obtained. The proton conductivity of the developed membranes were calculated and reported in **Table 6.13**.

Table 6.13: Obtained electrolyte resistance (R_b) and proton conductivity (σ) of the MWCNT and ionic liquid modified CP blends.

Sample Code	Membrane Resistance, R_b (Ω)		Proton Conductivity, σ (Scm^{-1}) ×10^{-4}	
	30ºC	**70ºC**	**30ºC**	**70ºC**
CPCN-1	128.46	97.43	3.08	4.07
CPCN-2	116.8	67.68	3.39	5.85
CPCN-3	107.2	54.23	3.69	7.31
CPCN-4	187.4	106	2.11	3.74
CPCN@IL-1	42.46	29.15	9.33	13.61
CPCN@IL-2	37.23	23.46	10.65	16.91
CPCN@IL-3	28.46	18.42	13.94	21.52
CPCN@IL-4	81.9	61.67	2.44	6.43

The proton conductivity of the CP blend was increases with the increase of MWCNT content. The addition of MWCNT particles to the CP blend increases ion transport sites of the membrane. The hooping sites for ion transport was enhanced which increases proton transport capacity of the membrane. The increase of IEC of the membrane in a CPCN membrane was already confirmed. The CPCN-3 membrane provides highest proton conductivity among the pure membrane. The CPCN-3 membrane has higher proton conductivity than the CPR-3 membrane. It was noticed that the increase of temperature improves proton conductivity. **Figure 6.27(a)** depicts the rise in proton conductivity of the membrane at higher temperatures. The mobility of the proton was increased, which increased the membrane's proton conductivity. Moreover, at medium temperature (70°C), bound water of the membrane plays a crucial role for the enhancement of proton conductivity. The addition of MWCNT particles to the CP blend increases bound water of the membrane. Due to the existence of bound water, proton transport was controlled by bound water regulated Grotthuss mechanism. Therefore, the proton

conductivity in a CPCN-3 membrane was maintained at a higher value. There was a sharp decline in proton conductivity for the CPCN-4 membrane. Despite the presence of bound water in a membrane, aggregated MWCNT blocked proton transport sites, lowering proton conductivity. The CPCN membrane was further modified with ionic liquid to enhance its proton conductivity. The addition of ionic liquid incorporated extra ion transport sites in the membrane which increases ion transport capacity. The increase in IEC of the ionic liquid modified CPCN membrane was already confirmed. The increase in IEC of the membrane enhances proton conductivity of the membrane. Moreover, the addition of low vapour pressure liquid to the membrane facilitates proton transport by Grotthuss mechanism. At low humidity, the ionic liquid acts as a hooping site for proton transport and improves proton conductivity. The ionic liquid modified CPCN membrane was shown to have better proton conductivity than the CPCN membrane. The addition of ionic liquid to the CPCN membrane enhances proton conductivity from 3.69×10^{-4} to 13.94×10^{-4} S/cm.

The activation energy of the CPCN and CPCN@IL membrane were obtained from the slope of Arrhenius plot. The Arrhenius plot of the membranes are represented in **Fig. 6.27(b)**. The activation energy of the membranes are obtained in the range of 5.76-19.40 kJ/mol. It was observed at the CPCN membrane provides higher activation energy than the ionic liquid modified membrane. The highest activation energy was found in a CPCN@IL-4 membrane. The addition of 0.5wt. % MWCNT to the CP blend significantly reduces its activation energy. The CPCN-1 membrane provides the lowest activation energy of 5.76 kJ/mol. It signifies that the proton transport was highly independent on temperature and was controlled by Grotthuss mechanism. The addition of more MWCNT to the CP blend increases its activation energy then decreases. The decline in activation energy was observed form CPCN-3 to CPCN-4 membrane. The incorporation of ionic liquid to the CPCN-1, CPCN-2 and CPCN-3 membrane decreases their activation energy. The proton transport was least dependent on temperature and controlled

by Grotthuss mechanism. The proton transport was facilitated by the bound water regulated Grotthuss mechanism. The increase of bound water in an ionic liquid modified membrane was already confirmed. Due to Grotthuss control mechanism, these membranes will provides higher proton conductivity. However, in a CPZr@IL-4 membrane, proton transport was influenced by temperature. The higher activation energy signifies that the proton transport was controlled by vehicular mechanism. Therefore, it provides lower proton conductivity as compared to other membranes.

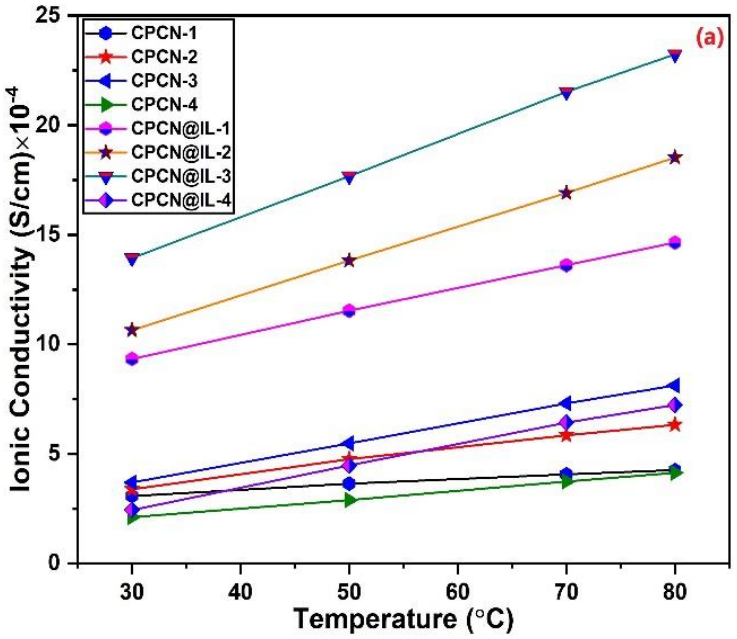

Figure 6.27 (a): Effect of temperature on the proton conductivity of MWCNT and ionic liquid modified CP blends.

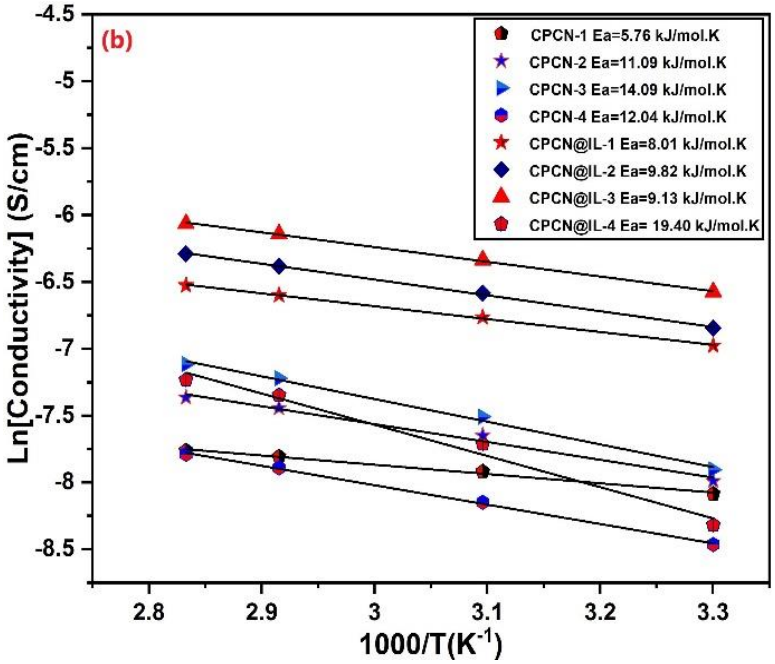

Figure 6.27 (b): Arrhenius plot for obtaining activation energy.

The selectivity of the CPCN and CPCN@IL- membranes are obtained and reported in **Table 6.14**. It was observed that the selectivity of the CPCN membrane was increases with the MWCNT content up to a certain extent then decreases. The highest selectivity was observed in a CPCN-3 membrane. The proton conductivity and methanol permeability of the membrane plays a crucial role which affects its selectivity. The membrane with good proton conductivity and excellent methanol blocking ability provides higher selectivity. The incorporation of ionic liquid to the CPCN membrane further improves selectivity. The CPCN@IL-3 membrane provides the highest selectivity among the fabricated membrane. It was found that the incorporation of ionic liquid to the CPCN-3 membrane increase the selectivity from 17.08×10^2 to 192.01×10^2 S.sec./cm^3. The selectivity of the CPCN@IL-3 membrane was 8 times more than the CPCN membrane. The ionic liquid enhances proton conductivity of the CPCN membrane. Moreover, the presence of bulk pendant group of ionic liquid block methanol transport channel thereby reducing methanol permeability. Therefore, ionic liquid modified CPCN membrane provides higher selectivity than the CPCN membrane. The ionic liquid modified CPCN membrane has a greater selectivity than the CPR membrane. However, the selectivity of the CPCN and CPCN@IL membranes were lower than the N117 membrane.

Table 6.14: Membrane selectivity of the MWCNT and ionic liquid modified CP blends.

Sample Code	**Proton Conductivity, σ (S/cm)×10^{-4}**	**Methanol Permeability, P (cm^2/sec.)×10^{-7}**	**Membrane Selectivity, S (S.sec./cm^3)×10^2**
CPCN-1	3.08	7.86	3.92
CPCN-2	3.39	5.04	6.73
CPCN-3	3.69	2.16	17.08
CPCN-4	2.11	9.16	2.31
CPCN@IL-1	9.33	0.926	100.75
CPCN@IL-2	10.65	0.843	126.33
CPCN@IL-3	13.94	0.726	192.01
CPCN@IL-4	2.44	0.558	43.72

The electrolyte resistance of the zirconia and ionic liquid modified CP membrane was evaluated by fitting the impedance values in a circuit model. After obtaining electrolyte resistance, proton conductivity of the membrane was calculated. The electrolyte resistance and proton conductivity of the membranes obtained at 30 and 70°C is reported in **Table 6.15**. It was observed that the addition of zirconia particles to the CP blend gradually decrease electrolyte resistance. It signifies that the migration sites of ion transport was increases. Due to the enhancement of ion migration sites, IEC of the membrane was increases. However, the aggregation of zirconia particles to the polymer matrix depleted ion migration sites. Due to aggregation of particles, IEC of the membrane was decreases. Therefore, CPZr-4 membrane provides higher electrolyte resistance as compared to the CPZr-3 membrane. At low temperature, IEC and free water of the membrane plays important role for proton conductivity. The membrane with higher IEC and free water content provides better proton conduction. The CPZr-3 membrane provides higher proton conductivity than the CPZr-4, CPZr-2 and CPZr-1 membrane. The presence of free water will facilitate proton conduction by Grotthuss mechanism. It was believed that the addition of filler reconstruct the architecture of polymer domain [**84**]. A phase separated semi-interpenetration network was developed in the polymer domain. The semi-interpenetration network of polymer domain improves the hooping sites for proton transport [**85**]. Therefore, the addition of zirconia to the CP blend improves the hooping site for proton transport and increases its proton conductivity. The proton conductivity achieved in a CPZr-3 membrane was significantly higher than that of the CPCN-3 and CP blends. Moreover, proton conductivity of the CPZr membrane was increased with increasing temperature. The effect of temperature on the proton conductivity of the membrane is represented in **Fig. 6.28(a)**. The bound water of the membrane plays important role for the transport of proton at medium temperature. The proton transport was controlled by bound water

regulated Grotthuss mechanism. The membrane with higher bound water facilitates higher proton conduction by Grotthuss mechanism. Further improvement in proton conductivity was noticed in a CPZr membrane after adding ionic liquid. The addition of ionic liquid creates extra hooping sites for proton transport in a polymer channel. Due the enhancement of hooping sites for proton transport, ionic liquid modified membrane provides higher proton conductivity. It was reported in a literature that the ion liquid improves ion migration sites in a membrane [**86, 87**]. The addition of ionic liquid creates extra charge carrier in a membrane which increases IEC. The increase of IEC in an ionic liquid modified membrane was already reported. The highest proton conductivity was achieved in a CPZr@IL-3 membrane (12.65×10^{-4} Scm^{-1}). The bound water and ionic liquid facilitates the proton conduction at reduced humidity conditions. The proton conductivity reported in a CPZr@IL-3 membrane was higher than the multiwall carbon nanotubes modified CP membrane as well as red mud modified membrane. However, its proton conductivity value was still inferior to the N117 membrane.

Table 6.15: Electrolyte resistance (R_b) and proton conductivity (σ) of the zirconia and ionic liquid modified CP blends obtained at 30ºC and 70ºC.

Sample Code	Electrolyte Resistance, R_b (Ω)		Proton Conductivity, σ (Scm^{-1}) ×10^{-4}	
	30ºC	70ºC	30ºC	70ºC
CPZr-1	76.26	54.45	5.20	7.28
CPZr-2	68.32	48.52	5.80	8.17
CPZr-3	57.46	41.12	6.91	9.64
CPZr-4	62.26	44.93	6.36	8.82
CPZr@IL-1	46.78	22.45	8.47	17.67
CPZr@IL-2	35.68	16.34	11.12	24.26
CPZr@IL-3	31.33	11.46	12.65	34.61
CPZr@IL-4	39.52	19.62	10.03	20.21

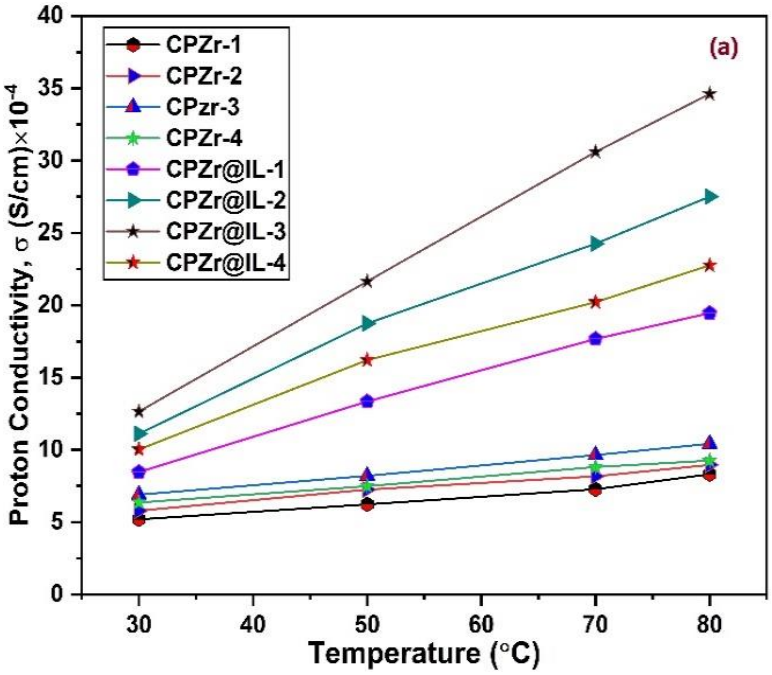

Figure 6.28 (a): Effect of temperature on the proton conductivity of zirconia and ionic liquid modified CP blends.

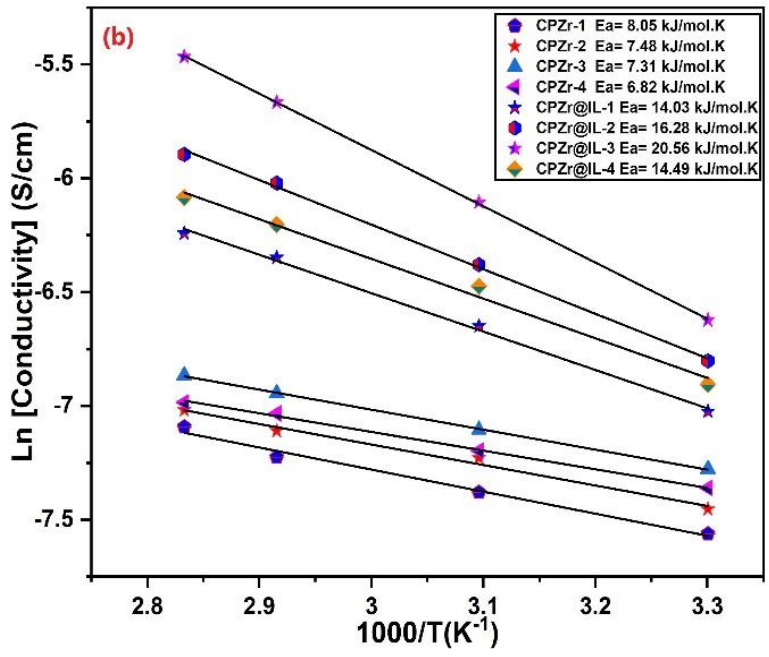

Figure 6.28 (b): Arrhenius plot for obtaining activation energy.

The amount of energy required for proton conduction in a CPZr and CPZr@IL membrane was obtained from the slope of Arrhenius plot. The Arrhenius plot the membrane is represented in **Fig. 6.28(b)**. The activation energy was obtained from the slope of Arrhenius plot and reported in the figure. The minimum energy required for proton transport was found in the range of 6.82-20.46 kJ/mol. It was observed that the addition of zirconia to the CP blend reduces its activation energy. It reveals that proton transport was least dependent by temperature with the increase of zirconia amount. The proton transport was dominated by Grotthuss mechanism. However, the addition of ionic liquid to the blend increases its activation energy. The proton transport was highly influenced by temperature. Moreover, the proton transport was controlled by vehicular mechanism. The selectivity of the membrane was calculated and reported in **Table 6.16**. It was observed that the addition of zirconia and ionic liquid to the CP blend gradually increases it selectivity. The highest selectivity was found in a CPZr@IL-3 membrane (11.712 $\times 10^3$ S.sec./cm^3). The selectivity of the CPZr@IL-3 membrane was higher than the CP blend and CPR membrane. It provides slightly lower selectivity than the CPCN@IL-3 membrane. Moreover, CPZr@IL-3 has lower selective than the commercial N117 membrane. It was reported that the developed membrane provides excellent methanol blocking ability. However, the proton conductivity of the membrane was achieved at lower value. Due to its lower proton conductivity, it provides lower selectivity than the N117 membrane. The CPCN@IL-3 membrane provides the highest selectivity among the fabricated membrane.

Table 6.16: Proton conductivity (σ), methanol permeability (P) and selectivity (S) values of the zirconia and ionic liquid modified CP blends.

Sample Code	Proton Conductivity, σ (S/cm)×10^{-4}	Methanol Permeability, P (cm^2/sec.)×10^{-7}	Membrane Selectivity, S (S.sec./cm^3)×10^2
CPZr-1	5.20	11.46	4.54
CPZr-2	5.80	9.81	5.91
CPZr-3	6.91	7.53	9.18
CPZr-4	6.36	6.18	10.29
CPZr@IL-1	8.47	1.35	62.74
CPZr@IL-2	11.12	1.21	91.90
CPZr@IL-3	12.65	1.08	117.12
CPZr@IL-4	10.03	0.94	106.70

6.5.2 SPEEK-PVA-Silica Hybrid Membrane

The proton conductivity of the SPEEK based hybrid membrane was evaluated by performing impedance test. The electrolyte resistance of the membrane was obtained from the Nyquist plot and equivalent circuit model. In a Nyquist plot, resistance was obtained from the intercept at high frequency region of semicircle. After evaluating bulk resistance, proton conductivity of the membrane was obtained. The proton conductivity of the SPEEK based hybrid membrane was compared with the Chitosan based hybrid membrane and commercial N117 & N112 membrane. The obtained proton conductivity of the SPEEK based hybrid membranes are reported in **Table 6.17**. The proton conductivity obtained at different temperature is shown in **Fig. 6.29(a)**. The proton conductivity obtained for the developed membranes agrees well with the literature study [**88**]. It was noticed that the increase of temperature increases proton conductivity. At 30°C, SPS-3 membrane provides the highest proton conductivity of 3.8×10^{-2} Scm^{-1}. The proton conductivity was controlled by free water regulated Grotthuss mechanism. Moreover, it was reported that IEC and DS of the membrane influence proton conductivity. The membrane with higher IEC and DS provides better proton conductivity. The proton

conductivity of the SPS-3 membrane was slightly lower than the N117 and N112 membrane [**25**]. Moreover, it provides significantly higher proton conductivity than the Chitosan based membrane. The proton conductivity of the SPS-3 membrane was compared with the graphene oxide modified SPEEK membrane. It was found that the proton conductivity in a SPS-3 was one order higher than the SPEEK-PVA-GO composite membrane [**89**]. However, its proton conductivity was marginally lower than the N112-GO membrane [**90**]. Although, the SPS-3 membrane provides excellent proton conductivity but major drawbacks of the SPEEK based membrane was their higher cost and methanol cross-over. It is desirable to develop cost effective membrane with higher proton conductivity and excellent methanol blocking ability.

Table 6.17: Comparison of the proton conductivity data of SPEEK-PVA-silica hybrid membranes obtained at different temperature and hydrated condition with the reported work.

Sample	Proton Conductivity, σ (S/cm)×10^{-2}				Activation Energy, E_a (kJ/mol.)	Reference
	30°C	50°C	70°C	80°C		
SPEEK	2.8	3.9	5	5.7	12.17	This work
SPEEK-PVA	2.6	3.27	4.14	4.49	9.89	This work
SPS-1	3.2	4.29	5.36	6.01	11.12	This work
SPS-2	3.5	4.58	5.84	6.52	10.59	This work
SPS-3	3.8	4.9	6.15	6.79	10.36	This work
SPS-4	2.7	3.75	4.83	5.56	12.66	This work
SPEEK-PVA-GO	0.1	0.27	0.36	0.6	1.4	[**80**]
N212	4.6	6	8	9	10.39	[**25**]

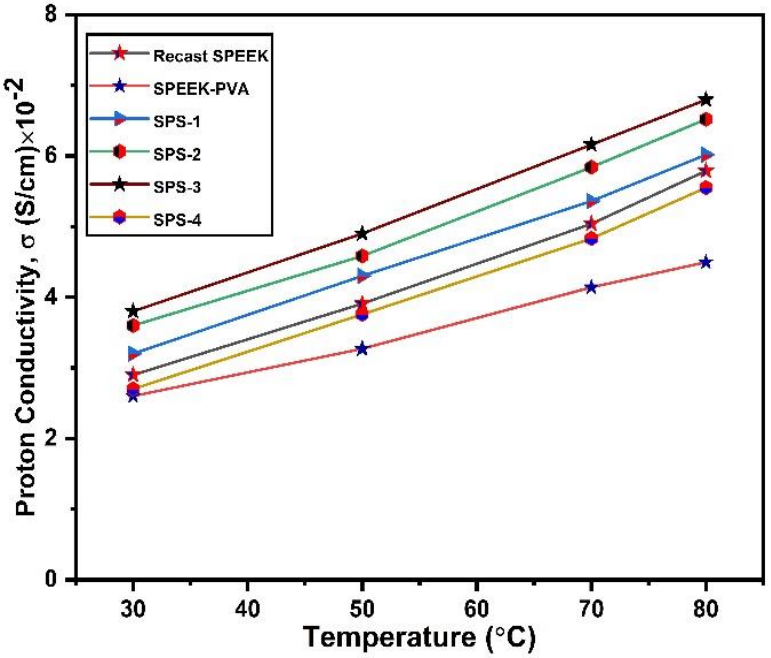

Figure 6.29 (a): Proton conductivity of the SPEEK-PVA-silica hybrid membranes obtained at different temperatures and hydrated condition.

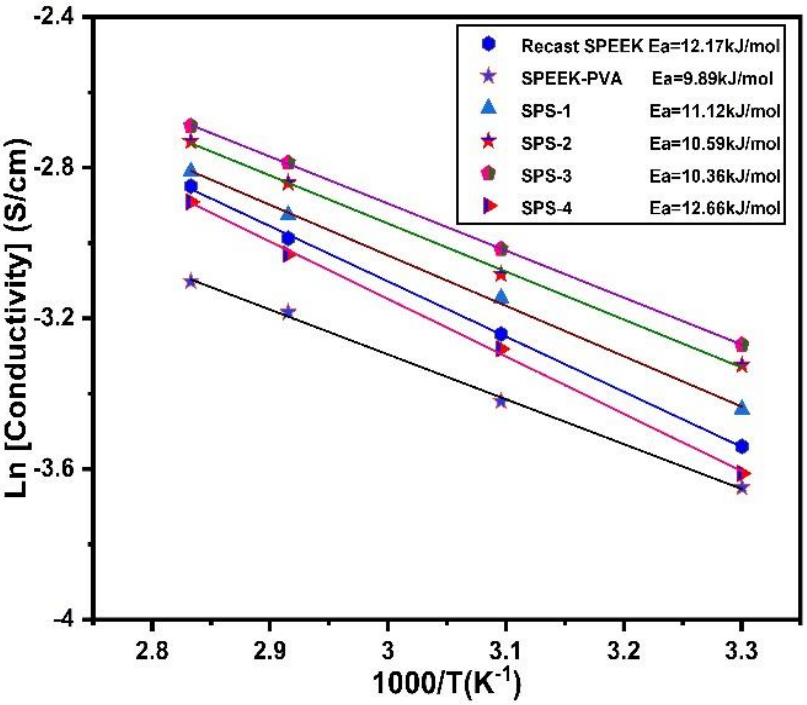

Figure 6.29 (b): Arrhenius plot for obtaining activation energy.

The activation energy of the SPEEK based hybrid membranes are obtained from the slope of Arrhenius plot. The Arrhenius plot of the SPEEK based hybrid membranes are shown in **Fig. 6.29(b)**. The activation energy of the membranes is reported in an Arrhenius plot. The activation energy of the SPEEK based hybrid membranes are obtained in the range of 9.98-12.66 kJ/mol. The activation energy range was similar to the Chitosan based membrane. Moreover, its activation energy was fall in the range of Nafion based membrane. The slight decrease in activation energy for proton transport was observed with the increase of silica amount. It implies that proton transport was least affected by temperature and was governed by the Grotthuss mechanism. At lower temperature, free water plays a crucial role and it facilitates proton transport by Grotthuss mechanism. However, at medium temperature, proton transport was controlled by bound water. In a SPS-4 membrane, mobility of the proton transport was highly dependent on temperature. The selectivity of the SPEEK based hybrid membranes are calculated and reported in **Table 6.18**. The SPS-3 membrane provides lower selectivity than the commercial N117 membrane [**91**]. However, the selectivity of SPS-3 membrane was superior to the Chitosan based hybrid membranes.

Table 6.18: Proton conductivity (σ), methanol permeability (P) and selectivity (S) values for SPEEK-PVA-silica hybrid membranes obtained at room temperature.

Sample Code	**Proton conductivity, σ (S/cm)×10^{-2}**	**Methanol permeability, K (cm^2/sec.)×10^{-7}**	**Membrane Selectivity, S (S.sec./cm^3)×10^4**	**Reference**
SPEEK	2.8	7.11	3.93	This work
SPEEK-PVA	2.6	6.23	4.17	This work
SPS-1	3.2	5.87	8.26	This work
SPS-2	3.5	4.16	8.41	This work
SPS-3	3.8	3.21	11.83	This work
SPS-4	2.7	2.09	12.93	This work
N117	7.1	5.16	13.76	[**20**]
N212-GO	4	0.792	5.051	[**77**]

6.6 Single Cell Performance Analysis of a DMFC

6.6.1 Performance evaluation using red mud modified membrane

6.6.1.1 Effect of methanol feed concentration

The fuel cell operated at low temperature provides poor performance due to uncontrolled water management. The fuel cell produces electricity by the electrochemical splitting of reactants at anode. Moreover, permeated reactant participates for electrochemical reaction at the cathode surface and generates water. The water produced at cathode interface was absorbed by the electrolyte membrane. The hydration state of the membrane was impacted by the presence of extra water. The membrane with proper hydration level improves proton conductivity. However, the presence of excess water created by the electrochemical process will obstruct the proton transfer channel of the electrolyte membrane. The presence of more water in an electrolyte membrane affects hydration level which drastically reduces its proton conductivity. The decrease in proton conductivity lowers power density and cell potential of the fuel cell. To improve cell performance, fuel cell should be operated at a medium temperature to avoid water management issue. At reduced humidity conditions, excess free water available in the membrane was evaporated. Moreover, the loss of free water in a membrane reduces hydration level. The bound water of the membrane plays a crucial role which increases cell performance. The strongly attached bound water facilitate proton transport by Grotthuss mechanism. The membrane with higher bound water will provides better proton conductivity. Moreover, the mobility of the proton was enhanced at medium temperature which improves proton conductivity. The performance of the fuel cell was measured at 70°C for various methanol input concentrations (0.5, 1 and 2M). During experiment, feed flow rate of diluted oxygen and methanol were maintained at 100ml/min and 1ml/min respectively. The cell performance was evaluated for CP and CPR-3 membrane. The polarization curve obtained for CPR-3 membrane is shown in **Fig. 6.30(a)**. The open circuit voltage and power density of the cell was gradually

increasing with the increase of methanol concentration. With the increase of methanol feed concentrations, more amount of methanol was participated for oxidation reaction. Due to oxidation reaction, proton was produced at anode and transported though the electrolyte membrane. The proton conductivity of the electrolyte membrane was increased, which increases cell voltage and power density. It was observed that as the current density increases, cell voltage was steadily decreases. The polarization loss caused voltage decay of the fuel cell. The fuel cell operated with 2M methanol feed provides the highest power density of 44mW/cm^2 at a current density of 140mA/cm^2. The cell performance for CPR-3 membrane was compared with the CP membrane. The polarization curve for CPR-3 and CP membrane obtained at 70°C and 2M methanol feed is shown in **Fig. 6.30(b)**. The CPR-3 membrane provides higher cell performance as compared to CP membrane. The CPR-3 membrane has a greater proton conductivity than the CP blends. Hence, CPR-3 membrane provides higher power density than the CP membrane. The power density achieved by CPR-3 membrane was slightly lower than the carbon nanotube fluid modified Chitosan membrane [**22**]. However, it produces lower power density than the Nafion membrane. The Nafion membrane has better proton conductivity than the CPR-3 membrane. Therefore, it produces lower power density than the commercial Nafion membrane. The peak power density of N117 membrane reported at 70°C and 2M methanol feed was 720 mW/cm^2 at a current density of 180 mA/cm^2. For potential application of the red mud modified membrane in a direct methanol fuel cell, power density should be achieved to a higher level. The higher power density can be achieved by improving the proton conductivity of the membrane. Therefore, further structural modification was required in a CPR membrane to enhance its proton conductivity.

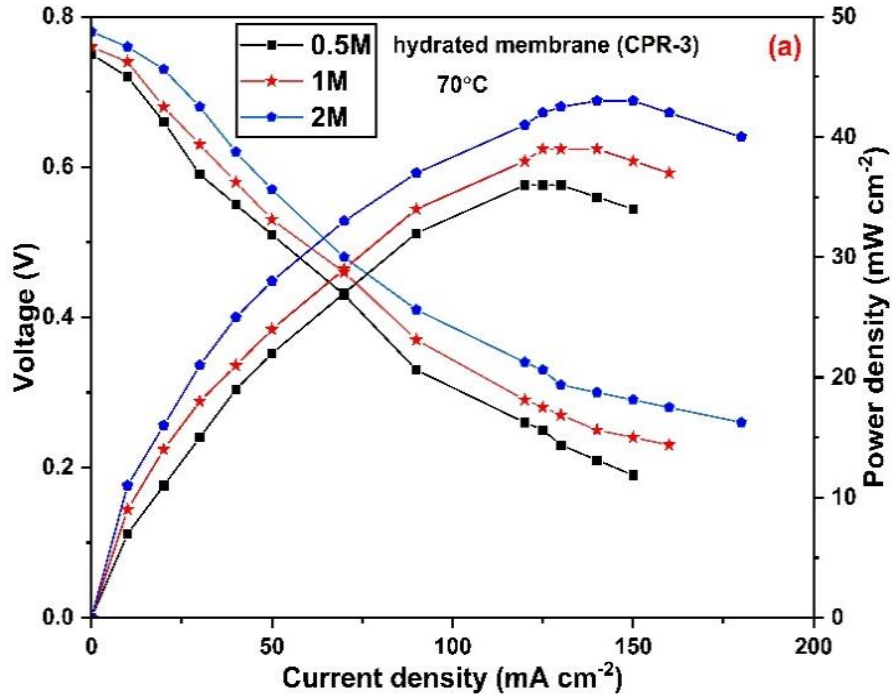

Figure 6.30: Polarization and power density curve of fuel cell obtained at 70°C for CPR-3 membrane. (a) Effect of methanol feed concentration.

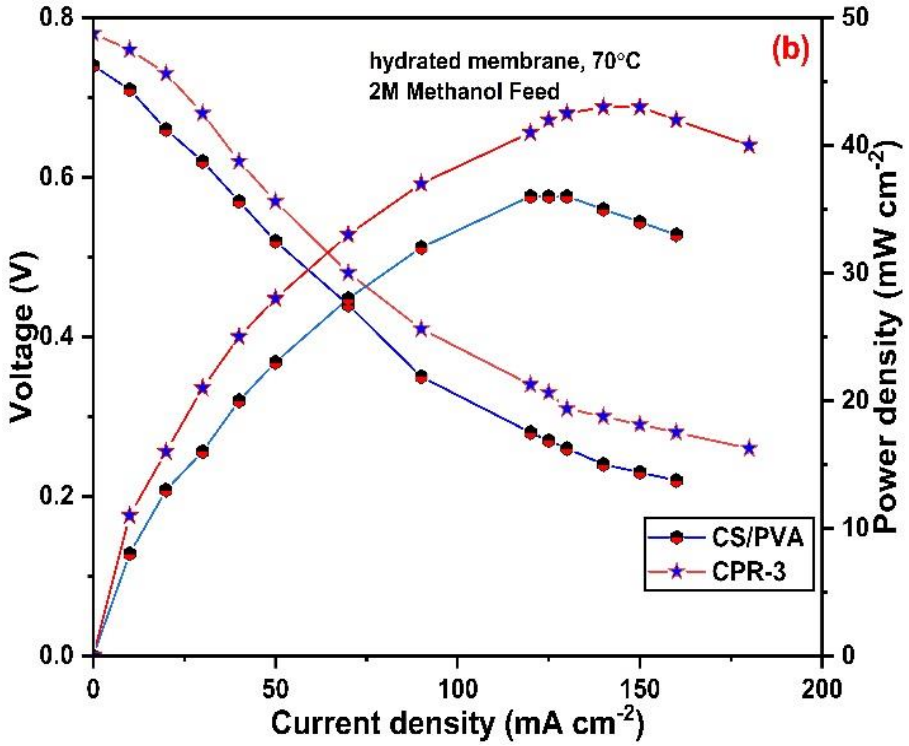

Figure 6.30 (b): Fuel cell performance for CP and CPR-3 membrane.

6.6.1.2 Long Term Durability Test of Fuel Cell

The long-term degrading stability of the fuel cell for CP and CPR-3 membranes was investigated by measuring cell performance at a constant current flow of 0.015 Acm^{-2}. The cell potential was recorded at 70°C and 2M methanol feed for 144h duration. The behavior of cell potential for the 144h duration of CPR-3 membrane and CP membrane is shown in **Fig. 6.31(a)**. The voltage decay was similar for both membrane till 30h and after that significant changes of voltage decay was noticed for both membranes. The higher voltage decay was occurred for CP membrane as compared to CPR-3 membrane. The polarization loss caused voltage reduction of the cell. The higher polarization loss was occurred in a CP membrane as compared to CPR-3 membrane. Moreover, at higher current density region, polarization loss was dominated by concentration loss [**92**]. The loss of methanol centration decline methanol oxidation at anode side. The loss of methanol was occurred due to methanol cross-over through the membrane. The amount of proton produced by oxidation reaction was reduces which decreases proton conductivity. The low proton conducting membrane reduces power density and cell voltage of fuel cell. There was a slight decay of cell voltage was noticed in a CPR-3 membrane. During durability test, 1.76% of cell voltage was declined which is insignificant. The cell performance during durability test was evaluated. The power density of fuel cell was obtained before and after durability test. The cell performance was evaluated at 70°C and 2M methanol feed for CPR-3 membrane. During experiment, methanol and diluted oxygen were supplied at a constant rates of 1ml/min and 100ml/min respectively. After performing durability test, power density achieved by the CPR-3 membrane was declined from 43 mW/cm^2 to 41 mW/cm^2. The decline of power density was due to the voltage decay by polarization loss.

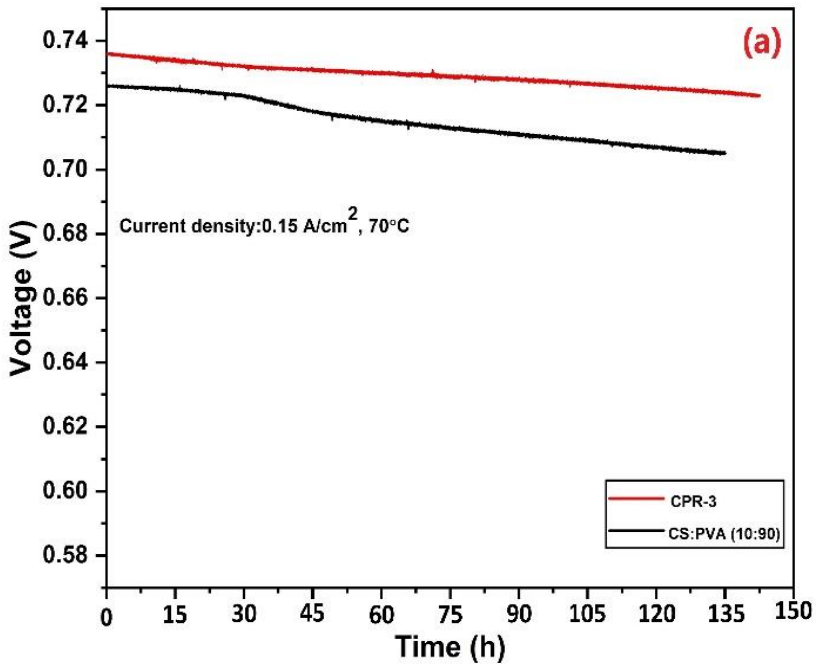

Figure 6.31 (a): Durability test of the fuel cell was conducted for 144hr. at constant current density of 0.15 A/cm^2 at 70°C. Voltage degradation curve.

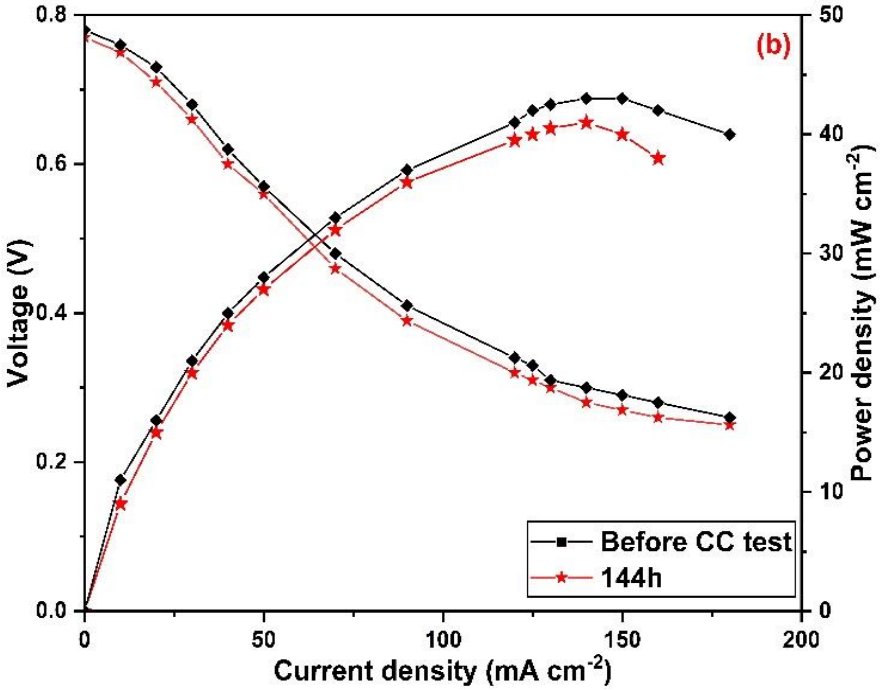

Figure 6.31 (b): Performance degradation curve of the fuel cell operating with a CPR-3 membrane.

6.6.2 Performance Evaluation using MWCNT Modified Membrane

The Chitosan membrane was further modified with multiwall carbon nanotubes and ionic liquid. The fuel cell performance was evaluated for the best performing membrane. It was reported that the CPCN-3 and CPCN@IL-3 membranes were provide higher selectivity among pure and ionic liquid modified membranes. Therefore, fuel cell performance was measured for these membranes at 70°C and 2M methanol feed. During experiment, feed flow rate of diluted oxygen and methanol were maintained at 100ml/min and 1ml/min respectively. The power density and cell voltage of the fuel cell was obtained from the polarization curve as shown in **Fig. 6.32**. As the current density increases, the cell voltage steadily drops. At a higher current density region, polarization loss was dominated by ohmic loss. The ohmic loss causes more polarization loss in a fuel cell. Due to ohmic loss, voltage decay was higher at higher current density region. The cell voltage was decreases due to polarization losses. The cell performance for CPCN-3 and CPCN@IL-3 membranes were compared. The CPCN@IL-3 membrane provides higher power density than the CPCN-3 membrane. The CPCN@IL-3 membrane provides the maximum power density of 82 mW/cm^2 at a current density of 370 mA/cm^2. The power density achieved in a CPCN@IL-3 membrane was significantly lower than the N117 membrane. The power density and cell voltage of fuel cell should be enhanced to a higher level for its prospective applications. To attain increased power density, Chitosan based membrane should be modified to achieve higher proton conductivity. Therefore, more study is required to build a Chitosan-based membrane with greater proton conductivity. Aside from proton conductivity, research should focus on the stability of membrane at extreme conditions. Moreover, durability of the membrane was influenced by mechanical and thermal stability of membrane. The research should concentrate on the fabrication of a highly stable membrane at low cost.

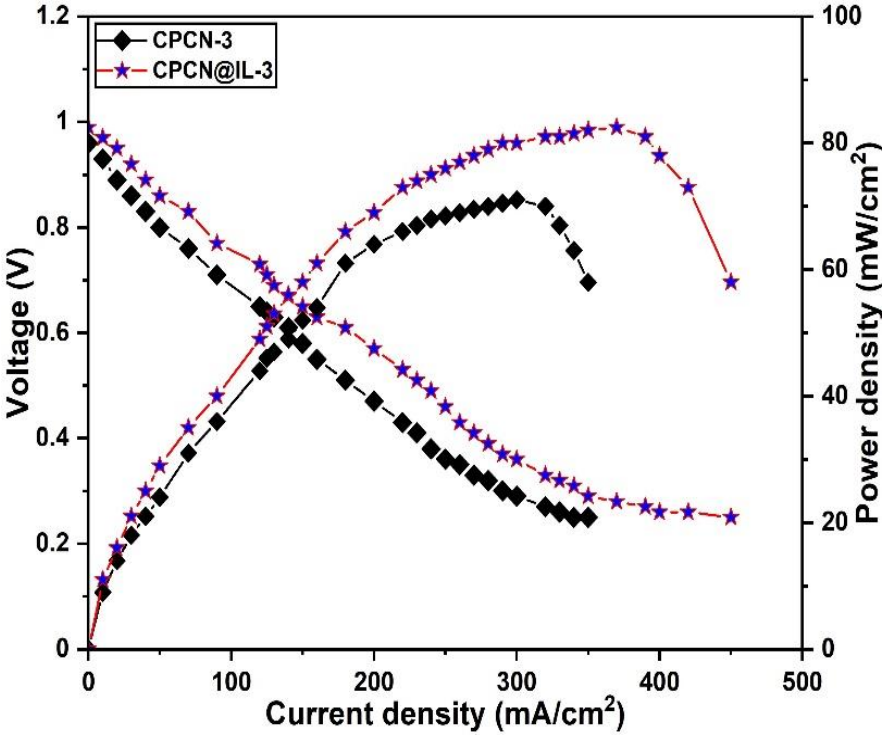

Figure 6.32: Polarization curve of a fuel cell obtained at 70°C and 2M methanol feed for CPCN-3 and CPCN@IL-3 membrane.

6.6.3 Performance Analysis using Zirconia Modified Hybrid Membrane

The Chitosan membrane was modified with the ionic liquid and hygroscopic zirconia to improve its proton conductivity and to achieve higher power density of fuel cell. The modified membrane has a greater proton conductivity than the MWCNT modified membrane. It was confirmed that the CPZr-3 and CPZr@IL-3 membrane provides highest proton conductivity among the zirconia and ionic liquid modified membranes. These membranes were used to evaluate cell performance for their higher proton conductivity. The fuel cell performance of the modified membrane was evaluated at 70°C and 2M methanol feed. The feed flow rate was maintained at 100ml/min and 1ml/min respectively. The polarization curve of the membranes are reported in **Fig. 6.33**. The CPZr@IL-3 membrane provides the highest power density of 97 mW/cm^2 at a current density of 440 mA/cm^2. The highest power density of 78 mW/cm^2 was achieved in a CPZr-3 membrane. The power density of these membranes were compared with the MWCNT followed by ionic liquid modified membranes. The ionic liquid modified CPZr-3 membrane provides maximum power density among the fabricated membranes. The power density achieved in a CPZr@IL-3 membrane was higher than the CPCN@IL-3 membrane. The ionic liquid incorporated CPZr-3 membrane provides higher power density due to its excellent proton conductivity. The ionic liquid modified CPZr-3 membrane provides good performance. However, the major drawbacks of the membranes was its higher swelling degree which reduces its dimension stability. Therefore, CPZr-3 membrane was considered to be a better candidate for fuel cell application. In a future, dimension stability of an ionic liquid modified membrane should be improved by reducing its swelling degree. The dimension stability of the membrane affects durability of the fuel cell. The power density achieved by CZr@IL-3 membrane was lower than the N117 membrane. The swelling degree of the membranes should be reduced to achieve fuel cell durability. Moreover, the proton conductivity of the membrane should be improved further to achieve higher power density.

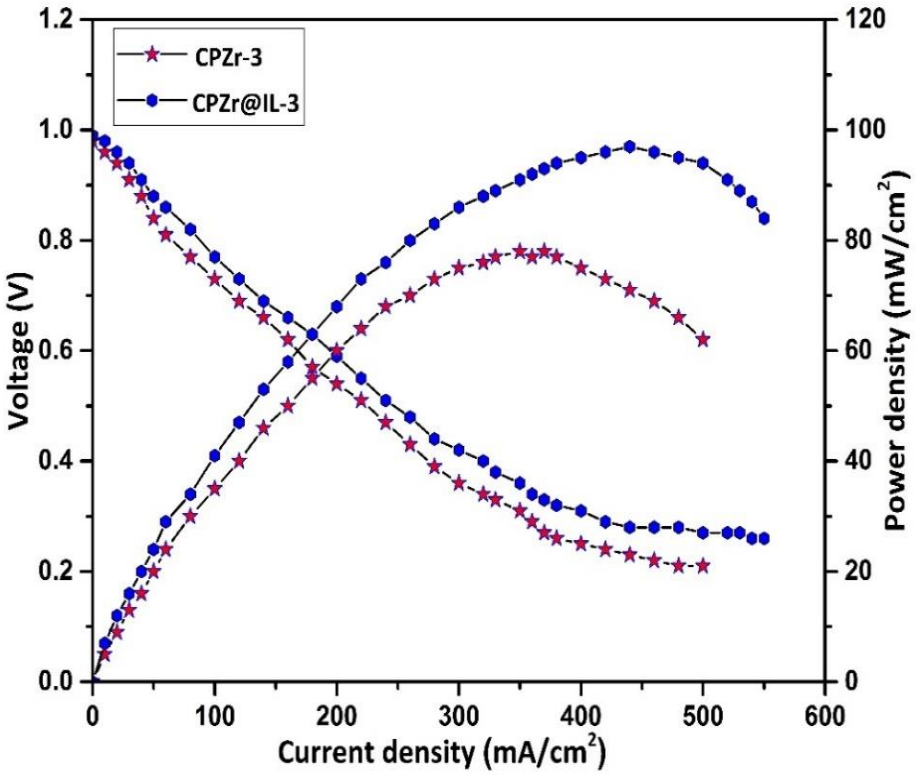

Figure 6.33: Polarization curve of a fuel cell obtained at 70°C and 2M methanol feed for CPZr-3 and CPZr@IL-3 membrane.

6.7 Mathematical Modelling of DMFC

The kinetic equation for methanol oxidation at anode and cathode flow channel was modelled to predict cell voltage and leakage current. Moreover, the influence of methanol concentration on cross-over rate was also predicted. The generation of leakage current was caused by the electrochemical oxidation of methanol at cathode interface. It has no use in a fuel cell and it reduces cell performance. If more methanol passes through the membrane, then more methanol participates for the oxidation reaction, resulting in a significant leakage current. Therefore, membrane with lower methanol cross-over was preferred to improve fuel cell performance by declining leakage current. The effect of methanol supply on leakage current was estimated by modelling the electrochemical oxidation reaction of methanol. The generation of leakage current at different methanol feed concentration in a fuel cell was predicted and represented in **Fig. 6.34**. It was observed that the supply of highly concentrated methanol at the anode side increases leakage current. The similar results were reported by Garcia et al. [**58**] and Wang et al. [**60**] on their theoretical studies. The effect of methanol supply on its cross-over rate through the membrane was predicted and shown in **Fig. 6.35**. The supply of highly concentrated methanol to the anode side increases the cross-over of methanol. It is believed that the slow kinetics of methanol oxidation at anode side causes higher methanol cross-over rate. The activity of Platinum/Ruthenium catalyst for methanol oxidation was very low. Due to its low activity, oxidation reaction was very slow. Due to slow oxidation mechanism, less amount of methanol are oxidized and rest are transported through the membrane via diffusion. Hence, higher methanol cross-over rate is observed when highly concentrated methanol is supplied to the anode flow channel. For better performance and improve fuel efficiency, methanol cross-over rate across the membrane should be declined. Fuel cross-over can be reduced by developing the highly performance anode catalyst to fastening the oxidation reaction. As the methanol cross-over increased, more methanol are oxidized at cathode interface, resulting in a

greater leakage current. The amount of leakage current produces at higher methanol feed concentration is significant which negatively affect cell performance. Therefore, it is appealing to operate a fuel cell at lower methanol feed concentration to reduces leakage current. However, at lower concentrations of methanol feed input, cell performance is poor. The fuel cell provide lower power density and cell voltage. Therefore, methanol supply is optimized to improve cell performance. It was also reported that fuel cell operating at higher current density region produces lower leakage current [**59**]. At higher current density, the electrochemical reaction at the anode surface occurs more quickly, allowing methanol to be oxidised faster and minimising methanol loss due to low cross-over. Hence, less amount of leakage current is generated at cathode side. Moreover, faster electrochemical improves power density of the fuel cell.Therefore, it is suggested that the fuel cell should be operated at higher current density to minimize leakage current.

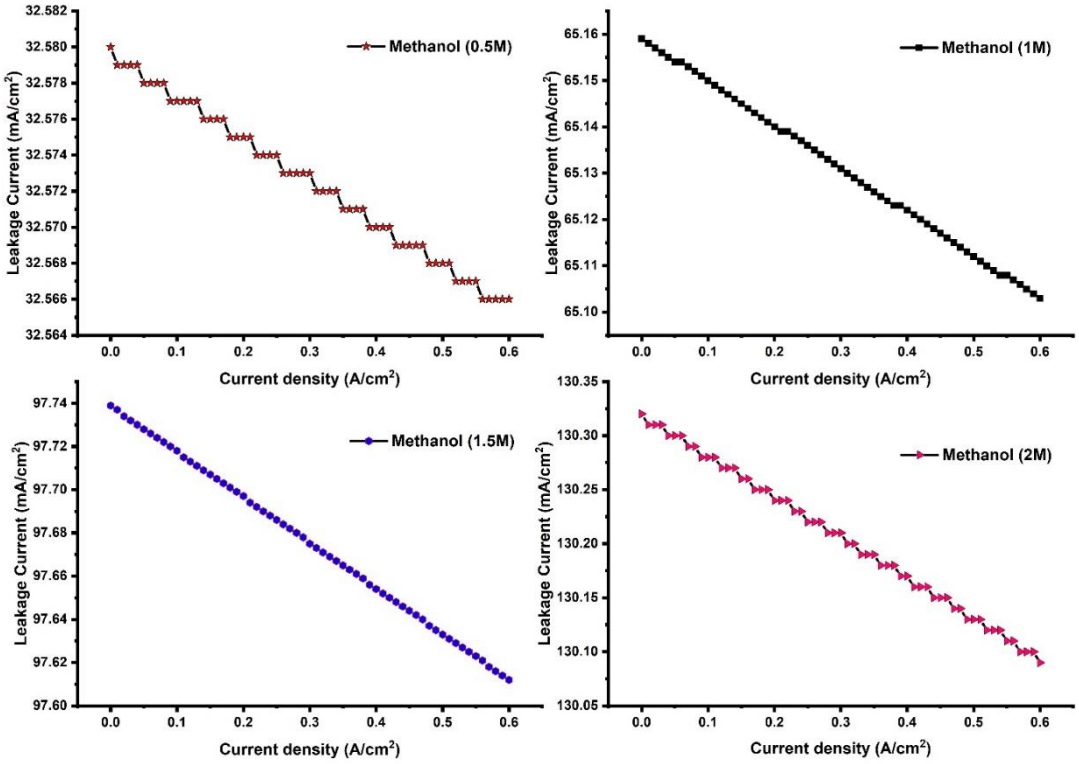

Figure 6.34: Influence of methanol input concentration on the generation of leakage current at cathode side of DMFC.

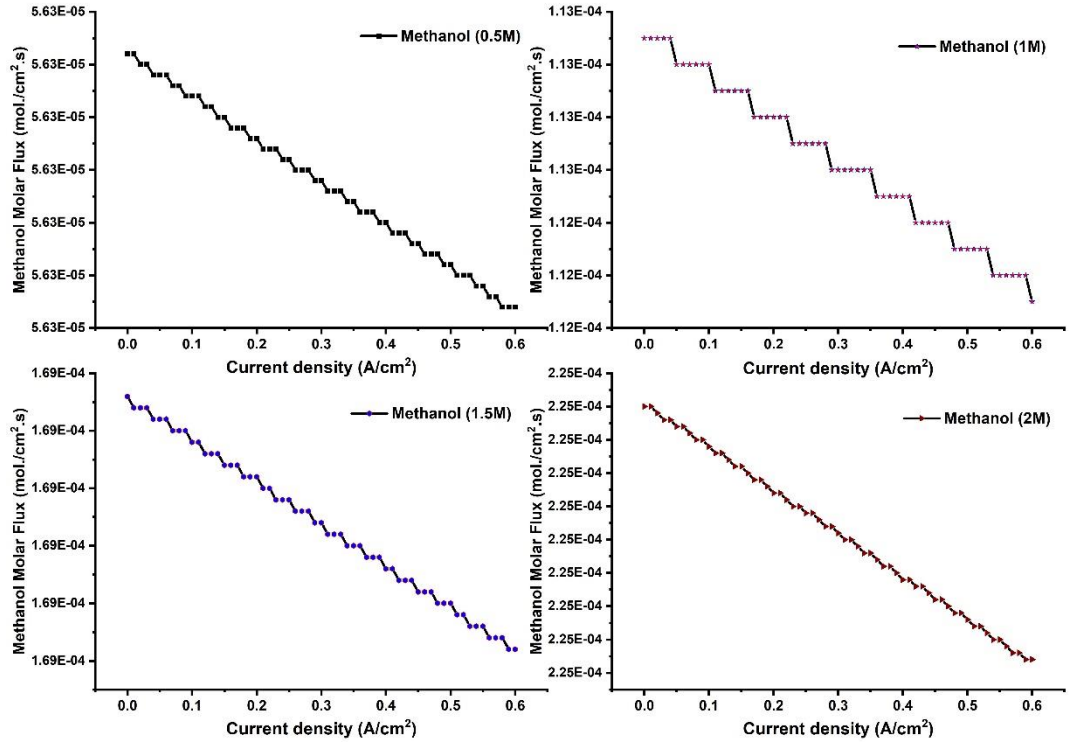

Figure 6.35: Prediction of methanol cross-over rate through the membrane. Influence of methanol input concentration on fuel cross-over rate.

The proposed model was simultaneously solved in a simulated environment and predicted the cell voltage at different concentration of methanol. The polarization curve of the DMFC was predicted at different concentration of methanol and shown in **Fig. 6.36**. The increase of methanol concentration at anode side increase cell voltage with power density. The increase of methanol concentration at feed side increases the amount of methanol oxidized at anode surface. The oxidation of methanol at anode produces more electric current. The electric current was collected by a current collector and stored in an external load. The generation of more electric current enhances cell voltage. The maximum cell voltage was predicted for 2M methanol feed at anode side. However, it was also observed that the increase of methanol feed concentration produces more leakage current. Hence, the methanol feed concentration should be optimized to reduce leakage current. To reduce leakage current, cross-over of methanol through the membrane should be minimized. The methanol passes through the membrane can be controlled by membrane architectures. The membrane considered in this research work should be modified to enhance its methanol blocking ability. It was also observed that the cell voltage of fuel cell gradually decreases with the increase of current density. With the increase of current density, cell voltage was reduces due to polarization loss. At a higher current density, polarization loss was dominated by ohmic loss. To avoid higher voltage loss, it was desirable to operate fuel cell at lower current density. However, at lower current density region, cell produces lower power density. However, it was noticed that operating fuel cell at higher current density produces more power density. Hence, ohmic loss should be minimized to reduce polarization loss at higher current density region. The ohmic loss was occurred due to electrolyte resistance of the membrane. The electrolyte membrane with higher proton conductivity reduces electrolyte resistance. Therefore, it was desirable to develop a high proton conducting membrane to reduce electrolyte resistance. Fuel cell operated at a higher current density region as well as methanol feed concentration provides more power density. For better

cell performance, fuel cell should be operated at a higher current density and methanol feed concentration. Moreover, it was suggested that the proton conductivity of the membrane should be enhanced to a higher level. The polarization curve predicted by the proposed model was validated with the experimental data. The experiment was conducted at 70°C and 2M methanol feed at anode side. The validation of proposed model with experimental results is shown in **Fig. 6.37**. The proposed model strongly agreed with the experimental data. The proposed model can be used to predict polarization curve of an active DMFC. The advantage of the proposed model was that it can be used efficiently at a less time.

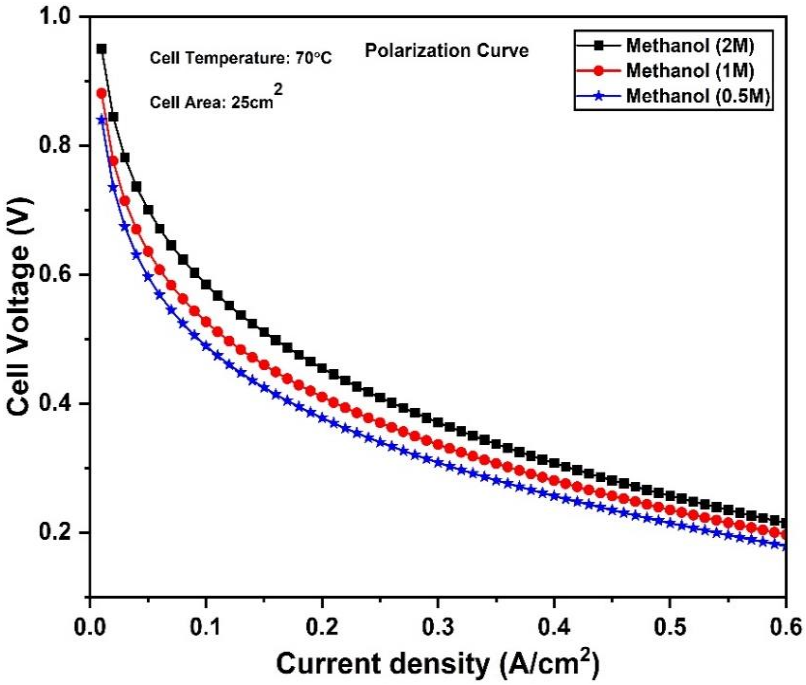

Figure 6.36: Prediction of the polarization curve of DMFC for different methanol feed concentration at anode side.

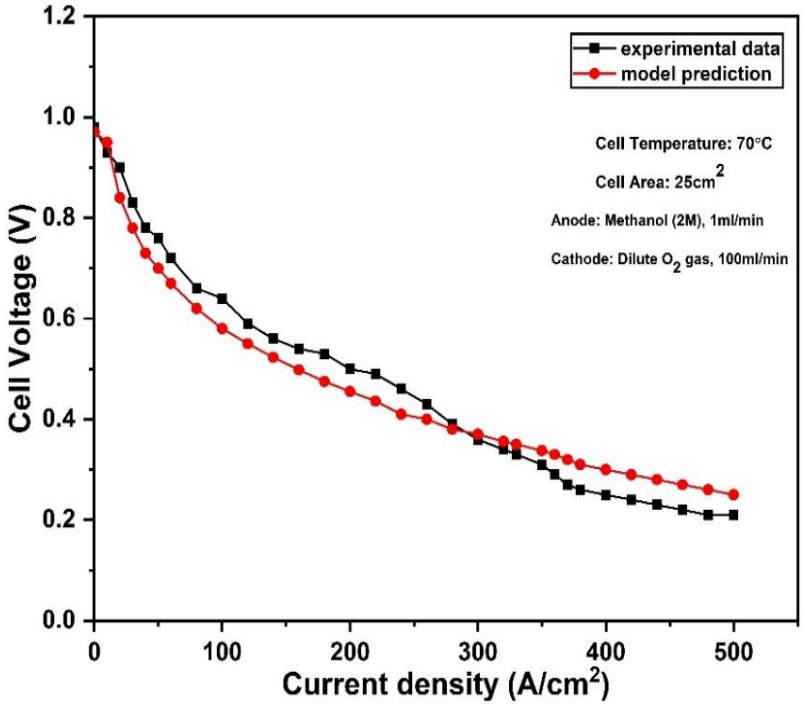

Figure 6.37: Validation of model polarization curve with the experimental data for a DMFC operating at 70°C and 2M methanol feed concentration.

The experimental data of our work was fitted to a well suited analytical model proposed by the researchers. In a literature, we have found the various modelling approach to predict the cell performance of active DMFC. However, there was a limited work for the analytical modelling of active DMFC. The analytical model proposed by the team of Srivastava et al. and Deng et al. were best suited for our experimental results. The model equation proposed by them were more relevant to our experimental conditions. Therefore, we have considered their analytical model to predict the cell performance of active DMFC. The experimental parameters were fitted to their analytical model and polarization curve was predicted. The polarization curve obtained by fitting the experimental parameters to a various analytical model is shown in **Fig. 6.38**. The polarization curve obtained from our proposed model was strongly agreed with the experimental results. It was observed that the model equation proposed in this study was more effective to predict the cell performance with a higher accuracy. However, the polarization curve obtained from the proposed model of Srivastava et al. and Deng et al. was not satisfactorily fitted with the experimental results. The model equation proposed by Deng et al. was partially fitted with our experimental results.

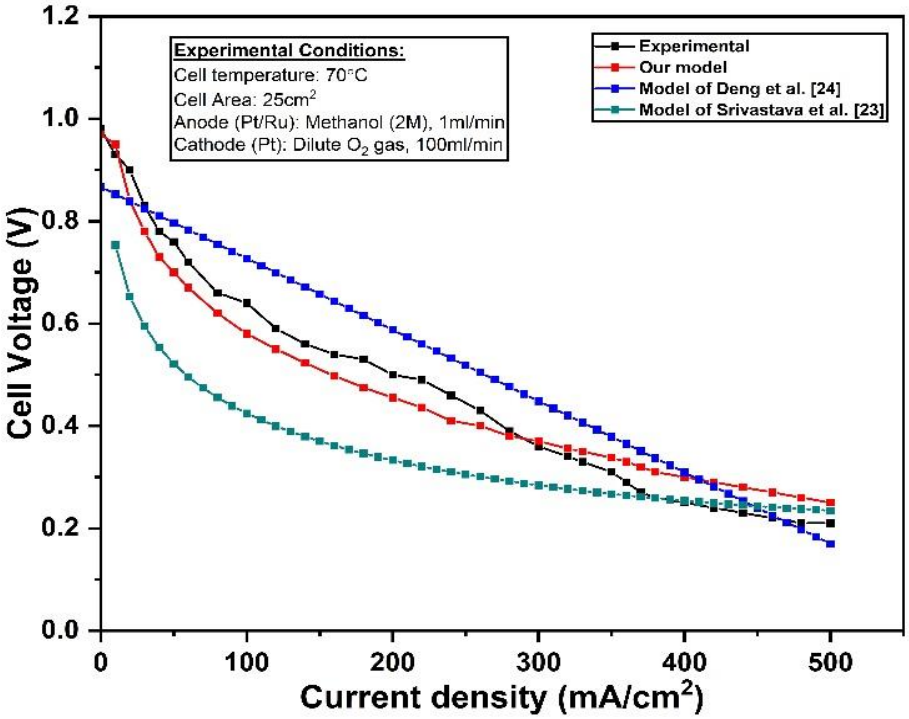

Figure 6.38: Comparison of experimental polarization curve with the various models.

CHAPTER 7

COMPARATIVE PERFORMANCE ANALYSIS

7. COMPARATIVE PERFORMANCE ANALYSIS

The physical, chemical, mechanical and thermal property of the developed membranes were compared to the properties of commercial N117 membrane. The methanol cross-over and proton conductivity are the crucial property of fuel cell membrane. Hence, these properties were compared with the prospective SPEEK based hybrid membrane and commercial Nafion membrane. Moreover, the performance of a single cell of fuel cell obtained by chitosan based membrane was compared to a Nafion-based fuel cell. The fuel cell performance was obtained at 70°C and 2M methanol supply. The properties of the membranes were compared to predict their feasibility to a moderate temperature fuel cell.

7.1 Physical, Mechanical and Thermal Properties

The physical, mechanical and thermal properties of the developed membranes are reported in **Table 7.1**. The CP blend cross-linked with sulphuric acid provides highest ion exchange capacity (IEC) among the Chitosan based membrane. It was also found that adding an ionic liquid to a CP blend improve its IEC. The IEC of ionic liquid modified CPZr and CPCN membranes are almost near to the IEC of commercial N117 membrane. The CPR membrane also provides good IEC and similar to the ionic liquid modified CPCN and CPZr membrane. Moreover, the cost of CPR membrane was very less as compared to the ionic liquid modified CPCN and CPZr membrane. Therefore, CPR membrane was an attractive candidate for the design of low cost fuel cell. The IEC of the chitosan based membrane was lower than the SPEEK based hybrid membrane. Moreover, SPEEK based hybrid membrane provides more IEC than the commercial N117 membrane. Among the fabricated membranes, SPEEK based hybrid membrane has highest IEC. However, the cost of SPEEK based hybrid membrane was very high which limits its potential application for the design of low cost fuel cell.

The addition of filler and ionic liquid to the CP blend increases water uptake capacity. The water uptake capacity of the developed membranes was significantly higher than the N117 and SPEEK based hybrid membrane. However, it was observed that the addition of filler and cross-linking agent improves bound water. The modified membrane has a higher bound water content, which is advantageous for fuel cell applications in low humidity conditions. The ionic liquid incorporated composite membrane has higher bound water as compared to other fabricated membranes. The CPCN and CPZr membrane provides lower swelling degree as compared to the ionic liquid modified membrane. Hence, these membrane can provide better dimension stability. The N117 membrane provides higher dimension stability due to its lower swelling area. The swelling area of the fabricated membrane should be reduced to a lower value to improve their dimension stability. The bound water content of the SPEEK based hybrid has lower than the Chitosan based membrane. Hence, it provide poor performance at reduced humidity conditions.

The tensile strength of the chitosan based membrane was compared with the SPEEK based hybrid membrane and N117 membrane. Among the chitosan based membranes, CP blend cross-linked with sulphuric acid provides highest tensile strength. The addition of filler and ionic liquid to a CP blend reduces its tensile strength. The tensile strength of CPZr membrane was similar to the CPCN membrane. The tensile stress obtained in a red mud, zirconia and carbon nanotube modified CP blend was similar to the N117 membrane. Hence, these membranes provides better mechanical stability and can be considered as a possible candidate for fuel cell application.

The glass transition temperature of the prepared membrane was compared to that of the commercial N117 membrane. The glass transition temperature of the CP blend was lower than the N117 membrane. It was observed that the glass transition temperature of the CPR, CPCN, CPCN@IL and CPZr@IL was slightly lower than the N117 membrane. The CPH blend

provides lower glass transition temperature among the fabricated membrane. Due to its lower glass transition temperature, it can provides a better flexibility and could be viable candidate for fuel cell application at stressed conditions.

Table 7.1: Physical, mechanical and thermal properties of the fabricated membranes.

Membrane Type	**IEC (meq/g)**	**Water Uptake Capacity (%)**	**Bound Water (%)**	**Swelling Area (%)**	**Tensile Strength (MPa)**	**T_g (°C)**
CP	0.575	133	---	----	42.08	120.57
CPH	**0.832**	138	---	----	**46.12**	**110.82**
CPR	0.71	149	12.26	----	12.28	121
CPCN	0.22	140	15.23	51.85	13	126.58
CPZr	0.23	117.31	16.79	**48.83**	13.56	134.77
CPCN@IL	0.76	184.38	20.63	74.16	9.41	124.38
CPZr@IL	0.728	**254.21**	**24.47**	118.64	10.59	126.17
SPEEK-PVA-silica	**1.64**	36	7.83	----	----	136
N117	0.93	25	2.15	13	11.94	132

Concluding Remarks:

- ✓ The CPH blend provides highest ion exchange capacity (IEC) among the Chitosan based membrane.
- ✓ Ionic liquid modified CPZr membrane provides higher water uptake capacity and bound water content. The major demerit of ionic liquid membrane is its excessive swelling which reduces its dimension and mechanical stability. The CPCN and CPZr membrane provides lower swelling degree as compared to the ionic liquid modified membrane. Hence, these membrane can provide better dimension stability. The N117 membrane provides higher dimension stability due to its lower swelling area.
- ✓ CPH provides highest tensile strength and lower glass transition temperature. The addition of filler and ionic liquid to a CP blend reduces its tensile strength. Due to its lower glass transition temperature, it can provides a better flexibility and could be viable candidate for fuel cell application at stressed conditions.

7.2 Proton Conductivity, Methanol Permeability and Membrane Selectivity

The proton conductivity, selectivity and methanol cross-over of the developed membranes were compared to that of the commercial N117 membrane. It was observed that the cross-linked and ionic liquid modified CP blend provides higher proton conductivity. However, the proton conductivity achieved in a Chitosan based membranes were significantly lower than the N117 membrane. The best performing membrane was the SPEEK based membrane which has highest proton conductivity as well as selectivity. However, it provides higher methanol cross-over as compared to the chitosan based membrane. The methanol cross-over value in a SPEEK based hybrid was slightly lower than N117 membrane. Moreover, the cost of SPEEK based hybrid was higher which limit its potential application. To improve selectivity of the chitosan based membrane, proton conductivity should be improved to a higher value. Moreover, the methanol cross-over across the membrane should be minimized. The red mud particles significantly reduces methanol permeability of the CP blend. However, it provides lower proton conductivity which reduces its selectivity. The CPH and CPCN@IL provides favourable proton conductivity as well as lower methanol cross-over. Due to their lower methanol permeability, CPH and CPCN@IL membrane provides higher membrane selectivity. The selectivity of CPH blend was superior to the zirconia and carbon nanotube incorporated CP blend. It was also noticed that the ionic liquid incorporated CP blend has higher activation energy. In these membranes, temperature plays significant impact on proton conductivity. The activation energy of the CP, CPH and CPR membrane was lower than the N117 membrane. The temperature has least effect on proton conductivity of the membrane. It was noticed that the activation energy of CPZr, CPCN@IL and SPEEK based hybrid was similar to the N117 membrane. However, the temperature dependency on proton transport was increases in a CPCN and CPZr@IL membrane. The activation energy of the CPCN and CPZr@IL was slightly higher than the N117 membrane.

Table 7.2: Proton conductivity, methanol permeability and selectivity of the fabricated membranes.

Membrane Type	Proton Conductivity (Scm^{-1})×10^{-3}	Methanol Permeability, ($cm^2/s.$)×10^{-7}	Membrane Selectivity, S ($S.sec./cm^3$)×10^3	Activation Energy, kJ/mol.
CP	0.16	2.42	0.54	4.80
CPH	1.38	0.34	32.94	4.26
CPR	0.351	0.72	4.87	2.38
CPCN	0.369	2.16	1.71	14.09
CPZr	0.691	7.53	0.91	7.31
CPCN@IL	1.394	0.726	19.2	9.13
CPZr@IL	1.26	1.08	11.71	20.56
SPEEK-PVA-Silica	38.2	3.21	118.3	10.36
N117	71	5.2	139.2	7.46

Concluding Remarks:

- ✓ Chitosan-PVA blend modified with cross-linking agent (sulphuric acid) and ionic liquid provides better proton conductivity. However, the conductivity value of modified membrane was lower than the commercial N117 membrane and SPEEK based membrane.
- ✓ The CP blend modified with crosslinking agent and ionic liquid provides excellent methanol blocking ability which is viable for fuel cell applications. However, the modified membrane provides lower selectivity due to their inferior proton conductivity. For improving fuel cell performance, selectivity of the membrane should be enhanced.
- ✓ The activation energy of the CP, CPH and CPR membrane was lower than the N117 membrane. The temperature has least effect on proton conductivity of the membrane.

7.3 Fuel Cell Performance

The fuel cell performance was evaluated at 70°C and 2M methanol feed. The cell performance of the developed membrane was compared with the commercial N117 membrane. The fuel cell performance of the developed and N117 membranes are reported in **Table 7.3**. Fuel cell performance was evaluated for CPR, CPCN, CPCN@IL, CPZr and CPZr@IL membranes. Among the developed membrane, ionic liquid modified CPZr membrane provides the highest

power density of 97 mW/cm^2 at a current density of 440 mA/cm^2. However, it provides lower power density as compared to the commercial N117 membrane. The proton conductivity achieved by the developed membrane was lower than the N117 membrane. Hence, it provides lower power density. The next best performing membrane was CPCN@IL-3 with a power density of 82 mW/cm^2. The red mud incorporated CP blend provides the power density of 44 mW/cm^2 at a current density of 140 mA/cm^2. The power density achieved by a CPR membrane was lower than the CPCN and CPZr based membrane. The CPR membrane was comparatively cheaper as compared to the CPCN and CPZr based membrane. Due to its lower development cost, it was considered to be an ideal candidate for fuel cell application. However, the power density achieved by CPR membrane was significantly lower than the commercial N117 membrane. For practical feasibility, power density of the CPR membrane should be enhanced. The power density can be enhanced by improving its proton transport channel and bound water intake. Therefore, further modification is required to improve proton conductivity of the CPR membrane.

Table 7.3: Fuel cell performance, current density and peak power density. Fuel cell performance was evaluated at 70°C and 2M methanol feed.

Membrane Type	Current density (mA/cm^2)	Peak Power density (mW/cm^2)
CPR	140	44
CPCN	280	71
CPCN@IL	370	82
CPZr	350	78
CPZr@IL	440	97
N117	720	180

Concluding Remarks:

- ✓ Among the fabricated membranes, ionic liquid modified CPZr membrane provides the highest power density of 97 mW/cm^2 at a current density of 440 mA/cm^2.
- ✓ The power density achieved by the fabricated membrane was lower than the commercial N117 membrane.

CHAPTER 8

CONCLUSIONS

8. CONCLUSIONS

I. Aim & Objective No. 1

❖ Fabrication of cost effective bio-membrane based on Chitosan.

Result Highlights/Conclusions:

- For developing a cost effective membrane, low cost chitosan and polyvinyl alcohol were blended followed by cross-linking with dilute sulfuric acid (2M). The effect of cross-linking agent on the properties of blends were studied.
- The Chitosan-PVA blend provides lower mechanical and thermal stability. Moreover, it has lower bound water content which reduces fuel cell performance at low humidity conditions.
- The cross-linking of Chitosan-PVA blend improves ion exchange capacity and bound water uptake. The modified membrane provides excellent methanol blocking ability.
- However, the cross-linked blend provides lower selectivity due to its poor proton conductivity as compared to the commercial Nafion membrane.
- For improving the performance of Chitosan-PVA blend, low cost red mud nanoparticles were incorporated to the blend. The main objective of the work was to develop a low cost membrane with better performance. The effect of red mud particles on the performance of Chitosan-PVA blend was studied.
- The addition of red mud particles to the Chitosan-PVA blend improve its mechanical and thermal stability. It was observed that the addition of red mud particles delays degradation of CP blend.
- The bound water of the membrane was increases which improves proton conductivity of the modified membrane. The proton transport was governed by Grotthuss mechanism.
- The significant finding of this work was that the addition of red mud particles decreases methanol permeability through the membrane. The red mud particles block methanol migration sites in a blend.
- However, the proton conductivity of the modified membrane was far lower than the commercial Nafion membrane. Due to its lower proton conductivity, it provides lower

power density in a DMFC. Hence, to improve power density of DMFC, Chitosan-PVA blend was further modified by fillers like multiwall carbon nanotubes, hygroscopic zirconia and ionic liquid.

- The Chitosan-PVA blend was further modified with multiwall carbon nanotubes, hygroscopic zirconia and ionic liquid. To optimize the cost of membrane, very less amount of multiwall carbon nanotubes and hygroscopic zirconia were used for membrane synthesis. Moreover, the cost of ionic liquid was very high. To make a cost effective membrane with improved properties, very little quantity (i.e. 0.05ml) of ionic liquid was used per batch of membrane synthesis.
- The addition of multiwall carbon nanotube and hygroscopic zirconia reduces swelling area of the membrane. Hence, the developed membrane provides better dimension stability.
- Moreover, the addition of zirconia and multiwall carbon nanotube improves mechanical and thermal stability of the chitosan membranes.
- The addition of filler and ionic liquid improves bound water of the membrane. The presence of higher bound water in a membrane improves proton conductivity at reduced humidity conditions.
- The chitosan membrane modified with ionic liquid and filler (multiwall carbon nanotube, zirconia) provides higher power density as compared to the red mud modified membrane.

II. Aim & Objective No. 2

❖ Improve thermal, mechanical and hydrolytic stability of the composite membrane.

Result Highlights/Conclusions:

- The tensile strength of the developed membrane was similar to the Nafion membrane as shown in **Table No. 7.1**. The cross-linked blend provides the highest tensile strength of 46.12 MPa.
- The cross-linking reaction delays the thermal degradation of polymer chain to a higher temperature. The polymer chain was degraded at a higher temperature.
- Carbon nanotubes and hygroscopic zirconia incorporated chitosan membrane provides better dimension stability due to their lower water uptake capacity and swelling degree.
- The ionic liquid modified membrane provides higher swelling degree which reduces its dimension stability. Moreover, bound water content of the membrane was enhanced which improves proton conductivity at reduced humidity conditions.
- The highest bound water was found in an ionic liquid modified chitosan membrane.
- Addition of filler to the chitosan membrane prevents the degradation of polymer chain at a lower temperature and enhances thermal stability. The polymer chains were strongly interacted with the filler and prevents the thermal degradation caused by oxidation reaction.

III. Aim & Objective No. 3

- To reduce fuel cross-over across the membrane.

Result Highlights/Conclusions:

- The results of methanol cross-over across the various developed membrane is reported in **Table No. 7.2.** The crosslinking of Chitosan-PVA blend with sulfuric acid reduces the methanol cross-over from 2.42×10^{-7} cm^2/sec. to 0.34×10^{-7} cm^2/sec.
- The methanol cross-over observed in a cross-linked blend was lower than the commercial Nafion membrane (5.2×10^{-7} cm^2/sec.)
- The addition of red mud nanoparticles to the Chitosan-PVA blend reduces its methanol cross-over. The methanol cross-over value observed in the membrane (0.72×10^{-7} cm^2/sec.) was slightly higher than the cross-linked Chitosan-PVA blend but its value was significantly lower than the commercial Nafion membrane.
- The ionic liquid modified membrane provides the similar methanol cross-over value as we observed in a red mud modified Chitosan-PVA blend.
- The methanol cross-over of the developed membranes were significantly lower than the commercial Nafion membrane.

IV. Aim & Objective No. 4

- To improve membrane selectivity and proton conductivity.

Result Highlights/Conclusions:

- The results of proton conductivity and selectivity of the various membranes is reported in **Table No. 7.2**. The cross-linking agent improves selectivity of the Chitosan-PVA blend by increasing its proton conductivity as well as reducing methanol cross-over.
- However, the proton conductivity of the cross-linked blend was far lower than the commercial Nafion membrane.
- To improve proton conductivity and selectivity, Chitosan-PVA blend was further modified with red mud nanoparticles, hygroscopic zirconia, multiwall carbon nanotubes and ionic liquid.
- The addition of red mud nanoparticles to the Chitosan-PVA blend reduces its methanol cross-over. However, the modified membrane provides lower selectivity due to its poor proton conductivity.
- The addition of multiwall carbon nanotubes and hygroscopic zirconia along with ionic liquid significantly improves the selectivity of the chitosan based membrane. The addition of ionic liquid improves ion migration sites in the membrane which increase proton conductivity. The highest selectivity was observed in an ionic liquid modified Chitosan-PVA-Carbon Nanotube (CPCN) and Chitosan-PVA-Zirconia (CPZr) membrane.
- The selectivity achieved by chitosan based membrane was lower than the commercial Nafion membrane and SPEEK based membrane.

V. Aim & Objective No. 5

- To improve power density of a fuel cell at low to moderate temperature.

Result Highlights/Conclusions:

- The Chitosan membrane was modified to improve the power density of a fuel cell. The power density of the developed membranes were evaluated at 70°C and 2M methanol feed.
- The maximum power density achieved by the developed membrane is reported in **Table No. 7.3**. The power density achieved by the developed membrane was compared to the commercial Nafion membrane.
- The Chitosan-PVA blend modified with red mud particles provides the maximum power density of 44 mW/cm^2 at a current density of 140 mA/cm^2. However, the developed membrane provides lower power density than the Nafion membrane (180 mW/cm^2).
- Among the developed membranes, ionic liquid modified Chitosan-PVA-Zirconia membrane provides the highest power density of 97 mW/cm^2 at a current density of 440 mA/cm^2.
- The Chitosan-PVA blend modified with multiwall carbon nanotubes and ionic liquid provides the power density of 82 mW/cm^2 at a current density of 370 mA/cm^2.
- The power density achieved by the developed membrane was lower than the commercial Nafion membrane.

VI. Aim & Objective No. 6

- ❖ Mathematical modelling of fuel cell.

Result Highlights/Conclusions:

- An analytical model of an active DMFC was proposed to predict the leakage current and polarization curve of the fuel cell.
- Effect of methanol feed concentration on methanol cross-over rate and leakage current was predicted.
- The proposed model was simultaneously solved to predict the polarization curve of the fuel cell with high accuracy and in a less time.
- The validation of proposed model with the experimental result is shown in **Fig. 6.36**.
- The experimental result was fitted with the proposed model along with the various model available in a literature. The experimental result was well fitted in a proposed model as shown in **Fig. 6.37**.
- The theoretical study concludes that the proposed model can be used to predict the performance of DMFC.

CHAPTER 9

SCOPE OF FUTURE WORK

9. SCOPE OF FUTURE WORK

There are some areas which may be addressed in future for the potential applications of DMFC.

I. The dimension and mechanical stability of the membrane should be improved.

II. The swelling area of the ionic liquid modified chitosan based membrane should be reduce to improve its dimension and mechanical stability.

III. More work should be conducted on the Chitosan based membrane modified with red mud as a filler.

IV. Proton conductivity of the membrane should be improved to a higher level.

V. Fuel cell performance can be optimized by performing at different operating conditions like methanol feed concentration, temperature, feed flow rate and humidity of membrane.

VI. The sluggish electrochemical oxidation of methanol at anode catalyst should be optimized to reduce leakage current. The sluggish kinetics can be improved by developing potential anode catalyst at low cost.

VII. Long term durability test of the fuel cell should be conducted to check its voltage decay and cell performance.

VIII. Validation of proposed theoretical model by including statistical parameters.

CHAPTER 10

REFERENCES

10. REFERENCES

1. Saikia K., Kakati B.K., Boro B., Verma A, (2018)Current Advances and Applications of Fuel Cell Technologies, Recent Advancements in Biofuels and Bioenergy Utilization, Singapore: Springer, 303-337.
2. Yi B.L. (2003) Fuel Cell- Principle Technology Application; Chemical Industry Press: Beijing, China.
3. Wang Y., Chen K.S., Mishler J., Cho S.C., Adroher X.C. (2010) A review of polymer electrolyte membrane fuel cells: Technology, applications, and needs on fundamental research, Applied Energy, The University of California, Irvine, CA 92697-3975, USA.
4. Shah V., Pandya N., Dharaiya U., Kansara Y., Kumar R. (2022) Direct Methanol Fuel Cells towards Sustainable Future: An Indian Perspective, International Journal for Research in Applied Science & Engineering Technology, 10.
5. Garcia B.L. and Weidner J.W. (2007) Review of Direct Methanol Fuel Cells (Book Chapter) Modern Aspects of Electrochemistry, 40. Springer, New York. DOI: 10.1007/978-0-387-46106-9_5
6. Lufrano F., Baglio V., Staiti P., Antonucci V. and Arico A.S. (2013) Performance analysis of polymer electrolyte membranes for direct methanol fuel cells, Journal of Power Sources, 243, 519–534, 2013.
7. Ahmad S., Nawaz T., Ali A., Orhan M.F., Samreen A., Kannan A.M. (2022) An overview of proton exchange membranes for fuel cells: Materials and manufacturing, International Journal of Hydrogen Energy, 47(44), 19086-19131.
8. Schmidt C., Gluck T., Schmidt-Naake G. (2008) Modification of Nafion Membranes by Impregnation with Ionic Liquids, Chem. Eng. Technol., 31, 13–22.
9. Sengul E., Erdener H., Akay G.R., Yucel H., Baç N. and Eroglu I. (2009) Effects of sulfonated polyether-ether ketone (sPEEK) and composite membranes on the proton exchange membrane fuel cell (PEMFC) performance, International Journal of Hydrogen Energy, 34, 4645–4652.
10. Kanakasabai P., Deshpande A.P., Varughese S. (2013) Novel Polymer Electrolyte Membranes Based on Semi-Interpenetrating Blends of Poly (vinyl alcohol) and Sulfonated Poly (ether ether ketone), Journal of Applied polymer science, 127 (3), 2140-2151.

11. Bagheri A., Javanbakht M., Beydaghi H., Salarizadeh P., Shabanikia A. and Amoli H.S. (2016) Sulfonated poly(etheretherketone) and sulfonated polyvinylidene fluoride-*co*-hexafluoropropylene based blend proton exchange membranes for direct methanol fuel cell applications, RSC Advances, 6, 39500–39510.
12. Wang J., Bai H., Zhang H., Zhao L., Chen H., Li Y. (2015) Anhydrous proton exchange membrane of sulfonated poly (ether ether ketone) enabled by polydopamine-modified silica nanoparticles. Electrochimica Acta, 152, 443-55.
13. Du L., Yan X., He G., Wu X., Hu Z., Wang Y. (2012) SPEEK proton exchange membranes modified with silica sulfuric acid nanoparticles. International Journal of Hydrogen Energy 37, 11853-61.
14. Shaari N., Kamarudin S.K. (2015) Chitosan and alginate types of bio-membrane in fuel cell application: An overview, Journal of Power Sources, 289, 71-80.
15. Liu X, Zhao X, Liu Y, Zhang T (2022) Review on preparation and adsorption properties of Chitosan and Chitosan composites, Polymer Bulletin, 79, 2633-2665.
16. Kumari S., Kishor R. (2020) Chitin and Chitosan: origin, properties and applications, Handbook of chitin and Chitosan, chapter 1, 1-33. DOI: 10.1016/B978-0-12-817970-3.00001-8
17. Tubbs, R.K. (1966) Sequence distribution of partially hydrolyzed poly (vinyl acetate): Journal of Polymer Science Part A-1; Polymer Chemistry, 4(3), 623-629.
18. Schildknecht C.E. (1973) Polyvinyl alcohol, properties and applications: Journal of Polymer Science; Polymer Letters Edition, Finch, Wiley, New York, 622.
19. Wu H., Zheng B, Zheng X, Wang J, Yuan W, Jiang Z (2007) Surface-modified Y zeolite-filled Chitosan membrane for direct methanol fuel cell, Journal of Power Sources, 173, 842-852.
20. Yang C.C., Lee Y.J., Yang M.J. (2009) Direct methanol fuel cell (DMFC) based on PVA/MMT composite polymer membranes, Journal of Power Sources,188(1), 30-37.
21. Ma J. & Sahai Y. (2013) Chitosan biopolymer for fuel cell applications. Carbohydrate Polymers, 92(2), 955–975.
22. Wang J, Gong C, Wen S, Liu H, Qin C, Xiong C, Dong L (2018) Proton exchange membrane based on Chitosan and solvent-free carbon nanotube fluids for fuel cells applications, Carbohydrate Polymers, 186, 200-207.
23. Seo J.A., Koh J.H., Roh D.K., Kim J.H. (2009) Preparation and characterization of crosslinked proton conducting membranes based on Chitosan and PSSA-MA copolymer, Solid State Ionics, 180, 998-1002.

24. Xiang Y., Yang M., Guo Z., Cui Z. (2009) Alternatively Chitosan sulfate blending membrane as methanol-blocking polymer electrolyte membrane for direct methanol fuel cell, Journal of Membrane Science, 337, 318-323.
25. Meenakshi S., Bhat S.D., Sahu A.K., Sridhar P., Pitchumani S., Shukla A.K. (2012) Chitosan-Polyvinyl Alcohol-Sulfonated Polyethersulfone Mixed-Matrix Membranes as Methanol-Barrier Electrolytes for DMFCs, Journal of Applied Polymer Science, 124, E73-E82. DOI: 10.1002/app.35522
26. Qu S., Li M., Zhang C., Sun Y., Duan J., Wang W., Li J. and Li X. (2019) Sulfonated Poly (ether ether ketone) doped with ammonium ionic liquids and nano-silicon dioxide for polymer electrolyte membranes, Polymers, 11, 7.
27. Greaves T.L. and Drummond C.J. (2008) Protic Ionic Liquids: Properties and Applications, Chemical Reviews, 108, 206-237.
28. Rosli N.A.H, Loh K.S., Wong W.Y., Yunus R.M., Lee T.K., Ahmad A. and Chong S.T. (2020) Review of Chitosan-Based Polymers as Proton Exchange Membranes and Roles of Chitosan-Supported Ionic Liquids, International Journal of Molecular Science, 21, 632.
29. Rhim J.W., Park H.B., Lee C.S., Jun J.H., Kim D.S., Lee Y.M. (2004) Cross-linked polyvinyl alcohol membranes containing sulfonic acid group: proton and methanol transport through membranes, Journal of Membrane Science, 238, 143-151.
30. Kim D.S., Park H.B., Rhim J.W., Lee Y.M. (2004) Preparation and characterization of cross-linked PVA/SiO_2 hybrid membranes containing sulfonic acid groups for direct methanol fuel cell applications, Journal of Membrane Science, 240, 37.
31. Lin C.W., Huang Y.F., Kannan A.M. (2007) Cross-linked polyvinyl alcohol and poly (styrene sulfonic acid-co-maleic anhydride) based semi-interpenetrating network as proton conducting membranes for direct methanol fuel cells, Journal of Power Sources, 171, 340-347.
32. Ariyaskul A.S., Huang R.Y., Douglas P.L., Pal R., Feng X., Chen P., Liu L. (2006) Blended Chitosan and polyvinyl alcohol membranes for the pervaporation dehydration of isopropanol, Journal of Membrane Science, 280, 815-823.
33. Zhou Y.S., Yang D.Z., Chen X.M., Xu Q., Lu F.M., Nie J. (2008) Electrospun water soluble carboxyethyl Chitosan/polyvinyl alcohol nanofibrous membrane as potential wound dressing for skin regeneration, Biomacromolecules, 9, 349-54.
34. Yang J.M., Su W.Y., Leu T.L., Wang M.C. (2004) Evaluation of Chitosan/PVA blended hydrogel membranes, Journal of Membrane Science, 236, 39.

35. Wu L.G., Zhu C.L., Liu M. (1994) Study of a new pervaporation membrane Part I. Preparation and characteristics of the new membrane, Journal Membrane Science, 90, 199-205.
36. Lin L.Y.F., Yen C.Y., Hung C.H., Hsiao Y.H., Ma C.C.M. (2007) A novel blends based on sulfonated montmorillonite modified Nafion®for DMFCs. Journal of Power Sources, 168, 162–166.
37. Murmu R., Sutar H. (2018) A Novel SPEEK-PVA-TiO_2 Proton Conducting Composite Membrane for PEMFC operations at Elevated Temperature, Journal of Polymer Materials, 35(4), 409-431.
38. Danwanichakul, P. and Sirikhajornnam, P. (2013) An Investigation of Chitosan-Grafted-Poly (vinyl alcohol) as an Electrolyte Membrane, Journal of Chemistry. DOI: 10.1155/2013/642871
39. Yang, J.M. and Chiu, H.C. (2012) Preparation and characterization of polyvinyl alcohol/Chitosan blended membrane for alkaline direct methanol fuel cells, Journal of membrane science, 419-420, 65-71.
40. Tripathi B.P. and Shahi V.K. (2008) Functionalized Organic-Inorganic Nanostructured *N*-*p*-Carboxy Benzyl Chitosan-Silica-PVA Hybrid Polyelectrolyte Complex as Proton Exchange Membrane for DMFC Applications, Journal of Physical Chemistry, 112, 15678-15690.
41. Acurio E., García-Cruz L., Montiel V. and Iniesta J. (2017) Preparation of Poly(Vinyl) Alcohol/Chitosan Hybrid Membranes Doped with Graphene Nanosheets, Advanced materials and technologies. DOI: 10.17277/amt.2017.01.pp.009-019
42. Appenzeller J., Martel R., Derycke V., Radosavljevic M., Wind S., Neumayer D. (2002) Carbon nanotubes as potential building blocks for future nanoelectronics. Microelectronic Engineering, 64, 391–397.
43. Sacca A., Gatto I., Carbone A., Pedicini R., Passalacqua E. (2006) ZrO_2-Nafion composite membranes for polymer electrolyte fuel cells (PEFCs) at intermediate temperature, Journal of Power Sources, 163(1), 47-51.
44. Goodwin S.E., Smith D.E., Gibson J.S., Jones R.G., Walsh D.A. (2017) Electroanalysis of Neutral Precursors in Protic Ionic Liquids and Synthesis of High-Ionicity Ionic Liquids, Langmuir, 33 (34), 8436-8446.
45. Watanabe M., Thomas M.L., Zhang S., Ueno K., Yasuda T., Dokko K. (2017) Application of Ionic Liquids to Energy Storage and Conversion Materials and Devices, Chemical Reviews, 117(10), 7190-7239.

46. Ueki T., Matsukawa K., Masuda T., Yoshida R. (2017) Protic Ionic Liquids for the Belousov–Zhabotinsky Reaction: Aspects of the BZ Reaction in Protic Ionic Liquids and Its Use for the Autonomous Coil–Globule Oscillation of a Linear Polymer. The Journal of Physical Chemistry B, 121 (17), 4592-4599.
47. Correia D.M., Fernandes L.C., Martins P.M., García-Astrain C., Costa C.M., Reguera J., Lanceros-Méndez S. (2020) Ionic Liquid–Polymer Composites: A New Platform for Multifunctional Applications, Advanced Functional Materials, 30, 24.
48. Kitazawa Y., Iwata K., Maizumi S., Ahn H., Kim S.Y., Ueno K., Park M.J., Watanabe M. (2014) Gelation of 15 Solvate Ionic Liquid by Self-Assembly of Block Copolymer and Characterization as Polymer Electrolyte, Macromolecules, 47 (17), 6009-6016.
49. Zakeri M., Bouzari-Lotf E., Nasef M.M., Ahmad A., Miyake M., Ting T.M., Sithambaranathan P. (2019) Fabrication and characterization of supported dual acidic ionic liquids for polymer electrolyte membrane fuel cell applications, Arabian Journal of Chemistry, 12(7), 1011-1023.
50. Murmu R, Sutar H (2018) Steady state analysis of water transport through sulfonated polyether ether ketone (SPEEK) membrane for fuel cell application, Journal of Polymer Materials, 35(1), 103-118.
51. Mahmoudzadeh M, Fassihi A, Emami J, Davies NM and Dorkoosh F (2013) Physicochemical, pharmaceutical and biological approaches toward designing optimized and efficient hydrophobically modified chitosan-based polymeric micelles as a nanocarrier system for targeted delivery of anticancer drugs, Journal of Drug Targeting, 21(8), 693-709.
52. Lupa L, Voda R, Popa A (2017) Adsorption behavior of cesium and strontium onto chitosan impregnated with ionic liquid, Separation Science and Technology, 53:7, 1107-1115.
53. Sngul E, Erdener H, Akay GR, Yucel H, Baç N, Eroglu I (2009) Efects of sulfonated polyether-ether ketone (sPEEK) and composite membranes on the proton exchange membrane fuel cell (PEMFC) performance. International Journal of Hydrogen Energy 34:4645–4652.
54. Kanakasabai P, Deshpande AP, Varughese S (2013) Novel polymer electrolyte membranes based on semi-interpenetrating blends of poly (vinyl alcohol) and sulfonated poly (ether ether ketone), Journal of Applied Polymer Science 127(3):2140–2151.

55. Colicchio I, Demco DA, Baias M, Keul H, Moeller H (2009) Infuence of the silica content in SPEEK–silica membranes prepared from the sol-gel process of polyethoxysiloxane: morphology and proton mobility. Journal of Membrane Science 337:125–135.
56. Shuguo Qu S, Minhui Li, Chenchen Z (2019) Sulfonated Poly (ether ether ketone) doped ammonium ionic liquids and nano silicon dioxide for polymer electrolyte membranes, Polymers 11:7.
57. Lue S.J., Pai Y.L., Shih C.M., Wu M.C., Lai S.M. (2015) Novel bilayer well-aligned Nafion/Graphene oxide composite membranes prepared using spin coating method for direct liquid fuel cells, Journal of Membrane Science,493,212-223.
58. García B.L., Sethuraman V.A., Weidner J.W., White R.E. & Dougal R. (2004) Mathematical Model of a Direct Methanol Fuel Cell. Journal of Fuel Cell Science and Technology, 1(1), 43. DOI: 10.1115/1.1782927
59. Kulikovsky A.A. (2007) Analytical Models of a Direct Methanol Fuel Cell, Advances in Fuel Cell, Volume 1, 337-417. DOI: 10.1016/S1752-301X(07)80011-1
60. Wang Z.H. and Wang C.Y. (2003) Mathematical Modelling of Liquid-Feed Direct Methanol Fuel Cells, Journal of Electrochemical Society, 150 (4), pp. A508-A519.
61. Patrabansh S. (2013) Dynamic modelling and simulation of a DMFC/UC based hybrid vehicular system, IEEE. DOI: 10.1109/IAS.2013.6682525
62. El-Hefian EA, Nasef MM, Yahaya AH (2010) The Preparation and Characterization of Chitosan / Poly (Vinyl Alcohol) Blended Films, E-Journal of Chemistry, 7(4), 1212-1219.
63. Choo K, Ching YC, Chuah CH, Julai S, Liou NS (2016), Preparation and Characterization of Polyvinyl Alcohol-Chitosan composite films reinforced with cellulose nanofiber, Materials, 9(8), 644.
64. Nakane K., Yamashita T., Iwakura K., Suzuki F. (1999) Properties and structure of poly(vinyl alcohol)/silica composites, Journal of Applied Polymer Science, 74(1), 133–138.
65. Zhang Y., Huang X., Duan B., Wu L., Li S., Yuan X. (2007) Preparation of electrospun Chitosan/poly(vinyl alcohol) membranes, Colloid and Polymer Science, 285, 855-863.
66. Li WH, Deng WH, Wang GE, Xu G (2020) Conductive MOFs, EnergyChem, 2(2), 100029.
67. Cheng H.P. (2002) Structure, collective hydrogen transfer, and formation of $(Si\text{-}OH)_4$ in $SiO_2\text{-}(H_2O)_n$ clusters, Journal of Chemical Physics, 116 (21).

68. Yang C.C., Li Y.J., Liou T.H. (2011) Preparation of novel poly(vinyl alcohol)/SiO_2 nanocomposite membranes by a sol–gel process and their application on alkaline DMFCs, Desalination, 276, 366-372.
69. Awang N., Jaafar J. and Ismail A.F. (2018) Thermal Stability and Water Content Study of Void-Free Electrospun SPEEK/Cloisite Membrane for Direct Methanol Fuel Cell Application, Polymers, 10, 194.
70. Gashoul F., Parnian M.J., Rowshanzamir S. (2016) A new study on improving the physicochemical and electrochemical properties of SPEEK nanocomposite membranes for medium temperature proton exchange membrane fuel cells using different loading of zirconium oxide nanoparticles, International Journal of Hydrogen Energy, 1-13.
71. Xu A., Wang Y., Gao J., Wang J. (2019) Facile fabrication of a homogeneous cellulose/polylactic acid composite film with improved biocompatibility, biodegradability and mechanical, Green Chemistry, 21, 4449–4456.
72. Jung H.Y., Kim J.W. (2012) Role of the glass transition temperature of Nafion 117 membrane in the preparation of the membrane electrode assembly in a direct methanol fuel cell (DMFC), International Journal of Hydrogen Energy, 37, 12580-12585.
73. Das A.K., Manohar M. and Shahi V.K. (2018) Cation-Exchange Membrane with Low Frictional Coefficient and High Limiting Current Density for Energy-Efficient Water Desalination, ACS Omega, 3, 10331-10340.
74. Kim D.S., Park H.B., Rhim J.W., Lee Y.M. (2005) Proton conductivity and methanol transport behavior of cross-linked PVA/PAA/silica hybrid membranes, Solid State Ionics, 176, 117-126.
75. Tripathi B.P. and Shahi V.K. (2008) Functionalized Organic-Inorganic Nanostructured *N*-*p*-Carboxy Benzyl Chitosan-Silica-PVA Hybrid Polyelectrolyte Complex as Proton Exchange Membrane for DMFC Applications, Journal of Physical Chemistry, 112, 15678-15690.
76. Xiang Y., Yang M., Guo Z., Cui Z. (2009) Alternatively Chitosan sulfate bending membrane as methanol-blocking polymer electrolyte membrane for direct methanol fuel cell, Journal of Membrane Science, 337, 318-323.
77. Choi B.G., Huh Y.S., Park Y.C., Jung D.H., Hong W.H., Park H.S. (2012) Enhanced transport properties in polymer electrolyte composite membranes with graphene oxide sheets, Carbon, 50:5395–5402.

78. Roy J.S., Bhattacharya G., Chauhan D., Deshmukh S.,·Upadhyay R., Priyadarshini R., Roy S.S. (2020) Potential use of smartly engineered red mud nanoparticles for removal of arsenate and pathogens from drinking water, SN Applied Sciences, 2:796.
79. Devi C.N., Selvaraj N., Mahesh V. (2014) Nano-Red Mud-Synthesis and Characterization, Design and Research Conference (AIMTDR 2014), IIT Guwahati, Assam, India.
80. Qiu M., Zhang B., Wu H., Cao L., He X., Li Y., Li J., Xu M., Jiang Z. (2019) Preparation of anion exchange membrane with enhanced conductivity and alkaline stability by incorporating ionic liquid modified carbon nanotubes, Journal of Membrane Science, 573, 1-10.
81. Paul D.K., McCreery R., Karan K. (2014) Proton transport property in supported Nafion Nanothin films by electrochemical impedance spectroscopy, Journal of the electrochemical society, 161 (14), F1395-F1402.
82. Lufrano E., Nicotera I., Enotiadis A., Rehman M.H.U. and Simari C. (2022) Elucidating the water and methanol dynamics in sulfonated polyether ether ketone nanocomposite membranes bearing layered double hydroxides, Membranes, 12, 419.
83. Hasanabadi N., Ghaffarian S.R. and Hasani-Sadrabadi M.M. (2011) Magnetic field aligned nanocomposite proton exchange membrane based on sulfonated poly(ether sulfone) and Fe_2O_3 nanoparticles for direct methanol fuel cell application, International Journal of Hydrogen Energy, 36(23), 15323-332.
84. Chikh L., Delhorbe V., Ficher O. (2011) Semi-Interpenetrating polymer networks as fuel cell membranes, Journal of Membrane Science, 368, 1-17.
85. Hedayatyanfard K., Bagheri-Khoulenjani S., Hashemi A., Ziai S.A. (2019) Semi-IPN films and electrospun nanofibers based Chitosan/PVA as an antibacterial wound dressing, Iranian Journal of Pharmaceutical Research, 18(3), 1156-1167.
86. Hua H., Yuan W., Jia Z., Baker G.L. (2012) Ionic liquid-based Random Copolymers as New Type of Polymer Electrolytes with a Low Glass Transition Temperature, RSC Advances. DOI: 10.1039/C4RA13432J
87. Liu S., Zhou L., Wang P., Shao Z., Yi B. (2013) Nonhumudified high temperature H_2/Cl_2 fuel cell using protic ionic liquids, Journal of Materials Chemistry, A2013, 1, 4423-4426.
88. Sahin A. (2018) The development of Speek/Pva/Teos blend membrane for proton exchange membrane fuel cells, Electrochimica Acta, 271, 127-136.

89. Reyes-Rodriguez J.L., Escorihuela J., Garcıa-Bernabe A., Enrique G., Solorza-Feriaa O. and Compan V. (2017) Proton conducting electrospun sulfonated polyether ether ketone graphene oxide composite membranes, RSC Advances, 7, 53481-53491.
90. Kumar R., Xu C. and Scott K. (2012) Graphite oxide/Nafion composite membranes for polymer electrolyte fuel cells, RSC Advances, 2, 8777-8782.
91. Prasad M., Mohanty S., Nayak S.K. (2014) Polymer electrolyte membrane from cloisite 30b based solid proton conductor and sulfonated polyether ether ketone/ polyvinylidene fluoride-co-hexafluoro propylene blends for direct methanol fuel cell, RSC Advances, 4, 61178-61186.
92. Park K.Y., Kim Y.D., Lee J.I., Saqib M., Shin J.S., Seo Y., Kim J.H. (2018) Operation protocols to improve durability of protonic ceramic fuel cells, ACS Applied Materials & Interfaces, 11, 1, 457-468.

CHAPTER 11

LIST OF REVISIONS

11. LIST OF REVISIONS

11.1 In response to observations of the Examiner No. I / II

Q1. Chapter -01, page no - 10, fig 1.2: figures should be arranged as per the order of the captions.

Response: Figures have been rearranged as per the captions of Figure 1.2. (**Page number-8** in the revised thesis).

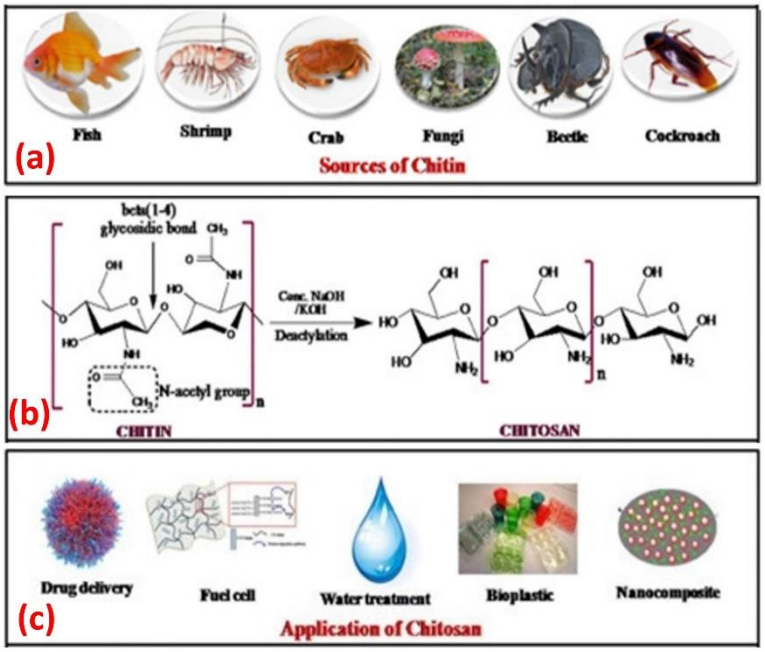

Figure 1.2: (a) Different sources of Chitin through which Chitosan is extracted. (b) Chemical treatment of Chitin to extract Chitosan. (c) Different applications of Chitosan. [**16**]

Q2. Chapter - 01, page no -12: what is the Grotthus mechanism, and its relation to bound moisture, hence, proton conductivity?

Response: Grotthus mechanism and its relation to bound moisture, hence, proton conductivity, has been explained in section 6.1, in Chapter-6, section 6.1, **page number-81 and 82** in the revised thesis.

- ✓ The mechanism of proton transport by Grotthuss mechanism is shown in **Fig. 6.1**. In Grotthuss mechanism, proton passes through the membrane by the formation of hydrogen

bond with the water [**66**]. The bonding between water and proton is called hydronium ion (H_3O^+). The resulting hydronium ion will transfer proton along the conduction pathway by subsequent rearrangement between nearly water molecules [**66**]. At moderate temperature (low humidity conditions), amount of free water presence in the membrane was escaped due to evaporation loss. In this condition, bound water plays a crucial role for fuel cell performance. The proton transport was controlled by bound water regulated Grotthuss mechanism [**65**]. The membrane with higher bound water content provides better proton conductivity at reduced humidity conditions.

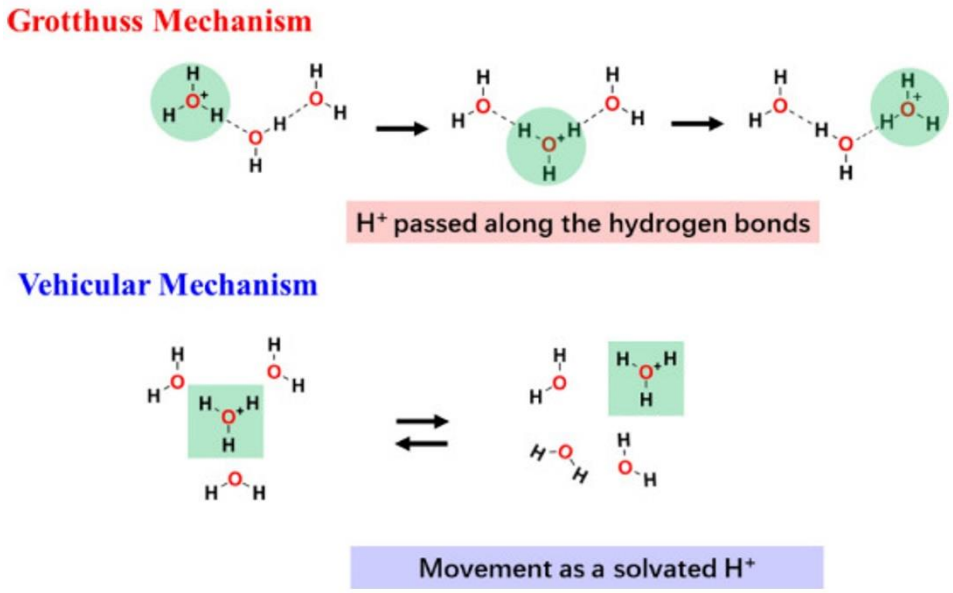

Fig. 6.1: Proton conduction by Grotthusss and vehicular mechanism. [66]

Q3. Chapter -03: The object of this present thesis according to my perception is as follows "To develop highly selective chitosan based low cost membranes (modified with red mud, ionic liquid with different fillers) able to deliver high power density.

<u>The objective stated in the thesis are actually the scopes required to be delivered in reaching the aimed objective.</u>

Response: The objectives of this thesis has been revised Chapter 03, **page number-16, 17 and 18**.

✓ **Aims & Objectives of this present thesis this is as follows;**

To develop highly selective chitosan based low cost membranes (modified with red mud, ionic liquid with different fillers) able to deliver high power density.

I. Fabrication of cost effective bio-membrane based on Chitosan.

In the current scenario, Nafion membrane is used as electrolyte membrane in a PEMFC. However, the cost of Nafion membrane is very high. The higher cost of membrane increases the cost of fuel cell. Therefore, the preparation of electrolyte membrane by a cheap material is more appealing. The use of low cost chitosan as membrane material is more attractive due to its excellent methanol blocking ability. The main objective of this work is to develop a cost effective chitosan based membrane focusing on higher proton conductivity as well as selectivity.

II. Improve thermal, mechanical and hydrolytic stability of the composite membrane.

The electrolyte membrane with better mechanical and thermal stability is desirable for fuel cell applications. The membrane with better mechanical stability provides excellent performance at stressed conditions. Moreover, it should have better hydrolytic stability. The membrane with poor hydrolytic stability reduces fuel cell performance. Due to poor hydrolytic stability, membrane swells more which drastically affects fuel cell performance. The chitosan membrane has poor hydrolytic stability due to its excessive swelling property. Moreover, it has also poor mechanical and thermal stability. Therefore, it should be blended with other polymers as well as fillers to improve its mechanical, thermal and hydrolytic stability.

III. Reduce fuel cross-over across the membrane.

The electrolyte membrane with higher methanol cross-over is not desirable for fuel cell application. Due to higher methanol cross-over, fuel loss was occurred in a fuel cell. Moreover, the permeated methanol takes part for oxidation reaction at cathode interface and produces leakage current. The generation of more leakage current drastically reduces fuel cell performance. Therefore, it is more appealing to develop a cost effective membrane with lower methanol cross-over. The chitosan is a potential candidate for the development of electrolyte membrane due to its good methanol blocking ability.

IV. Improve membrane selectivity and proton conductivity.

The electrolyte membrane with better proton conductivity is desirable for fuel cell application. The membrane with higher proton conductivity as well as excellent methanol blocking ability provides excellent performance. The chitosan membrane has lower proton conductivity. Due to its poor proton conductivity, it has lower selectivity. Hence, pure chitosan membrane provides poor performance. Therefore, it is desirable to improve its proton conductivity by adding fillers.

V. Improve power density of a fuel cell at low to moderate temperature.

The highly selective membrane is preferred for fuel cell application. The highly selective membrane provides better cell performance. The more power density will be achieved by the highly selective membrane. The main objective of this work is to develop highly selective chitosan based membrane to achieve high power density.

VI. Mathematical modelling of fuel cell.

An analytical model will be developed to predict fuel cell performance at different operating conditions. The model equation will be developed by steady state assumption in a flow channel of fuel cell attack. The model equation will be solved to predict leakage current and polarization curve of a fuel cell. Finally, the polarization curve predicted by the analytical model will be compared with the experimental polarization curve.

VII. To compare the performance of Chitosan based membrane with a potential SPEEK based membrane and commercial Nafion Membrane.

The SPEEK membrane is considered to be a potential candidate for fuel cell application. The main drawbacks of the SPEEK based membrane is its higher cost. The properties of chitosan based membranes will be compared with the commercial Nafion membrane and prospective SPEEK based membrane. The properties of the chitosan based membranes will be compared to confirm its feasibility towards fuel cell applications.

Q4. Chapter 4, page 25: Fig. 4.1(a) should be for red mud and 4.1(b) should be for silica. Please correct the captions.

Response: The caption of Fig. 4.1(a) and Fig. 4.1(b) has been corrected in Chapter 4, **page number-22** in the revised thesis. The corrected captions of the Fig. 4.1(a) and Fig. 4.1(b) is shown below

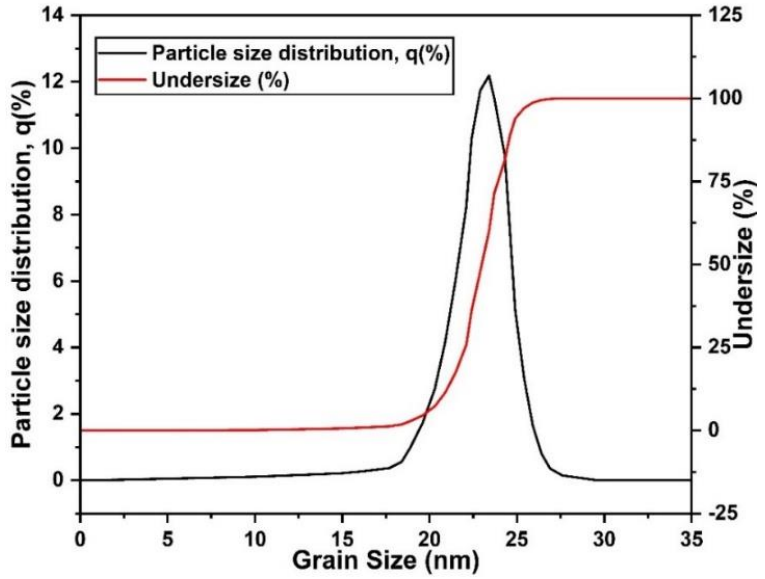

Figure 4.1 (a): Grain size plot of finely produced red mud particles.

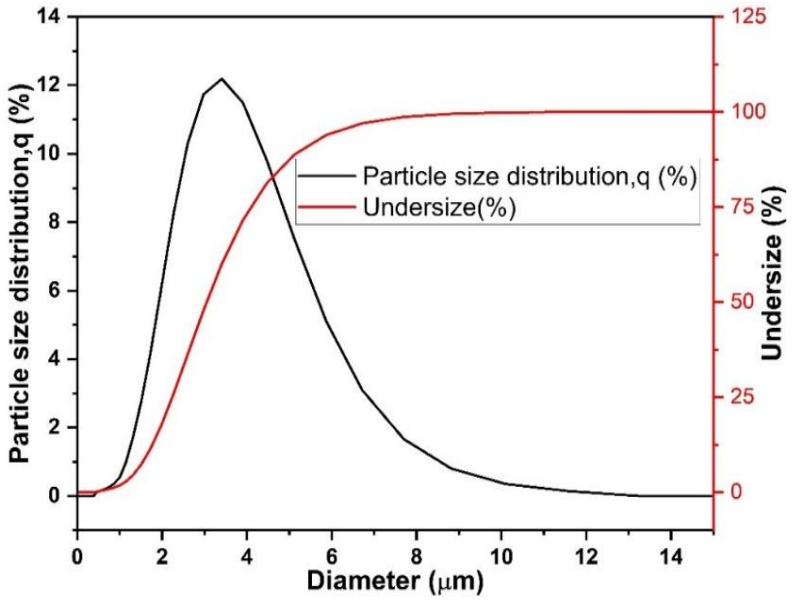

Figure 4.1 (b): Grain size plot of finely produced silica particles.

Q 5. Sec-4.3 .2: "after cross-linking the blend was kept in a controlled chamber". What do you mean by controlled chamber?

Response: Controlled chamber means the blends are kept in a chamber to prevent the contact with suspended particulate matter. It is mentioned in **page number-24** in the revised thesis.

- ✓ After cross-linking reaction, all the blends were removed from the sulfuric acid solution and kept it in a controlled chamber (**used as a desiccator**) for 2 days.

Q 6. ls there any Literature evidence for fig. 4.2 and fig.4.4?

Response: The literature evidence for Fig. 4.2 and Fig. 4.4 has been explained in Chapter 4, **page number-24, 25 and 27** in the revised thesis.

- ✓ The sulfuric acid produces two ions in the solution i.e. H^+ and SO_4^{2-}. The sulfuric acid converts the amine group of Chitosan to NH_3^+ in the blend. The $-NH_2$ group of Chitosan was protonated by H^+ ion to form NH_3^+ ion. A new ionic bond was created due to the interaction between the NH_3^+ and SO_4^{2-} ion [**26**].

- ✓ The amine group of Chitosan was interacted with the base of ionic liquid to form a strong covalent bond [**17**]. Due to the addition of ionic liquid to the composite, sulfonate (SO_3) group was impregnated which has the potential to improve its ion exchange capacity [**44**]. The hydroxyl group of Chitosan interacts with the positive ion of an ionic liquid, resulting in the creation of an electron donor electron receiver (EDA) complex [**50**]. In this case, the ionic liquid's cation (N^+) functions as a receptor for electrons, while the Chitosan's hydroxyl group (OH^-) acts as a donor of electrons [**51**].

Q 7. Sec-4.3.2, page-32: why presence of sulphonate group in electrolytic membrane improved ion transfer capacity and proton conductivity "? Please explain briefly here with reference.

Response: It is confirmed from the literature that the sulphonate group improves ion transport capacity of the membrane. The sulfonate group of membrane acts as a hooping site for ion transport which improves proton conductivity. The detailed mechanism along with the supportive reference is explained in Chapter 4, **page number-24** in the revised thesis.

- ✓ During crosslinking reaction, SO_4^{2-} ion diffuses in to the membrane and created an extra ionic sites in the membrane. The creation of an extra ionic sites in a cross-linked membrane

is responsible for the enhancement of IEC. The ionic sites in a blend membrane act as a proton transport channel. The increase of ion transport sites in a blend increases ion exchange capacity [**26, 29**].

Q 8. Page-33, Ch-4: After addition of ionic liquid what zirconia is doing or helping and in what capacity for the developed membranes? Please explain briefly here with reference.

Response: The addition of ionic liquid to a CP blend improves its ion exchange capacity. The presence of hygroscopic zirconia in a blend improve its water retention capacity which will be good for fuel cell operation at low humidity conditions. The effect of ionic liquid and zirconia on the ion exchange capacity of membrane is explained with the supportive reference in Chapter 6, section 6.1, **page number-91** in the revised thesis.

- ✓ The addition of filler to a polymer domain depleted ion migration sites thereby reducing IEC. The similar result was reported in a literature [**30, 43 & 50**]. However, the modification of CPZr hybrid membrane with ionic liquid increases IEC. The presence of ionic liquid in a membrane creates extra ion migration sites for ion transport. Therefore, ionic liquid membrane provides better IEC than the CPZr hybrid membrane. Adding an aprotic liquid to the hybrid membrane introduces additional imidazolium cations and increases IEC [**71**].

Q 9. Page-36, fig-4.7, Ch-4: ls there any literature evidence for fig 4.7 or is there any experimental evidence for the proposed mechanism?

Response: The possible reaction scheme is proposed based on the literature evidence. The reaction mechanism is explained with the supportive literature evidence in Chapter 4, **page number-31** in the revised thesis.

- ✓ During the sulfonation of PEEK, sulfonate group (S=O) was inserted to the PEEK backbone leaving out water as a condensation product [**50, 53**].
- ✓ The hydroxyl group of polyvinyl alcohol was strongly interacted with the sulfonate group of SPEEK to from hydrogen bond [**54**]. However, the addition of silica disturbs the interaction between SPEEK and polyvinyl alcohol. The silica has higher reactivity towards the sulfonate group of SPEEK. The silica atom will be reacted with the sulfonate group of SPEEK and the possible reaction scheme is represented in Fig. 4.7(b) [**55, 56**]. The polyvinyl alcohol was strongly reacted with the silanol group of silica, forming a strong

intermolecular bond [**54**].

Q 10. Page -39, Ch-4; what is the relation between the phase transition from glassy to rubbery and the glass transition temperature of membrane? Please discuss here briefly.

Response: The glass transition temperature is the temperature at which glassy phase of membrane is converted to rubbery phase. The membrane with lower glass transition temperature provides higher flexibility and mechanically stable. The definition and significance of glass transition temperature is explained in Chapter 4, **page number-35 and 36** in the revised thesis.

- ✓ When void fraction increases, glass transition temperature of the membrane was significantly reduces. The polymer chain will move freely, accelerating the phase shift from glassy to rubbery. The temperature at which glassy phase of polymer converted to rubbery phase is called glass transition temperature. The membrane with lower glass transition temperature is less rigid and highly flexible. However, the membrane with higher void fraction provides poor mechanical properties and excessive fuel loss due to fuel cross-over. Due to its higher void fraction, glass transition temperature of the membrane was increases which makes the membrane more rigid and less flexible.

Q 11. Page -40, Ch-4: How do you define partial molar volume of the membrane?

Response: To determine the partial molar volume of the membrane, its volume is measured. A known amount of solvent is used to dissolve the membrane. After dissolution, sample volume is measured and it is called partial molar volume of membrane. It is explained in Chapter 4, **page number-36** in the revised thesis.

- ✓ To determine the partial molar volume of the membrane, its volume is measured. A known amount of solvent was used to dissolve the membrane. After dissolution, sample volume was measured.

Q 12. Ch-4, page-41: How do you define sample thickness (L) and area (A)?

Response: The average thickness (cm) and diameter of the membranes are measured by digital varnier caliper. It is mentioned in Chapter 4, **page number-37** in the revised thesis.

- ✓ The average thickness and diameter of the membrane was measured by digital varnier caliper.

Q 13. Page-45, Ch-4: ln DSC analysis: ls it freezing water or free water to calculate W_b (bound water)? I guess this particular mistake has been recurred couple of time in the thesis.

Response: The freezing water has been corrected to free water in Chapter 4, **page number-40** in the revised thesis.

- ✓ The quantity of free water presence in the sample was used to compute bound water (%). The quantity of free water presence in the sample was obtained from the area of first crystallization peak observed during cooling cycle.

Q 14. Page-46, sec-4.6: where is the photograph of membrane electrode assembly (MEA)?"

Response: The photograph of membrane electrode assembly has been included in the Chapter 4, section-4.6, **page number-42** in the revised thesis. The new figure can be read as Fig. 4.9 in the revised thesis.

Figure 4.9: Single cell membrane electrode assembly setup with EIS work station.

Q 15. Page-47, Ch-4: what is the Tafel kinetics? Please discuss briefly.

Response: It is a fundamental equation in electrochemistry which follows the mathematical relationship between current and applied electrochemical potential. It is explained in Chapter 4, **page number-44** in the revised thesis.

- ✓ **Tafel kinetics:**

  Tafel kinetics relates the rate of an electrochemical reaction to the over potential. It describes the dependency of electric current through an electrode on voltage difference between the electrode and electrolyte.

  Tafel equation can be used for predicting anode and cathode side over potential. The general expression of tafel equation for a single electrode is given below

  $$\eta = \pm A.\ \log_{10}\left(\frac{I}{I_0}\right) \qquad (4.14)$$

  Here, plus sign refers to an anode side reaction and minus sign refers to cathode side reaction. η is the over potential of the cell (Volt), A is tafel slope (Volt), I is current density (A/cm^2) and I_0 is the exchange current density (A/cm^2). It assumes that the concentrations at electrode interface are practically equal to the concentrations in the bulk electrolyte. It also assumes that the electrode mass transfer rate is much greater than the reaction rate.

Q 16. Page-48, Ch-4, equation-4.14: How ohmic loss was calculated?

Response: The ohmic loss was calculated from the last expression of **equation-4.15**. The ohmic loss was calculated at different current density (I_{cell}) using the known parameters of δ_m and k. It is explained in Chapter 4, **page number-45** in the revised thesis.

- ✓ $V_{Cell} = U_{O_2} - U^{MeOH} - \eta_A - \eta_C - \frac{\delta_M I_{Cell}}{K}$ (4.15)
- ✓ The last term in the expression represents ohmic loss across the membrane. Ohmic loss was calculated at different current density (I_{cell}) by using the known parameters of δ_m and k.

Q 17. Page-50, fig- 4.9: Nomenclature of thickness of ADL, ACL, and membrane layers, are define as t_b, t_a, t_m, respectively, where as in boundary conditions provided in page 49 , the same are expressed as l_b, l_a, and l_m, respectively Also in this figure, exist concentration of the membrane layer (C_{III}^m) is missing.

Response: The nomenclature of thickness of the membrane is corrected in Chapter 4, **page number-45** in the revised thesis. The schematic diagram of the anode flow channel is also modified by including the exit concentration of methanol flow. The modified schematic diagram is shown in Fig. 4.10, **page number-46** in the revised thesis.

✓ ADL: Thickness (t_b); At X=0: c=c_b; At X=X_1: c=c_I^b

ACL: Thickness (t_a); At X=X_I: c=c_I^a; At X=X_{II}: c=c_{II}^a

Membrane: Thickness (t_m); At X=X_{II}: c=c_{II}^m; At X=X_{III}: c=c_{III}^m

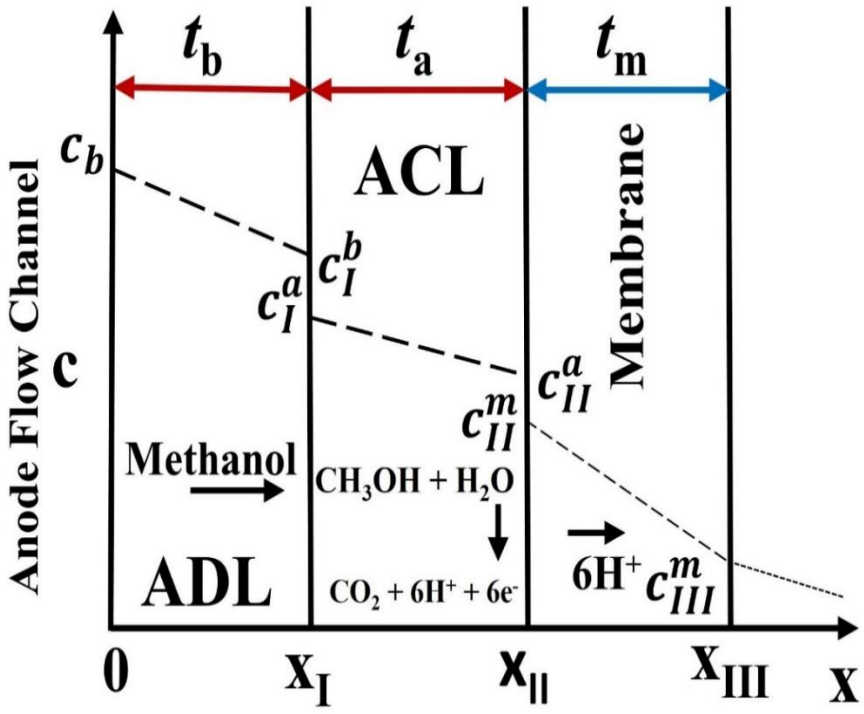

Figure 4.10: A simplistic one dimensional approach of anode flow channel in a DMFC.

Q 18. Page-51, Ch-4: The analytical solution of molar flux was done by equation 4.16 not equation 6. Proper nomenclature of equation 4.16 is missing.

Response: The equation number 4.16 is corrected to 4.17 and nomenclature of the equation is included in Chapter 4, **page number-47** in the revised thesis.

$$N_{m,cross} = -D_m \frac{dc^m_{MeOH}}{dx} + m_d \frac{I_{Cell}}{F} \frac{c^a_{MeOH}}{c^a_w} \qquad (4.17)$$

- ✓ Here, $N_{m,cross}$ is the molar flux of methanol transported through the test membrane. D_m is the diffusivity of methanol through the membrane, F is the Faradays constant, c^a_{MeOH} is the concentration of methanol at anode interface.

Q 19. Fig 4.10 is missing.

Response: A new figure has been added following question no.14 and new figure no. is fig. 4.9. So, the previous figure no. 4.9 is now revised to fig. 4.10 (**page number-46** in the revised thesis).

Q 20. Ch-4, page-52: How your proposed model is different from A.A KULIKOVOSKY?

Response: A.A. Kulikovosky [**59**] proposed the model by considering the diffusion of methanol and oxidation reaction at anode flow channel. In this study, the model was proposed by considering the diffusion and oxidation of methanol at anode flow channel as well as reduction of oxygen at cathode catalyst layer. Thus the reduction of O_2 at cathode catalyst layer is the distinguishing feature of the present model which thus differs from earlier Kulikovosky model. The assumptions of the proposed model is explained in Chapter 4, **page number-48** in the revised thesis.

- ✓ A.A. Kulikovsky [**59**] proposed a theoretical model to predict anode side over potential. In his study, diffusion, oxidation reaction of methanol was considered for developing the model. The kinetics of methanol oxidation and oxygen reduction at AFC and cathode catalyst layer was considered in this model.

Q 21. Ch-5, page- 57: why peak at 600 cm^{-1} makes CP blend incompatible?

Response: The infrared peak appeared at 600 cm^{-1} attributes C-C bond interaction in a blend. The peak appeared at 600cm^{-1} signifies the miscibility or compatibility of the blend. The effect of C-C bond interaction on the compatibility of blend is reported in Chapter 5, **page number-53** and highlighted in the revised thesis.

- ✓ The presence of a prominent peak at 600cm^{-1} confirms C-C interaction between chitosan and polyvinyl alcohol. There was no C-C bond interaction in a CP blend. The absence of C-C bond interaction signifies its non-compatibility structure [**62**].

Q22. Page-73, sec-5.3.3: Where is equation 8?

Response: This is actually equation-4.11, **page number-67** in the revised thesis.

- ✓ The average size of CNT crystal present in the hybrid membrane was calculated by Scherer's equation (**equation-4.11**).

$$\mathbf{D}=\frac{K\lambda}{\beta Cos\theta} \qquad \mathbf{(4.11)}$$

Q 23. Page-75, sec-5.4.1: There is no rectangular box in Fig 5.12(c) please rewrite the section as per your figures.

Response: Section-5.4.1, **page number 69**, Fig. 12(c) can be read as Fig. 13 (c). The sentence is corrected in the revised thesis as follows

- ✓ The well dispersed zirconia particles was observed in all the membranes except CPZr-4. In a CPZr-4 membrane, zirconia particles were aggregated which is highlighted by rectangular box in Fig. 5.13(c).

Q 24. Ch-6, page-94: Last it should be freeze water not freezing water.

Response: Freezing water has been corrected to free water in Chapter 6, **page number-87** in the revised thesis.

- ✓ The bound and free water of the hybrid membrane was experimentally determined and reported in **Table 6.3**.

Q 25. lon exchange capacity (lEC), water uptake, DSC analysis, TGA analysis, mechanical strength analysis: Each of this section should have a concluding remark conveying the best membrane configurations evolved out of those analyses. The accompanying tables may also be highlighted for the best membrane blend evolved.

Response: The results of each analysis has been presented in a separate section with concluding remarks in the revised thesis (**page number-183, 185 and 186**). In the comparative analysis table, properties of best membranes are highlighted (**page number-183**).

<u>Section-7.1</u> (Page number-183)

- ✓ The CPH blend provides highest ion exchange capacity (IEC) among the Chitosan based membrane.

- ✓ Ionic liquid modified CPZr membrane provides higher water uptake capacity and bound water content. The major demerit of ionic liquid membrane is its excessive swelling which reduces its dimension and mechanical stability. The CPCN and CPZr membrane provides lower swelling degree as compared to the ionic liquid modified membrane. Hence, these membrane can provide better dimension stability. The N117 membrane provides higher dimension stability due to its lower swelling area.
- ✓ CPH provides highest tensile strength and lower glass transition temperature. The addition of filler and ionic liquid to a CP blend reduces its tensile strength. Due to its lower glass transition temperature, it can provides a better flexibility and could be viable candidate for fuel cell application at stressed conditions.

Table 7.1: Physical, mechanical and thermal properties of the fabricated membranes.

Membrane Type	**IEC (meq/g)**	**Water Uptake Capacity (%)**	**Bound Water (%)**	**Swelling Area (%)**	**Tensile Strength (MPa)**	**T_g (°C)**
CP	0.575	133	---	----	42.08	120.57
CPH	**0.832**	138	---	----	**46.12**	**110.82**
CPR	0.71	149	12.26	----	12.28	121
CPCN	0.22	140	15.23	51.85	13	126.58
CPZr	0.23	117.31	16.79	**48.83**	13.56	134.77
CPCN@IL	0.76	184.38	20.63	74.16	9.41	124.38
CPZr@IL	0.728	**254.21**	**24.47**	118.64	10.59	126.17
SPEEK-PVA-silica	**1.64**	36	7.83	----	----	136
N117	0.93	25	2.15	13	11.94	132

<u>Section-7.2</u> (**Page number-185**)

- ✓ Chitosan-PVA blend modified with cross-linking agent (sulphuric acid) and ionic liquid provides better proton conductivity. However, the conductivity value of modified membrane was lower than the commercial N117 membrane and SPEEK based membrane.
- ✓ The CP blend modified with crosslinking agent and ionic liquid provides excellent methanol blocking ability which is viable for fuel cell applications. However, the modified membrane provides lower selectivity due to their inferior proton conductivity. For improving fuel cell performance, selectivity of the membrane should be enhanced.
- ✓ The activation energy of the CP, CPH and CPR membrane was lower than the N117 membrane. The temperature has least effect on proton conductivity of the membrane.

Section-7.3 (**Page number-186**)

- ✓ Among the fabricated membranes, ionic liquid modified CPZr membrane provides the highest power density of 97 mW/cm^2 at a current density of 440 mA/cm^2.
- ✓ The power density achieved by the fabricated membrane was lower than the commercial N117 membrane.

Q 26. Fig-6.10: why derivative weight change is important here but not in other figures?

Response: The derivative weight change is important to analyze the weight loss curve of sample. But unfortunately the derivative weight change curve of all samples was not studied in this thudy. The derivative weight change curve of CPR and CPZr membrane was studied and reported in **page number-108 and 112**.

Q 27. Could the Author explain explicitly the role of free and bound water at low and moderately high temperature in proton conductivity by Grotthus and vehicular mechanisms?

Response: The role of free and bound water at low and moderate temperature in proton conductivity by Grotthus and vehicular mechanism is explained in Chapter 6, **page number-81 and 82** in the revised thesis.

- ✓ In a membrane, higher proton conductivity was achieved by proton transport via the Gotthus mechanism. The proton transport via Grotthuss mechanism was regulated by the presence of free water. At lower temperature, fuel cell performance was influenced by the availability of free water as well as IEC of the membrane. The membrane achieved increased proton conductivity by free water, and proton transport was controlled by the Grotthuss mechanism.

- ✓ However, at moderate temperature (low humidity conditions), amount of free water presence in the membrane was escaped due to evaporation loss. In this condition, bound water plays a crucial role for fuel cell performance. The proton transport was controlled by bound water regulated Grotthuss mechanism [**65**]. Moreover, free water will act as a vehicle to transport proton by vehicular mechanism. The amount of proton transport by vehicular mechanism was significantly lower than that of Grotthuss mechanism. The membrane with higher bound water content is considered to be a potential candidate of fuel cell application at moderate temperature.

Q 28. Ch-6, fig-6.29 (a): it is the polarization curve for CPR-3 that should have been revealed in fig caption.

Response: A new figure number (Fig. 6.1) is added in the Chapter 6 and Fig. 29(a) is changed to Fig. 30. The caption of Fig. 30 is corrected in Chapter 6, **page number-165**.

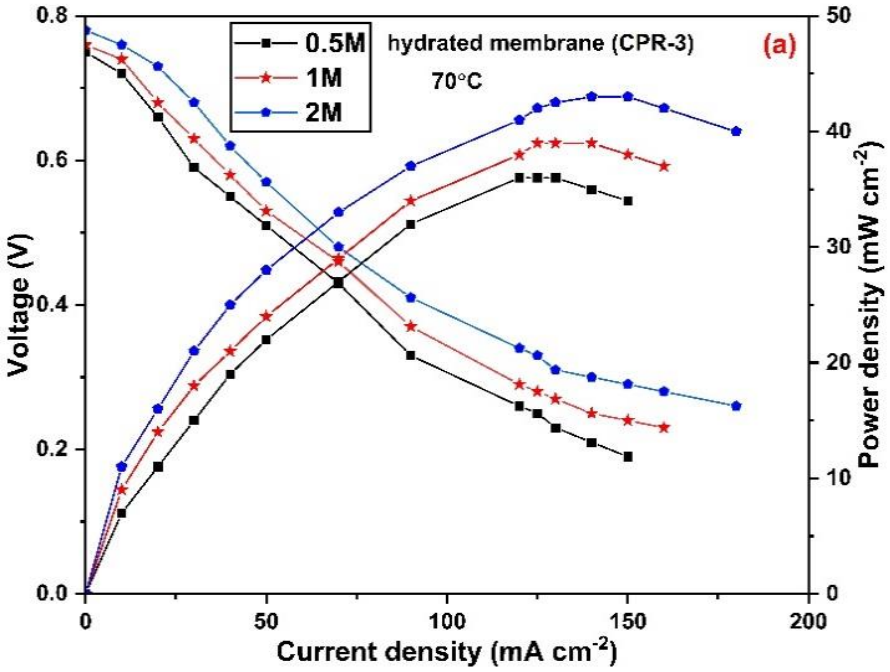

Figure 6.30: Polarization and power density curve of fuel cell obtained at 70°C for CPR-3 membrane. (a) Effect of methanol feed concentration.

Q 29. Ch-1, page-48: please explain polarization loss in terms of active, ohmic and concentration polarization loss.

Response: Polarization loss in terms of active, ohmic and concentration polarization loss is explained in Chapter 1, **page number-44 and 45** and highlighted in the revised thesis.

- ✓ Polarization curve characterizes the voltage with the function of current. It also predicts the efficiency of fuel cell at any operating current. During current flow, voltage loss was occurred due to the resistance of current flow at anode and cathode interface. It was affected due to the limitations of reaction rate, mass transport and resistance at catalyst surface. Due to the loss of current, sharp drop of open circuit voltage was occurred. Due to the voltage drop, fuel cell efficiency decreases. The polarization loss was categorized in to three types i.e. active, ohmic and concentration polarization loss. The voltage loss occurred due to the limitations of reaction rate is called active polarization loss. The limitations of mass transport incurred concentration polarization loss. The ohmic loss was occurred due to the

resistance of current at catalyst interface.

Q 30. Ch-6, page -177: there is no durability test for CPCN-3 and CPCN@IL-3 and CpZr3 and CPZ@lL-3 as well.

Response: The durability test of the above membrane was not conducted as required equipment was not present.

Q 31. Ch-6, page -182: How the fuel cell to be operated at higher current density to minimize leakage current.

Response: At higher current density, the electrochemical reaction at the anode surface occurs more quickly, allowing methanol to be oxidized faster and minimizing methanol cross-over. Hence, less amount of leakage current is generated at cathode side. Moreover, faster electrochemical improves power density of the fuel cell. The effect of operating condition on power density of the fuel cell is explained in Chapter 6, **page number-173** in the revised thesis.

- ✓ It was also reported that fuel cell operating at higher current density region produces lower leakage current [**59**]. At higher current density, the electrochemical reaction at the anode surface occurs more quickly, allowing methanol to be oxidized faster and minimizing methanol loss due to low cross-over. Hence, less amount of leakage current is generated at cathode side. Moreover, faster electrochemical improves power density of the fuel cell. Therefore, it is suggested that the fuel cell should be operated at higher current density to minimize leakage current.

Q32. Page -184, Ch-6: The increase in methanol concentration at anode side increases cell voltage with current density "not and current density".

Response: The above sentence was corrected in Chapter 6, **page number-175** in the revised thesis.

- ✓ The increase of methanol concentration at anode side increase cell voltage with power density.

Q33. There was lot of grammatical mistakes in manuscripts like "(was introduces)" please rectify those.

Response: The grammatical mistakes of this thesis has been corrected.

11.2 In response to observations of the Examiner No. I / II

(1) Though the CPH blend showed better water uptake, tensile strength and IEC, and very poor methane permeability (Table 6.1), but in the study CP blend was used for further analysis. The reason is not explained well.

Response: The objective of this thesis was to investigate the influence of fillers, ionic liquid and cross-linking agent on the properties of chitosan-polyvinyl alcohol blend for its potential use in a fuel cell. Hence, further research was not conducted on a cross-linked blend.

- ✓ **Aims & Objectives of this present thesis this is as follows;**

To develop highly selective chitosan based low cost membranes (modified with red mud, ionic liquid with different fillers) able to deliver high power density.

(2) It is reported that addition of red mud increases the absorption of water in CPR membrane. More the amount of red mud, more the water uptake (Table 6.2). It reveals that if we go on increasing percentage of red mud (without changing chitosan-PVA blend), more will be water uptake. Then how the membrane will manage to survive (Young's modulus is decreasing)? Where is the limitation?

Response: The increase of weight (%) of red mud in a Chitosan-PVA blend increases water uptake capacity which is more appealing. But when the amount red mud content exceeds 3% (weight) in a Chitosan-PVA blend, agglomeration occurs (**page number-56 and 57**). Due to agglomeration, membrane becomes highly porous and decreases its tensile strength (**page number-129**). Hence, it will not survive at stressed conditions.

- ✓ When we have added more red mud particles during synthesis, hard aggregation was observed.
- ✓ During hard aggregation, the red mud particles were aggregated strongly and form a cluster of particles.
- ✓ The formation of cluster creates more void space in a membrane.
- ✓ As the amount of red mud increased, the tensile strength of the membrane was decreases. The tensile strength of CPR-2 and CPR-3 membrane was 18 and 11MPa respectively. Due to decline their tensile strength, mechanical stability of the membrane were reduces.

(3) In FESEM analysis (Chapter 5), the formation of filler cluster (aggregates) on the surface of CPCN- 3 membrane has been reported and is shown in Fig. 5.7(b). However, in Chapter 6 (page 94), it is stated that CPCN-3 had the maximum water uptake compared to CPCN-1 and CPCN-2. Where as in CPCN-4, water uptake was dropped drastically. Discussion in Chapter 6 supports formation of aggregates in CPCN-4 (not in CPCN-3). Need to be explained.

Response: This is actually Fig. 5.7(b) (Chapter 5, FESEM Analysis, **page number-62**). Although, it is stated for CPCN-4 in the figure caption, it was incorrectly referred as CPCN-3 during the discussion. It is corrected in the discussion section in the revised thesis. The formation of cluster was started in a CPCN-4 membrane not in CPCN-3 membrane. Due to the aggregation of filler, water uptake was dropped drastically.

✓ The formation of filler cluster on the surface of CPCN-4 membrane is shown in Fig. 5.7(b).

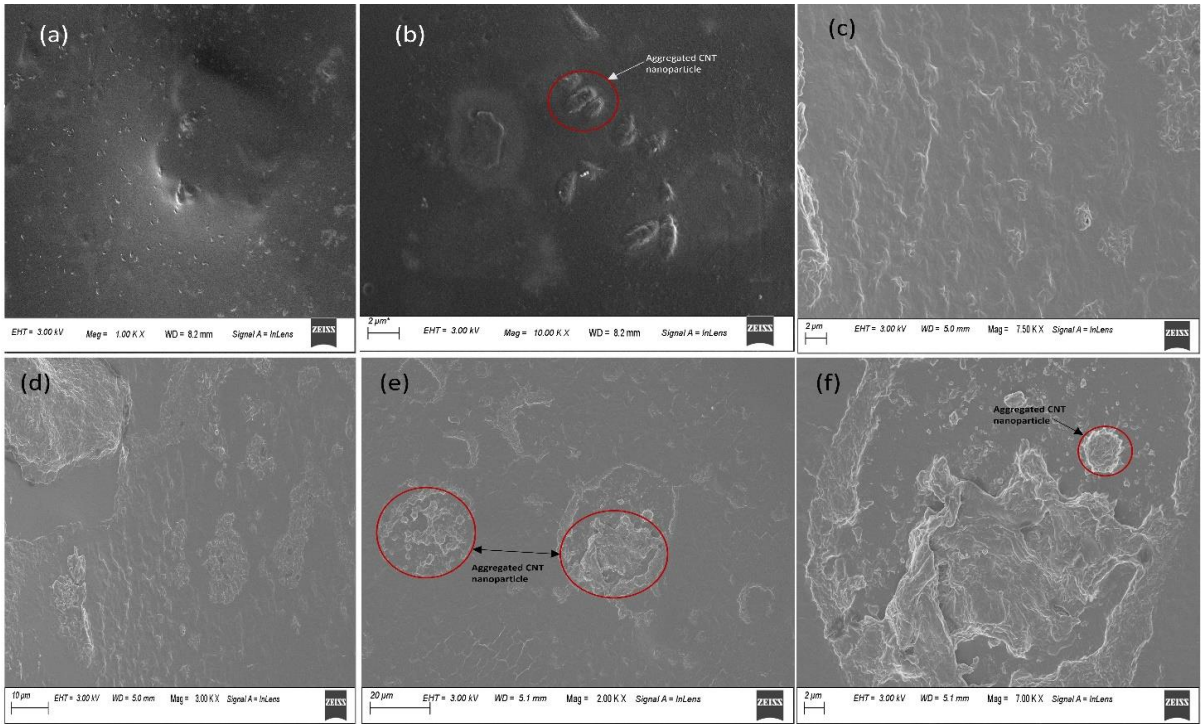

Figure 5.7. FESEM images of the membrane (a) CPCN-1 (b) CPCN-4 (c) CPCN@IL-1, Mag=7.50KX (d) CPCN@IL-1, Mag=3.00KX (e) CPCN@IL-4, Mag=2.00KX (f) CPCN@IL-4, Mag=7.00KX.

(4) CPH blend showed (Table 6.10) highest proton conductivity and the lowest methanol permeability among the chitosan-PVA blends studied by the researcher. It is also stated in line No.13 of the Page 152 that CPH showed higher selectivity. But in line No.19 of the same page it is mentioned differently.

Response: The CPH membrane shows higher proton conductivity among the neat and cross-linked CP blend. But its selectivity value is lower than the commercial Nafion (N117) membrane. In line no. 19, **page number-I43**; selectivity of CPH membrane is compared with the commercial Nafion (N117) membrane.

- ✓ The proton conductivity of the CPH membrane was lower than the commercial N117 membrane. Due to its inferior proton conductivity, it provides lower selectivity than the commercial N117 membrane.

(5) Though the comparison of model predicted data and the experimental data (Figure 6.35 and 6.36) showed very well fitting, no statistical data (like standard deviation, correlation coefficient etc.) has been reported.

Response: The statistical data like standard deviation and correlation coefficient etc. was not used during model fitting. It is included in the scope of future work (**page number-196**).

<u>Scope of future work:</u>

- ✓ Validation of proposed theoretical model by including statistical parameters.